

Summer 7-12-2019

Cyclic AMP efflux inhibition as a potential therapeutic target for acute leukemia: small molecule discovery and validation

Dominique R. Perez
University of New Mexico

Follow this and additional works at: https://digitalrepository.unm.edu/biom_etds

 Part of the [Medicine and Health Sciences Commons](#)

Recommended Citation

Perez, Dominique R.. "Cyclic AMP efflux inhibition as a potential therapeutic target for acute leukemia: small molecule discovery and validation." (2019). https://digitalrepository.unm.edu/biom_etds/198

This Dissertation is brought to you for free and open access by the Electronic Theses and Dissertations at UNM Digital Repository. It has been accepted for inclusion in Biomedical Sciences ETDs by an authorized administrator of UNM Digital Repository. For more information, please contact amywinter@unm.edu.

Dominique R. Perez

Candidate

Biomedical Sciences - Pathology

Department

This dissertation is approved, and it is acceptable in quality and form for publication:

Approved by the Dissertation Committee:

Larry A. Sklar, Chairperson

Alexandre Chigaev

Ksenia Matlawska-Wasowska

Bruce S. Edwards

Bridget S. Wilson

**CYCLIC AMP EFFLUX INHIBITION AS A POTENTIAL
THERAPEUTIC TARGET FOR ACUTE LEUKEMIA:
SMALL MOLECULE DISCOVERY AND VALIDATION**

by

DOMINIQUE R. PEREZ

B. S., Biology, New Mexico Institute of Mining & Technology, 2006
B. S., Psychology, New Mexico Institute of Mining & Technology, 2006

DISSERTATION

Submitted in Partial Fulfillment of the
Requirements for the Degree of

**Doctor of Philosophy
Biomedical Sciences**

The University of New Mexico
Albuquerque, New Mexico

July 2019

ii

DEDICATION

This dissertation is dedicated in memoriam of Benjamin Madrid, Gregorio Perez,
and Susan Young.

I miss you.

ACKNOWLEDGMENTS

I am incredibly honored to have had two amazing mentors, Drs. Larry A. Sklar and Alexandre Chigaev. I don't think that many graduate students can say that their mentors bled for their dissertation projects, but mine did. Thank you for your donations of PBMCs. Larry, I have always admired your leadership, and your dedication to the Center for Molecular Discovery. The wisdom that you've shared has been indispensable, and I am proud to be able to say that I was your student. Thank you for encouraging me to publish early and often. Alex, I waited years for the privilege to work with you, and I am glad that you took me on as a student. After all your years in science, you're still enthusiastic about new data, and it's truly inspirational. I love that you always have an interesting perspective on research. I'll miss our Friday idea-sharing sessions.

I am also lucky to have had a remarkable dissertation committee. Dr. Ksenia Matlawska-Wasowska, you have been an excellent collaborator and friend. I have learned so much from you, about leukemia, life as a scientist, and everything in between. Thank you for the primary samples, all the fruitful conversations, and the tremendous support that you've given me. Dr. Bruce S. Edwards, you are so extraordinarily talented and insightful. Without you and the numerous applications that you've created, none of our high throughput data could be analyzed. I mean it when I say that SynScreen has changed my life. Dr. Bridget S. Wilson, you are a wonderful role model. I am grateful for your objectivity and perspectives on research. You have been a great resource for all things leukemia, and I have always appreciated your constructive criticism.

I would not be the scientist that I am today were it not for Steve Goodgame and Dr. Snezna Rogelj. Steve, you were the first to teach me biology and experimental design. Your patience and dedication to teaching are truly admirable. You sacrificed every Saturday for years to teach high school students everything from geology to engineering. It is amazing to see that you're now cultivating young scientists on an international level. Snezna, you have inspired so many students at NM Tech. Your passion for science is unparalleled. Thank you for taking the extra time to teach me laboratory and research techniques. If it were not for you, I would have ended up in a career in outside of science, and I am forever grateful.

To all of the members of the UNM Center for Molecular Discovery past and present, you are some of my closest friends, and I consider you like a second family. I have been so fortunate to have been a part of this group for the last twelve years. I love that as a group, we have always been a source of support and encouragement for each other. I could write pages of acknowledgments to each one of you, but for the sake of brevity, I will contact you all directly. I do, however, need to give special recognition to two remarkable women. Dr. Anna Waller, in many ways, you are the glue of this lab, and I can't express how amazing you are. Yelena Smagley, thank you for all of your help and friendship over the years.

To my family, thank you so much for your unwavering support, and for believing that I could succeed. My parents have always encouraged me to learn. I appreciate

that you were both so patient with my incessant questions as I grew up. My sisters, Jamie and Cassie, have carved their own paths, and truly inspire me. My extended family is amazing, and a constant source of laughter. Lisa, you are one of my favorite people of all time, and I am very grateful for all that you've done for me. Mom, "I love you more."

CYCLIC AMP EFFLUX INHIBITION AS A POTENTIAL THERAPEUTIC TARGET FOR ACUTE LEUKEMIA: SMALL MOLECULE DISCOVERY AND VALIDATION

by

DOMINIQUE R. PEREZ

B. S., Biology, New Mexico Institute of Mining & Technology, 2006

B. S., Psychology, New Mexico Institute of Mining & Technology, 2006

Ph. D., Biomedical Sciences, University of New Mexico, 2019

ABSTRACT

Evasion of apoptosis and resistance to chemotherapy are major therapeutic challenges for acute leukemias. Presumably as a means to promote cell survival, multiple elements of the cyclic AMP (cAMP) pathway are aberrantly regulated in acute leukemias. Furthermore, increased intracellular cAMP (icAMP) is known to induce apoptosis. Therefore, modulation of icAMP has long been a target in leukemias. The central hypothesis of this dissertation is that malignant cells produce and remove excess intracellular cAMP to evade apoptosis and promote survival. Consequently, inhibition of cAMP efflux could selectively trigger leukemia cell death. We designed a novel assay to assess icAMP efflux from cells, and used this in a high throughput screen to identify several molecules as *inhibitors of cAMP efflux (ICE)*. We determined that cAMP efflux mechanisms are relatively absent in normal peripheral blood mononuclear cells (PBMCs), but are active in leukemia cell lines. We also

validated the ability of ICE to increase cAMP pathway activity. We demonstrated that ICE selectively induce apoptosis in leukemia cells. Because chemotherapy resistance can occur by cAMP efflux transporters, this dissertation also addresses the possibility of using ICE in combination with current therapeutics. We demonstrate that combinations of ICE with leukemia chemotherapeutic agents produce synergistic effects against acute leukemia cells *in vitro* and *ex vivo*. In conclusion, we believe that our data support inhibition of efflux as a mechanism in cAMP pathway targeting that merits further investigation for the development of cancer therapeutics.

TABLE OF CONTENTS

CHAPTER 1: Introduction.....	1
1.1 Acute leukemias — Novel therapeutics are urgently required	1
1.1.1 Biology and etiology of acute leukemias	1
1.1.2 Treatment paradigms in acute leukemias	3
1.2 cAMP-dependent pathway - A meaningful target in hematological malignancies	5
1.2.1 The cellular roles of cAMP and its regulation.....	5
1.2.2 Overview of cAMP targets in acute leukemias.....	8
1.2.3 History of cAMP targeting in cancer (with a focus on hematological malignancies).....	9
1.3 Targeting cAMP transporters/efflux – an unexplored approach to modulation of the cyclic nucleotide pathway	10
1.4 Summary and Discussion	12
CHAPTER 2: A high throughput flow cytometry assay for identification of inhibitors of 3', 5'-cyclic adenosine monophosphate efflux.....	16
2.1 Summary	16
2.2 Introduction.....	17
2.3 Materials	25
2.3.1 Components for Fluorescent Cyclic AMP Loading.....	25

2.3.2 cAMP Efflux Assay Components	26
2.3.3 High Throughput Screening Components	27
2.4 Methods.....	28
2.4.1 Loading F-cAMP into cells.....	28
2.4.2 Optimization of F-cAMP efflux positive control and determining cell F-cAMP efflux ability	29
2.4.3 High throughput F-cAMP efflux assay	32
2.5 Notes.....	35
2.6 Acknowledgements.....	41
CHAPTER 3: Cyclic AMP efflux inhibitors as potential therapeutic agents for leukemia	42
3.1 Abstract	42
3.2 Introduction.....	43
3.3 Results.....	46
3.3.1 A screen for ICE identifies six potentially active compounds	46
3.3.2 Correlation between ICE ability to block F-cAMP efflux and viability loss	49
3.3.3 CREB/AFT-1 phosphorylation in response to ICE.....	49
3.3.4 VLA-4 deactivation in response to ICE.....	51
3.3.5 Adenylyl cyclase inhibition reduces ICE-induced cell viability loss	52

3.3.6 Normal primary peripheral blood mononuclear cells (PBMCs) did not significantly efflux cAMP.....	55
3.3.7 ICE induce apoptosis of U937 cells.....	56
3.3.8 ICE decrease viability and show cancer cell specificity.....	57
3.3.9 Leukemic cells have different abilities to efflux cAMP	59
3.3.10 The primary cAMP transporter, MRP4/ABCC4, is differentially expressed by leukemic cell lines	61
3.3.11 ICE decrease primary ALL patient sample viability	62
3.4 Discussion.....	65
3.5 Materials and methods.....	72
3.5.1 Ethics.....	72
3.5.2 Cells and reagents	72
3.5.3 PBMCs.....	73
3.5.4 Primary ALL patient samples	73
3.5.5 cAMP efflux assay	73
3.5.6 High throughput screening (HTS).....	74
3.5.7 Compound validation.....	75
3.5.8 Detection of CREB/AFT-1 phosphorylation in response to ICE.....	75
3.5.9 Kinetic analysis of VLA-4 deactivation.....	76

3.5.10 Viability.....	77
3.5.11 Determination of cell viability by 7-AAD exclusion.....	77
3.5.12 Apoptosis	78
3.5.13 Quantitation of ABCC4	79
3.5.14 Data analysis.....	79
3.6 Acknowledgments.....	80
3.7 Disclosure of potential conflicts of interest.....	80
3.8 Grant support.....	80
CHAPTER 4: High throughput flow cytometry identifies small molecule inhibitors for drug repurposing in T-ALL	81
4.1 Abstract	82
4.2 Introduction.....	82
4.3 Material and Methods	86
4.3.1 Reagents.....	86
4.3.2 T-ALL cell lines	86
4.3.3 T-ALL patient samples and patient derived xenografts (PDX).....	86
4.3.4 Compounds	87
4.3.5 High Throughput Flow Cytometry Viability Testing	88
4.3.6 Data analysis	89

4.4 Results and Discussion	90
4.4.1 Drug sensitivity screening in T-ALL cell lines	90
4.4.2 Hypoxia cytotoxicity ratio (HCR) in T-ALL cell lines	93
4.4.3 Drug sensitivity screening in T-ALL primary samples and PDX	97
4.5 Acknowledgements.....	104
CHAPTER 5: High-throughput flow cytometry (HTFC) drug combination discovery with novel synergy analysis software, SynScreen	105
5.1 Abstract	105
5.2 Introduction.....	106
5.3 Materials and Methods	109
5.3.1 Development of the SynScreen application	109
5.3.2 HTFC Assays and Data Collection.....	113
5.3.3 Preparation of Data for SynScreen Analysis	114
5.3.4 SynScreen Software Determination of Drug-Drug Interactions in HTFC Data	115
5.3.5 Validation of Synscreen and Application to Other Screening Platforms.	120
5.4 Results and Discussion	120
5.4.1 Validation of SynScreen Analysis for HTFC Assays	120
5.4.2 Application of SynScreen Analysis to Other Screening Platforms.....	122

5.4.3 SynScreen Facilitates Drug Combination Analysis.....	125
5.4.4 Limitations of the SynScreen Software Application	127
5.4.5 SynScreen is an Optimal Application for HTFC Drug Combination Analysis	128
5.5 Acknowledgements.....	129
5.6 Conflicts of Interest.....	130
CHAPTER 6: Drug combination screen of cyclic AMP efflux inhibitors with leukemia chemotherapeutics elicits synergy in acute leukemia cells	
6.1 Abstract	131
6.2 Introduction	132
6.3 Results.....	135
6.3.1 HTFC assays were designed to test ICE+LCA combinations.....	135
6.3.2 AML cell lines show enhanced sensitivity to ICE+LCA combinations.....	137
6.3.3 B-ALL cell lines exhibit sensitivity to some ICE+LCA combinations	141
6.3.4 Primary B-ALL samples have limited sensitivity to ICE, LCA, or ICE+LCA combinations	146
6.4 Discussion	153
6.5 Materials and Methods.....	157
6.5.1 Reagents and compounds	157

6.5.2 Cell lines	158
6.5.3 B-ALL patient samples	158
6.5.4 HTFC drug combination setup	159
6.5.5 HTFC viability assays	160
6.5.6 HTFC proliferation assay.....	162
6.5.7 Primary cell F-cAMP assay.....	162
CHAPTER 7: Clioquinol: to harm or heal	164
7.1 Abstract	164
7.2 Introduction.....	165
7.3 Subacute myelo-optic neuropathy: clioquinol's fall from grace.....	166
7.4 Clioquinol makes a comeback against neurodegenerative diseases	167
7.5 Clioquinol may be a rising star against cancer too	170
7.6 ATP-binding cassette transporters, potential culprits in clioquinol-associated subacute myelo-optic neuropathy?	172
7.7 Single nucleotide polymorphisms in ABCC4 and ABCC11 in Japanese population dramatically increase sensitivity to nucleotide-like drugs	173
7.7.1 ABCC4	173
7.7.2 ABCC11.....	174

7.8 Possible beneficial effects of single nucleotide polymorphisms in ABCC transporters.....	176
7.9 Could clioquinol's effect on cAMP be relevant to clioquinol's action in Alzheimer's disease?	179
7.10 The cAMP/PKA/CREB signaling pathway as a possible target in Alzheimer's disease	182
7.11 Concluding remarks and future perspectives.....	185
7.12 Glossary	187
ATP-binding cassette (ABC) transporter:.....	187
7.13 Acknowledgments	190
7.14 Conflict of interest statement.....	190
CHAPTER 8: Discussion and future directions.....	191
8.1 Discussion.....	191
Future Directions	194
8.2.1 Determine the effects of ICE on endogenous cAMP signaling.....	194
8.2.2 Evaluate ICE effects in vivo.....	196
8.3 Concluding remarks.....	199
APPENDICES.....	200
APPENDIX A: Abbreviations used	200

APPENDIX B: Supplemental material for Chapter 4	202
APPENDIX C: Supplemental material for Chapter 5.....	211
APPENDIX D: Supplementary material for Chapter 6	217
REFERENCES.....	279

LIST OF FIGURES

Figure 1.1 Basic schematic of cAMP compartmentalization and effectors.....	7
Figure 2.1 Structure of the fluorescent cAMP analog (F-cAMP) used in this assay..	19
Figure 2.2 Cell line MK571 optimization and determination of cell F-cAMP efflux ability.....	21
Figure 2.3 Sample data from a 384-well F-cAMP efflux assay plate collected as in step 3.3.9.....	22
Figure 2.4 Sample configuration for a 384-well compound mother plate, as described in Note 15.....	22
Figure 2.5 Sample data from hit compound dose-response validation.....	23
Figure 2.6 Results of ICE hit compounds after overnight incubation on U937 leukemia cell vitality in flow cytometric secondary assays.....	24
Figure 3.1 Effect of MK-571 (MRPs selective inhibitor) on efflux of a fluorescently tagged cAMP (F-cAMP).....	47
Figure 3.2 Relationship between ICE ability to block F-cAMP efflux and loss of cell viability.....	49
Figure 3.3 Binding of anti-phospho-CREB/AFT-1-specific antibody in response to ICE.	50
Figure 3.4 Dissociation of the VLA-4-specific fluorescent ligand in response to ICE.	52
Figure 3.5 Effect of the selective inhibitor of soluble adenylyl cyclase (KH7) on cell viability loss induced by ICE.....	54
Figure 3.6 cAMP efflux activity of U937 cells and human PBMCs.....	55

Figure 3.7 Effects of ICE on apoptosis of U937 cells.	57
Figure 3.8 Effects of ICE on cell viability of U937 cells, the B-ALL cell lines 697, Reh, MHH Call 3, RS4;11, Sup B15, and Nalm 6, and normal human PBMCs.....	59
Figure 3.9 Retention of F-cAMP in hematopoietic cell lines.	61
Figure 3.10 Determination of ATP-binding cassette transporter ABCC4-specific binding sites on B-ALL cell lines.....	62
Figure 3.11 Effects of ICE on cell viability of primary ALL patient samples.....	65
Figure 3.12 Mechanisms for cAMP-dependent regulation of cell death.	71
Figure 4.1 Drug response profiles of the T-ALL cell lines.....	92
Figure 4.2 Hypoxia Cytotoxicity Ratios (HCR) for five T-ALL cell lines treated with 31 small molecule inhibitors.....	94
Figure 4.3 Representative patterns of T-ALL sensitivity to kinase inhibitors in oxygen deprived environment.	95
Figure 4.4 Response of T-ALL primary samples ($n = 2$) and patient derived xenografts ($n = 5$) to small molecule inhibitors ($n = 31$).....	99
Figure 5.1 SynScreen facilitates the assessment of drug combination effects from an HTFC screen.	118
Figure 5.2 An example of SynScreen analysis of multiplex HTFC drug combination data.....	123
Figure 5.3 Validation of SynScreen analysis of drug combination effects and the determination of synergy.....	124
Figure 6.1 Diagram of the 64-well ICE+LCA combination matrix.....	137

Figure 6.2 Representative drug interaction analysis of ICE+LCA combination effects on U937 cell viability.....	139
Figure 6.3 ICE+LCA combination effects on U937 cells after 48 h.....	140
Figure 6.4 Representative drug interaction analysis of ICE+LCA combination effects on B-ALL cell viability.....	142
Figure 6.5 ICE+LCA combination effects on B-ALL cell line proliferation.....	145
Figure 6.6 Representative drug interaction analysis of ICE+LCA combination effects on U937 cell viability.....	147
Figure 6.7 Comparison of ICE+LCA combination effects on B-ALL cell line and primary sample viability.....	151
Figure 7.1 Chemical structures of substrates of ABCC4, ABCC5 and ABCC11, and other related compounds.....	165
Figure 7.2 Schematic illustration of the role of SNP rs17822931 (G538A; G180R) in ABCC11 functional activity (modified from ref. [5]).	175
Figure 7.3 A model for the role of integrin in consolidation of LTP.....	180
Figure 7.4 A model that summarizes hypotheses relating cAMP accumulation with the pathogenesis of SMON, AD and other diseases.....	181
Figure 8.1 Preliminary data – ICE effects on endogenous intracellular and extracellular cAMP.....	195
Figure 8.2 Preliminary ICE <i>in vivo</i> data.....	198

LIST OF TABLES

Table 2.1 Volumes of MK571 and DMSO added to each well.	30
Table 3.1 Hit compounds identified in the screen for inhibition of cAMP efflux.	48
Table 3.2 The hematologic cell lines included in the study, their subtype and genetic rearrangements [131].	58
Table 3.3 Genotypic and phenotypic profile of B-ALL patient samples.	64
Table 3.4 Previously reported anticancer activity of the compounds identified as ICE.	67
Table 3.5 Previously reported molecular/ signaling mechanisms related to anticancer activity of the compounds identified as ICE.....	68
Table 5.1 Synergistic effects of the repurposed compound, clioquinol, with a conventional cytotoxic drug, cytarabine.....	118
Table 6.1 Compounds used in drug combination assays.	136
Table 6.2 The AML cell lines used in these studies and their characteristics.	138
Table 6.3 Summary of synergistic data points from ICE+LCA combination viability assays in AML cell lines.....	140
Table 6.4 The B-ALL cell lines used in these studies and their characteristics.....	141
Table 6.5 Summary of synergistic data points from ICE+LCA combination viability assays in B-ALL cell lines.....	144
Table 6.6 Summary of synergistic data points from ICE+LCA combination proliferation assays in B-ALL cell lines.....	145
Table 6.7 Characteristics of the tested primary B-ALL cell lines.	148

Table 6.8 Summary of primary B-ALL sample F-cAMP retention and viability. . **Error!**

Bookmark not defined.

Table 6.9 Summary of synergistic data points from ICE+LCA combination viability

assays in primary B-ALL samples.....**Error! Bookmark not defined.**

CHAPTER 1: Introduction

1.1 Acute leukemias — Novel therapeutics are urgently required

1.1.1 Biology and etiology of acute leukemias

While not the most prevalent malignancy in the United States, leukemia ranks among the top ten cancers in terms of both morbidity and mortality [8]. These hematological malignancies involve aberrant proliferation of blood cells with immature phenotypes. Acute leukemias are typically identified by the presence of > 20% blast cells in the peripheral blood or bone marrow [12]. Due to inherent characteristics related to a reduced differentiation state, and the ability to rapidly propagate, acute leukemias have worse prognoses than chronic leukemias. Over the last ten years, the rates of acute myeloid (AML) and acute lymphoblastic leukemia (ALL) diagnoses have modestly increased by 2.2% and 0.6%, respectively [14]. Because these diseases are subject to the growth of blast cells, there is a strong need for the development of novel approaches to treat these malignancies.

As such, our work specifically focuses on acute AML and B-cell lineage ALL (B-ALL). AML is most prominent in elderly adults over 65 years in age. Annually, 21,450 cases are diagnosed in the United States, and 10,920 cases succumb to the disease [8]. The five year overall survival for this disease is a disheartening 28.3% for adults [8] and about 60% for children [17]. B-ALL primarily affects children under 17 years of age, with about 6,000 new cases diagnosed and 1,500 deaths each year [18]. This disease is considered > 80% curable, however there is much room for improvement.

The primary classification of acute leukemia is based on the presence of chromosomal abnormalities and translocations and immunotyping. For example, 25-30% of B-ALL have hyperdiploidy [19], while a surprising 40-50% of AML are cytogenetically normal [12]. An analysis of primary AML samples determined an average of 13 mutated genes per sample [20]. It has also been reported that > 80% of B-ALL cases contain deletions within genes related to B cell development [14]. *De novo* B-ALL genomes also contain 10-20 gene coding mutations [21]. The main role of these genetic alterations in acute leukemia cells is to promote survival.

Most commonly, the etiology of acute leukemias is attributed to the combination of mutations that increase pro-survival signaling and reduce tumor suppressor genes [22]. Many factors are potentially implicated in leukemogenesis, and most include aberrancies that increase cell proliferation. Due to potential mutations, rapid growth, and deviant signaling, leukemia cells have the capacity to overcome normal mechanisms that would typically result in cell death. For example, AMLs overexpress vascular endothelial growth factor (VEGF), and this promotes angiogenesis of the surrounding bone marrow [23]. This altered microenvironment results in vascular leakage of the surrounding endothelium and increased production of nitric oxide (NO) [24]. Because NO is immunosuppressive [25], this leukemia-microenvironment feedback system allows malignant cells to escape cell death through the normal immune response.

1.1.2 Treatment paradigms in acute leukemias

Treatment for acute leukemia typically begins with induction therapy, wherein chemotherapeutics are used to induce remission of the disease. In this approach, the goals are to reduce the population of blast cells and/or induce them to differentiate. Most commonly, this stage of treatment involves drugs that are used in many other cancers and diseases, and hence their mechanisms of action are non-specific for leukemia. These drugs are aimed at killing all cells that are proliferating by inducing DNA damage or interfering with cell replication mechanisms. For some AML and B-ALL patients, allogeneic stem cell transplants are a treatment option as well.

The standard of care for AML is the use of cytosine arabinoside (cytarabine; AraC) with an anthracycline (e.g., daunorubicin, idarubicin, doxorubicin) for 7-10 days [26]. Over 80% of patients can achieve a complete response with this treatment, but often relapse will occur over time [27]. This is followed by consolidation therapy, which is typically high dose AraC [28]. Refractory or relapsed AML is also treated with high dose AraC, or the FLAG (fludarabine, AraC, granulocyte colony-stimulating factor (G-CSF)) regimen, but these result in modest complete remission rates of 32% and 47.5%, respectively.

B-ALL induction therapy involves 4-6 weeks of a glucocorticoid (e.g., dexamethasone or prednisone), asparaginase, vincristine, and an anthracycline. This is followed by several months of consolidation and maintenance therapies, which consist of some induction agents, as well as 6-mercaptopurine or 6-thioguanine, or methotrexate [19]. Like AML, the time elapsed between remission and relapse was

associated with better overall survival. In one longitudinal study of pediatric B-ALL patients, only 8.8% of participants relapsed within 5 years [29], although other reports have indicated relapse rates of about 15-20% [23]. Nonetheless, a small percentage of B-ALL patients are vulnerable to the development of extramedullary disease in the central nervous system (CNS) [30].

For both AML and B-ALL, remission is often determined by the minimal residual disease in the patient. Most commonly, this is classified as < 1 leukemic blast in 10,000-100,000 cells in the bone marrow [19, 30]. The length of remission varies by patient, although some mutations and translocations have been associated with longer event free survival (EFS). For example, AML cases with *NPM1* mutations are considered to have favorable risk, while those containing an internal tandem duplication of fms-related tyrosine kinase 3 (*FLT3-ITD*) have adverse risk [31]. However, it should be noted that about 40% of AML cases are deemed 'cytogenetically normal' [12]. In B-ALL, the *ETV6-RUNX1* fusion protein is associated with better treatment response and longer time to relapse [32]. Rearrangements of the mixed-lineage leukemia (*MLL*) gene are considered prognostically less favorable[32]. Despite the fact that these and other cytogenetic factors are characteristically associated with prognosis, many patient responses to treatment are individual, and even those with similar cytogenetic factors could have opposite responses to the same therapy.

The treatment paradigms for acute leukemias are not without fault. Primarily due to their lack of selectivity for leukemic cells, leukemia chemotherapeutic agents (LCA)

can cause systemic damage to the patient. Most notably, anthracyclines and other chemotherapeutics exhibit cardiotoxicity. This is probably because, like cancer cells, the heart is highly metabolically active. Survivors of pediatric ALL are at increased risk for the long-term development of heart disease [33]. LCA are associated with damage to the liver and kidneys, as these are the primary organs for drug metabolism. Patients with ALL are also at risk for osteonecrosis [34, 35]. Furthermore, leukemia treatments have been related to long-term cognitive impairment, including memory, attention, and executive function deficits [36, 37]. Hence, the development of drugs that are more selective for malignant cells could seriously reduce the incidence of adverse side effects suffered by patients.

1.2 cAMP-dependent pathway - A meaningful target in hematological malignancies

1.2.1 The cellular roles of cAMP and its regulation

In 1958, the first second messenger in cells, 3',5'-cyclic adenosine monophosphate (cAMP) [38], was identified. This molecule is critically important for all cells, and is at the crux of many cellular processes that regulate growth, survival, differentiation, and the transcription of a myriad of genes. cAMP signal transduction can result in activation of pro-survival or death pathways, depending upon cell type and conditions [39]. The primary downstream effectors of cAMP are protein kinase A (PKA) and exchange proteins activated by cAMP (EPAC). While these two effectors can activate multiple transcription factors, the one most commonly associated with

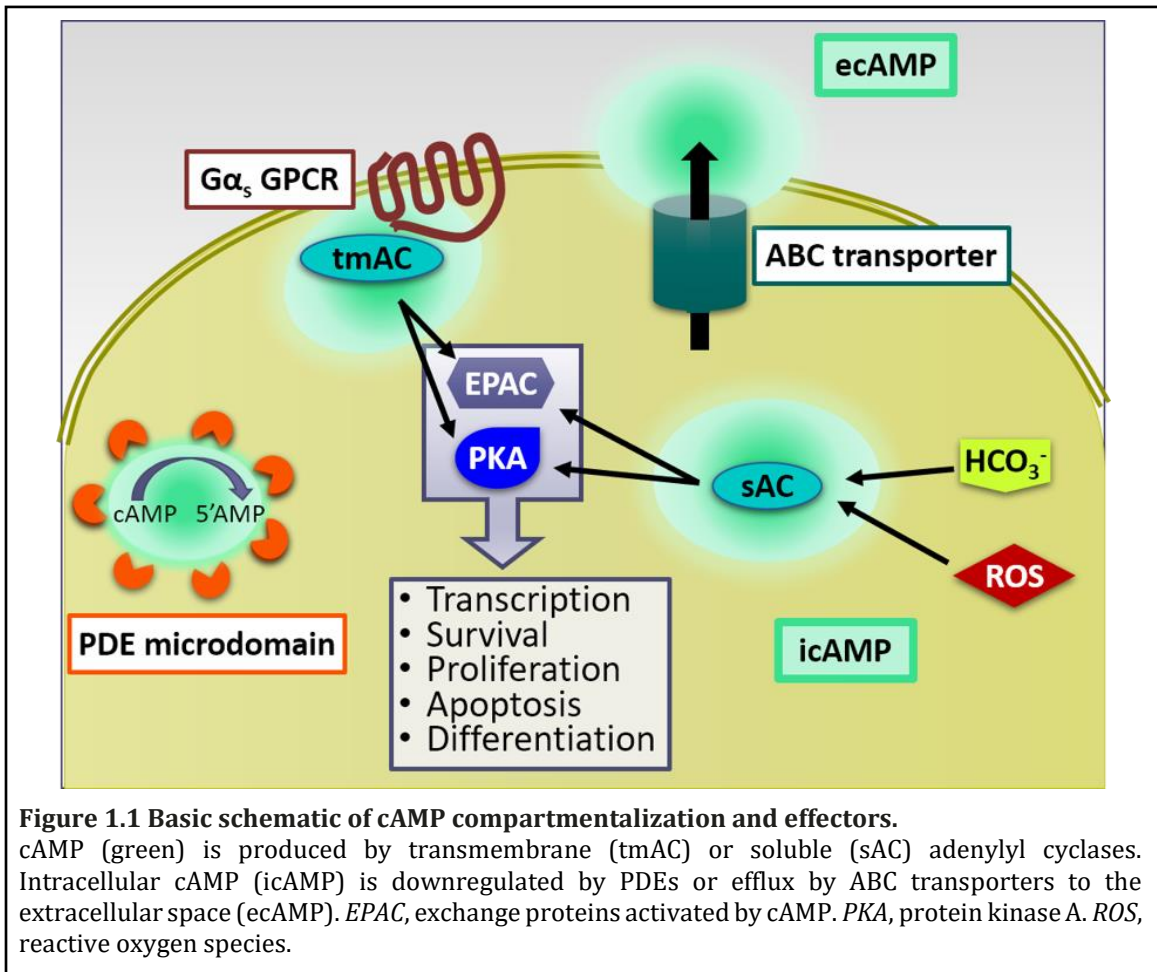
cAMP pathway signaling is the cAMP response element binding (CREB). CREB activity is associated with transcription of many pro-survival genes, including cyclins A, D1, and D2 [40].

Canonical cAMP synthesis involves activation of any of nine transmembrane-associated adenylyl cyclases (tmAC), which are stimulated by $G\alpha_s$ -coupled receptors. Activation of G_i -coupled receptors inhibits tmAC activity, and hence reduces intracellular cAMP (icAMP). Because cAMP signaling occurs spatially throughout the cell, it can also be generated by an alternative mechanism, soluble adenylyl cyclase (sAC; ADCY10). This enzyme is responsible for cAMP production in cytosolic microdomains, such as the cytoplasm, or within the nucleus or mitochondria [41-43]. Unlike tmACs, sAC is activated by bicarbonate (HCO_3^-) or oxidative stress [42, 44]. Elevated icAMP triggers intrinsic apoptosis by PKA signaling. PKA can activate the transcription factor cAMP response element binding (CREB) protein to up-regulate expression of the pro-apoptotic protein Bim [2]. Additionally, sAC stimulation of PKA can cause translocation of pro-apoptotic Bax into mitochondria [45, 46].

icAMP concentrations can be modulated by two different mechanisms. The most commonly studied cAMP regulators are phosphodiesterases (PDEs). These enzymes hydrolyze cyclic nucleotides. The PDEs 1-4, 7, 8, 10, and 11 are capable of degrading cAMP to 5'-AMP [47]. The fact that cAMP can exist outside the cell (ecAMP) was first described in 1963 [48]. Decades later, it was determined that icAMP can be extruded from cells by its active removal via the ATP-binding cassette (ABC) transporters. Members of the multidrug resistance (MRP) family of transporters, ABCC4 (MRP4),

ABCC5 (MRP5), and ABCC11 (MRP8), are reported to efflux cAMP [47]. The primary focus of this dissertation is modulation of this process by small molecules .

Because cAMP activity occurs in discrete locations, many cAMP regulatory proteins can be complexed to facilitate signaling. A-kinase anchoring proteins (AKAPs) are scaffolding proteins that allow adenylyl cyclases, PKA, and PDEs to be kept in close proximity to one another [49]. Hence, the compartmentalization of icAMP into microdomains near the plasma membrane, mitochondria, nucleus, or regulatory proteins, is a critical determinant of its concentration and activity [50-52] (Figure 1.1).



1.2.2 Overview of cAMP targets in acute leukemias

Considering that (a) icAMP regulation is altered in hematopoietic malignancies, and (b) increased icAMP reduces blood cell survival, the cAMP pathway has long been of interest as a target for leukemia therapeutics [39, 47, 53-55]. Many cAMP-associated proteins are dysregulated in acute leukemias. The primary tmAC expressed in lymphoid cells is adenylyl cyclase 7 [56], and the expression of this protein inversely correlates with AML survival [57]. PDE activity is 10-20-fold higher in leukemia and lymphoma cells in comparison to normal blood cells [58]. It should also be noted that glucocorticoids, which are used to treat B-ALL, have been shown to downregulate PDE activity [59]. Of note, genomic studies on primary AML and adult ALL samples have reported overexpression of CREB and/or its active, phosphorylated form [60-65], and another study identified downregulation of ICER (inducible cAMP early repressor), an antagonist of CREB [66]. In B-ALL samples, there is an increased incidence of mutations in transcripts for *CREBBP*, the binding protein for CREB. These *CREBBP* mutations were associated with dominant-negative or deleted activity [67, 68]. In sum, acute leukemia cells are associated with both increased pro-survival cAMP activity by having increased CREB signaling, as well as downregulation of pro-apoptotic factors associated with the cAMP pathway.

1.2.3 History of cAMP targeting in cancer (with a focus on hematological malignancies)

Most previous attempts to modulate cAMP for cancer therapeutics have focused on the use of cAMP analogs, or by targeting canonical proteins of the pathway through: 1) stimulation of cAMP production by G α s-coupled receptors, or 2) inhibition of cAMP degradation by PDEs. These efforts have had modest success, and will be summarized here.

Few cAMP modulating agents targeting cancer have been tested in clinical trials. Despite demonstrating anticancer effects *in vitro* and *in vivo*, phase I clinical trials with the analog 8-Cl-cAMP in patients with refractory solid tumors resulted in hypocalcemia and toxicity to normal tissues [69-71]. A phase II clinical trial evaluated the use of the PDE-inhibitor theophylline for CLL patients. Of the 25 CLL patients treated with theophylline, only one achieved a complete response, and 18 patients maintained a stable disease state [72].

Nonetheless, cAMP pathway modulation has been well investigated as a target in hematopoietic malignancies *in vitro* and *in vivo*. Elevation of icAMP by the use of cAMP analogs has demonstrated the ability to induce cell cycle arrest (G₁ or G₂ phase), differentiation, and/or intrinsic apoptosis in leukemia, lymphoma, myeloma, and normal B cells *in vitro*, most often through PKA-mediated mechanisms [2, 3, 10, 73-77]. Similar results have been reported from studies where cAMP production was stimulated via activation of tmAC [78-81]. PDE inhibitors have also been employed to increase cAMP signaling in hematopoietic cells. Meyers, *et al.* provided evidence that

PDE4 inhibition induced cell death in B-CLL cell lines, but not in normal B and T cells [56]. This selectivity is plausible, since leukemia and lymphoma cells have exhibited elevated PDE expression and activity [55, 58, 82]. Mitton, *et al.* used small molecule CREB inhibitors to reduce the expression of pro-survival genes in AML cells *in vitro* and *in vivo*, and they showed that this approach induced cell cycle arrest and apoptosis. Nevertheless, it is important to note that elevated icAMP can also rescue blood cancer cells from apoptosis, although those studies involved activation of cAMP signaling after substantial DNA damage had occurred in the treated cells [83-88]. Consequently, there is still substantial evidence to support cAMP pathway targeting in hematological malignancies.

1.3 Targeting cAMP transporters/efflux - an unexplored approach to modulation of the cyclic nucleotide pathway

While the intracellular concentrations of cyclic nucleotides are canonically regulated by degradation by PDE microdomains [52], efflux mechanisms by ABC transporters are less explored. This class of proteins consists of 7 families (ABC-A through ABC-G), in which two molecules of ATP are used to translocate substrates into the extracellular space. As previously mentioned, cAMP and cGMP are transported by members of the ABCC (MRP) family, ABCC4 (MRP4), ABCC5 (MRP5), and ABCC11 (MRP8). These transporters are distributed variably throughout the body, with ABCC4 having highest expression in the bladder, kidney, and prostate [89]. The affinity of these transporters varies for cAMP or cGMP. ABCC5 has a greater

affinity for cGMP, whereas ABCC4 is preferential for cAMP [90]. ABCC4, ABCC5, and ABCC11 regulate xenobiotic metabolism, and they can efflux antiviral drugs (PMEA, ganciclovir) as well as chemotherapeutic agents (fluorouracil, mercaptopurine, thioguanine, camptothecins, methotrexate). Importantly, these proteins also serve a role in the transport of natural, endogenous substrates. These include eicosanoids (e.g., prostaglandins E1 and E2, leukotriene C4), estradiol-17 β -glucuronide, folic acid, bile acids (taurocholate, glycocholate), and some steroids (e.g., DHEAS) [91]. Furthermore, the cyclic nucleotide transporters also play a major role in relieving oxidative stress, as they remove glutathione conjugates from the cell [92].

Past work in which cAMP efflux was inhibited by small molecules was performed in epithelial cell lines, and primarily focused on cAMP concentration changes and the activity of pathway-associated proteins [93, 94]. The efflux capacity of leukemia cells has been reported as an important factor for predicting patient outcomes [95]. However, the analysis of cAMP-specific efflux activity has not been extensive. The expression of ABCC4 is inversely correlated with hematopoietic cell differentiation [96]. Previous studies relied on the use of indiscriminate ABC transporter inhibitors (e.g., probenecid) or silencing RNA to block expression of cAMP effluxing proteins [97-99]. These approaches, however, lacked the efficiency and breadth necessary for resolving the utility of targeting cAMP efflux for cancer therapeutics. The recent development of a high throughput-amenable assay to assess cAMP efflux activity would allow for this trait to be measured quickly on a sample-by-sample basis (**Chapter 2**) [100, 101].

It should be underscored that competition between substrates can allow them to inhibit one another. Hence, it is possible that some molecules identified as inhibitors of a given transporter may instead reduce the efflux of other substrates, but not actually block the activity of that transporter. Extensive mechanistic studies must be conducted to validate the mechanism of action of efflux inhibitors on transporters. It should be noted that all substrates of a transporter have the potential to inhibit the transport other substrates of the same transporter. Therefore, molecules that affect similar pathways could initially be identified as efflux inhibitors, but may in fact potentially have mechanism(s) of action that are unrelated to antagonism of transport proteins.

1.4 Summary and Discussion

The introduction to this work has highlighted the need for new treatment regimens for acute leukemias. We have described the vital roles that cAMP signaling plays in the regulation of cell proliferation, survival, and apoptosis. We provided justification for targeting the cAMP pathway, since pathway-associated proteins are dysregulated in these malignancies. We also introduced the concept that the reduction of cyclic nucleotide efflux activity could potentially provide multiple anticancer benefits. As such, *we hypothesize that malignant cells produce and remove excess icAMP to evade apoptosis and promote survival. Therefore, inhibition of cAMP efflux should increase icAMP and selectively trigger leukemia cell death.* We propose that small molecule cAMP efflux inhibition, specifically by repurposed drugs, has the

potential to expedite the translation of cAMP pathway-targeted therapeutics. Because we propose that elevated cAMP efflux activity is an adaptation of malignant cells that is not apparent in normal blood cells, drugs developed from this approach would be selective for leukemia or other cancer cells as compared to normal blood cells or tissue.

To test this hypothesis, we first designed and patented a novel assay to assess icAMP efflux from cells, by measuring cellular retention of a fluorescent cAMP analog (F-cAMP). We then adapted this assay for use in a high throughput flow cytometry (HTFC) screen (**Chapter 2**) [100, 101]. After screening two collections of off-patent FDA-approved drugs and biologically active compounds, we identified and validated six compounds as *inhibitors of cAMP efflux (ICE)* (**Chapters 2 and 3**) [6, 100].

In **Chapter 3**, we describe work to support the main components of our hypothesis. We determined that cAMP efflux mechanisms are relatively absent in normal peripheral blood mononuclear cells (PBMCs), but are active in leukemia cell lines. We also validated the ability of ICE to increase cAMP pathway activity. We demonstrated that ICE induce apoptosis, and that this process requires functional SAC. Furthermore, ICE reduced the viability of leukemia cell lines and *ex vivo* primary patient samples at much lower concentrations than required for PBMCs, supporting our hypothesis that cAMP efflux inhibition is a selective target for malignant cells. Our data suggest that cAMP efflux targeting is independent of leukemia cell line genetic rearrangement or mutation status.

With that promising data, we developed and optimized approaches for testing ICE in pre-clinical studies. We completed work with T-cell ALL (T-ALL) cells to optimize HTFC approaches for determining chemotherapeutic effects on primary sample viability *ex vivo* (**Chapter 4**). We therein determined that hypoxia was not a significant factor for affecting most responses to tyrosine kinase inhibitors.

To facilitate the analysis of drug interactions and to determine potential drug interactions, **Chapter 5** introduces SynScreen software, an application that allows for high throughput data from multiple experimental replicates to be compared simultaneously. This software served as a basis for the development drug combination studies.

Because chemotherapy resistance can occur by cAMP efflux transporters [102, 103], this dissertation also addresses the possibility of using ICE in combination with current therapeutics to produce synergistic effects against leukemias (**Chapter 6**). Synergism produced by these drug combinations would be beneficial for decreasing leukemia cell burden, and potentially to reduce the likelihood of resistance, drug-related toxicities, and/or relapse.

We complete this dissertation with a discussion of the role of one ICE compound, clioquinol, and several disease states (**Chapter 7**). We propose that the occurrences of subacute myelo-optic neuropathy (SMON) may be associated with single nucleotide polymorphisms (SNPs) in cAMP efflux transporters. We also suggest that the efficacy of clioquinol in Alzheimer's disease [104] may be related to its effects on the cAMP pathway.

The summation of the proposed studies could provide support for a new class of antileukemia drugs to be tested in clinical trials. The goal of the current project is to establish a framework for testing the possibility of repurposing the identified compounds as a potential future therapeutic option. The proposed work is significant because it could substantiate inhibition of efflux as a paradigm shift in cAMP pathway targeting for cancer therapeutics.

CHAPTER 2: A high throughput flow cytometry assay for identification of inhibitors of 3', 5'-cyclic adenosine monophosphate efflux

Dominique Perez^{1,2}, Peter C. Simons^{1,2}, Yelena Smagley^{1,2}, Larry A. Sklar^{1,2}, and
Alexandre Chigaev^{1,2}

¹ University of New Mexico Cancer Center, ² University of New Mexico Center for
Molecular Discovery, Albuquerque, NM, USA

In **High Throughput Screening: Methods and Protocols** (Janzen, W. P., ed) pp.
227-244, Humana Press, 2016.

doi: 10.1007/978-1-4939-3673-1_15. PMID: 27316999

2.1 Summary

Assays to identify small molecule inhibitors of cell transporters have long been used to develop potential therapies for reversing drug resistance in cancer cells. In flow cytometry, these approaches rely on the use of fluorescent substrates of transporters. Compounds which prevent the loss of cell fluorescence have typically been pursued as inhibitors of specific transporters, but further drug development has been largely unsuccessful. One possible reason for this low success rate could be a substantial overlap in pump substrate specificities and functions between

transporters of different families. Additionally, the fluorescent substrates are often synthetic dyes that exhibit promiscuity among transporters as well. Here, we describe an assay in which a fluorescent analog of a natural metabolite, 3',5'-cyclic adenosine monophosphate (F-cAMP), is actively effluxed by malignant leukemia cells. The F-cAMP is loaded into the cell cytoplasm using a procedure based on the osmotic lysis of pinocytotic vesicles. The flow cytometric analysis of the fluorescence retained in F-cAMP loaded cells incubated with various compounds can subsequently identify inhibitors of cyclic AMP efflux (ICE).

2.2 Introduction

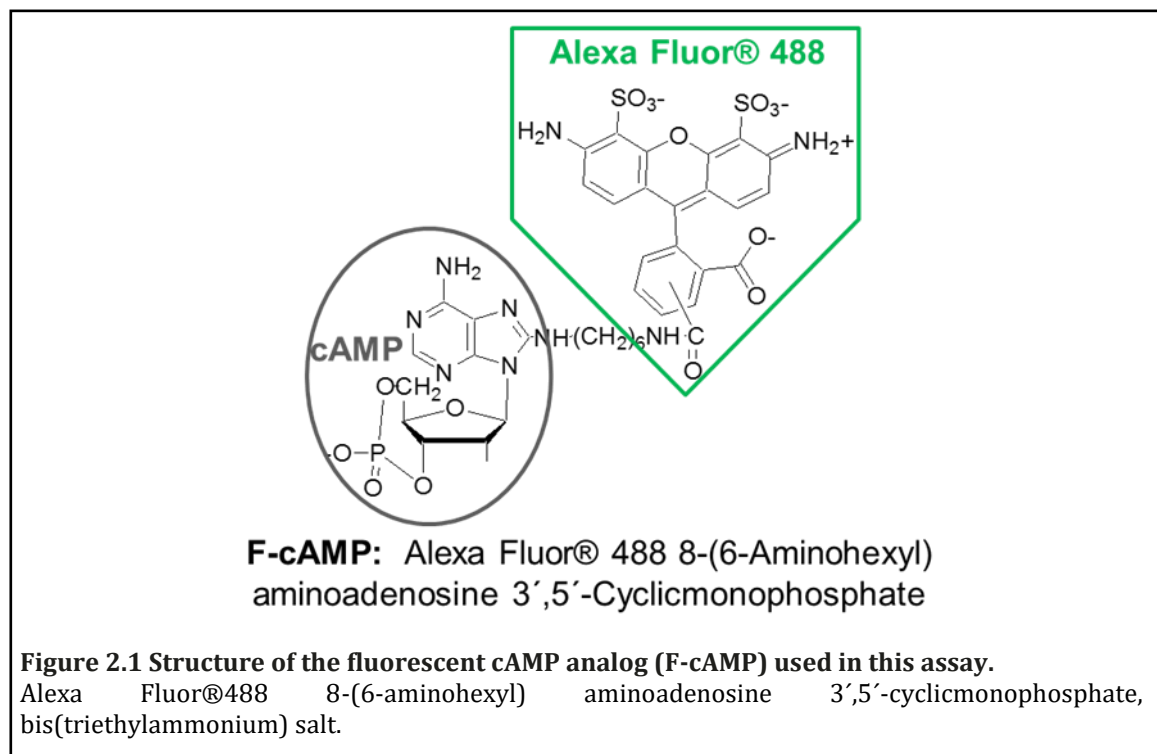
ATP-binding cassette (ABC) transporters are often associated with multidrug resistance in relapsed cancers. ABC transporters are also implicated in the initiation and progression of metastatic malignancies due to their increased expression in cancer stem cells [105, 106]. As a result, the development of novel approaches to study ABC transporter activity to identify small molecule modulators or inhibitors is vital for translation to cancer therapy. Previously, high throughput assays for transporter inhibition have relied upon the use of inside-out vesicles containing specific transporters, or of cancer cell lines which have been induced or engineered to acquire drug resistance [107-110]. In both cases, these approaches have been largely dependent on measuring the intracellular fluorescence of synthetic substrates remaining in cells after exposure to compounds. While several small molecules identified in this manner were capable of reducing the multidrug resistance of cancer

cells *in vivo*, few of these molecules have been successful in clinical trials [108, 111, 112]. This may be due in part to the limitations of these transporter efflux assays.

Often, synthetic fluorescent dyes known to be substrates of a particular transporter are used as probes to screen for hit compounds. A major limitation of this technique is the considerable similarity in cell transporter structures, and therefore substrates are capable of being effluxed by a multitude of transporters [113]. Thus, the inhibitory compounds identified in these assays fail to exhibit specificity toward the originally investigated transporter. Other attempts at measuring efflux of cellular metabolites have used radioactive conjugates of substrates to evaluate changes in intracellular concentrations. However, this results in lower throughput data collection [97]. The approach described here differs from earlier methods because it uses a fluorescent conjugate of a natural metabolite of cell membrane transporters, 3',5'-cyclic adenosine monophosphate (cAMP), and measures its efflux from cells through unmodulated, endogenously expressed transport proteins, allowing for thousands of samples to be measured in a short period of time.

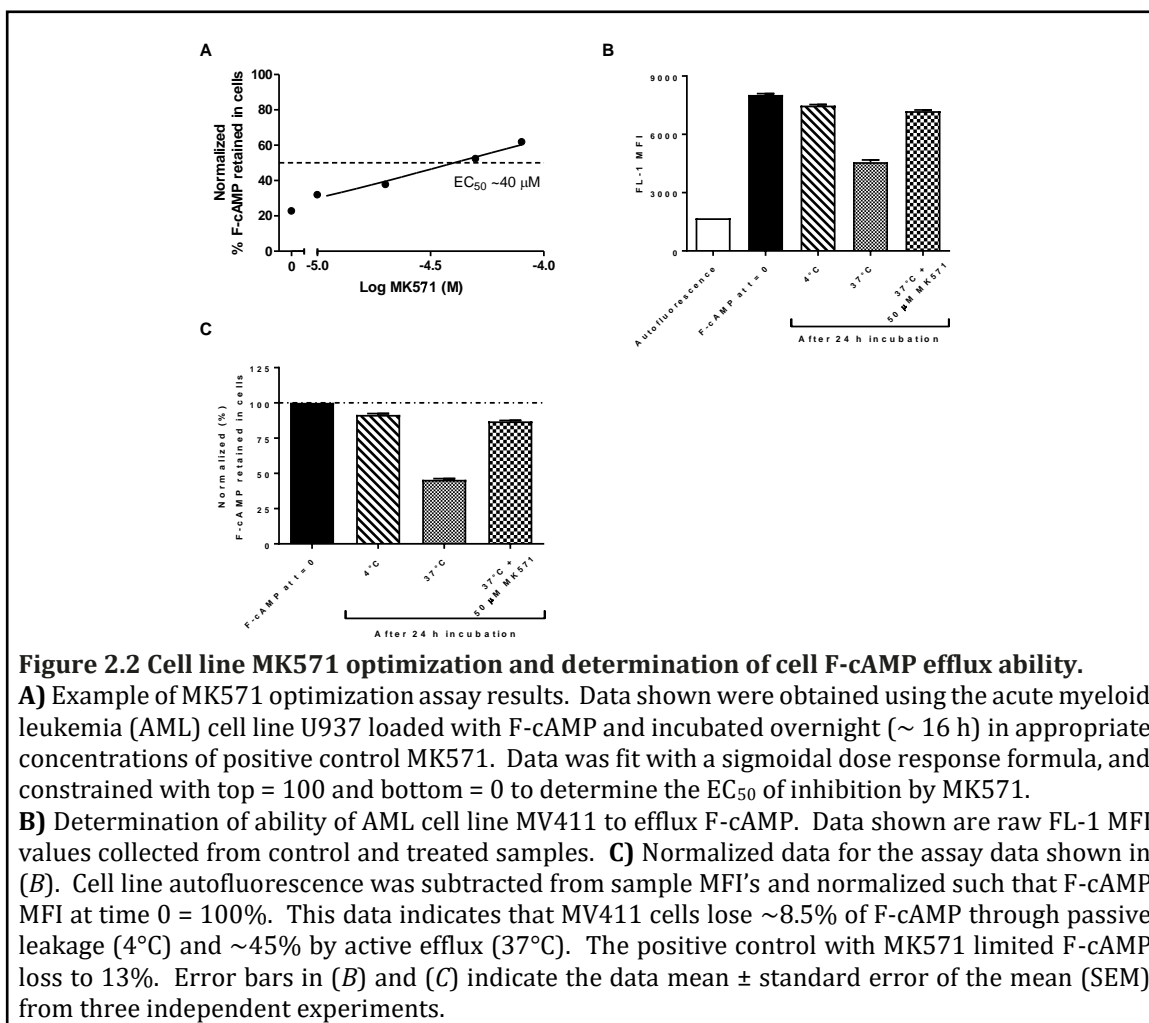
The cAMP signaling pathway has been a focus of cancer research due to its relationship to multiple intracellular signaling components and, specifically, programmed cell death, apoptosis. Existing evidence indicates aberrant cAMP regulation in malignant cells in comparison to normal, healthy cells [47]. It has long been known that the increased concentration of intracellular cAMP is capable of triggering cell death in certain cancer cells [73]. Typically, such research has relied

upon modulation of the major cAMP-synthesizing enzymes adenylate cyclases (AC) or phosphodiesterases (PDEs) that hydrolyze cAMP to increase cytosolic cAMP and reduce cancer cell survival [47, 114]. Until recently, one additional step of the cAMP signaling pathway that could be targeted for drug discovery has been overlooked: cAMP efflux by ABC transporters. The approach described here utilizes high throughput flow cytometry for measurement of the efflux of a fluorescent cAMP analog (F-cAMP, **Figure 2.1**) from leukemic cells. This assay assesses the intrinsic ability of cells to efflux cAMP through their endogenously expressed transporters rather than through analysis of the activity of specific protein targets. It thus allows the measurement of the inherent efflux potential of a cancer cell,



As a proof of this concept, we demonstrate the accumulation and release of F-cAMP with flow cytometry (**Figure 2.2**). We present here the results of a high throughput screen (HTS) for the identification of ICE from two libraries: the SPECTRUM Collection (2320 compounds – 60% drugs, 25% natural products, 15% bioactive components) and the Prestwick Chemical Library (~1200 previously FDA-approved drugs). The acute myelogenous leukemia (AML) cell line U937 was screened according to the methods described in this chapter, and the cells were incubated with compounds overnight (~18 h; **Figures 2.3 and 2.4**). From this screen, 51 hits were identified as having F-cAMP fluorescence ≥ 2 standard deviations above the plate mean negative control values. (**Figure 2.4**). These hits were validated by testing the compound F-cAMP efflux inhibition in 8-point dose responses ranging from 60 μM to 9 nM (**Figure 2.5A**). For this validation, the F-cAMP mean or median fluorescence intensity (MFI) values were normalized based on F-cAMP fluorescence at time = 0. The dose-response curves were fit with sigmoidal curves, and those compounds which exhibited EC_{50} values $< 30 \mu\text{M}$ and had well-behaved sigmoidal dose response curves were selected for further validation (**Figure 2.5B**). This yielded 8 compounds of interest (artemisinin, parthenolide, patulin, quinalizarin, harmalol, pyriithione zinc, clioquinol, and cryptotanshinone). Bioinformatics analysis of the compound structures allowed for the identification of 3 additional related small molecules: artesunate, artemether, and dihydroartemisinin. The 11 compounds of interest were tested in dose response in flow cytometric apoptosis and cell cycle secondary assays to measure the effects of ICE on U937 cell vitality after overnight incubation (**Figure**

2.6). Additional CellTiter-Glo® viability measurements found that 6 of the hit compounds (artesunate, dihydroartemisinin, clioquinol, cryptotanshinone, parthenolide, and patulin) were selectively inhibitory to leukemia cells at EC₅₀ concentrations much lower than those determined for healthy human primary blood mononuclear cells (PBMCs; data not shown). Subsequent testing of the hit compounds to determine mechanisms of action confirmed that the molecules work by modulation of the cAMP pathway and induce programmed cell death. Thus, the utility of the F-cAMP efflux assay approach to identify ICE for leukemia therapeutics has been validated.



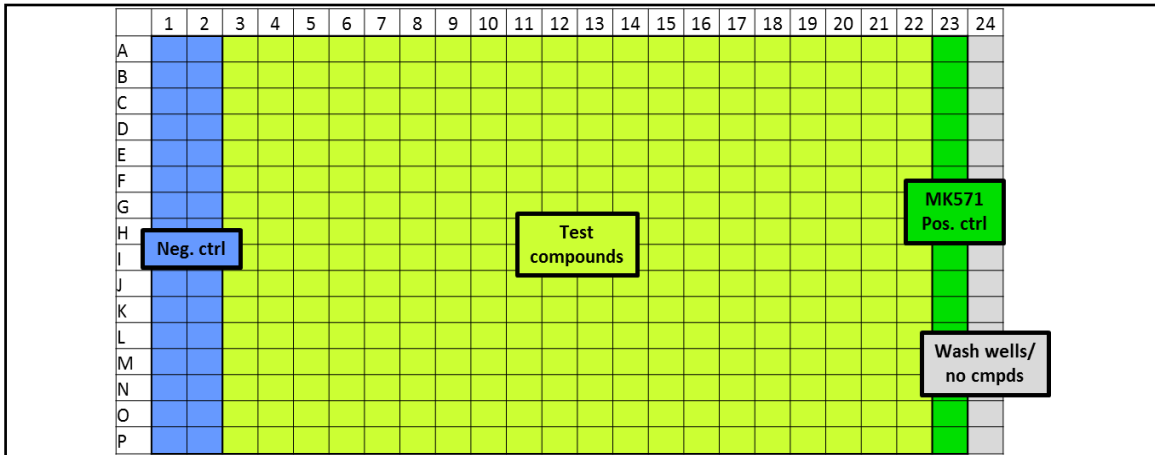


Figure 2.3 Sample configuration for a 384-well compound mother plate, as described in [Note 15](#).

Solubilized reagents are added to the plate at a minimum volume of 6 μ L. Test compounds may be used in a single-point or dose response manner. This plate incorporates both negative (compound solvent) and positive (MK-571) controls so that normalized ability to efflux F-cAMP and Z' values can be determined for each plate. If reagent availability is limited, fewer wells per plate may be used for positive controls.

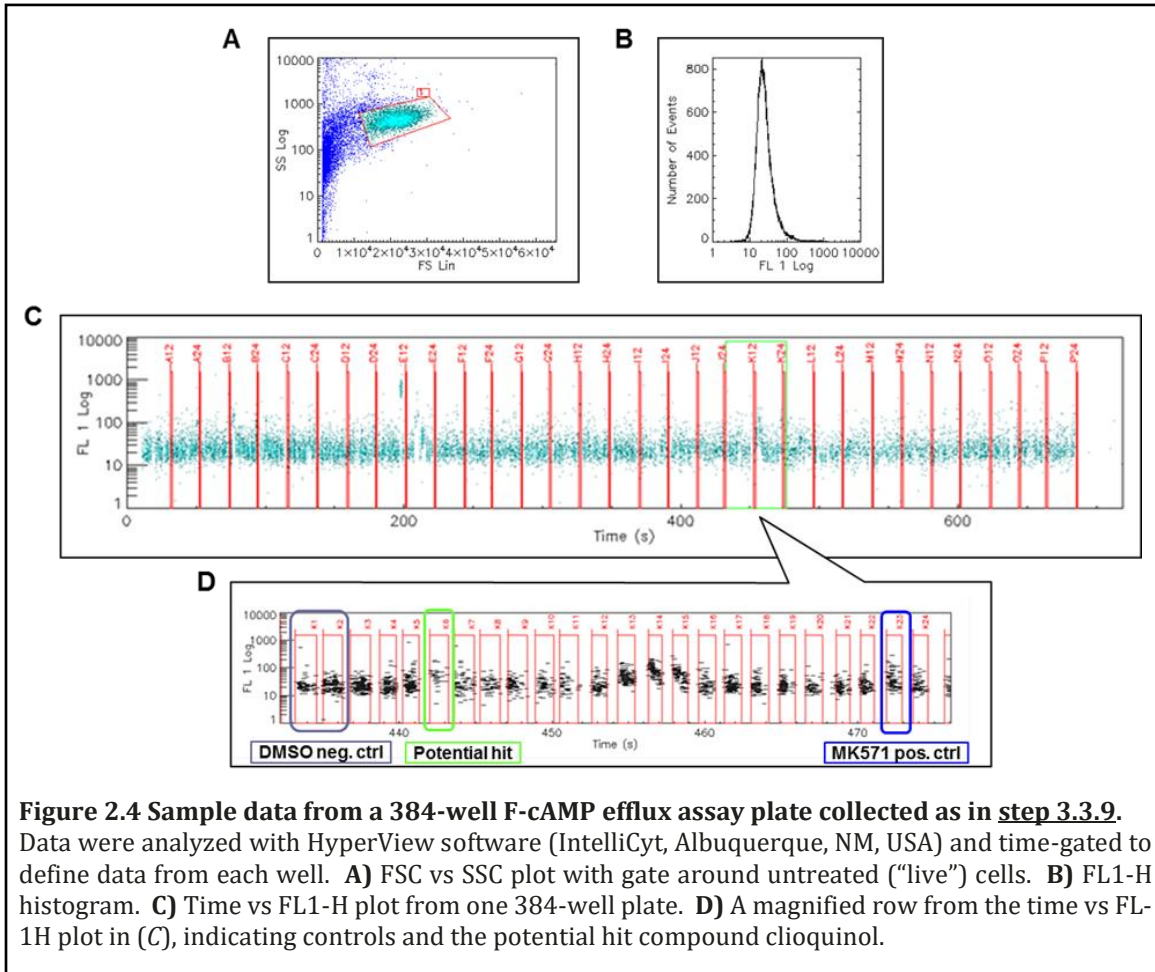
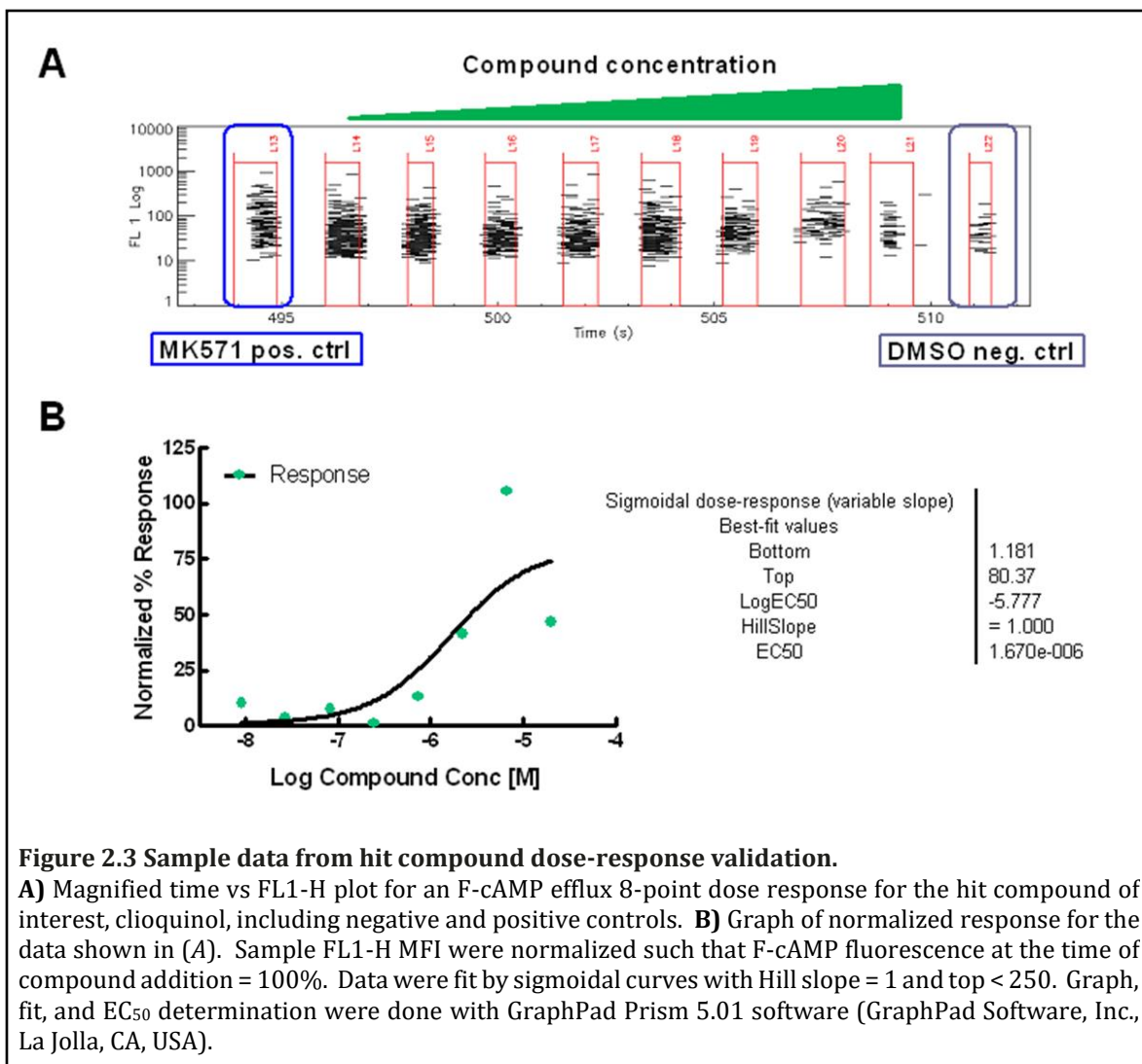
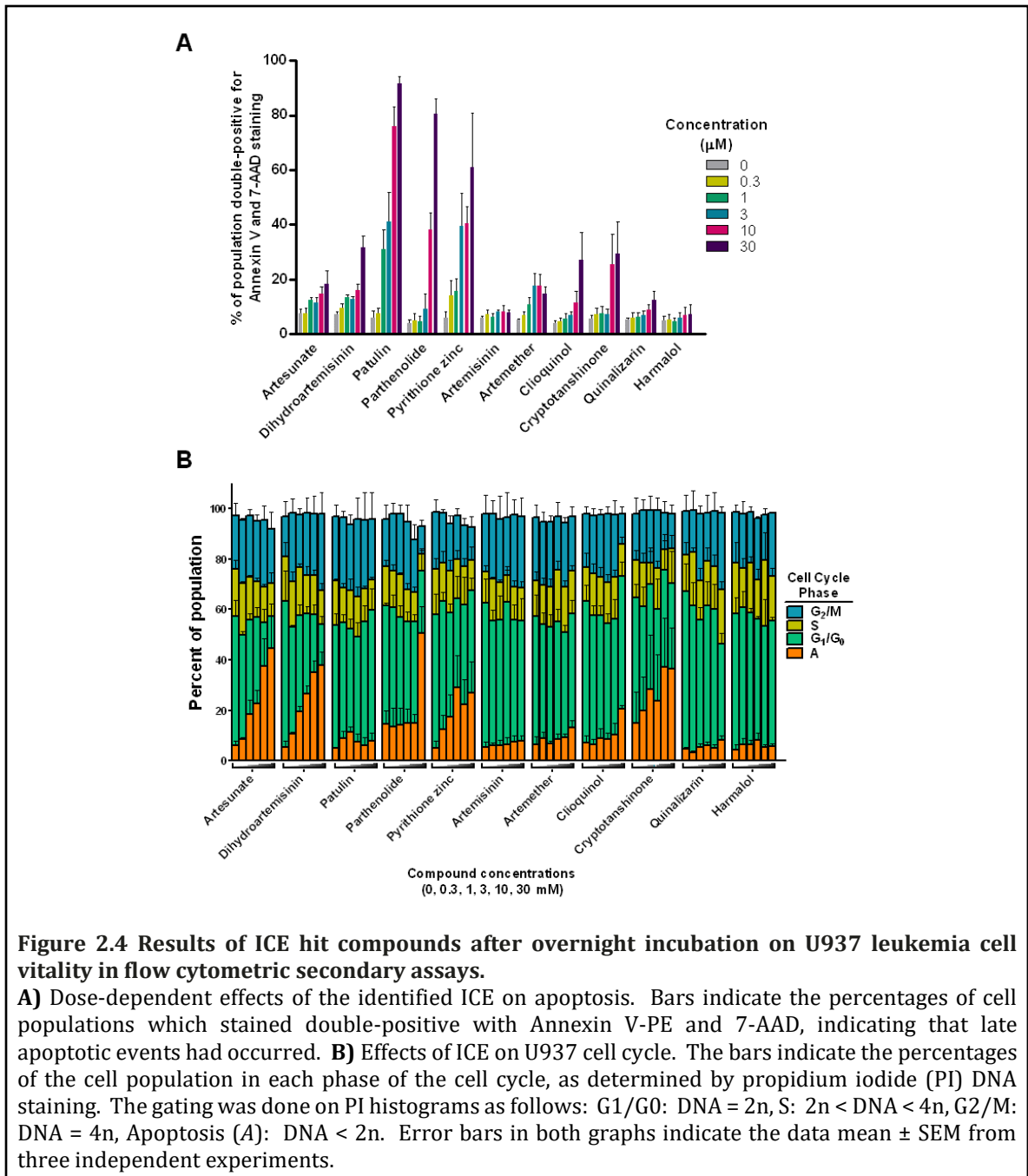


Figure 2.4 Sample data from a 384-well F-cAMP efflux assay plate collected as in [step 3.3.9](#).

Data were analyzed with HyperView software (IntelliCyt, Albuquerque, NM, USA) and time-gated to define data from each well. **A)** FSC vs SSC plot with gate around untreated ("live") cells. **B)** FL1-H histogram. **C)** Time vs FL1-H plot from one 384-well plate. **D)** A magnified row from the time vs FL1-H plot in (C), indicating controls and the potential hit compound clioquinol.





2.3 Materials

All solutions should be prepared following proper aseptic techniques. Dispose of waste materials according to appropriate regulations. All fluid component handling and storage is done in polypropylene tubes: 1.7 mL microcentrifuge, 15 mL conical, 50 mL conical. Cells are grown and incubated in a humidified 37°C, 5% CO₂ incubator unless otherwise specified.

2.3.1 Components for Fluorescent Cyclic AMP Loading

1. 50 mL NF-RPMI: RPMI-1640, 5 mg/L phenol red, 2 mM L-glutamine, 100 units/mL penicillin, 100 µg/mL streptomycin, 10 mM HEPES. No fetal bovine serum (FBS).
2. 50 mL cRPMI: RPMI-1640, phenol red, 2 mM L-glutamine, 100 units/mL penicillin, 100 µg/mL streptomycin, 10 mM HEPES, and 10% heat-inactivated fetal bovine serum (FBS; *see Note 1*).
3. Fluorescent cAMP analog (F-cAMP), Alexa Fluor®488 8-(6-aminohexyl) aminoadenosine 3',5'-cyclicmonophosphate, bis(triethylammonium) salt (*see Figure 2.1 and Note 2*).
4. Hypertonic solution: 10% w/v polyethylene glycol (PEG), 500 mM sucrose in NF-RPMI. 0.1 g poly(ethylene glycol) (PEG) 1,000, 0.17 g sucrose, 0.9 mL NF-RPMI. In a 15 mL conical tube, add 0.9 mL NF-RPMI, then weigh and add 0.1 g PEG and mix thoroughly by vortexing (*see Note 3*).

5. In a sterile tissue culture hood, push the solution through a 3-10 mL syringe fitted with a 0.2 μm nylon membrane filter (Pall Corporation) and transfer into a sterile 1.7 mL microcentrifuge tube.
6. Hypotonic solution: 40% purified, deionized water, 60% cRPMI. Add 1 mL sterile water to 1.5 mL cRPMI in microcentrifuge tube. Mix by light vortexing. Filter-sterilize as in **step 2.1.5**.
7. Cells known to efflux cAMP, $1-2 \times 10^7$ in a 50 mL conical polypropylene tube (*see Note 4*).
8. 1.7 mL microcentrifuge tube.
9. Centrifuge(s) with capacity for 50 mL conical and 1.7 mL microcentrifuge tubes.
10. T-75 tissue culture flask for F-cAMP loaded cell equilibration.

2.3.2 cAMP Efflux Assay Components

1. 1 mL untreated cells (no F-cAMP loaded) at $\geq 4 \times 10^5$ /mL for autofluorescence testing.
2. F-cAMP loaded cells from **step 2.1**.
3. Sterile 12-well cell culture plate with lid (or other means of covering for incubation).
4. 20 mL cRPMI.
5. $\geq 60 \mu\text{L}$ 30 mM MK571 positive control, solubilized in dimethyl sulfoxide (DMSO).
6. $\geq 80 \mu\text{L}$ DMSO

7. Flow cytometer with 488 nm laser, 530/30 bandpass optical filter, and multiwell plate auto-sampling capabilities.
8. 15 sample tubes for flow cytometer.

2.3.3 High Throughput Screening Components

1. 1 mL untreated cells (no F-cAMP loaded) at $\geq 4 \times 10^5$ /mL for autofluorescence testing.
2. F-cAMP loaded cells from **step 2.1**.
3. Multiwell plates, preferably 384-well, for compound mother plates and the high throughput F-cAMP efflux assay (*see Note 5*).
4. Compound mother plates: 384 well plates which contain positive and negative controls, as well as compounds of interest to be tested in the high throughput F-cAMP efflux assay.
5. ≥ 110 μ L 10 mM MK571 positive control per compound mother plate.
6. ≥ 225 μ L DMSO negative control per compound mother plate.
7. Proper seals (e.g., DMSO resistant adhesive foil microplate seals) and storage equipment, such as dessicators and/or -20°C freezer, for the compound mother plates (*see Note 6*).
8. Liquid dispensing equipment: this can either be an automated system or multichannel pipettors capable of delivering 5 μ L volumes to wells in 384-well plates (*see Note 7*).
9. 100 nL pintool or analogous compound transfer equipment (*see Note 8*).

10. 384-well plate lids or seals for the assay plates (*see Note 9*).
11. Multiwell plate vortexer.
12. Flow cytometer with 488 nm laser, 530/30 bandpass optical filter, and multiwell plate auto-sampling capabilities.
13. Software which can resolve data from individual wells after high throughput flow cytometry analysis.

2.4 Methods

2.4.1 Loading F-cAMP into cells

1. Centrifuge cells at $160 \times g_{\max}$ for 10 min and remove supernatant.
2. Wash/remove serum from cell medium: Resuspend cells in 1 mL NF-RPMI with slow pipetting, add an additional 19 mL NF-RPMI, gently mix, and centrifuge for 10 min. Discard supernatant.
3. While cells are centrifuging, prepare the F-cAMP loading solution. In a microcentrifuge tube, add 200 μ L hypertonic solution and 10 μ L of 5 mM F-cAMP (250 μ M final).
4. Again resuspend the cells in 1 mL NF-RPMI with slow pipetting and transfer to 1.7 mL microcentrifuge tube.
5. Centrifuge the cells at $\sim 120 \times g_{\max}$ for 2 min and remove the supernatant.
6. Gently resuspend the cells in the 210 μ L of F-cAMP loading solution (*see step 3.1.3 above*).

7. Incubate the cells with F-cAMP loading solution at room temperature for 10 min, with gentle mixing by hand or 1-2 sec at ~1,600 rpm every 3 min during this incubation (*see Note 10*).
8. Centrifuge the cells $\sim 120 \times g_{\max}$ for 2 min, remove the supernatant, and resuspend the cells in 1 mL of hypotonic solution.
9. Incubate the cells in hypotonic solution for 2 min at room temperature, with gentle mixing at 1 min.
10. Centrifuge the cells $\sim 120 \times g_{\max}$ for 2 min, remove the supernatant, and gently resuspend the cells in 1 mL of cRPMI.
11. Transfer the 1 mL of resuspended cells to a T-75 tissue culture flask containing 24 mL cRPMI and gently mix. If 10^7 cells were used for the F-cAMP loading, then this gives a final concentration of 4×10^5 cells/mL.
12. Place the T-75 flask in the incubator to allow the F-cAMP loaded cells to recover for 30-120 min (*see Note 11*).

2.4.2 Optimization of F-cAMP efflux positive control and determining cell F-cAMP efflux ability

This protocol will allow for optimization of the F-cAMP efflux assay and conditions. This step should be performed before the high throughput F-cAMP efflux assay is attempted. Once the positive control and incubation time(s) are determined for a particular cell line, this step may be skipped.

1. Add 500 μL cRPMI to each well of a 12-well tissue culture plate, then add 500 μL of F-cAMP loaded cells to all wells and mix by gentle pipetting (final concentration = 2×10^5 cells/mL. Save two 1 mL samples of F-cAMP loaded cells for control purposes, to be used in **steps 3.2.5** through **3.2.8**.
2. Add DMSO and 30 mM MK571 to the wells (**Table 1**) for $n = 2$ for each concentration tested and mix by gentle pipetting (*see Notes 12-13*). Do not exceed a final concentration of 1% DMSO per sample, as this can be toxic to cells.
3. Incubate the lidded tissue culture plate overnight (16-24 h) under normal cell culture conditions (*see Note 14*).
4. *Run control samples immediately after the plate is placed in the incubator, to collect fluorescence data to be used for normalization of the treated samples.*

Table 2.1 Volumes of MK571 and DMSO added to each well.

Each well contains 1 mL and F-cAMP loaded cells to give final DMSO concentration = 1%.

Final conc. MK571 (μM)	30 mM MK571 (μL)	DMSO added (μL)
0	--	10.0
10	1.0	9.0
25	2.5	7.5
50	5.0	5.0
75	7.5	2.5
100	10.0	--

5. Run untreated, non-F-cAMP loaded cells on the flow cytometer, using the 488 nm laser for excitation and collecting fluorescence data with a 530/30 bandpass optical filter. Collect $\geq 3,000$ events. Create an FSC vs SSC density plot and set a “live cell” gate on the major population of the cells. Then, create an FL-1 channel histogram based on the live cell gate. Data from this untreated sample will provide the baseline/ autofluorescence of the cell line.
6. Run a 1 mL sample of the F-cAMP loaded cells through the flow cytometer with the same settings and parameters detailed in **step 3.2.5** above. Ensure that the FL-1 channel histogram does not go off scale; adjust settings so that the entirety of the histogram is visible (*see Note 15*). This sample will serve as the “100% F-cAMP fluorescence” control for time = 0 of the assay.
7. Place the remaining 1 mL sample of F-cAMP loaded cells at 4°C for the duration of the MK571 optimization plate incubation time.
8. After incubation, run the 4°C-incubated F-cAMP loaded cell sample in the flow cytometer under the same settings used in **step 3.2.5**. This will provide a measurement for the F-cAMP “passive efflux” ability of the cell line (*see Note 16*).
9. Gently mix the contents of each well in the MK571 optimization plate by pipetting, collect individual samples, and interrogate with the flow cytometer (*see Note 17*). Set a gated event count limit for each sample of $\geq 1,000$ events.
10. To process the F-cAMP efflux data, use MFI values from data collected in **steps 3.2.5 through 3.2.8**.

11. Subtract the autofluorescence MFI value (**step 3.2.5**) from the MFIs of all of the F-cAMP loaded samples, including the F-cAMP fluorescence control collected at time = 0 (**step 3.2.6**).
12. Divide the MFIs from each sample by the MFI collected from the 100% F-cAMP fluorescence/ time = 0 control (**step 3.2.6**). This will indicate the percentage of F-cAMP remaining within the cells under each condition.
13. Fit the MK571 dose response data with a variable slope sigmoidal dose response equation constrained with “bottom” equal to 0 and “top” equal to 100 (fluorescence at initial staining). This will determine the EC₅₀ of MK571 for cAMP efflux inhibition. Example data from an overnight MK571 optimization assay with U937 cells is shown in **Figure 2.2A**.
14. Once an optimal MK571 concentration is determined for a particular cell type, the assay described here may be used to determine the efflux ability of F-cAMP loaded samples at other iterations or incubation times. Example data from an assay to determine the MV411 leukemia cell line cAMP efflux ability is shown in **Figure 2.2B**. The MV411 F-cAMP efflux assay data normalized according to **steps 3.2.11** and **3.2.12** is shown in **Figure 2.2C**.

2.4.3 High throughput F-cAMP efflux assay

The following protocol is designed for a 384-well high throughput assay (*see Note 18*). For information on modifications which may be done to conduct the assay in 96-well plates, *see Note 19*. If no adjustments were made to the protocol

completed in **Method 3.1** (25 mL F-cAMP loaded cells at 4×10^5 cells/mL), then this protocol will allow for the creation of 10, 384-well assay plates.

1. Create a compound mother plate with solubilized compounds at 100x final assay concentration. Dedicate wells for negative control (compound solvent) and positive control (MK571; see **Notes 20-21** and **Fig. 3** for example plate map). Alternatively, an acoustic dispenser may be used to deliver compounds directly to assay plates in **step 3.3.3**, and if so, the creation of separate compound mother plates is not necessary.
2. Dispense 5 μ L cRPMI to all wells of the 384-well assay plates with a liquid handler or multichannel pipettor.
3. With a 384-well pintool (or other similar liquid transfer equipment), transfer 100 nL from the compound mother plates to the assay plates (see **Note 8**).
4. Dispense 5 μ L F-cAMP loaded cells to the negative and positive control, and compound-treated wells in the assay plates (see **Note 21**). If the added cells were originally at a density of 4×10^5 /mL, then this provides a final cell density of 2×10^5 /mL, or 2000 cells/ 10 μ L final volume well. Save two, 1 mL aliquots of excess F-cAMP loaded cells for flow cytometer optimization and fluorescence testing.
5. Seal the assay plates and store upside down in the incubator for desired incubation time (see **Note 9**).
6. Conduct cytometer optimization and fluorescence testing according to **steps 3.2.5 through 3.2.7**.

7. After assay plate incubation, run the 4°C-incubated F-cAMP loaded cell “passive efflux” sample as in **step 3.2.8**.
8. Vortex (2000 rpm) each F-cAMP efflux assay plate 15s before running samples through the high throughput flow cytometer (*see Note 22*). Add an FL-1 vs time density plot to the cytometer collection parameters to allow for well data separation during analysis.
9. Use high throughput flow cytometry analysis software to identify cells and FL-1 MFI from individual wells (*see Fig. 4* for example data).
10. To analyze well/compound data, exclude samples with < 50 events. Normalize data according to **steps 3.2.11** and **3.2.12** (*see Note 23*). Calculate the Z' values for each plate for quality control purposes. Assay plates which indicate a Z' factor of ≥ 0.3 should be considered acceptable [115]. Hit compounds may be determined per the user’s preference. We identified hits as samples with MFI values ≥ 2 standard deviations above the plate mean negative control values.
11. To further validate sample data and decrease the number of false-positive hits, compounds were assayed in a high-throughput dose response assay. Plates were set up as in the HTS, with the exception that the plate formats contained 10-well dose responses for each hit compound, at final concentrations ranging from 30 μM to 4 nM.

2.5 Notes

1. If the cells used in this assay are typically cultured in another medium, please substitute that medium for all instances of cRPMI in this protocol.
2. Other fluorescently-conjugated cAMP may be utilized, but fluorophores conjugated to cAMP at sites which do not mimic the molecule shown in **Figure 2.1** have not been tested nor validated for this assay.
3. Dissolving PEG 1000 in NF-RPMI may be somewhat difficult. Continue vortexing and tilting tube back and forth. If the PEG still does not readily enter solution, wait a few hours or overnight for the flakes to dissolve. Otherwise, placing the tube in a 37°C water bath for 5-15 min may help.
4. We have tested F-cAMP loading in leukemia cell lines, at numbers up to 18×10^6 under the conditions described in this method. For adherent or other cell types, it would be best to optimize the assay starting at cells and gradually testing other cell counts and F-cAMP concentrations to suit your needs. If the assay volumes and/or cell densities that you require are higher than those described in this protocol, adjust the component volumes and cell numbers loaded with F-cAMP accordingly (*see Note 19*).
5. You will need at least 10, 384-well plates for the cAMP assay, and a number of plates to create compound mother plates. The high-throughput F-cAMP efflux assay protocol described here is for a small assay volume (10 μ L). It would be best to have small volume flat-welled plates or conical wells for these assay

plates. In our experience, this assay has worked with both polystyrene and polypropylene multiwell plates.

The compound mother plates need to have the same well format as the assay plates (e.g., 384 wells). The compound mother plates should have well structures optimized for the transfer of small volumes of reagents. We found that wells with conical bottoms were optimal for our 100 nL compound transfers by pintoole.

6. The compound mother plates may be saved and reused if stored properly. The plates should be foil-sealed, preferably after being flushed with nitrogen gas to remove excess oxygen and moisture from the wells. The plates can be stored at -20°C (typically best for long-term compound storage, avoiding several freeze-thaws) or in a climate-controlled, low humidity, high nitrogen desiccator. Plates stored in a desiccator may be stable for up to 3 months, depending on the properties of individual compounds.
7. Take note of the “dead volume” specifications of your liquid dispensing equipment. When following the described protocol, ensure that the volumes of the reagents used are adjusted to meet these minimum requirements before beginning the high throughput F-cAMP efflux assay.
8. The wells in this assay will have a final volume of 10 μ L F-cAMP loaded cells in culture medium. A compound delivery of 100 nL will ensure that the DMSO concentration remain below 1%. If a 100 nL pintoole or equivalent is unavailable, then intermediate compound dilution plates will need to be

prepared to allow for 1 μL volumes to be transferred to assay wells while maintaining DMSO at $\leq 1\%$.

To prepare intermediate compound dilution plates, stock from the compound mother plates is diluted 1:10 in culture medium. This is accomplished in additional 384-well plates, by combining 9 μL of culture medium with 1 μL of the well contents from the compound mother plates. Mix well contents thoroughly by pipetting or plate vortexer before making 1 μL transfers from the intermediate compound dilution plates into the assay plates **(step 3.3.3)**.

9. Depending on the optimal culturing conditions for the cell line tested, the assay plates may be incubated with fitted lids or sealed with gas-permeable, solid polymer, or foil seals. Take into consideration that the assay plates will contain small volumes (10.1 μL final), and incubation with lids or gas-permeable seals may result in some evaporation of well volumes, especially on the edges of the assay plates. We found that leukemia cell line responses to the F-cAMP efflux assay were best when non-permeable seals were used on the assay plates. Gas permeable plate covers seemed to decrease cell viability, as evidenced in population shifts on flow cytometer FSC vs SSC density plots when plates were analyzed after incubation.
10. We have not tested the sensitivity of F-cAMP loaded cells incubated and equilibrated in full-light conditions. It is best to incubate the cells in the dark to minimize the potential for ambient light to reduce treated cell MFI's.

11. It is possible for the cells to be used in the efflux assay immediately, but because the plasma membranes have been subjected to stress from the osmotic lysis of pinocytic vesicles in the F-cAMP loading procedure, it would be beneficial to allow the membrane integrity to be regained before proceeding. This step allows the cells to recuperate before testing with compounds. Different cell lines will recover at different rates. Check the cells with a light microscope to determine whether the cells appear healthy and rounded before advancing to the efflux assay.
12. MK571 is a known inhibitor of ABC C-family transporters (also known as multidrug resistance proteins), and it is often used as a positive control for cAMP efflux. The concentrations tested here are used to generate a dose response curve to determine the EC₅₀ of MK571 cAMP efflux inhibition. Alternative concentrations may also be tested. With U937 cells, we determined an MK571 EC₅₀ of ~40 μM, and used a final concentration of 100 μM in our HTS assays to ensure effective cAMP efflux inhibition (**Fig. 2A**).
13. Because this optimization step does not require many F-cAMP loaded cells, multiple plates, MK571 concentrations, and incubation times may be tested as well.
14. The MK571 optimization incubation should be for the anticipated amount of time in which the HTS assay will be completed. We have conducted this assay at varying times from 16-48 h. Please note, however, that cells which do not actively efflux cAMP well, or too short an incubation time may not produce

data with any significant effects or dose-dependent efflux inhibition by MK571. Incubation times which are too long (~48 h) could lead to increased levels of apoptosis, depending on the sensitivity to the cells to high concentrations of MK571.

15. If the FL-1 channel cytometer settings had to be adjusted in this step, run the untreated, non-loaded cells (**step 3.2.5**) again to ensure proper assessment of the cell line autofluorescence for the assay readings.
16. For some cell lines, incubation at 4°C can cause apoptosis, and this is evident in shifting of the population on the FSC vs SSC plot. Only use data from events which fall within the “live cell” gate created with the untreated/ autofluorescence cells.
17. All or partial aliquots of the wells may be collected during this step. If only a few hundred microliters of each well are sampled, this allows for the remainder of the plate to continue to be incubated, allowing for aliquots to be collected at multiple time points.
18. All plate setup and compound handling for HTS can be done in ambient conditions outside of a tissue culture hood.
19. Considerations for completing the high throughput F-cAMP efflux assay in 96-well plates: a) The compound mother plates and assay plates should have the same well configurations, to ease compound transfer. b) Assays conducted in 96-well plates typically require higher minimum volumes per well for samples to be collected by high throughput flow cytometry. These minimum volumes

are contingent on the geometry of the plate wells, of course, but it can be expected that the wells would require $\geq 50 \mu\text{L}$ final volumes. c) While the volume per well can vary from the $10 \mu\text{L}$ final volume described in this protocol, it is ideal to maintain final well concentrations of $\leq 1\%$ DMSO and 2×10^5 cells/mL.

20. In this step, any number of compound mother plates may be created for use with the 10 assay plates. Therefore, individual compound mother plates may be used multiple times to increase the sample size tested per compound, or each assay plate may be tested with different compound mother plates. For our tests to identify “inhibitors of cAMP efflux”, our compound mother plates consisted of $6 \mu\text{L}$ final volume per well. There were 10 mM DMSO-solubilized compounds in all wells in columns 3-22, the negative control was in columns 1-2, and the positive control was in column 23 of the 384-well plate (**Fig. 3**). Alternatively, if compounds of interest are already known, the compound mother plate can be made to test the compounds in dose response, with negative controls in columns 1 and 13, and dose series in columns 2-10 and 12-22. The MK571 positive control can be incorporated into the plate as a dose response series, or as few wells in column 23 at a static concentration.
21. For example, if the compound mother plates were set up as shown in **Fig. 3**, F-cAMP loaded cells would be added to all wells in columns 1-23 of the assay plates. Because column 24 would not have any compound or cells added, these wells would serve as “wash” wells.

22. In our assay, we used flow cytometers configured with HyperCyt® autosampling systems (IntelliCyt), with peristaltic pump speeds at 15 rpm, and aspiration for 1 sec/well (up times between wells could be set from 300-500 ms). This allowed for approximately 2 μ L (~400 cells) to be sampled from each well.
23. In some instances, the positive and negative controls data may indicate a gradient of MFI values dependent on well position on the plate. In such cases, it would help to normalize F-cAMP efflux for the samples on a per-row basis (e.g., using only the positive and negative control MFI values from Row H to normalize the Row H sample MFIs).

2.6 Acknowledgements

This work was supported by The Oxnard Foundation, University of New Mexico Clinical & Translational Science Center Pilot Award 1UL1RR031977, and New Mexico Cancer Nanotechnology Training Center grant R25CA153825.

CHAPTER 3: Cyclic AMP efflux inhibitors as potential therapeutic agents for leukemia

Dominique R. Perez¹⁻³, Yelena Smagley^{1,2}, Matthew Garcia^{1,2}, Mark B. Carter^{1,2}, Annette Evangelisti¹⁻³, Ksenia Matlawska-Wasowska^{1,4}, Stuart S. Winter^{1,4}, Larry A. Sklar¹⁻³, and Alexandre Chigaev¹⁻³

¹ Comprehensive Cancer Center, ² Center for Molecular Discovery, ³ Department of Pathology, ⁴ Department of Pediatrics, University of New Mexico Health Sciences Center, Albuquerque, NM, USA

Oncotarget. 2016 Jun 7 (23) 33960-82

doi: 10.18632/oncotarget.8986 PMID: 27129155

3.1 Abstract

Apoptotic evasion is a hallmark of cancer. We propose that some cancers may evade cell death by regulating 3'-5'-cyclic adenosine monophosphate (cAMP), which is associated with pro-apoptotic signaling. We hypothesize that leukemic cells possess mechanisms that efflux cAMP from the cytoplasm, thus protecting them from apoptosis. Accordingly, cAMP efflux inhibition should result in: cAMP accumulation, activation of cAMP-dependent downstream signaling, viability loss, and apoptosis. We developed a novel assay to assess cAMP efflux and performed screens to identify inhibitors. In an acute myeloid leukemia (AML) model, several identified compounds

reduced cAMP efflux, appropriately modulated pathways that are responsive to cAMP elevation (cAMP-responsive element-binding protein phosphorylation, and deactivation of Very Late Antigen-4 integrin), and induced mitochondrial depolarization and caspase activation. Blocking adenylyl cyclase activity was sufficient to reduce effects of the most potent compounds. These compounds also decreased cAMP efflux and viability of B-lineage acute lymphoblastic leukemia (B-ALL) cell lines and primary patient samples, but not of normal primary peripheral blood mononuclear cells. Our data suggest that cAMP efflux is a functional feature that could be therapeutically targeted in leukemia. Furthermore, because some of the identified drugs are currently used for treating other illnesses, this work creates an opportunity for repurposing.

3.2 Introduction

Apoptosis serves as a natural barrier to cancer development, and targeting this cancer hallmark represents an indispensable therapeutic strategy [116]. Apoptosis can be induced via two major pathways, extrinsic and intrinsic, and in acute myelogenous leukemia (AML) the latter can be directly triggered by elevation of cAMP, which acts synergistically with first-line antileukemic agents [2]. This creates a unique situation, where an additional targetable pathway, previously unexploited by traditional chemotherapeutics, may exist in AML cells [2].

The effect of intracellular cAMP (icAMP) elevation is tissue/cell specific. In certain tumors, including pituitary, adrenocortical and thyroid adenomas and carcinomas, the cAMP/ protein kinase A (PKA) pathway provides signals required for tumor development and/or cell survival. In leukemias/lymphomas, cAMP elevation can be pro-apoptotic, whereas in leukocytes/macrophages it is reported to be anti-apoptotic (see Tables 1 and 2 in ref. [39] and [83]). Additionally, cAMP can have both pro- and anti-apoptotic activity within the same cell depending upon experimental conditions. icAMP compartmentalization may also contribute to the complexity of signaling [117]. Nonetheless, a significant body of literature suggests that modulating the cAMP pathway provides a number of promising targets for treating leukemia [53].

AML (IPC-81) and multiple myeloma cells undergo rapid apoptosis after cAMP elevation [4, 118]. In S49 T-cell lymphoma cells, apoptosis can be induced through a cAMP/PKA-dependent pathway [3]. Increasing icAMP by using cAMP analogues [73], adenylyl cyclase (AC) stimulators [119], or phosphodiesterase (PDE) inhibitors [56, 120] has been a focus of cancer therapeutics research [39, 114]. This approach has been supported by the fact that the concentration of cyclic nucleotides is elevated in the plasma and urine of individuals with certain leukemias [121, 122], and in some cases these levels correlate with disease progression [122]. In this report, we hypothesize that one mechanism for malignant cell apoptotic evasion could be active efflux of cAMP [114]. Rather than relying on PDEs to degrade icAMP, active cAMP removal from the cytoplasm can provide a survival advantage. We envision that cAMP efflux prevents an elevation of icAMP that could trigger up-regulation of the Bcl-2

interacting mediator of cell death (Bim/BCL2L1) protein [2, 77], or down-regulation of the myeloid cell leukemia 1 (Mcl-1) protein [4, 10]. Inhibition of cAMP efflux alone should be sufficient to selectively trigger death in cells that rely on this anti-apoptotic mechanism for survival. To test this idea, we decided to identify drug-like compounds that are capable of blocking cAMP efflux.

To identify “inhibitors of cAMP efflux” (ICE), we developed and validated a novel assay for the detection of cAMP efflux (in press), using a well characterized model for AML known to efflux cAMP through ABCC4, the multidrug resistance-associated protein-4 (MRP4) transporter [97]. Next, we screened libraries composed of biologically active substances and off-patent drugs. We validated the “hits” in secondary assays that assessed the compound effects on cell signaling, viability and apoptosis. The ICE were also tested for their effects on cAMP efflux inhibition and viability in B-lineage acute lymphoblastic leukemia (B-ALL) cells, primary B-ALL bone marrow patient samples, and healthy human primary blood mononuclear cells (PBMCs). The most promising compounds showed dose-dependent, selective inhibition of leukemic cells vs. PBMCs. Our hypothesis was further supported by measurements of cAMP-dependent activation of downstream effectors after exposure to ICE compounds. Because several identified ICE are FDA-approved drugs, our studies provide a potential path for drug repurposing against leukemias.

3.3 Results

3.3.1 A screen for ICE identifies six potentially active compounds

To identify ICE, we took advantage of a model system where cAMP efflux is well studied: U937 cells, which can actively extrude cAMP into extracellular media [97]. In these cells, a rapid increase of cAMP efflux can be triggered through the elevation of the icAMP concentration using G-alphaS GPCR-specific ligands, blocking PDE-dependent cAMP hydrolysis, and by other pharmacological manipulations. The cAMP efflux is ATP- and MRP inhibitor-dependent, and shRNA knockdown has shown that the cAMP efflux is mediated by MRP4/ABCC4. Moreover, an increase of icAMP was sufficient to induce differentiation of U937 and other AML cell lines [97].

To study cAMP efflux, we loaded U937 cells with fluorescently tagged cAMP (F-cAMP). MK-571, (MRPs selective inhibitor) [97], was used as a positive control. **Figure 3.1** shows that MK-571 down-modulated cAMP efflux in a dose-dependent manner, with $EC_{50} \sim 30 \mu\text{M}$. This value was very close to the IC_{50} previously reported for MRP4/ABCC4 [123]. Thus, the fluorescent tag (Alexa Fluor®488) did not significantly affect the ability of cells to efflux cAMP nor of MK-571 to block this process.

These experiments served as the basis for a screen to identify compounds that could block cAMP efflux. F-cAMP-loaded U937 cells were screened against compounds from the Prestwick Chemical Library (~1200 previously FDA-approved drugs) and the SPECTRUM Collection (2320 compounds – 60% drugs, 25% natural products, 15% bioactive components). The screen identified 51 hits, which were

tested in dose-response to validate their activities (data not shown), yielding seven potentially active ICE compounds: artemisinin, clioquinol, quinalizarin, harmalol, cryptotanshinone, parthenolide, and patulin. Three additional structurally-related compounds (dihydroartemisinin, artemether, artesunate) were also included for evaluation in secondary assays. Based on further validation, only artesunate, clioquinol, cryptotanshinone, dihydroartemisinin, patulin, and parthenolide were chosen for extended studies (**Table 3.1**). The detailed screening data will be published elsewhere [124].

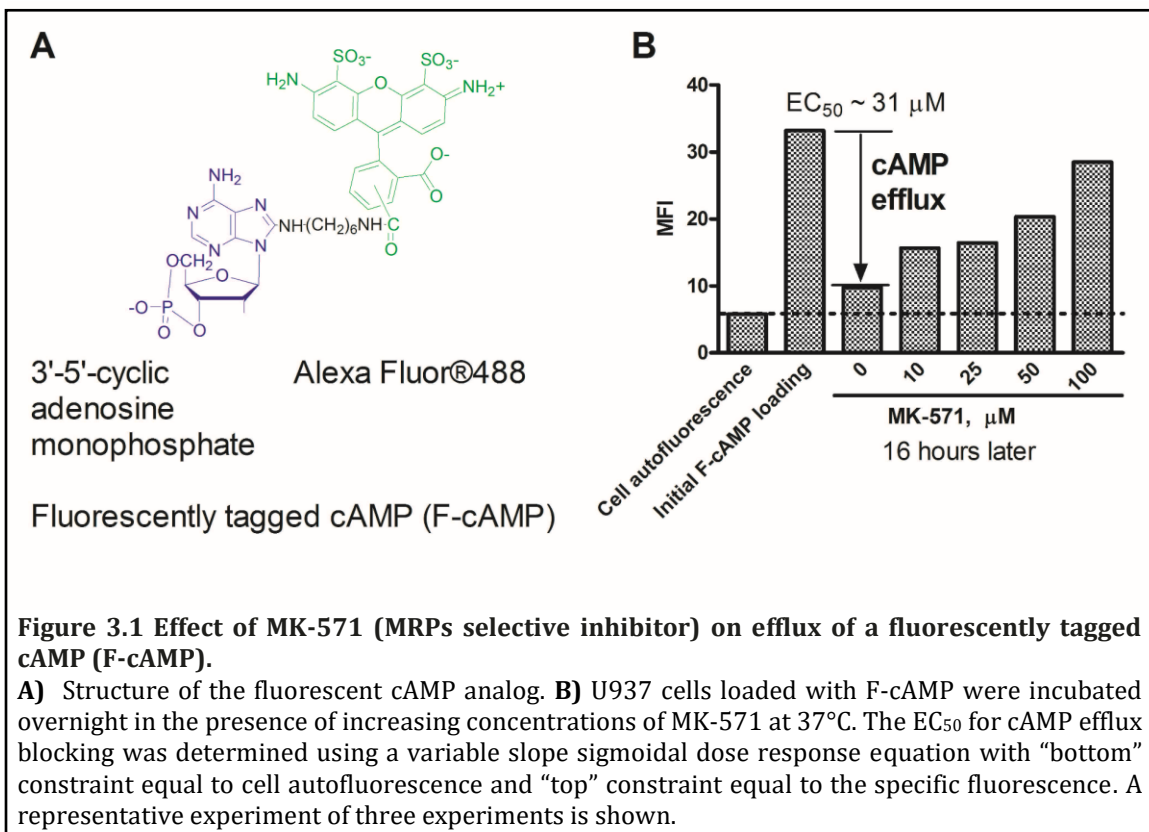
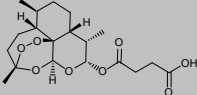
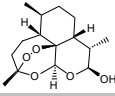
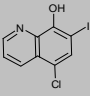
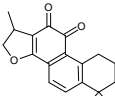
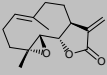
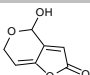
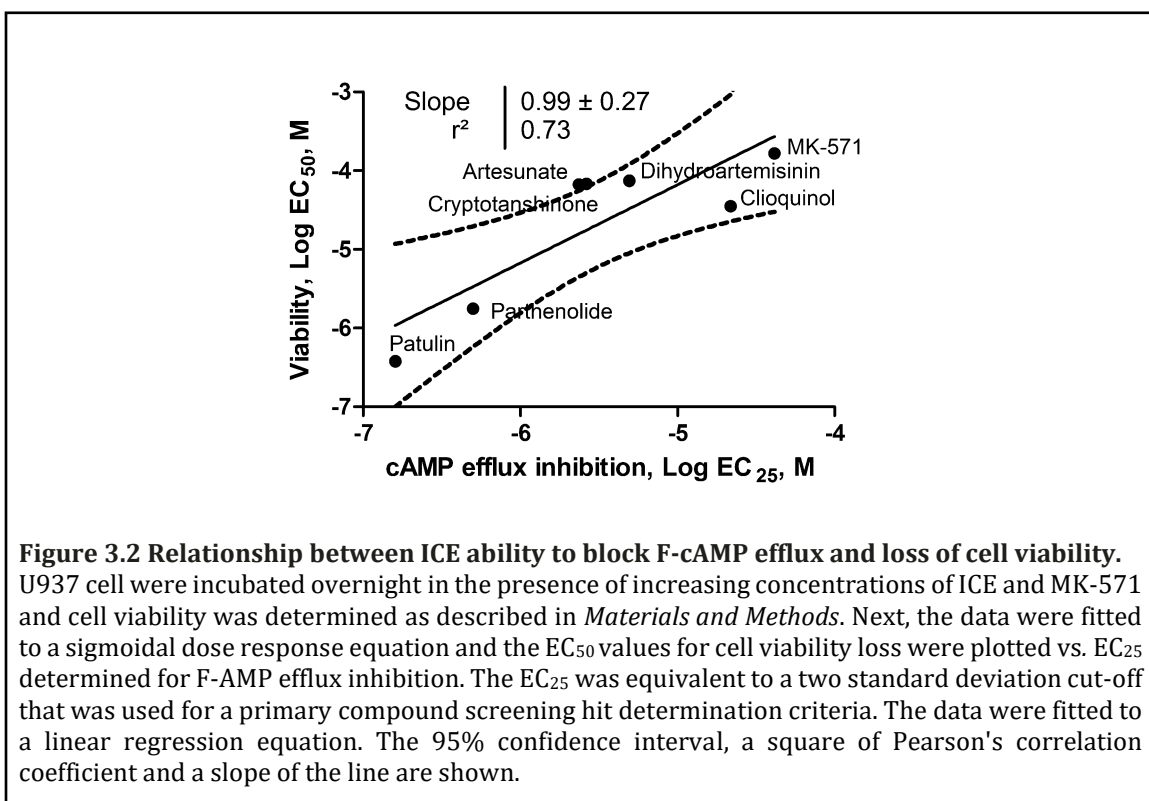


Table 3.1 Hit compounds identified in the screen for inhibition of cAMP efflux.

Hit compound	Structure	Notes
Artesunate		In 2007, FDA approved investigational new drug protocol #76,725 entitled "Intravenous Artesunate for Treatment of Severe Malaria in the United States".
Dihydroartemisinin		Artesunate is hydrolysed to its active metabolite dihydroartemisinin. Along with artemisinin currently used as antimalarial drugs in Asia.
Clioquinol		Clioquinol (Iodochlorhydroxyquin) is the FDA approved antifungal and antiprotozoal drug. A phase I trial for clioquinol in patients with hematologic malignancies has been reported [125].
Cryptotanshinone		A major tanshinone isolated from <i>Salvia miltiorrhiza</i> . It was shown to inhibit cancer cell proliferation [126].
Parthenolide		A sesquiterpene lactone from <i>Tanacetum parthenium</i> . An orally bioavailable parthenolide analog selectively eradicates acute myelogenous leukemia stem and progenitor cells [127].
Patulin		A mycotoxin produced from <i>Penicillium</i> and <i>Aspergillus</i> . Patulin-induced apoptosis in human leukemia cells is mediated through the mitochondrial pathway [128].

3.3.2 Correlation between ICE ability to block F-cAMP efflux and viability loss

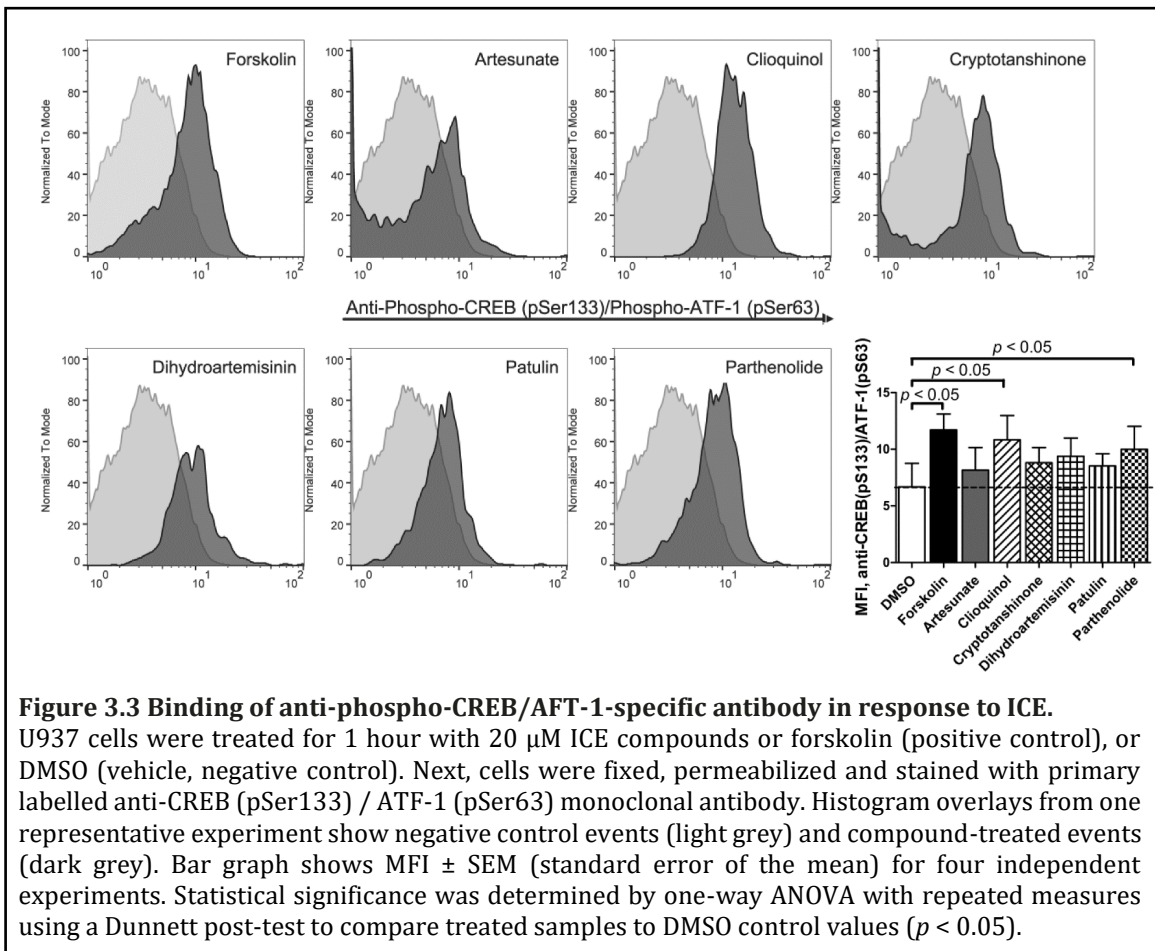
Next, we compared ICE efficacy for blocking F-cAMP efflux with their ability to trigger loss of cell viability (**Figure 3.2**). A strong positive correlation ($r^2=0.73$) has been observed. The values for all six ICE compounds and MK-571 control ranked in the same order and were located within 95% confidence interval. Moreover, the slope of the regression line was equal to 1. This suggests that the relative potency of ICE in affecting cell viability varies in parallel with the ability to block F-cAMP efflux.



3.3.3 CREB/AFT-1 phosphorylation in response to ICE

Next, to evaluate whether reducing cAMP efflux would result in an elevation of cytoplasmic cAMP-dependent cell signaling, we studied the effects of ICE on phosphorylation of cAMP-responsive element-binding protein (CREB; Ser133) and

activating transcription factor-1 (ATF-1; Ser63), classical cAMP effectors that activate target genes through cAMP response elements (CRE). This pathway is also directly implicated in cAMP-induced apoptosis in leukemia [2]. All studied compounds showed increased binding of anti-CREB (pS133) / ATF-1 (pS63) specific antibodies as compared to vehicle control (**Figure 3.3**). For two compounds (clioquinol and parthenolide), the binding of antibodies was comparable to the adenylate cyclase stimulator forskolin positive control. Thus, ICE compounds can stimulate CREB/ATF-1 phosphorylation.



3.3.4 VLA-4 deactivation in response to ICE

Another signaling pathway that in leukocytes can be triggered by the elevation of cytoplasmic cyclic nucleotides is the conformational deactivation of the Very Late Antigen-4 (VLA-4, alpha4 beta1 integrin), an adhesion molecule implicated in homing and retention of early hematopoietic progenitors in the bone marrow. The elevation of icAMP using G-alphaS GPCR-specific ligands, forskolin and by other pharmacological manipulations results in rapid dissociation of the VLA-4-specific ligand-mimicking probe, LDV-FITC [129]. We studied the effect of ICE on VLA-4 deactivation using the same previously characterized model system (**Figure 3.4**). Studied compounds triggered rapid dissociation of LDV-FITC in U937 cells pre-activated through a non-desensitizing mutant of the FPR1. In several experiments, the effects of parthenolide and patulin exceeded the effects of the positive control, forskolin (**Figure 3.4**). Cryptotanshinone induced rapid and reversible VLA-4 deactivation that looked similar to the effect of a cell-permeable cyclic nucleotide analog [130]. Thus, ICE compounds were also capable of triggering an integrin deactivation pathway, where the role of elevated cyclic nucleotide concentration is critical [129, 130].

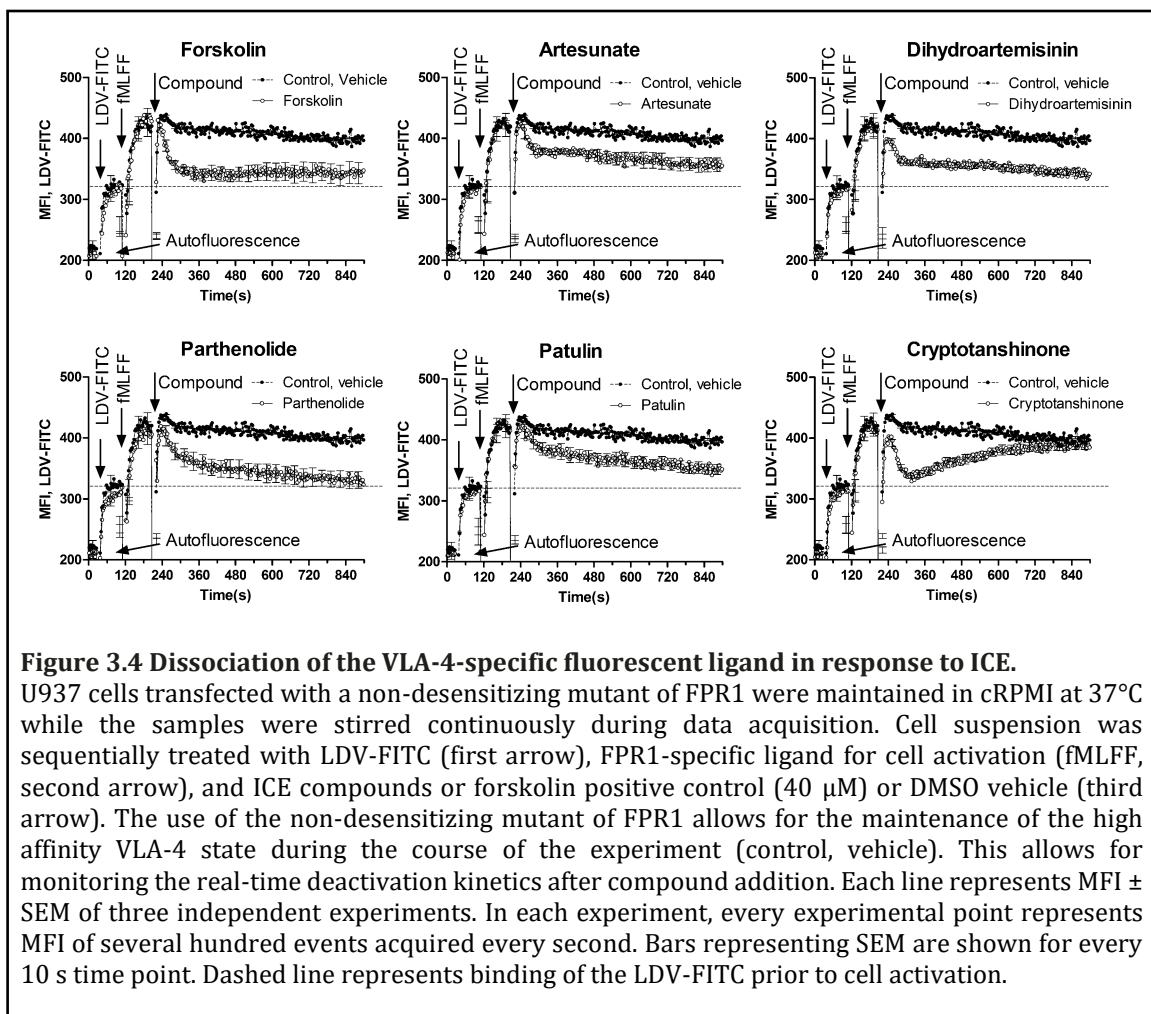


Figure 3.4 Dissociation of the VLA-4-specific fluorescent ligand in response to ICE.

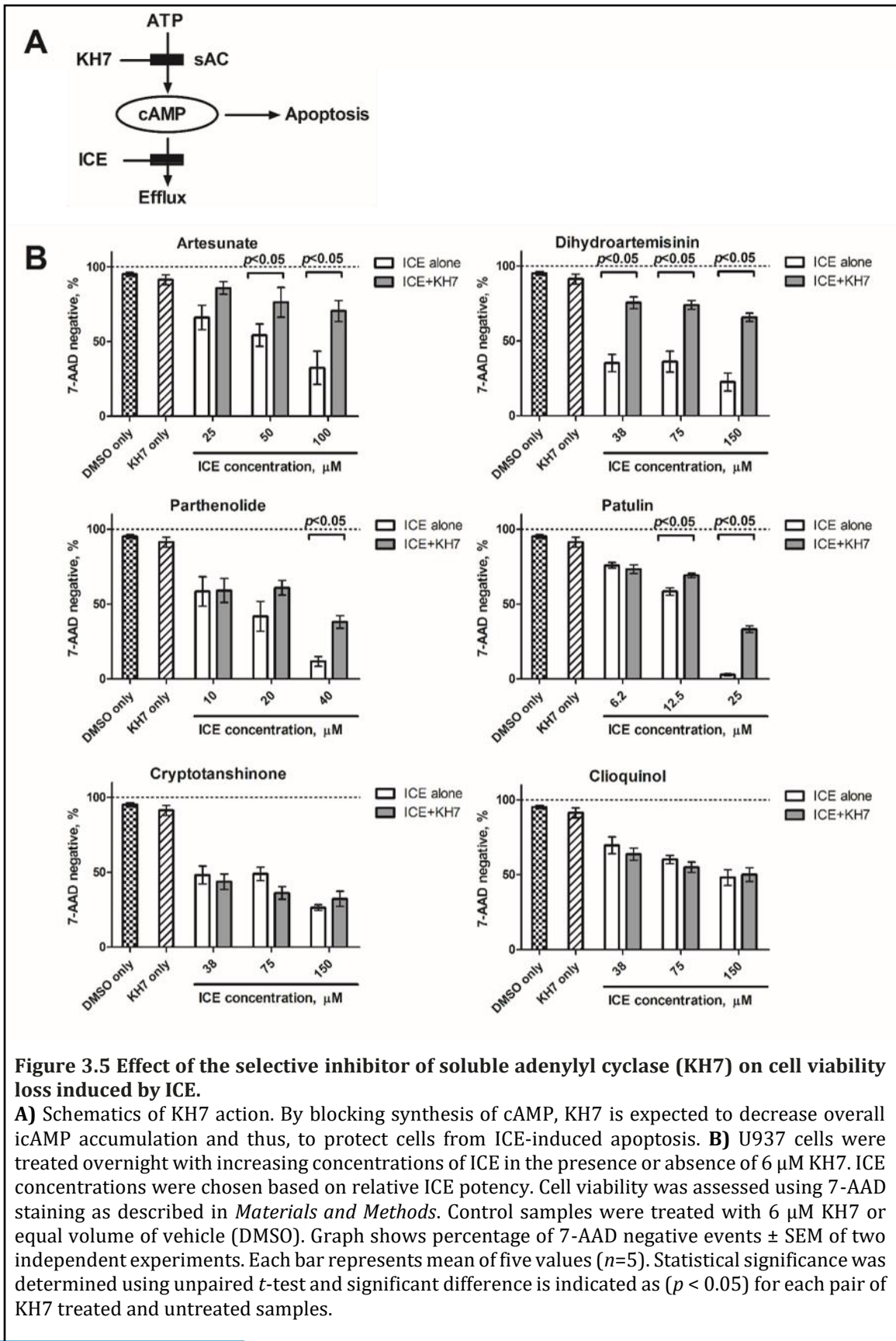
U937 cells transfected with a non-desensitizing mutant of FPR1 were maintained in cRPMI at 37°C while the samples were stirred continuously during data acquisition. Cell suspension was sequentially treated with LDV-FITC (first arrow), FPR1-specific ligand for cell activation (fMLFF, second arrow), and ICE compounds or forskolin positive control (40 μ M) or DMSO vehicle (third arrow). The use of the non-desensitizing mutant of FPR1 allows for the maintenance of the high affinity VLA-4 state during the course of the experiment (control, vehicle). This allows for monitoring the real-time deactivation kinetics after compound addition. Each line represents MFI \pm SEM of three independent experiments. In each experiment, every experimental point represents MFI of several hundred events acquired every second. Bars representing SEM are shown for every 10 s time point. Dashed line represents binding of the LDV-FITC prior to cell activation.

3.3.5 Adenylyl cyclase inhibition reduces ICE-induced cell viability loss

Because synthesis is a source for icAMP accumulation, and soluble adenylyl cyclase (sAC) is directly implicated in the mitochondrial pathway of apoptosis, we studied how blocking the AC by the selective sAC inhibitor, KH7, influences ICE effects. Based on the data published by Kumar *et al.*, 2009 [45], we expected that blocking cAMP production would reduce ICE potency (**Figure 3.5A**). In fact, we detected a significant protective effect of KH7 on the cell viability loss induced by the four most potent ICE compounds (**Figure 3.5B**). The lack of effect for less potent ICE

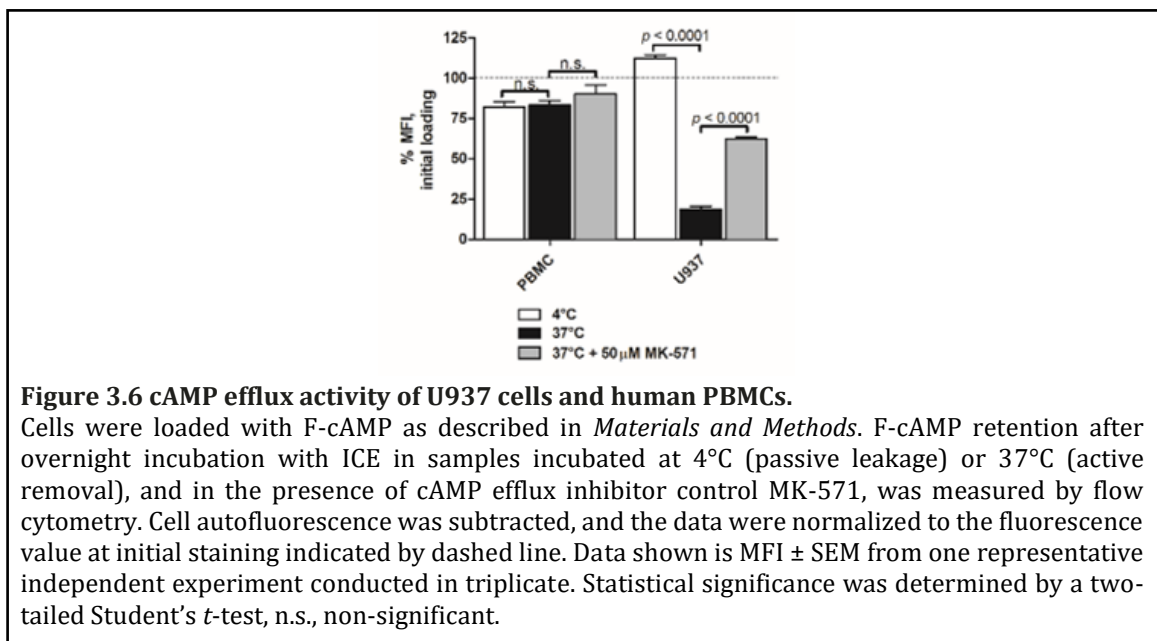
could be due to a lesser effect on viability: KH7 displayed the most prominent effect in samples where control viability was far below 50%. Thus, inhibition of sAC activity was sufficient to reduce the effects of the most potent ICE.

Hence, compounds identified in an assay based on blocking cAMP efflux can reduce cell viability, and stimulate two signaling pathways that are each modulated by elevation of icAMP, CREB phosphorylation and VLA-4 deactivation. Moreover, blocking of sAC activity prevented ICE-induced cell viability loss. These data are consistent with an ICE molecular mechanism involving elevation of icAMP. The accumulation of icAMP as the result of decreased cAMP efflux in U937 cells was first demonstrated by Copsel, *et al.* [97].



3.3.6 Normal primary peripheral blood mononuclear cells (PBMCs) did not significantly efflux cAMP

According to our hypothesis, active cAMP efflux represents a novel apoptosis evasion mechanism that is activated in certain malignant cells, and normal cells should lack this cAMP efflux ability. To test this proposition, we compared F-cAMP efflux in U937 cells and normal PBMCs (**Figure 3.6**). After 24 h incubation, PBMCs loaded with F-cAMP retained ~80-90 % of the probe fluorescence when incubated at 37°C or at 4°C, whereas U937 cells lost ~80 % of the probe fluorescence only at 37°C. A significant part of this loss was blocked by incubation with efflux inhibitor MK-571, indicating active participation of ABCC family transporters. No decrease in the probe fluorescence was detected at 4°C, suggesting that cell membrane integrity was well preserved and passive probe leak had not occurred. This result suggests that active cAMP removal cannot be detected in normal PBMCs in the same time frame as in the AML model.



3.3.7 ICE induce apoptosis of U937 cells

The effect of ICE on U937 cell apoptosis after overnight incubation has been studied using the MultiCyt 4-Plex Apoptosis kit that reports four different apoptosis endpoints: effector caspases 3 and 7 activation, phosphatidylserine surface expression, mitochondrial membrane depolarization and cell membrane integrity. The ICE induced apoptosis in a dose-dependent manner, and the EC₅₀ values for all four apoptosis endpoints were determined to range from 2-3 μ M to several hundred μ M (**Figure 3.7**). The relative sensitivity of different apoptosis endpoints reflected different consecutive steps of the intrinsic pathway. Mitochondrial depolarization and membrane damage were the most sensitive while the effector caspase activation was the least. Cryptotanshinone showed a very small effect on annexin-V binding and caspase activation, even at the highest ICE concentrations. These EC₅₀s were excluded from further analyses (as indicated by NC).

To simplify analysis, the data were color-coded (heat map) according to the determined EC₅₀ values (**Figure 3.7**). The most potent compounds (EC₅₀ values 1-10 μ M) in the apoptosis assay were: patulin, parthenolide, and dihydroartemisinin (white color). In addition, the relative ranking was largely independent on the particular endpoint. Mean EC₅₀s calculated for each compound are shown at the bottom of a heat map and indicate relative potency of studied ICE. Thus, U937 cells treated with ICE exhibited a dose-dependent increase in apoptosis.

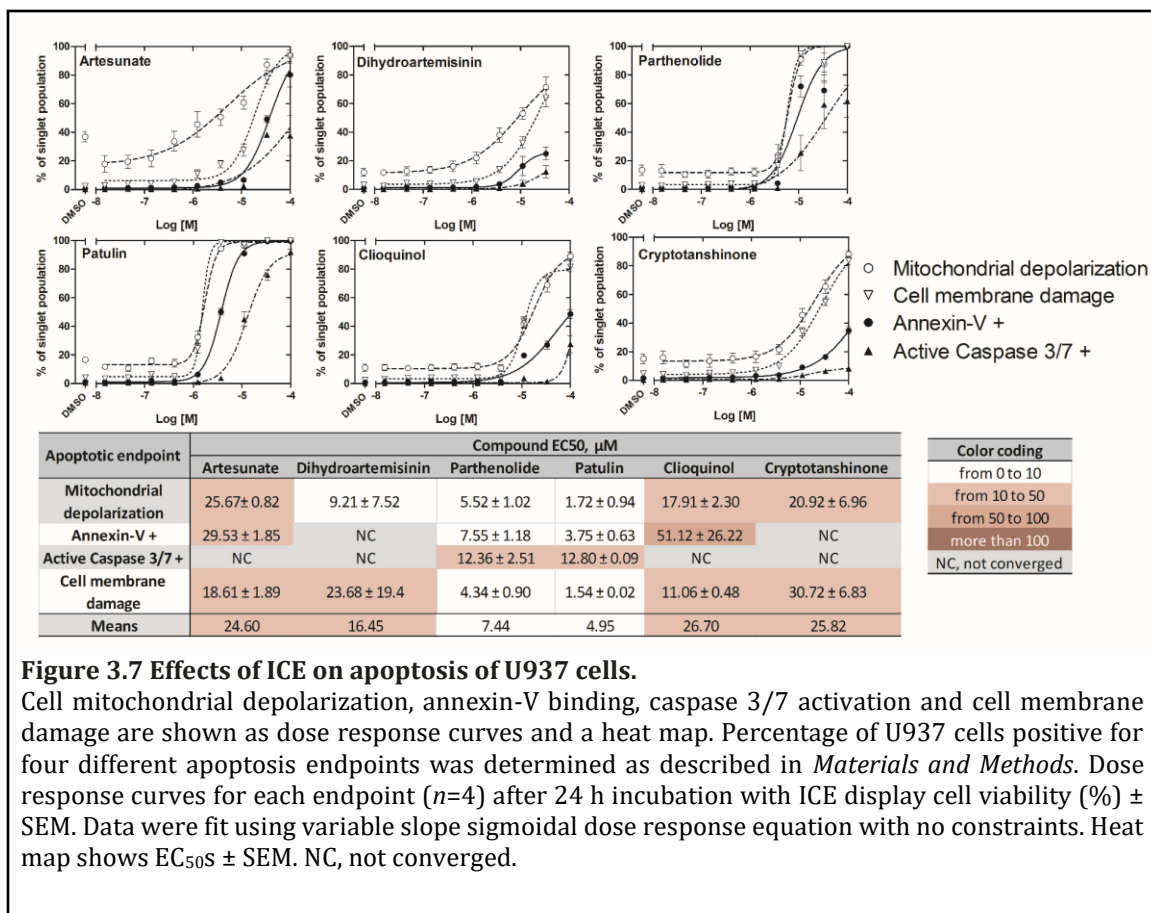


Figure 3.7 Effects of ICE on apoptosis of U937 cells.

Cell mitochondrial depolarization, annexin-V binding, caspase 3/7 activation and cell membrane damage are shown as dose response curves and a heat map. Percentage of U937 cells positive for four different apoptosis endpoints was determined as described in *Materials and Methods*. Dose response curves for each endpoint ($n=4$) after 24 h incubation with ICE display cell viability (%) \pm SEM. Data were fit using variable slope sigmoidal dose response equation with no constraints. Heat map shows EC₅₀s \pm SEM. NC, not converged.

3.3.8 ICE decrease viability and show cancer cell specificity

Next, we tested the effect of ICE on the viability of U937 cells and B-ALL cell lines (**Table 3.2**). On U937 cells, several compounds were more potent than the positive control MK-571 (**Figure 3.8**). In general, B-ALL cell lines showed more sensitivity than the U937 cells to several of the selected compounds. However, B-ALL lines showed a decreased sensitivity to the two structurally related drugs: artesunate and dihydroartemisinin. The EC₅₀ values for the ICE with each B-ALL line ranged from low nanomolar to $\sim 300 \mu\text{M}$ (**Figure 3.8**). It can be noted, however, that the compounds, which consistently decreased viability ranked in the same order across all six B-ALL lines: patulin, parthenolide, clioquinol, cryptotanshinone.

To investigate the potential selectivity of the compounds, we compared ICE effects on cell viability in leukemic and non-malignant cells (PBMCs from healthy volunteers). The EC₅₀ values indicated that for the most potent of the tested compounds to be efficacious, PBMCs required a concentration of at least an order of magnitude higher than was necessary for the leukemic cell lines (**Figure 3.8**, notice the darker color-coding for PBMCs). This difference was expected, since normal PBMCs do not have an established system for cAMP efflux (**Figure 3.6**), and therefore should be less sensitive to ICE.

Table 3.2 The hematologic cell lines included in the study, their subtype and genetic rearrangements [131].

* - Two cell lines were shown to have identical genetic rearrangement and a fusion gene.

Cell line	Subtype	Genetic rearrangement	Fusion gene
U937	AML	t(10;11)(p12;q14)	PICALM/MLL10(AF10)
697	B-ALL	t(1;19)(q23;p13)	TCF3(E2A)/PBX1*
Nalm-6	B-ALL	t(5;12)(q33;p13)	ETV6/PDGRFB
Sup-B15	B-ALL	t(9;22)(q34;q11)	P190 BCR/ABL1
Reh	B-ALL	t(12;21)(q13;q22)	ETV6(TEL)/RUNX1(AML1)
RS4;11	B-ALL	t(4;11)(q21;q23)	MLL/MLLT2(AF4)
MHH-Call 3	B-ALL	t(1;19)(q23;p13)	TCF3(E2A)/PBX1*

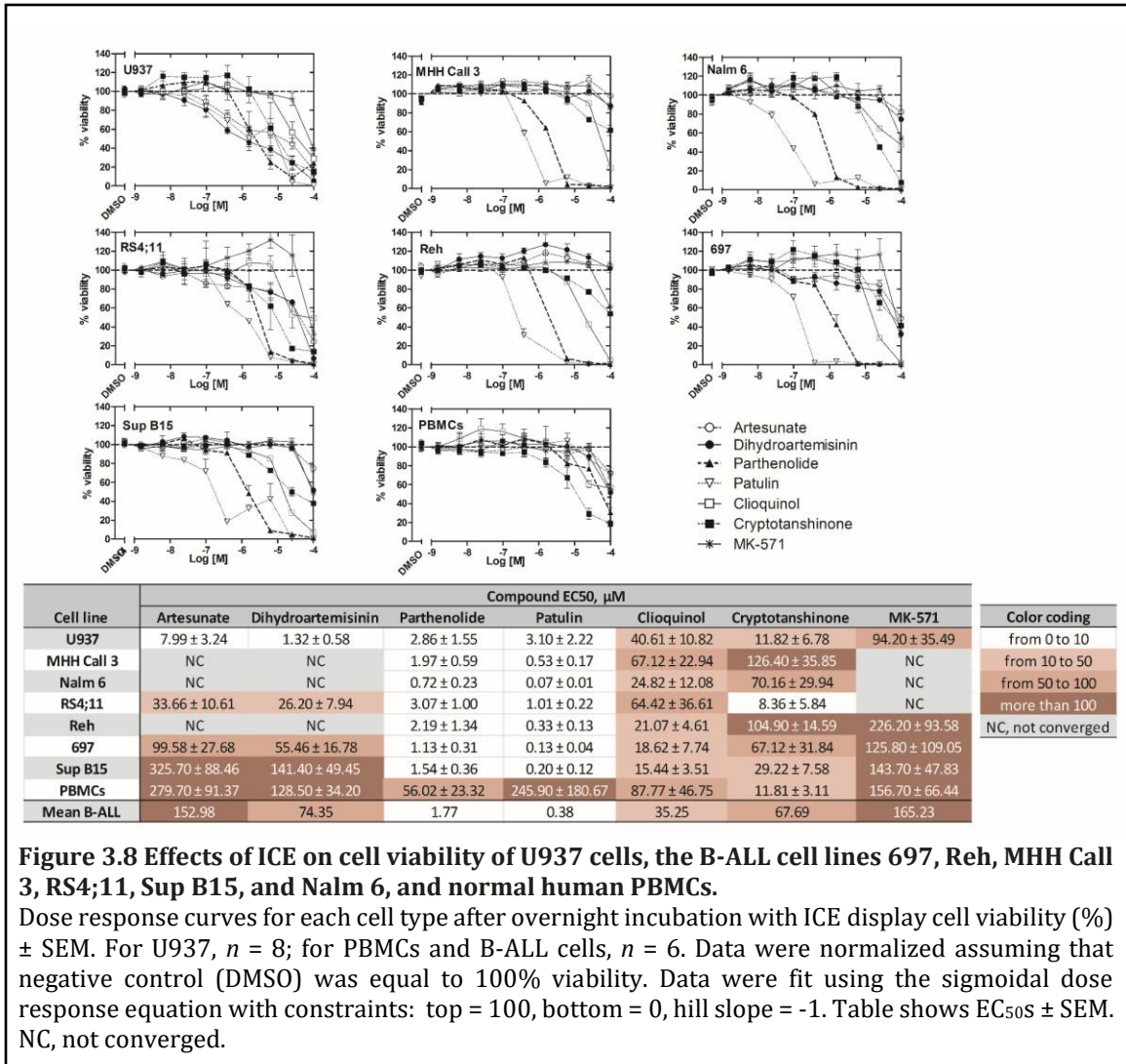


Figure 3.8 Effects of ICE on cell viability of U937 cells, the B-ALL cell lines 697, Reh, MHH Call 3, RS4;11, Sup B15, and Nalm 6, and normal human PBMCs.

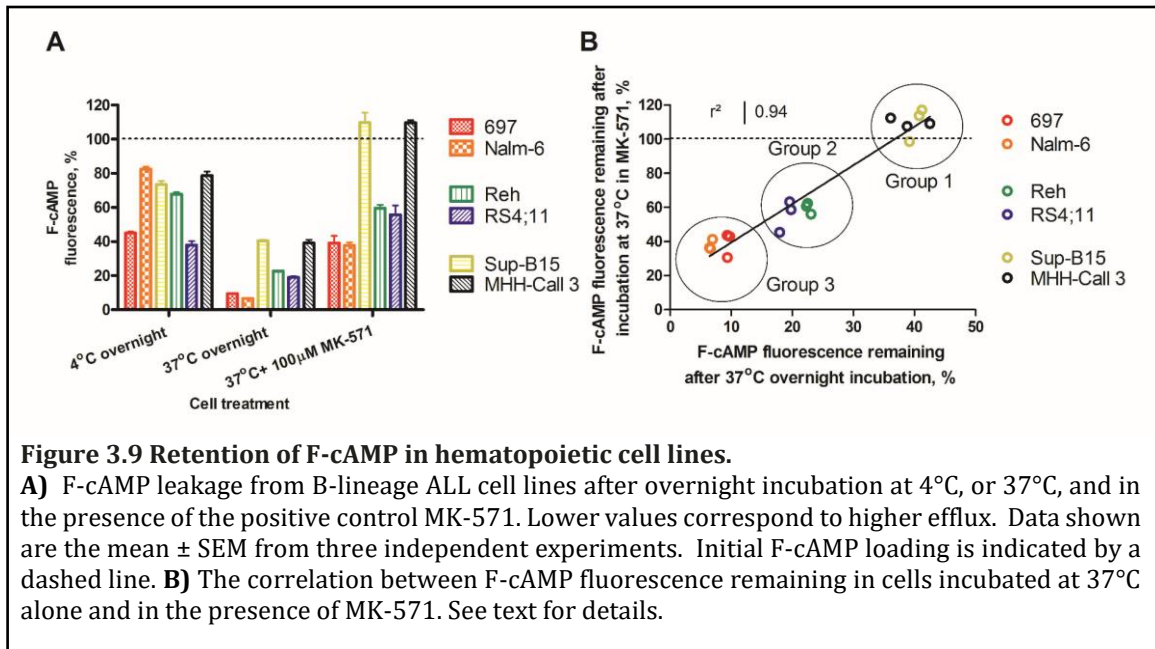
Dose response curves for each cell type after overnight incubation with ICE display cell viability (%) \pm SEM. For U937, $n = 8$; for PBMCs and B-ALL cells, $n = 6$. Data were normalized assuming that negative control (DMSO) was equal to 100% viability. Data were fit using the sigmoidal dose response equation with constraints: top = 100, bottom = 0, hill slope = -1. Table shows EC₅₀s \pm SEM. NC, not converged.

3.3.9 Leukemic cells have different abilities to efflux cAMP

To further study cAMP efflux in leukemic cells, the B-ALL cell lines were loaded with F-cAMP, and its efflux from the cells was evaluated. After incubation at 4°C (passive leakage), the cells lost 20-60% of their fluorescence from the initial F-cAMP loading. Incubation at 37°C (active efflux) resulted in F-cAMP removal that ranged from ~60% to ~90%, with no apparent relationship between 4°C and 37°C samples

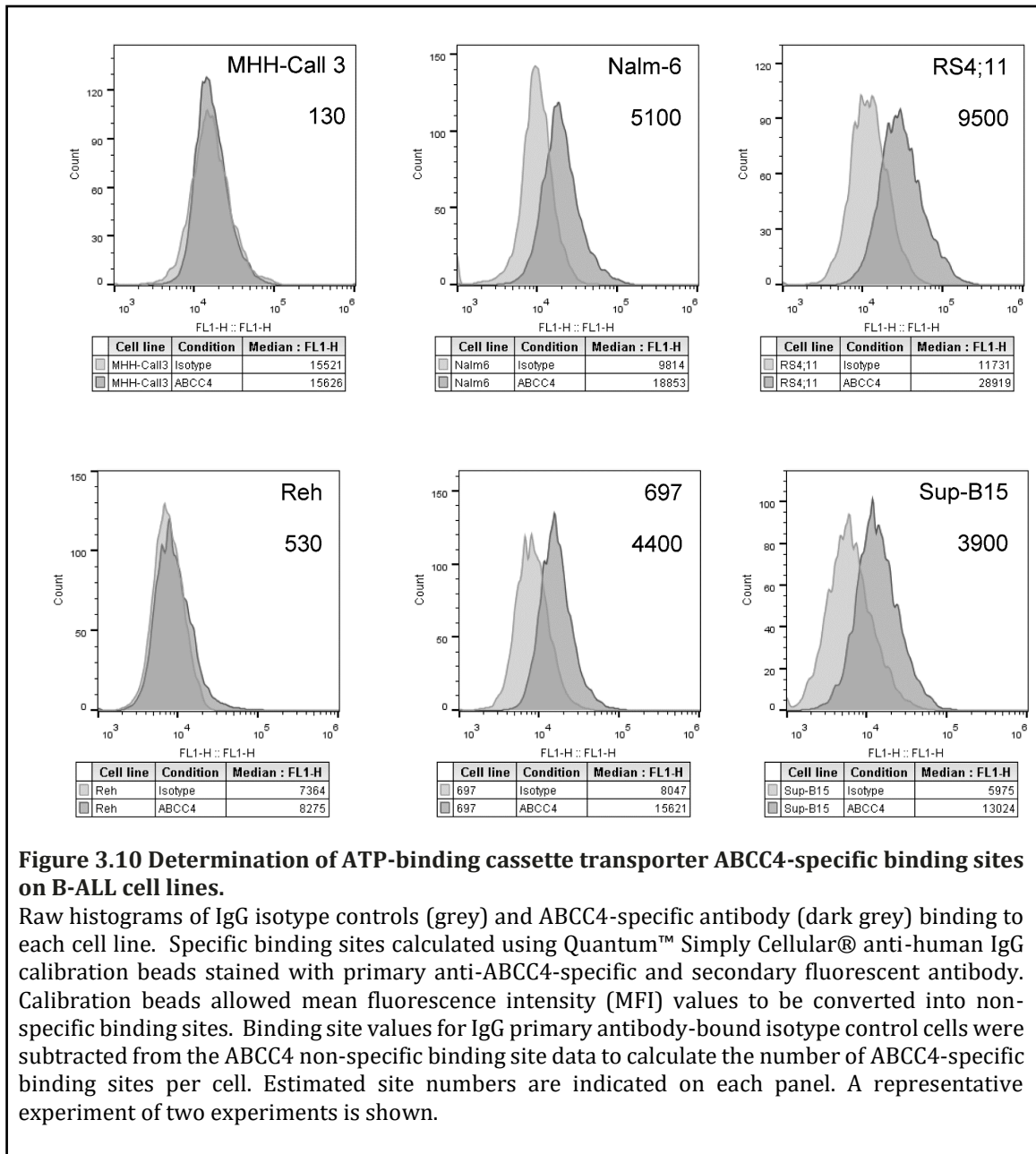
(**Figure 3.9A**). For example, Nalm-6 and 697 cells showed dissimilar passive leakage, but both cell lines exhibited similar active F-cAMP removal abilities.

The cell lines also exhibited varied sensitivity to MK-571, a control for transporter-dependent efflux. We found a strong relationship between levels of F-cAMP remaining in cells at 37°C, both alone and in the presence of MK-571. Based on this parameter, cell lines could be stratified into three groups, which indicated correlations between ability to actively efflux cAMP and MK-571 inhibition of cAMP removal. *Group 1:* Sup-B15 and MHH-Call3 removed ~60% of the F-cAMP by active efflux, which was blocked completely by MK-571. *Group 2:* Reh and RS4;11 cells removed 75-80% of the F-cAMP by active efflux, and ~30-40% with MK-571. *Group 3:* 697 and Nalm-6 cells removed > 90% of the F-cAMP by active efflux, and 60-70% with MK-571 (**Figure 3.9B**). Thus, the cell lines that effluxed F-cAMP poorly were better inhibited by MK-571, and those that were efficient in the removal of F-cAMP were less inhibited by MK-571. This suggests that for cell lines in Groups 2 and 3, an additional MK-571-insensitive mechanism participated in the removal of F-cAMP.



3.3.10 The primary cAMP transporter, MRP4/ABCC4, is differentially expressed by leukemic cell lines

cAMP is primarily released by cells via the ABCC4 (MRP4) and ABCC5 (MRP5) transporters [90]. The affinity of ABCC4 for cAMP is \sim 10-fold greater than that of ABCC5 (k_m values of 44.5 μ M and 379 μ M, respectively) [90, 132]. Therefore, we hypothesized that the presence of ABCC4 on leukemic cells would correlate with their ability to efflux F-cAMP. ABCC4 phenotypes were determined for the B-ALL cell lines, and the number of ABCC4-specific binding sites ranged from \sim 100 on MHH-Call3 to \sim 10⁴ on RS4;11 cells (**Figure 3.10**). However, no apparent correlation between ABCC4 expression and F-cAMP efflux were detected (compare **Figure 3.9** and **Figure 3.10**). This suggests that other transporters and/or mechanisms may play additional roles in leukemic cell removal of cAMP.



3.3.11 ICE decrease primary ALL patient sample viability

To further establish the effectiveness of ICE in reducing cancer cell viability, primary cells from six B-ALL patients (**Table 3.3**) were tested *ex vivo*. The results showed dose-dependent decreases in patient sample viability after exposure to the

compounds (**Figure 3.11**). To verify the relative ranking of ICE, the mean EC_{50} values for each compound were plotted against the mean EC_{50} values determined for all B-ALL cell lines. The result indicated a strong correlation for most patient samples (**Figure 3.11B**). This result suggests that the data obtained using cell lines adequately reflect the relative compound potency detected in patient samples, and therefore, cell lines can be used to test ICE derivatives in future medicinal chemistry applications.

Moreover, the overall shape of the dose-response curves obtained for different patient samples revealed an interesting pattern: the shape of the curves was more patient-specific rather than compound-specific. For example, in the samples from patients no. 1 and no. 5, we observed a significant increase in cell viability vs. vehicle treated sample at lower concentrations of dihydroartemisinin, clioquinol or parthenolide (see points above the dashed line, **Figure 3.11A**). This behavior was also evident in viability data from B-ALL cell lines (**Figure 3.8**). These results are consistent with the report that small or transient increases in icAMP can be anti-apoptotic and therefore, can support cell survival [2, 39]. Under identical conditions, the same compounds elicited no such effect in the samples obtained from patients no. 2 or no. 4. Another difference can be observed when the slopes of the dose-response curves are analyzed. It appears that in some patient samples, the slopes are steeper than in others. These data suggest that certain traits of a particular patient sample play a significant role in the response to different ICE compounds. It might be useful to correlate genotypic and phenotypic profiles of patient samples with these dose-

response curve parameters. However, this will require further studies with larger numbers of patient samples with diverse genotypic and phenotypic profiles.

Table 3.3 Genotypic and phenotypic profile of B-ALL patient samples.

* – have MLL-AF4 rearrangement

Abbreviations: *ALL*: acute lymphoblastic leukemia; *WBC*: white blood cell; *FISH*: fluorescent in situ hybridization; *STD*: standard risk; *VHR*: very high risk

Patient	Age	Gender	WBC	Ploidy	Phenotype	Risk	Cytogenetics/FISH
124-12	4	F	2.9			STD	46,XX,del(9)(p13),der(19)t(1;19)(q23;p13.3)[10]/46,idem,add(5)(p13),add(9)(p21),del(10)(q23)[2]/46,idem,t(1;13)(p13;q14)[3]/46,XX[5]
238-13*	18	M	629.2	diploid	CD34+ CD19+ CD22dim	VHR	46,XY,t(4;11)(q21;q23)[cp6]/49,XY,+X,+1,t(4;11)(q21;q23),+21[5]/46,X,-Y,t(4;11)(q21;q23),+mar[3]
329-13*	26	F	53.1		CD10+ CD19+ CD22+	VHR	46,XY,t(4;11)(q21;q23)[cp6]/49,XY,+X,+1,t(4;11)(q21;q23),+21[5]/46,X,-Y,t(4;11)(q21;q23),+mar[3]
017-14	22	M	39.5		CD10+ CD19+ CD22+	VHR	45,XY,-7,t(9;22)(q34;q11.2)[16]/46,XY[4] complement with translocation t(9;22) and monosomy 7 in sixteen of twenty cells analyzed; BCR/ABL1 transcript ratio: 0.37. Ratios>0.1
280-13	2	M	22.0	0.92 hypoploid	CD10+ CD19+ CD34+	STD	46,XY[4]
116-13	7	F	4.0	diploid	CD10+ CD19+ CD34+	STD	46,XX

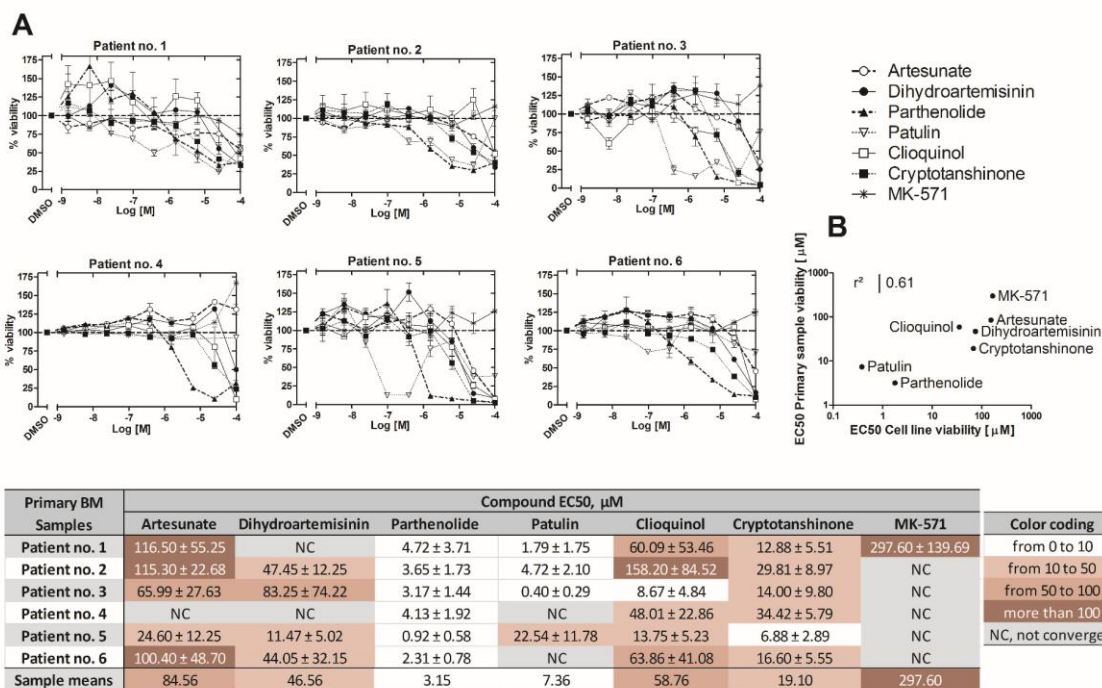


Figure 3.11 Effects of ICE on cell viability of primary ALL patient samples.

A) Compound dose response curves for each patient sample tested in duplicate. Data were normalized assuming that negative control (DMSO) was equal to 100% viability. Data were fit using the sigmoidal dose response equation with constraints: top = 100, bottom = 0, hill slope = -1. Table shows $\text{EC}_{50} \pm \text{SEM}$. NC, not converged. **B)** Correlation between mean compound EC_{50} values obtained from B-ALL cell line data (Fig. 8) and mean EC_{50} values from primary B-ALL patient samples. The coefficient of determination (r^2) was calculated from the Pearson correlation coefficient.

3.4 Discussion

For many years, researchers have been eager to develop methods to robustly modulate icAMP in cancer cells, and all known steps of the cAMP-related signaling pathway have been targeted [53]. Only recently, researchers have realized that icAMP can be also modulated by cyclic nucleotide efflux transporters. The finding that blocking cAMP efflux or down-regulation of efflux transporters can trigger cAMP elevation and downstream signaling [97] has opened new avenues for developing a novel class of anticancer therapeutics via inhibitors of cAMP efflux. Analysis of the proteins capable of cyclic nucleotide efflux also suggests notable possibilities.

The cAMP transporter ABCC4 has increased expression in blood cancer cells as compared to normal hematopoietic cells [133], and its expression decreases significantly upon cell differentiation [96]. ABC transporters are likewise upregulated in stem-like cells, which may suggest that these cells require active removal of cAMP or other structurally-related compounds in order to remain in a pluripotent state, and that the metabolic specificity of these cells requires active transport of certain metabolites [134]. These cancer stem cells are also associated with higher resistance to typical cancer therapeutics [135]. However, our results for ABCC4-expression did not define any clear correlations between cAMP efflux and ABCC4 expression in the cell lines. It is possible that other transporters capable of cAMP efflux (ABCC5 or ABCC11 [132, 136]) are present, or that there is a difference in the efflux capacity of different transporters. This may indicate that the ability to inhibit cAMP transport is substrate- or condition-dependent.

Of the active compounds identified in our screen for ICE, the majority were sesquiterpene lactones: parthenolide is derived from the feverfew (*Tanacetum parthenium*) plant; artemisinin and dihydroartemisinin are from *Artemisia annua*; and artesunate and artemether are semi-synthetic artemisinin derivatives. Cryptotanshinone is also plant-derived (*Salvia miltiorrhiza*), whereas clioquinol is an antimicrobial hydroxyquinolone derivative, and patulin is an antibiotic mycotoxin produced by *Aspergillus* and *Penicillium*. These compounds have been reported to exhibit anticancer activity in a number of model systems (**Table 3.4**), and the reported anticancer effects of these compounds were often similar to those seen in

our assays (**Table 3.5**). However, none of the compounds has previously been reported to modulate cyclic nucleotide efflux.

Table 3.4 Previously reported anticancer activity of the compounds identified as ICE.

Compound	Tested cancer types
Patulin	kidney [137], oral squamous cell carcinoma [138], glioblastoma [139], colon [140-142], colorectal [143], hematological [128, 144], liver [145]
Parthenolide	Melanoma [146, 147], cervical [148, 149], hematological [127, 150, 151], breast [152]
Artesunate	Ovarian [153], cervical [154], Kaposi's sarcoma [155], squamous carcinoma [156], breast [157, 158], liver [159], pancreatic [160, 161], hematological [162-166], colorectal [165, 167], neuroblastoma [168], lung [165, 169], osteosarcoma [170]
Dihydroartemisinin	ovarian [153, 171], breast [172], liver [172, 173], melanoma [174], pancreatic [175-179], lung [180-182], cervical [154], hematological [183-188], prostate [189], glioma [190], osteosarcoma [191]
Clioquinol	hematological [125, 192-194], breast [195, 196], cervical [197], prostate [198-200]
Cryptotanshinone	hematological [201, 202], prostate [126, 203, 204], breast [126, 205], melanoma [206, 207], lung [207], rhabdomyosarcoma [126]

Artemisinin, dihydroartemisinin, artesunate and artemether are currently used worldwide for the treatment of malaria. Artemether is a component of the drug Coartem manufactured by Novartis and approved by the US Food and Drug Administration in 2009. Several ongoing clinical trials of artemisinin derivatives to treat hepatocellular carcinoma, breast cancer, cervical intraepithelial neoplasia, as well as a trial evaluating “biological activity of oral clioquinol in patients with relapsed or refractory hematological malignancy” initiated by Dr. Mark Minden from Ontario Cancer Institute Princess Margaret Hospital in Canada, can be found on clinicaltrials.gov. Therefore, these drugs have the highest potential to be repurposed

into current treatment regimens. Poor water-solubility and bioavailability of parthenolide prompted medical chemistry efforts to improve these characteristics [208]. However, since these drugs were identified from two relatively small libraries totaling ~3500 compounds, we envision that larger efforts to identify compounds capable of blocking cAMP efflux may lead to better drugs. This is especially important because of the unique signaling role of cAMP in apoptosis.

Table 3.5 Previously reported molecular/ signaling mechanisms related to anticancer activity of the compounds identified as ICE.

Abbreviations: *VEGF*: vascular endothelial growth factor; *NF-κB*: nuclear factor kappa-B; *AP-1*: activator protein 1; *MAPK*: mitogen-activated protein kinase; *ERK*: extracellular signal-regulated kinases; *STAT*: signal transducer and activator of transcription; *ROS*: reactive oxygen species; *PI3K*: phosphatidylinositol-4,5-bisphosphate 3-kinase; *Akt*: protein kinase B; *mTOR*: mammalian target of rapamycin; *eIF-4E*: eukaryotic initiation factor 4E; *UPR*: unfolded protein response

Compound	Cell cycle arrest	Anticancer effects	Potential mechanism(s) of action
Parthenolide	G ₁ [147, 209], S [210]	↓VEGF expression & metastasis [147, 211, 212]; ↑p53 activation [127]; ↓cyclin D1 [147, 209]	↓NF-κB & AP-1 activation [127, 147, 211, 213, 214]; ↓MAPK/ERK signaling [213, 214]; ↓STAT signaling [215]; ↑ROS [127, 151, 215]
Dihydroartemisinin	G ₁ [176], G ₂ [173, 187, 191]	↓VEGF expression & angiogenesis [185, 187, 188]; ↓cyclin B, CDC25 [173]	↓NF-κB activation [176, 191]; ↓MAPK/ERK, PI3K/Akt signaling [183, 189]; ↑ROS [172, 181, 190]
Artesunate	G ₁ [156, 216], S [167], G ₂ [165, 170]	↓metastasis/ migration [166, 169]; ↓VEGF expression/ angiogenesis [156, 162, 166]; ↓cyclins B & D1, Cdks 2, 4, 6 [156]; ↑p21, p27 [156]	↓NFκB & AP-1 activation [169, 217, 218]; ↓nitric oxide, cAMP-mediated, Wnt/β-catenin, PI3K/Akt signaling [167, 217, 218]; ↑ROS [156, 158, 164]
Cryptotanshinone	G ₁ [206], G ₂ [206]	↓cyclin D1, Bcl-2 [126, 201, 202]; ↑p53, Chk1, Chk2 [206]	↓mTOR, STAT3 signaling [202, 203]; ↓eIF-4E [126]
Clioquinol	G ₁ [196]	↓cyclin D1 [196]; ↑p21, p27, p53 [192]	↓NF-κB activation [194, 198]; ionophore/chelator activity [192, 194, 198]; proteasome inhibition [193, 195]
Patulin	G ₁ [219], G ₂ [143]	↓ERK1/2 activation [138, 220]; ↑UPR [138, 220]; ↑intracellular [Ca ²⁺] [221]	↑ROS, DNA damage [143, 145, 219, 220, 222]; ↓glutathione [220, 222]

As a messenger, cAMP plays significant regulatory roles within cells. Multiple signaling mechanisms critical for leukemogenesis can be down-modulated by cAMP. At least two cAMP/PKA-related pathways can be involved in the induction of cAMP-dependent apoptosis in cancer cells: 1) the mitochondrial-mediated (intrinsic) pathway, and 2) modulation of the NF- κ B signaling pathway (**Figure 3.12**). The proapoptotic intrinsic mechanism promoted by cAMP depends upon PKA [77], which can phosphorylate CREB, and results in transcription of the apoptotic activator Bim/BCL2L11 [2]. cAMP modulation of NF- κ B can affect transcription of pro-survival genes [15]. Our data suggest that inhibition of cAMP transport by ICE was able to elicit many of these effects.

Targeting cancer through a “pathway-dependent approach” that consists of different means of elevating cAMP is considered a viable option for novel therapeutic development [53]. It appears that every potential step of the pathway, including cAMP synthesis, degradation, and downstream signaling, has been taken into consideration to stimulate icAMP accumulation [53, 223, 224]. Classically, cyclic nucleotide analogs or other cAMP-elevating agents have been used to treat hematological malignancies by slowing cell growth and differentiating cancer cells [114]. However, while modestly effective, these compounds exhibit toxicity in non-cancerous tissues [69, 71, 225]. Our data suggest that targeting cAMP efflux with small molecules could be an efficient way to raise icAMP in certain types of cancer, and this could potentially result in the development of a new class of pathway-specific therapeutics. Because increased cAMP efflux is not a typical trait of healthy cells, the identified ICE exhibited

specificity toward leukemic cells. The relatively efficient targeting of cAMP transport in cancers would directly depend on cell- or patient-specific characteristics and efflux ability. We anticipate that identification of drugs that inhibit this transport could allow for selective targeting of cancers that capitalize on cAMP pathway modulation for survival, and this merits further investigation into the effects of ICE on multiple ABC transporters. The fact that the machinery responsible for apoptotic evasion by cAMP efflux can also potentially support the removal of structurally related chemotherapy drugs (e.g., ara-C), and thus may contribute to multidrug resistance [226-228], makes this work unusually promising.

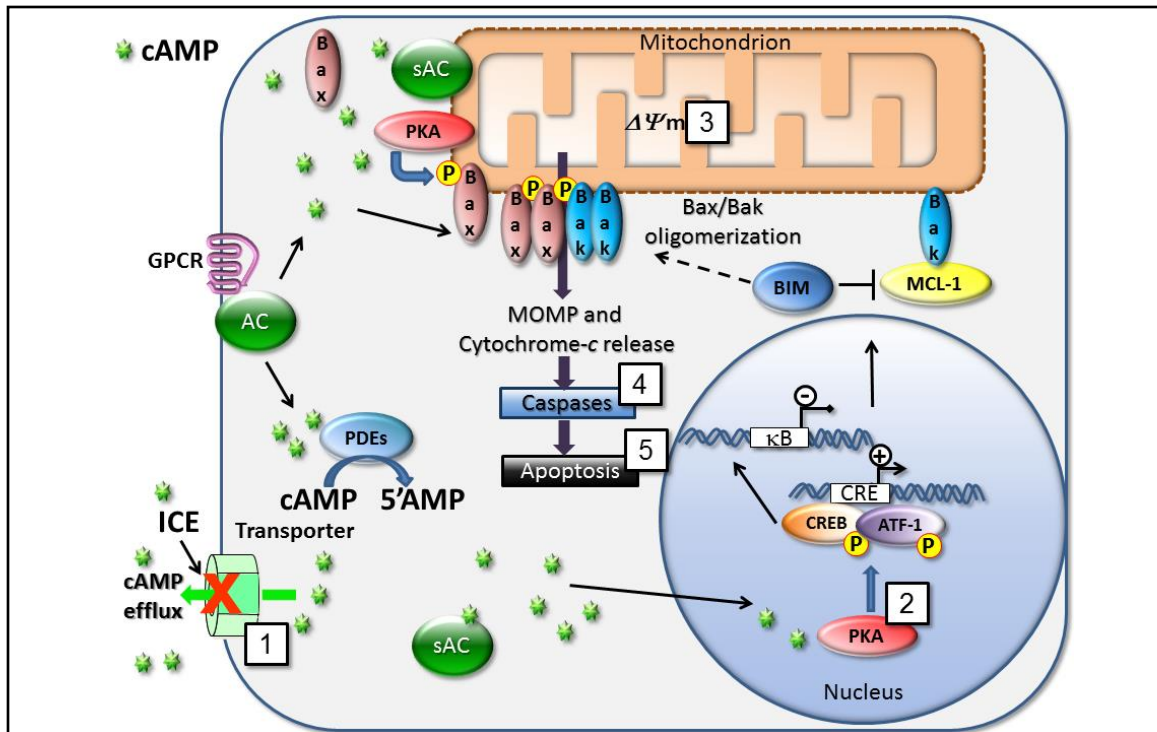


Figure 3.12 Mechanisms for cAMP-dependent regulation of cell death.

cAMP is produced by various pools of soluble and membrane-bound adenylyl cyclases (sAC and AC). Blocking cAMP efflux with ICE **1**) triggers several signaling endpoints that are related to the modulation of pro-apoptotic and cell survival pathways. Here, we detected phosphorylation of CREB/ATF-1 **2**), mitochondrial depolarization **3**), effector caspases 3 and 7 activation **4**), and apoptosis **5**) in the form of annexin-V binding and cell membrane damage. Blocking adenylyl cyclase activity using selective inhibitor of soluble adenylyl cyclase (KH7) was sufficient to reduce effects of most potent compounds. Various molecular mechanisms are implicated in effects of cAMP on apoptosis induction. In AML cells pro-apoptotic protein Bim/BCL2L11 expression is up-regulated via CRE/CREB in a cAMP-dependent manner [2]. Induction of Bim represents a crucial event in the cAMP-induced apoptosis in murine T-cell lymphoma and human acute leukemia [3]. cAMP is also shown to inhibit MCL-1 protein transcription in human MM cells [4] or human B-precursor cells [10]. Relocalization of the cytosolic sAC pool toward mitochondria leads to PKA activation and phosphorylation of the pro-apoptotic protein Bax that activates mitochondrial apoptotic pathway [13]. Also, cAMP is implicated in a regulation of NF- κ B action [15], which is a potential target in AML [16].

3.5 Materials and methods

3.5.1 Ethics

All blood samples from healthy volunteers were obtained with written, informed consent per local institutional research guidelines according to the University of New Mexico Human Research Protections Office protocol 11-225. Bone marrow samples acquired from pediatric B-ALL patients were taken upon written, informed consent according to the University of New Mexico Human Research Protections Office protocol 05-435.

3.5.2 Cells and reagents

Alexa Fluor®488 8-(6-aminohexyl) aminoadenosine 3',5'-cyclicmonophosphate, bis(triethylammonium) salt (F-cAMP) (Life Technologies, cat. A35775). The VLA-4-specific probe 4-((N'-2-methylphenyl)ureido)-phenylacetyl-L-leucyl-L-aspartyl-L-valyl-L-prolyl-L-alanyl-L-alanyl-L-lysine-FITC (LDV-FITC) was synthesized at AIBioTech. The selective inhibitor of soluble adenylyl cyclase, KH7, was purchased from Cayman Chemical Company (cat. 330676-02-3). All other reagents and hit compounds for secondary assays were from Sigma-Aldrich.

Cell lines, purchased from ATCC and DSMZ, were cultured in RPMI-1640 medium supplemented with 2 mM L-glutamine, 100 U/ml penicillin-streptomycin and 10% heat-inactivated fetal bovine serum (FBS; 20% for MHH-Call3), hereafter referred to as cRPMI, and incubated in a humidified atmosphere with 5% CO₂ at 37°C.

3.5.3 PBMCs

Healthy PBMCs were obtained from volunteers. Mononuclear cells were purified using Mono-Poly resolving medium (MP Biomedicals, cat. 091698049) according to manufacturer's instructions. PBMCs were resuspended in cRPMI and kept on ice prior to use.

3.5.4 Primary ALL patient samples

Bone marrow samples were acquired at diagnosis from pediatric B-ALL patients. Mononuclear cells were enriched by centrifugation in Ficoll-Paque (GE Healthcare, cat. 17-1440-02) and aliquoted for storage in liquid nitrogen until use. Samples were thawed in a 37°C water bath, resuspended in 20% FBS cRPMI, and centrifuged to remove freezing medium. Cells were resuspended in conditioned medium (DMEM, 10% FBS, 50 U/ml penicillin-streptomycin, 2 mM L-glutamine) from HS-5 stromal cell cultures.

3.5.5 cAMP efflux assay

Cells were loaded with F-cAMP as described [229]. Briefly, cells were resuspended in a hypertonic solution containing 10% polyethylene glycol 1000, 0.5 M sucrose, and 250 μ M F-cAMP in cRPMI without FBS, incubated 10 min at room temperature, washed, and then resuspended in hypotonic solution (60% cRPMI, 40% sterile water) for 2 min at room temperature to complete F-cAMP loading. Cells were resuspended in cRPMI and equilibrated for 2 h under normal culture conditions.

For testing cAMP efflux, an aliquot of loaded cells was kept at 4°C to serve as control, and the remaining cells were incubated in the presence of vehicle or compounds overnight. Samples were evaluated using Accuri C6 or BD FACScan flow cytometers (Becton Dickinson (BD)).

3.5.6 High throughput screening (HTS)

Liquid handling was accomplished with a Biomek FX Multichannel system (Beckman-Coulter, Fullerton, CA, USA) and/or Biotek Multiflo system (Winooski, VT, USA). F-cAMP-loaded U937 cells (2000/well) were seeded into 384-well polypropylene plates (Greiner Bio-One 784201, Monroe, NC, USA). Cells were treated with compounds (10 µM final concentration) from the Prestwick Chemical Library (Illkirch, France) or SPECTRUM Collection (MicroSource, Gaylordsville, CT, USA) delivered by pintool (V&P Scientific, San Diego, CA), at a final DMSO concentration of 1%. Plates were foil-sealed with AlumaSeal 384™ (Excel Scientific, Victorville, CA, USA), and incubated inverted overnight. Sample plates were analyzed by CyAn flow cytometers (Beckman-Coulter) configured with HyperCyt high-throughput auto-sampler systems (IntelliCyt, Albuquerque, NM, USA) using 488 nm excitation to assess FL-1 (530/40) MFI levels.

Data were analyzed with HyperView software (IntelliCyt) and time-gated to determine data from each well. Wells with ≥ 50 events were evaluated for FL-1 MFI

values. Samples with MFI values ≥ 2 standard deviations above the plate mean negative control values were considered “hit” compounds.

3.5.7 Compound validation

To validate sample data and decrease the number of false-positive hits, compounds were assayed in a high-throughput dose response assay. Plates were set up as in the HTS, with the exception that the plate formats contained 10-well dose responses for each hit compound, at final concentrations ranging from 30 μM to 4 nM.

For B-ALL cell lines, tests of hit compound inhibition of cAMP efflux were conducted as in the HTS, with compounds in 10-well dose responses ranging from 100 μM – 1.53 nM, at cell densities of 5000/well.

The dose response data were normalized for percent response based on sample FL-1 MFI values in comparison to untreated F-cAMP-loaded cells kept at 4°C overnight or at time = 0, and were fitted by GraphPad Prism 5 software (GraphPad Software, La Jolla, CA, USA) for sigmoidal dose response with constrained hill slope = 1. Compounds with S-shaped dose response curves and EC_{50} values less than 3 μM were selected for secondary assays.

3.5.8 Detection of CREB/AFT-1 phosphorylation in response to ICE

Cells were suspended at 10^6 cells/ml in cRPMI and incubated for 1 hour at 37°C with 20 μM ICE compounds or forskolin (positive control). Negative control samples were treated with DMSO at equal volume. Cells were fixed with 20x volume of pre-

warmed 1x solution BD Phosflow™ Lyse/Fix Buffer (cat. 558049), incubated at 37°C for 10 minutes, permeabilized with BD Phosflow™ Perm buffer II (cat. 558052), and incubated on ice for 30 minutes. Permeabilized cells were then washed and stained with BD Phosflow™ Alexa Fluor® 488 Mouse Anti-CREB (pS133) / ATF-1 (pS63) clone J151-21 (cat. 558435) according to the manufacturer's instructions.

3.5.9 Kinetic analysis of VLA-4 deactivation

Kinetic analysis of the binding and dissociation of the LDV-FITC probe was described previously [230]. Briefly, flow cytometric data were acquired at 37°C while the samples were stirred continuously with a stir bar (Bel-Art Products). First, U937 cells transfected with a non-desensitizing mutant of the Formyl Peptide Receptor FPR1 [231] were analyzed for 30–120 s to establish a baseline. The FPR1 mutant triggers VLA-4 activation, which persists for hundreds of seconds, allowing for integrin deactivation to be detected. Next, the LDV-FITC was added and acquisition was re-established. For cell activation, the high affinity FPR-specific agonist (N-formyl-L-methionyl-L-leucyl-L-phenylalanyl-L-phenylalanine, fMLFF) was added at a saturating concentration (100 nM), and acquisition was re-established. Finally, 40 μM of ICE, forskolin (positive control) or vehicle (negative control) were added. Acquisition was re-established, and data were acquired continuously for up to 1024 s.

The concentration of the LDV-FITC probe used in deactivation experiments (4 nM) was below the dissociation constant (K_d) for its binding to resting VLA-4 (low

affinity state, $K_d \sim 12$ nM), and above the K_d for physiologically activated VLA-4 (high affinity state, $K_d \sim 1-2$ nM). Therefore, the transition from low to high affinity state led to increased binding of the probe. This was detected as an increase in the median fluorescence intensity (MFI). VLA-4 deactivation led to the dissociation of the probe and decreased MFI [129].

3.5.10 Viability

Cell viability was determined with the CellTiter-Glo® Luminescent Cell Viability Assay (Promega). Greiner 655083 had 100 μ L cRPMI +/- 4×10^4 cells/well, and dose response curves of compounds ranged from 100 μ M to 1.53 nM (1% DMSO). Wells with DMSO-only served as negative controls. Samples were incubated overnight, and the assay was completed according to the manufacturer's protocol. Plates were analyzed using a Victor³V™ 1420 Multilabel Counter (Perkin Elmer).

For primary ALL patient samples, media consisted of 50% cRPMI, 50% conditioned DMEM from HS-5 stromal cell cultures and compounds. Cell densities ranged from 28,000-68,000 cells/well, and plates were foil-sealed prior to incubation.

3.5.11 Determination of cell viability by 7-AAD exclusion

Cells treated with ICE and control samples were incubated with 1 μ g/ml of 7-AAD for 20-60 minutes at 4°C on a rotator in the dark, and analyzed by flow cytometry

according to manufacturer instructions. Gates were set on 7-AAD negative and positive events based on histograms. Percent of 7-AAD negative events is shown.

3.5.12 Apoptosis

Apoptosis was determined using MultiCyt® 4-Plex Apoptosis Screening Kit (IntelliCyt, cat. 90053). The kit provides four different apoptosis endpoints that include effector caspases 3 and 7 activation, phosphatidylserine surface expression, mitochondrial membrane depolarization and cell membrane integrity. The activation of caspases is detected using NucView™ 488 Caspase3/7-specific substrate that exhibits increase in fluorescence upon cleavage by activated enzyme. Surface phosphatidylserine is detected by the binding of labelled annexin-V. Another fluorescent dye accumulates in intact mitochondria and upon mitochondrial membrane depolarization it leaks into the cytoplasm and exhibits a decrease in fluorescence. Cell membrane damage is detected by the uptake of a proprietary DNA intercalating agent analogous to 7-aminoactinomycin D.

384-well plates (Greiner 784201), pre-loaded with 5 µL cRPMI were stamped using a pintool with 100 nL of DMSO-solubilized compounds from the 100-fold concentrated stock solution. Next, 5 µL U937 cells (2×10^6 /ml in cRPMI) were added to wells and mixed, and plates were foil-sealed. Compounds (**Table 3.1**) were tested in dose response at final concentrations ranging from 15.2 nM to 100 µM (1% DMSO final). Vehicle (DMSO) was used as a negative control. After 24 h incubation under culture conditions, the IntelliCyt MultiCyt 4-Plex Apoptosis Screening Kit was used

according to manufacturer's protocol. The data were acquired using iQue Screener Platform (IntelliCyt). Singlet cell populations were analyzed for individual measures of apoptosis, and gates were set based on control histograms.

3.5.13 Quantitation of ABCC4

ABCC4 transporters in fixed B-ALL cell lines were enumerated by flow cytometry using: primary mouse anti-human ABCC4 or IgG1 negative isotype-matched control (Abcam®, Cambridge, MA, USA), FITC-conjugated AffiniPure F(ab')₂ of goat anti-mouse IgG secondary antibody (Jackson Laboratories, West Grove, PA, USA), and Quantum™ Simply Cellular® anti-human IgG calibration beads (Bangs Laboratories, Fishers, IN, USA) according to manufacturers' protocols. Post-labeling, all samples were analyzed for FL-1 MFI. The calibration beads were used to generate a linear regression, which associated MFI to the antibody-binding capacity of the beads. This regression was used to calculate the number of antibody binding sites (ABS) per cell sample. For each cell type, the calculated ABS for isotype control samples were subtracted from ABS of the ABCC4 samples to determine specific binding sites.

3.5.14 Data analysis

The kinetic data were converted to MFI versus time using FCSQuery software developed by Dr. Bruce Edwards (University of New Mexico). Analysis of apoptosis was done using ForeCyt software (IntelliCyt). Curve fits and statistics were done

using GraphPad Prism software version 5.01 (GraphPad Software), as described in figure captions.

3.6 Acknowledgments

We would like to thank Dr. Bruce Edwards (University of New Mexico) for providing FCSQuery and HyperView software and Dr. Anna Waller for thoughtful input and discussions.

3.7 Disclosure of potential conflicts of interest

Larry A. Sklar is a co-inventor of HyperCyt, a high throughput flow cytometry platform used for drug identification utilized in the current manuscript, and is a co-founder of IntelliCyt, a company that manufactures HyperCyt. Other authors declare no conflicts of interest.

3.8 Grant support

This work was supported by The Oxnard Foundation (to A.C. and L.A.S.), University of New Mexico Clinical & Translational Science Center Pilot Award 1UL1RR031977 (to A.C.), and New Mexico Cancer Nanotechnology Training Center grant R25CA153825 (to D.R.P).

CHAPTER 4: High throughput flow cytometry identifies small molecule inhibitors for drug repurposing in T-ALL

Dominique R. Perez^{1,2,4}, Christian K. Nickl^{3,4}, Anna Waller^{1,2,4}, Cristina Delgado-Martin⁵, Travis Woods^{1,2,4}, Nitesh D. Sharma^{3,4}, Michelle L Hermiston⁵, Mignon L. Loh⁵, Stephen P. Hunger⁶, Stuart S. Winter⁷, Alexandre Chigaev^{1,2,4}, Bruce Edwards^{1,2,4}, Larry A. Sklar^{1,2,4,#}, Ksenia Matlawska-Wasowska^{3,4,#}

¹ Department of Pathology, ² Center for Molecular Discovery, ³ Department of Pediatrics, Division of Pediatric Research, Health Sciences Center, University of New Mexico, Albuquerque, NM, USA

⁴ University of New Mexico Comprehensive Cancer Center, Albuquerque, NM, USA

⁵ Department of Pediatrics, University of California, San Francisco, Benioff Children's Hospital, San Francisco, CA, USA

⁶ Department of Pediatrics and the Center for Childhood Cancer Research, Children's Hospital of Philadelphia and the Perelman School of Medicine at the University of Pennsylvania, Philadelphia, Pennsylvania, USA

⁷ Children's Minnesota Research Institute, Children's Minnesota, Minneapolis, Minnesota, USA

These authors contributed equally to this work

SLAS Discovery. 2018 Aug 23 (7):732-741.

doi: 10.1177/2472555218774248. PMID: 29746793.

4.1 Abstract

Kinase inhibitors have dramatically increased patient survival in a multitude of cancers, including hematological malignancies. However, kinase inhibitors have not yet been integrated into current clinical trials for patients with T-cell lineage acute lymphoblastic leukemia (T-ALL). In this study, we used a high throughput flow cytometry (HTFC) approach to test a collection of small molecule inhibitors including 26 FDA-approved tyrosine kinase inhibitors in a panel of T-ALL cell lines and patient derived xenografts. Because hypoxia is known to cause resistance to chemotherapy, we developed a synthetic niche that mimics the low oxygen levels found in leukemic bone marrow to evaluate the effects of hypoxia on the tested inhibitors. Drug sensitivity screening was performed using the Agilent BioCel automated liquid handling system integrated with the HyperCyt HT flow cytometry platform, and the uptake of propidium iodide was used as an indication of cell viability. The HTFC dose-response testing identified several compounds that were efficacious in both normal and hypoxic conditions. This study shows that some clinically approved kinase inhibitors target T-ALL in the hypoxic niche of the bone marrow.

4.2 Introduction

T-cell lineage acute lymphoblastic leukemia (T-ALL) is an aggressive hematopoietic malignancy, which arises in the thymus from malignantly transformed T-cell progenitors [232]. It comprises ~15% of newly diagnosed children and young adults with ALL. Currently, patients with T-ALL require intensified therapies, for

which risk-adjusted treatments are primarily determined by minimal residual disease (MRD) response [233]. Importantly, patients with high-risk T-ALL do not benefit from further therapy intensification and often experience additional adverse events. Although cure rates have shown dramatic improvement over time, poor outcomes are still observed in patients who failed induction or relapsed after conventional chemotherapy. Affected patients are typically adolescents or young adults for whom a second remission is often very short. Therefore, the development of novel treatment programs for pediatric T-ALL is essential. Novel therapies could cure patients for whom cure has been elusive, or could provide bridging therapies to eradicate persistent MRD and facilitate stem cell transplantation.

Tyrosine kinase inhibitors (TKIs) have revolutionized modern pharmacology, leading to increased survival in a multitude of solid tumors, as well as precursor B-cell ALL (B-ALL) and chronic myelogenous leukemia (CML) with *BCR-ABL1* fusion [234]. While B-ALL and CML have become an intensive area of study for kinase-directed therapies, TKIs have not yet been integrated into current therapies for patients with T-ALL. To date, a few studies have investigated the efficacy of kinase pathway inhibition in T-ALL aberrantly overexpressing *FLT3*, *JAK-STAT* or *mTOR*, *etc.* [235-237]. However, the development of targeted therapies is challenged by the high degree of heterogeneity in T-ALL, in which most cytogenetic or molecular driver mutations occur at very low frequencies [232].

Genome wide studies have played a prominent role in drug response profiling [236] but the repertoire of specific biomarkers for targeted therapies remains limited

in T-ALL. Notably, kinase signaling pathways are critically involved in all aspects of cellular function. In cancer cells, they drive aberrant signaling, regulating cell proliferation, cell survival and chemoresistance. Dysregulation of tyrosine kinase and other kinase signaling pathways is commonly seen in T-ALL, providing an opportunity for therapeutic intervention [238]. Such pathways might be targeted with FDA-approved small molecule inhibitors which are available for drug repurposing, and the development of novel targeted therapies. Because kinase inhibitors have relatively safe adverse event profiles, they have generally been able to safely integrated into dose-intensified therapies in leukemia treatment regimens [234]. We hypothesized that T-ALL may be sensitive to treatment with clinically approved kinase inhibitors. Therefore, we tested a library of FDA-approved inhibitors to identify the most potent drug candidates with antitumor activity against T-ALL.

One critical factor that influences cancer cell sensitivity to drug treatment is the microenvironment, with an emphasis on hypoxia [239, 240]. Many promising drug candidates with demonstrated antitumor potential in *in vitro* assays paradoxically fail in pre-clinical trials *in vivo* because the microenvironment niche serves as a site for resistance to chemotherapy. On the other hand, some inhibitors show increased antitumor activity towards hypoxic cells, suggesting that conventional drug sensitivity testing under normoxic conditions may result in overlooking promising drug candidates [239].

Recent works suggest Src activation as an important mechanism by which cancer cells maintain chemoresistance under hypoxia to promote cell survival, progression,

and metastasis of a variety of human cancers [240]. In T-ALL, the hypoxic bone marrow niche is commonly infiltrated with rapidly proliferating T-cell lymphoblasts. A growing body of evidence indicates that the hypoxia present in the bone marrow microenvironment alters the activity of multiple clinically approved TKIs contributing to drug resistance [240]. Therefore, novel approaches that will identify drug candidates that effectively target leukemic cells in the hypoxic microenvironment are warranted.

We utilized the unique drug screening capabilities of the University of New Mexico Center for Molecular Discovery [241] to identify small molecule kinase inhibitors for drug repurposing in T-ALL. In addition to T-ALL cell lines, we performed drug sensitivity profiling using T-ALL primary samples and patient derived xenografts, which were maintained as monoculture in serum-rich media. We established a high throughput flow cytometry synthetic niche which mimics the low oxygen levels found in leukemic human bone marrow to assess leukemic cells for sensitivity against clinically approved inhibitors. We successfully identified inhibitors that were efficacious in normoxia as well as niche-mimicking conditions and which have not been used in modern T-ALL regimens. Our HTFC screening platform provides a rapid and convenient tool for the implementation of new therapeutic options and drug repositioning opportunities for suspension target cells such as leukemic blasts.

4.3 Material and Methods

4.3.1 Reagents

All reagents were purchased from Thermo Fisher Scientific (Waltham, MA) unless specified otherwise.

4.3.2 T-ALL cell lines

Human T-ALL cell lines (Loucy, ALL-SIL, Jurkat, CCRF-CEM) were purchased from DSZM-German Collection of Microorganisms and Cell cultures. CUTLL1 cell line was a generous gift from Dr. Ferrando at the Columbia University. The cells were cultured in RPMI-1640 medium supplemented with 10% FBS, 2mM L-glutamine and 100 U/ml penicillin G in a 5% CO₂ incubator at 37°C.

4.3.3 T-ALL patient samples and patient derived xenografts (PDX)

Cryopreserved primary samples were obtained from patients enrolled in Children's Oncology Group T-ALL trial AALL0434 and/or the University of New Mexico Health Sciences Center. All patients or their parent(s)/guardian(s) provided written, informed consent for future research in accordance with the Declaration of Helsinki and local institutional human research guidelines. The Institutional Animal Care and Use Committee approved the animal studies. Characteristics of patient derived xenografts (PDX) are listed in **Appendix B, Table S4.1**. PDX were established by injecting 1-2 x 10⁶ cells via tail vein into non-obese diabetic/severe combined immunodeficiency NOD.Cg-Prkdc^{scid}Il2rg^{tm1Wjl}/SzJ mice. Leukemia engraftment was

assessed by flow cytometry analyses of peripheral blood with fluorescent labeled anti-human APC-CD45+ and anti-mouse BV21-CD45+ antibody (BD Biosciences, San Jose, CA). Leukemic cells were purified via centrifugation in Ficoll-Paque/Percoll density gradient (GE Healthcare, Piscataway, NJ). The cells were preserved with freezing medium (90% FBS, 10% DMSO) and stored in liquid nitrogen. PDX samples were used at low passage up to 3 to limit the effect of mouse positive selection on PDX divergence from the original tumor sample. The cells were thawed and rested for ~4 hours at 37°C in complete RPMI-1460 medium supplemented with 2mM L-glutamine, 10% FBS, 10% human AB serum (Sigma-Aldrich, St. Louis, MI), 50 ng/ml SCF (Peprotech, Rocky Hill, NJ), 20 ng/ml Flt3L (Peprotech), 10 ng/ml IL7 (Peprotech), and 116 ng/ml insulin (Sigma-Aldrich).

4.3.4 Compounds

We investigated several drug classes, including: TKIs ($n = 26$), cyclin dependent kinase inhibitors ($n = 2$; alvocidib and palbociclib), Hedgehog signaling inhibitor ($n = 1$; vismodegib) and proteasome inhibitors ($n = 2$; bortezomib and carfilzomib), all purchased from LC Laboratories (Woburn, MA) (**Appendix B, Table S4.2**). The compounds were solubilized in DMSO (250 μ M for alvocidib, bortezomib and carfilzomib; 20 mM for vandetanib, 25 mM for all others) and stored frozen at -80°C.

4.3.5 High Throughput Flow Cytometry Viability Testing

An Echo® 555 Liquid Handler (Labcyte, San Jose, CA) was used both to create intermediate source plates and to add inhibitors to assay plates. The HTFC assays were conducted in 384-well Greiner Bio-One 784201 polypropylene plates (Monroe, NC). The thirty-one drugs were added to the plates to generate 10-point dose responses, with assay final DMSO concentration at <1%. Each compound was tested at clinically relevant concentration range (0.005–100 μ M except for bortezomib and carfilzomib that were tested at 0.05–1000 nM) (**Appendix B, Table S4.1**). The cells were resuspended in fresh media and 15 μ L was added to wells with a Biotek Multiflo system (Winooski, VT). The cell lines were tested at 5000 cells per well, and the primary samples were tested at 4500-6000 cells per well. The assay plates were incubated in a humidified atmosphere at 37°C and 5% CO₂. The hypoxic incubation, 1% O₂, was achieved in a Cytomat™ 24 C 10 (ThermoFisher, Waltham, MA). The assay plates were covered with polystyrene lids for the first 24 h of incubation and sealed with a PlateLoc Thermal Microplate Sealer (Agilent, Santa Clara, CA) for the remainder of the incubation. Plates from normoxic conditions were flushed with ambient air for 1.2 sec prior to sealing, and those from hypoxic conditions were flushed with 100% N₂. Three replicate experiments were performed for the cell lines, which were incubated for 72 hr. Due to the limited availability of primary samples, those experiments were done in single replicates, but with multiple plates to allow for 48 and 72 h incubations. On average, eight 384-well plates (3072 wells) were analyzed per day. With continuous round-the-clock automation, we have the

potential to analyze ~ 100 x 384 or 1536 well plates per day, but our throughput was based on the availability of cells and primary samples.

The cell viability assay was performed as previously described [11]. Briefly, 5 μ L of propidium iodide (PI; Sigma-Aldrich, St. Louis, MO) was added to all wells of the assay plates to a final concentration of 0.75 μ g/mL. The plates were then incubated on rotators at 4°C for 20-45 min. The HTFC data were collected with a HyperCyt® platform (IntelliCyt, Albuquerque, NM) configured to an Accuri C6 Plus flow cytometer (BD Biosciences, Franklin Lakes, NJ). The data were analyzed with HyperView software (IntelliCyt). The samples were gated on forward and side scatter to isolate the cell populations, and a binary gate was used on the histograms for fluorescence in the FL-3 channel to distinguish PI positive and negative populations.

4.3.6 Data analysis

The data were normalized to the mean viability from negative control wells = 100% viability for inhibitor-treated samples. GraphPad Prism 7 software (La Jolla, CA) was used to plot and fit the data. Half-maximal effective concentration (EC_{50}) values were calculated based on least squares fit of the data to a four-parameter sigmoidal dose response curve. EC_{50} values are only reported for compounds that yielded a maximum response values of 20% or greater. For EC_{50} values calculated to be beyond the concentration range tested and for those samples which yielded maximal responses < 20% ,they are reported as “>100 μ M”. The hypoxia cytotoxicity ratio (HCR) was determined for each drug and cell line as $EC_{50}^{normoxia}/EC_{50}^{hypoxia}$. For

each cell line and compound, the HCR from independent experiments were compared with a two-tailed paired *t*-test.

4.4 Results and Discussion

4.4.1 Drug sensitivity screening in T-ALL cell lines

To determine the sensitivity of T-ALL cells to tyrosine kinase pathway inhibition in T-ALL, we compiled a library of 26 FDA-approved TKIs with clinically proven efficacy against multiple tyrosine kinases including, PDGFR, VEGFR, EGFR, ALK, *etc.* (**Appendix B, Table S4.2**). Due to growing interest in kinases that regulate cell cycle, we also added two cyclin dependent kinase inhibitors: alvocidib, targeting CDK7/CDK9 (under clinical development), and the FDA-approved CDK4/6 inhibitor, palbociclib. Our drug panel also included vismodegib, a Hedgehog pathway inhibitor, which was recently reported as a novel therapeutic option for T-ALL [242]. Because bortezomib, a reversible inhibitor of 26S proteasome has been introduced into clinical trials in relapsed/refractory T-ALL (NCT02112916), we used bortezomib as a reference and also added a second generation, non-reversible proteasome inhibitor, carfilzomib, to our screening library.

Drug sensitivity screening of five T-ALL cell lines revealed a differential response to the compounds tested under normoxia conditions (**Figure 4.1**). Despite the heterogeneity of the inhibitor responses, all the cell lines demonstrated high sensitivity to six kinase inhibitors: afatinib, axitinib, crizotinib, ponatinib and sunitinib, which induced cytotoxic responses of $EC_{50} \leq 10 \mu M$ and alvocidib ($EC_{50} \leq 1$

μM) after 72 h incubation (**Figure 4.1A,C; Appendix B, Table S4.3**). Interestingly, alvocidib was the most efficacious among all the tested kinase inhibitors, with demonstrated cytotoxic activity at $\text{EC}_{50} \leq 1 \mu\text{M}$ across all the cell lines. In addition, the proteasome inhibitors bortezomib and carfilzomib were also effective against all T-ALL cells at nanomolar concentration range ($\text{EC}_{50} \leq 1 \mu\text{M}$). Another six inhibitors (bosutinib, cabozantinib, ceritinib, dasatinib, erlotinib and lapatinib) were efficacious in at least three out of five cell lines tested ($\text{EC}_{50} \leq 10 \mu\text{M}$) (**Figure 4.1A; Appendix B, Table S4.3**). The remaining compounds were less potent ($\text{EC}_{50} > 10 \mu\text{M}$), showing selectivity against a single T-ALL cell line (e.g., vandetanib, $\text{EC}_{50} = 3.4 \mu\text{M}$ in Loucy cells) or did not induce a significant response in the tested cells.

To further delineate the cytotoxic activity of kinase inhibitors, we determined the maximum response of each drug at the highest tested dose (100 μM for each inhibitor except for alvocidib, bortezomib and carfilzomib, for which the highest tested dose was 1 μM). As seen in **Figure 4.1B**, most of the tested agents effectively eradicated leukemic cells at the highest tested concentration, indicating that their cytotoxic activity increases substantially as the maximum tested dose was approached.

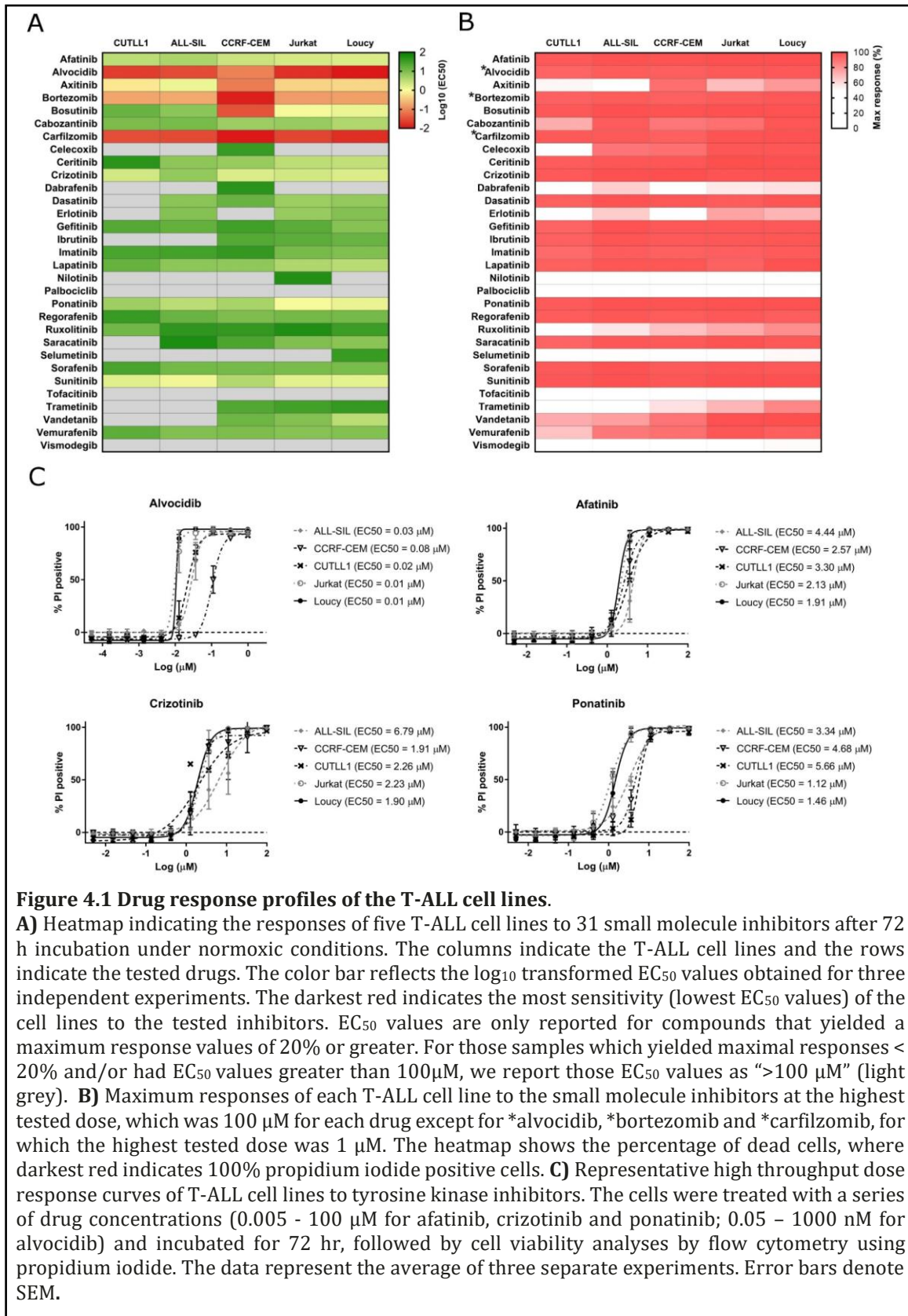


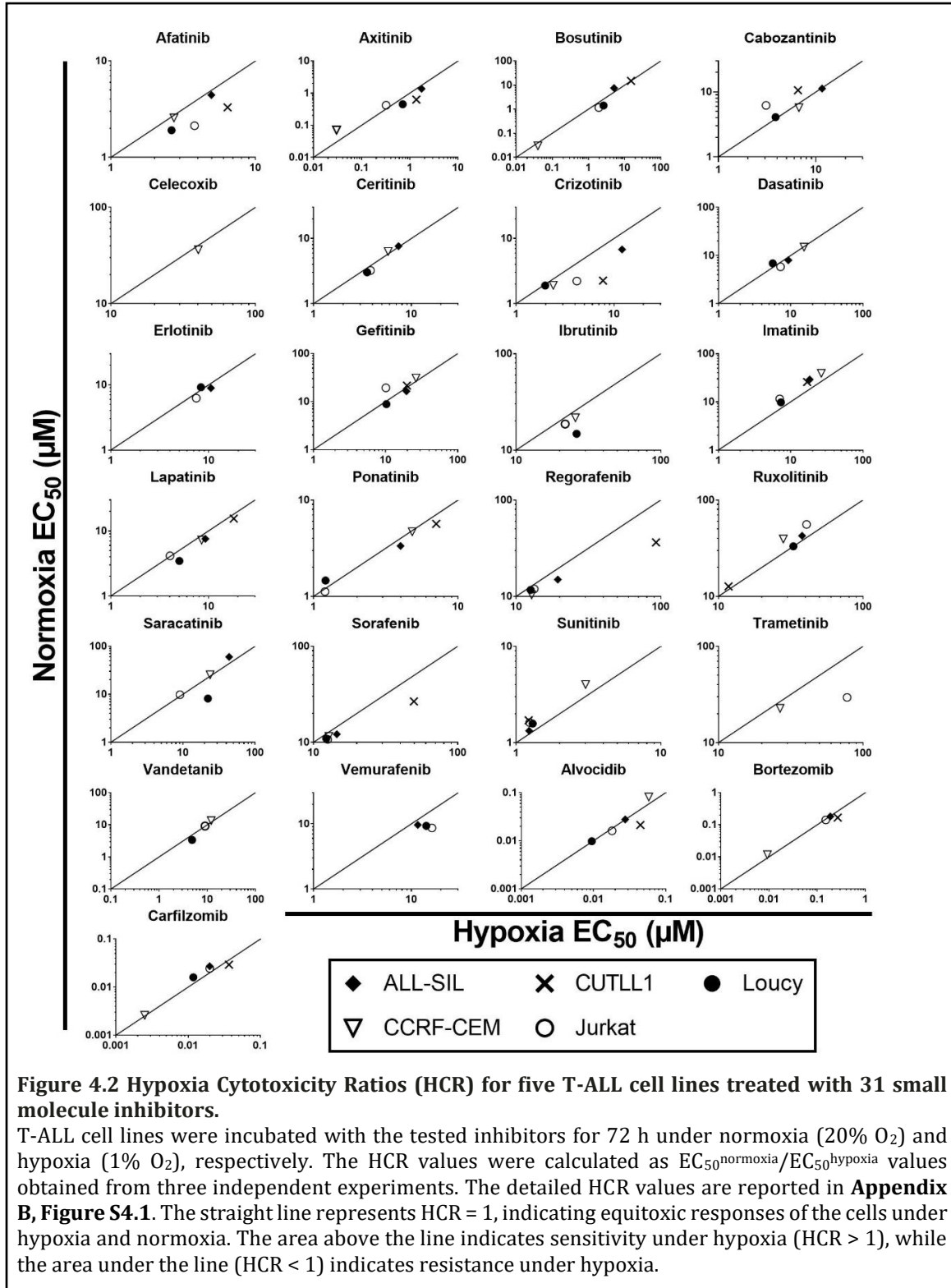
Figure 4.1 Drug response profiles of the T-ALL cell lines.

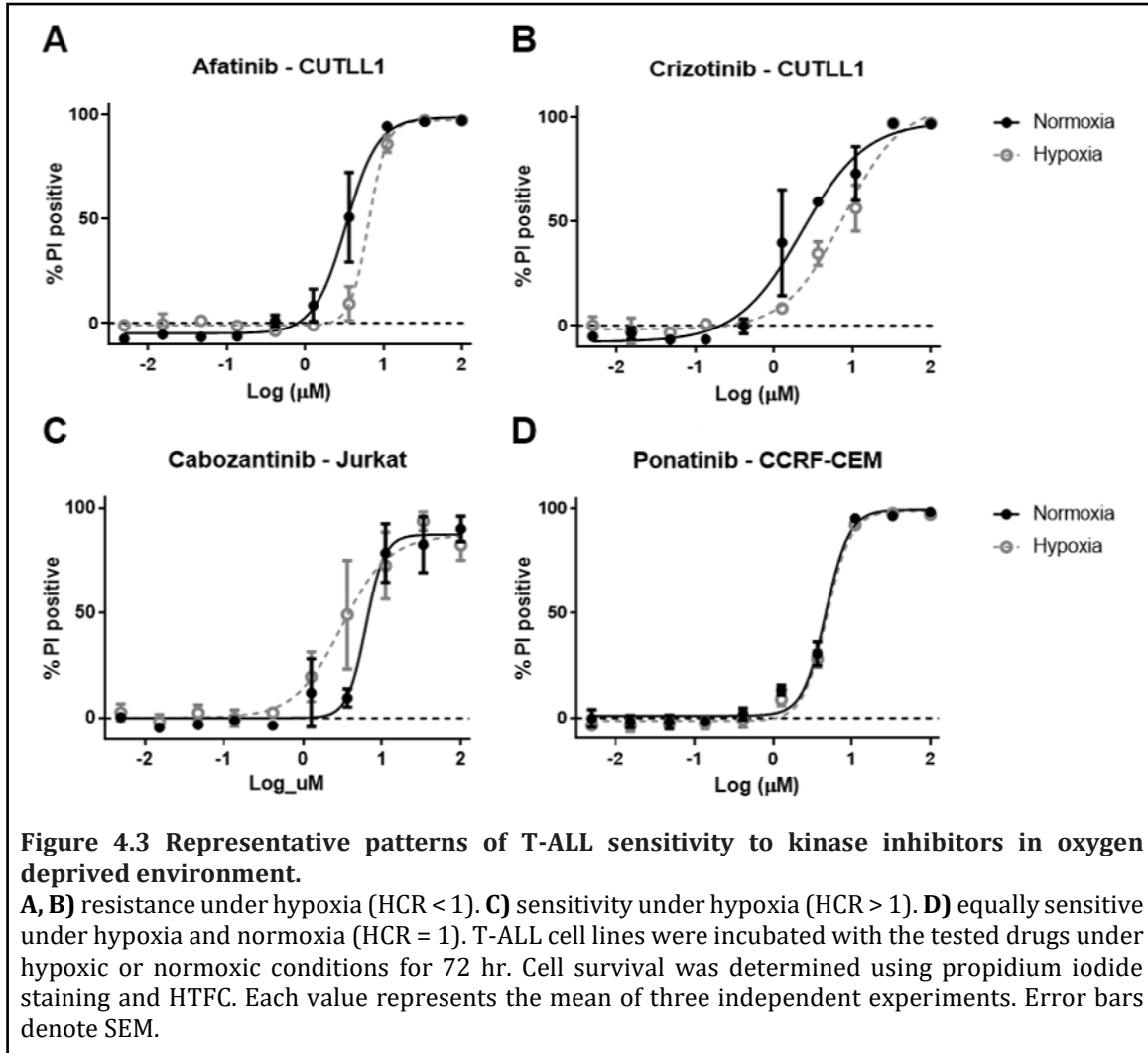
A) Heatmap indicating the responses of five T-ALL cell lines to 31 small molecule inhibitors after 72 h incubation under normoxic conditions. The columns indicate the T-ALL cell lines and the rows indicate the tested drugs. The color bar reflects the \log_{10} transformed EC₅₀ values obtained for three independent experiments. The darkest red indicates the most sensitivity (lowest EC₅₀ values) of the cell lines to the tested inhibitors. EC₅₀ values are only reported for compounds that yielded a maximum response values of 20% or greater. For those samples which yielded maximal responses < 20% and/or had EC₅₀ values greater than 100 μM, we report those EC₅₀ values as “>100 μM” (light grey). **B)** Maximum responses of each T-ALL cell line to the small molecule inhibitors at the highest tested dose, which was 100 μM for each drug except for *alvocidib, *bortezomib and *carfilizomib, for which the highest tested dose was 1 μM. The heatmap shows the percentage of dead cells, where darkest red indicates 100% propidium iodide positive cells. **C)** Representative high throughput dose response curves of T-ALL cell lines to tyrosine kinase inhibitors. The cells were treated with a series of drug concentrations (0.005 - 100 μM for afatinib, crizotinib and ponatinib; 0.05 - 1000 nM for alvocidib) and incubated for 72 hr, followed by cell viability analyses by flow cytometry using propidium iodide. The data represent the average of three separate experiments. Error bars denote SEM.

Since first described by Coustan-Smith *et al.*, patients with early T-cell precursor phenotype (ETP-ALL) have received much attention for their increased risk for relapse [243]. In our study, Loucy cells, which show a transcriptional program related to ETP-ALL, were highly sensitive to the tested drugs similar to the other four more differentiated T-ALL cell lines (**Figure 4.1; Appendix B, Table S4.3**). Our results identify attractive kinase inhibitor candidates and suggest that kinase inhibitors might be promising targeted therapies, and are worthy of further exploration as potential treatment options in T-ALL.

4.4.2 Hypoxia cytotoxicity ratio (HCR) in T-ALL cell lines

To test whether hypoxia modulates the activity of the tested compounds, we performed drug sensitivity profiling in T-ALL cell lines under hypoxia (1% O₂). The results were integrated with the data obtained for the cells incubated in normoxic conditions (20% O₂) as described above. The hypoxia cytotoxicity rate (HCR) for the T-ALL cell lines ($n = 5$) treated with inhibitors for 72 h are presented in **Figures 4.2-4.3** and **Appendix B, Figure S4.1**. Here we demonstrate that hypoxia can induce differential responses in T-ALL cells exposed to clinically approved kinase inhibitors.





Unexpectedly, most of the tested inhibitors were generally equipotent under hypoxic and normoxic conditions (HCR = 1; arbitrarily set to 0.8-1.2). However, specific patterns of drug response indicative of increased sensitivity under hypoxia (HCR >1.2) or decreased sensitivity under hypoxia (HCR <0.8) were also observed (**Figures 4.2-4.3; Appendix B, Figure S4.1**). Interestingly, imatinib was preferentially more efficacious under hypoxia in all the tested cell lines (HCR 1.33 - 1.63). Sensitivity to ruxolitinib and sunitinib was also elevated under hypoxic conditions in at least three

out of five T-ALL cell lines. Nevertheless, several of the tested compounds including, afatinib and crizotinib, were more active in normoxia (three cell lines or more), suggesting decreased sensitivity under hypoxia (**Figures 4.2-4.3; Appendix B, Figure S4.1**). We have not observed any specific pattern of response among the tested drugs and cell lines since all three patterns of drug response could be observed in many cases. For example, axitinib was less potent under hypoxia in CUTLL1 (HCR = 0.46), Loucy (HCR = 0.62) cells, but its antitumor activity was increased under hypoxia in CCRF-CEM (HCR = 2.11) and Jurkat (HCR = 1.30) cells (**Figure 4.2, Appendix B, Figure S4.1**). Our EC₅₀ results indicate that despite distinct HCR values for individual drugs, the majority of the kinase inhibitors were equally sensitive or marginally less active under hypoxia conditions in the tested T-ALL cell lines. This was consistent with the observation of reduced cell survival at the maximum tested dose under hypoxia (**Appendix B, Figure S4.2**). The results of our study indicate that hypoxic T-ALL cells are highly responsive to kinase inhibitors and should be further investigated in the context of hypoxia sensitive therapies in T-ALL. Further studies will be required to determine the effects of other tumor microenvironment factors such as adhesion molecules or extracellular matrix components on drug sensitivity in leukemia. Our results underscore the potential importance of hypoxia testing in drug profiling studies and provide compelling evidence for the application of HTFC to search for hypoxia selective drug candidates.

4.4.3 Drug sensitivity screening in T-ALL primary samples and PDX

With evidence that kinase inhibitors are effective against T-ALL cell lines, we next utilized our platform to evaluate drug sensitivity in T-ALL primary samples ($n = 2$) and patient derived-xenografts ($n = 5$). Primary tissue is often considered a limiting factor in high throughput studies, which require a high number of cells. In this study, we utilized PDX models of T-ALL, which were shown to better preserve both the genomic integrity and the tumor heterogeneity observed in patients [244]. Therefore, PDX models are proposed as an attractive alternative strategy for drug profiling studies when sufficient primary tissue is not available. We tested a small set of T-ALL samples for which phenotypic and genomic data were available (**Appendix B, Table S4.1**). Patient and PDX samples were subjected to high-throughput flow cytometry screening for sensitivity to 31 small molecule inhibitors under conditions described in Material and Methods. Untreated cells demonstrated excellent cell viability in serum-rich monoculture, which varied between 70-95% up to 72 h incubation (**Appendix B, Table S4.4**), which was comparable to the viability of the T-ALL cell lines.

We observed that the sensitivity of T-ALL cells to kinase inhibitors was heterogeneous but also sample-dependent (**Figure 4.4**). Primary cells and PDX models were less sensitive to kinase signaling inhibition compared to the cell lines (**Figures 4.1, 4.4**). This is consistent with previous studies showing that primary samples or relevant PDX are more resistant, and often respond differently, to investigational agents in comparison to cell lines [6, 245]. T-ALLs with ETP phenotype

and/or harboring *MLLT10* and/or *KMT2A* gene rearrangements are slowly proliferating leukemias, which often present stem-like features. PDX obtained from such patients were included in our sample set (**Appendix B, Table S4.1**). Cell stemness and a low proliferation rate may affect cellular responses to drugs whose cytotoxic activity relies on the proliferative activity of the leukemic cells. Such differences in cell proliferative activity may also affect engraftment kinetics [244]. In our study, PASGJG, which was insensitive to the tested inhibitors, engrafted more slowly than PATZZM or PASNXS, which were more sensitive to the tested agents (data not shown). Secondly, we observed that the primary specimens (12-089 and 15-093) had an overall better response to kinase inhibitors compared to PDX (**Figure 4.4B**). This interesting observation needs to be further explored, considering the relatively small sample size in our study. Recent data indicate that PDX maintain oncogenic translocations and preserve ~75% of the genomic lesions initially identified in patients [244]. However, PDX undergo mouse-specific tumor evolution, which is comparable to that of cell lines, but still may affect drug response [246].

Among the PDX samples, PATRAP and PATZZM were more sensitive to the tested drugs than PASNXS (**Figure 4.4**). PASGJG and PASSPP were resistant to all the tested inhibitors, suggesting that some T-ALL samples demonstrate high resistance to kinase signaling inhibition, which can be associated with kinome reprogramming and/or adaptive bypass response leading to drug resistance [247]. This may also be related to the genetic and molecular features of the tested cells. Some of our PDX models were developed from samples that harbor genomic lesions e.g. *KMT2A* gene

rearrangements, which are associated with high-risk and refractory disease (Appendix B, Table S4.1) [232, 248].

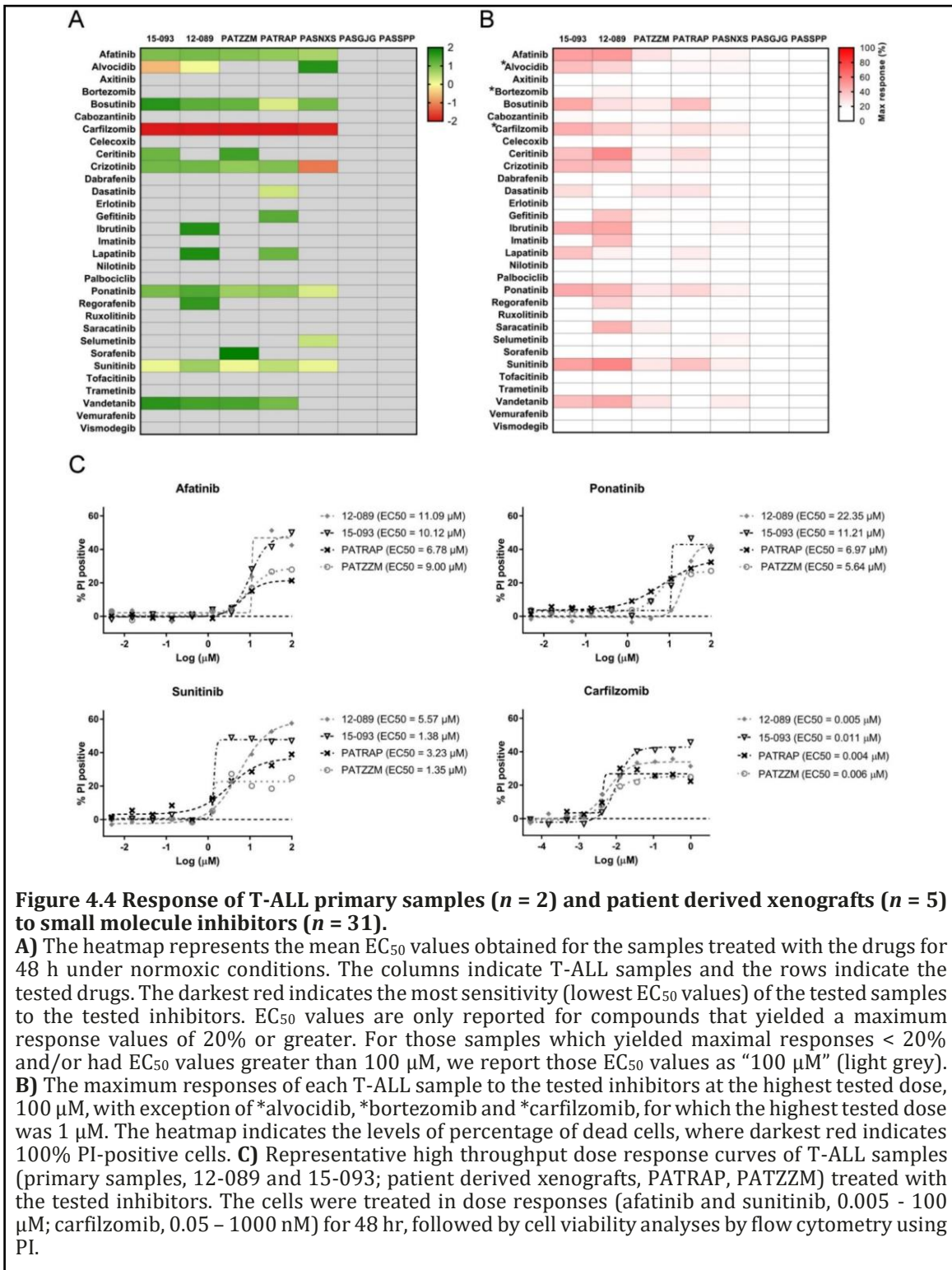


Figure 4.4 Response of T-ALL primary samples ($n = 2$) and patient derived xenografts ($n = 5$) to small molecule inhibitors ($n = 31$).

A) The heatmap represents the mean EC₅₀ values obtained for the samples treated with the drugs for 48 h under normoxic conditions. The columns indicate T-ALL samples and the rows indicate the tested drugs. The darkest red indicates the most sensitivity (lowest EC₅₀ values) of the tested samples to the tested inhibitors. EC₅₀ values are only reported for compounds that yielded a maximum response values of 20% or greater. For those samples which yielded maximal responses < 20% and/or had EC₅₀ values greater than 100 μM, we report those EC₅₀ values as "100 μM" (light grey). **B)** The maximum responses of each T-ALL sample to the tested inhibitors at the highest tested dose, 100 μM, with exception of *alvociclib, *bortezomib and *carfilzomib, for which the highest tested dose was 1 μM. The heatmap indicates the levels of percentage of dead cells, where darkest red indicates 100% PI-positive cells. **C)** Representative high throughput dose response curves of T-ALL samples (primary samples, 12-089 and 15-093; patient derived xenografts, PATRAP, PATZZM) treated with the tested inhibitors. The cells were treated in dose responses (afatinib and sunitinib, 0.005 - 100 μM; carfilzomib, 0.05 - 1000 nM) for 48 hr, followed by cell viability analyses by flow cytometry using PI.

Interestingly, several samples demonstrated decreased sensitivity at 72 h compared to 48 hr, which might be related to the heterogeneous and clonal architecture of the tested samples, and/or induction of spontaneous cell death, and/or induction of quiescence in some cell subpopulations of T-ALL (**Figure 4.4; Appendix B, Figure S4.3**). Sensitivity to afatinib and sunitinib ($EC_{50} \leq 10 \mu\text{M}$) was detected in five out of seven tested T-ALL samples (~70% samples) after 48 h incubation (**Figure 4.4, Appendix B, Table S4.5**). Bortezomib, which is currently being tested in the COG AALL1231 clinical trial (NCT02112916), had no activity in the tested cells (the highest concentration tested was $1\mu\text{M}$), compared to carfilzomib, the second generation proteasome inhibitor that was highly efficacious ($EC_{50} \leq 1 \mu\text{M}$) in the T-ALL patient samples and PDX (five out of seven samples) (**Figure 4.4A,C, Appendix B, Table S4.4**). In addition, ponatinib and crizotinib were efficacious against at least three out of seven samples (~42%), with the lowest EC_{50} values observed for PASNXS (ponatinib, $EC_{50} = 1.92 \mu\text{M}$; crizotinib, $EC_{50} = 0.69 \mu\text{M}$) (**Figure 4.4A; Appendix B, Table S4.5**). Strikingly, selumetinib was uniquely selective against PASNXS ($EC_{50} = 2.70 \mu\text{M}$) while dasatinib was preferentially effective in PATRAP ($EC_{50} = 2.43 \mu\text{M}$) (**Figure 4.4; Appendix B, Table S4.5A**). The analyses of the maximum responses of the tested inhibitors at the highest concentration tested further revealed the high heterogeneity of the drug responses (**Figure 4.4B**). Although the patient and PDX samples were overall less sensitive to the tested drugs compared to the cell lines, similar trends of drug response were observed (**Figures 4.1B, 4.4B**). With a few exceptions (*e.g.* axitinib, erlotinib), the inhibitors which were

found to be the most potent against T-ALL cell lines, induced a decrease in T-ALL cell survival at the highest tested concentration across the majority of the samples (*e.g.* afatinib, ponatinib, sunitinib). In addition, we investigated the sensitivity of normal peripheral blood mononuclear cells to the tested inhibitors. We found that the most potent inhibitors were also cytotoxic towards normal cells, indicating that they were not specific to leukemic cells (**Appendix B, Figure S4.5**).

Our observation that several T-ALL samples were generally more susceptible to multiple kinase inhibitors (**Figure 4.4**) strongly supports the rationale for targeting the deregulated kinome in T-ALL. However, it is worth noting that most of the tested samples were highly selective towards one or a few specific inhibitors, suggesting that high-throughput drug screening may rapidly detect unique sensitivities of individual patient cells to the tested drugs [236]. Our data underscore the roles of personalized medicine in the development of modern therapies in T-ALL.

Recently, two independent reports implicated dasatinib as a novel targeted therapy in a subset of T-ALL [244, 245]. While dasatinib was effective against our tested T-ALL cell lines, only one T-ALL sample was preferentially sensitive to this inhibitor in our study (**Figures 4.1 and 4.4**). Interestingly, there were other promising inhibitors that demonstrated greater activity against T-ALL cells than dasatinib, and are worthy of further investigation (**Figures 4.1, 4.4**). One interesting observation in this study was sensitivity to cyclin dependent kinase inhibition. Alvocidib (CDK7/CDK9 inhibitor), which is currently under development as a

combination therapy for AML (NCT01349972, NCT02520011)[249], was efficacious against T-ALL cell lines and some patient samples (**Figures 4.1, 4.4**).

The results of our study also indicate that T-ALL cells show good response to several TKIs, which target multiple kinases including PDGFR, VEGFR (ponatinib, sunitinib, axitinib), EGFR (afatinib), ALK (ceritinib, crizotinib) (**Figures 4.1, 4.4**). Although preliminary, these findings provide a foundation for future studies on targeting the T-ALL kinome by FDA-approved multi-target inhibitors. It will be critical to test active agents in murine models of T-ALL, either genetically engineered or injected with PDX.

Overall, our analyses show that T-ALL samples were less sensitive than the cell lines. Importantly, our approach includes culturing T-ALL primary samples and PDX at 10% FBS and 10% human AB serum concentration. Serum may sequester drugs via their binding to serum proteins and therefore limit their cytotoxic response. Furthermore, the growth factors present in the culture medium may accelerate pro-survival signaling as opposed to serum-free culturing systems, which may affect cell metabolism and eventually sensitize the cells to the tested agents. Taking this into account, it would be critical to establish the minimum levels of serum facilitating drug response profiling without compromising cell viability in our monoculture systems. We successfully utilized a conditioned medium from stromal cells to maintain the viability of B-ALL cells in our previous reports [6]. Frismantas *et al.* [244] have recently reported serum free co-cultures of PDX and/or primary cells on hTERT-immortalized mesenchymal stroma cells as a novel strategy to facilitate the survival

of ALL cells, including T-ALL. The authors postulated that stromal co-cultures are better predictors of drug response in the context of *in vivo* validation studies. Still, they were able to demonstrate a significant correlation between both serum-free co-culture and serum-supplemented monoculture systems.

The results of this study demonstrate that a flow cytometry-based PI screen can be effectively used in HTFC to identify small molecule inhibitors as a targetable therapy in T-ALL. Common plate reader-based viability assays, such as MTT and CellTiter Glo, require cell lysis, and thus provide only one metric from a treated sample. In contrast, a flow cytometry approach with PI allows for rich information to be collected from a treated sample in addition to simple viability assessments. Flow cytometry enables particle count and analysis of a sample on a cell-by-cell basis, and hence, drug effects within a heterogeneous population may be determined (**Appendix B, Figure S4.4**). The PI assay used here provided phenotypic analysis of the TKI-treated T-ALL cells. Our data suggest that primary patient samples can be screened within 72 hours and yield results that may inform personalized therapies with the potential to compare drug activity on PBMC (**Appendix B, Figure S4.5**) and patient samples (**Figure 4.4**) to circulating drug levels (**Appendix B, Table S4.2**) (See, for example, the potential of sunitinib to provide a therapeutic window between PBMC and patient sample with an achievable dose). Thus, our approach provides a reproducible tool for functional screening and novel therapeutics.

4.5 Acknowledgements

We would like to acknowledge the Shared Flow Cytometry Resource, Animal Resource Facility and the Animal Models Shared Resource at the UNM Comprehensive Cancer Center. Material was provided in part by the Children's Oncology Group (AALL15B1-Q to KMW). We apologize all authors whose work could not be cited due to space constraints. This project was supported in part by the National Center for Research Resources and the National Center for Advancing Translational Sciences of the NIH through Grant number 8UL1TR000041, and by the National Cancer Institutes and the Cancer Center Support Grant through Grant Number P30CA118100. Other grant support: Dedicated Health Research Funds from the University of New Mexico School of Medicine (KMW). DRP was supported by funding from NIH Minority Institutional Research Training Program Award T32 HL007736. SPH has received honoraria from Jazz pharmaceuticals, Spectrum Pharmaceuticals and Erytech, and consulting fees from Novartis.

CHAPTER 5: High-throughput flow cytometry (HTFC) drug combination discovery with novel synergy analysis software, SynScreen

Dominique R Perez^{1,2}, Bruce S Edwards^{1,2,3‡}, Larry A Sklar^{1,2,3‡}, Alexandre Chigaev^{1,2,3‡*}

¹ Department of Pathology, ² Center for Molecular Discovery, Health Sciences Center, University of New Mexico Albuquerque, NM

³ University of New Mexico Comprehensive Cancer Center, Albuquerque, NM

‡ B.S.E., L.A.S. and A.C. contributed equally

SLAS Discovery. 2018 Aug 23 (7):751-760.

doi: 10.1177/2472555218775913 PMID: 29842834

5.1 Abstract

Classical therapeutic regimens are subject to toxicity, low efficacy, and/or the development of drug resistance. Thus, the discovery of synergistic drug combinations would permit treatment with lower, tolerable dosages of each agent and restored sensitivity. We describe the development and use of the SynScreen software application, which allows for visual and mathematical determinations of compound concentrations that produce super-additive effects. This software uses non-linear

regression fits of dose-responses to determine synergism by the Bliss independence and Loewe additivity analysis models. We demonstrate the utility of SynScreen with data analysis from *in vitro* HTFC combination screens with repurposed drugs and multiplexed synergy analysis of multiple biologic parameters in parallel. The applicability of SynScreen was confirmed by testing open-source data sets used in published drug combination literature. A key benefit of SynScreen for high-throughput drug combination screening is that observed measurements are graphically depicted in comparison to a three-dimensional surface that represents the theoretical responses at which Bliss additivity would occur. These images and summary tables for the calculated drug interactions are automatically exported. This allows for substantial data sets to be visually assessed, expediting the quick identification of efficacious drug combinations, thereby facilitating the design of confirmatory studies and clinical trials.

5.2 Introduction

Drug discovery research is progressively moving toward the identification of combinations which interact synergistically by both targeted and unbiased screening approaches. There are multiple motivations for pursuing these efforts. The predominant paradigm is that drug combinations could decrease the incidence of refractory and resistant disease responses to treatment. Off-patent and generic drugs may be repurposed for use in combinations to elicit responses more favorable than their use individually. Recent studies have illustrated the advantages of multi-

targeted drug combinations that do not have synergistic interactions [250]. However, synergistic drug interactions could potentially reduce the dosages and duration of treatment required for therapeutics with adverse side effects. Furthermore, some hypothesize that the nature of targeted drug interactions may provide an indication of potential crosstalk between biological pathways [251, 252]. The experimental designs for drug combination studies are fairly straightforward. In these strategies, drugs are tested with concentrations in fixed or non-fixed ratios, and the latter approach may be expanded into matrix or factorial arrays. The analysis of drug combinations used simultaneously or sequentially may provide contradicting outcomes, the results of which could provide insight into the mechanistic nature of the drug interactions.

Drug interactions with respect to synergy are generally determined by the following methods: Highest Single Agent (also referred to as Gaddum non-interaction effect)[253], Bliss independence model [254], and Loewe additivity model [255], an application of which is the median effect analysis developed by Chou-Talalay [256]. Additionally, combination data may be compared to single agent dose-responses by isobolograms, combination thresholding, curve shift analyses, or by zero-interaction potency [257, 258]. There are both benefits and disadvantages for each model, and therefore it is practical to use multiple analyses to reliably determine synergism. For in-depth descriptions of these models, their advantages and constraints, please see the review by Fouquier and Guedj [257].

While technology has allowed for HTFC screening of vast, multiple drug combination testing, there are few resources that facilitate the assessment of high throughput (HT) results, thus creating a bottleneck for the validation of drug interaction data toward preclinical studies. There is currently a myriad of free (Combenefit [259], CompuSyn [260], MixLow [261]) and commercial (CalcuSyn, Chalice™, Genendata Screener®) software available for drug combination analysis. Please refer to Table 1 in Di Veroli, *et al.* [259] Fortunately, most such applications provide analyses by multiple means. However, one limitation of evaluating HT drug combination data is due to the means by which the data are displayed, typically in tables or two-dimensional graphs [262, 263]. The visualizations of such drug combination analyses are unintuitive, and require thoughtful assessment prior to the determination of specific compounds and concentrations that will be pursued in confirmatory assays. This is especially problematic for drug combinations tested in matrices, wherein some of the breadth of the results can be lost with two-dimensional representations. Consequently, response surface approaches have proven useful to display results of matrix combination testing [258]. Nonetheless, many of these common methods require that the user view single agent or predicted non-interaction responses separately from observed drug interaction data.

Here, we introduce a novel application for drug combination analysis that is especially utile for the implementation of HTFC data, SynScreen (<https://github.com/bestwards/FlowProg>). An unlimited amount of normalized assay data from single or multiple screening runs can be imported and analyzed by

multiple drug interaction models. The results are plotted in real-time and provide three-dimensional simultaneous visualizations of both observed single and combination drug responses in comparison to a response surface that corresponds to a theoretical threshold of additivity. These graphics are automatically exported, and can be collated to allow for the quick assessment of synergy, thus expediting the process of triaging hit drug combinations for further confirmatory assays.

5.3 Materials and Methods

5.3.1 Development of the SynScreen application

SynScreen was implemented as a graphical user interface (GUI) package to be used within MATLAB software (Mathworks, Natick, MA). A copy of the software will be available from the authors on request.

5.3.1.1 Data normalization and curve fitting

Two models were used to evaluate the possibility that a combination of two compounds resulted in a response that was additive, greater than additive (synergistic) or less than additive (antagonistic). Both models rely upon nonlinear curve fits to dose-response data produced by single compounds.

First, response data were normalized to controls such that the negative control produced the minimum response (e.g., 0% cytotoxicity in presence of DMSO-containing diluent alone) and the positive control represented the expected maximal response (e.g., 100% cytotoxicity):

$$\text{normalized fa} = (\text{DRUGXfa} - \text{ncntrlfa}) / (\text{pcntrlfa} - \text{ncntrlfa})$$

in which DRUGXfa, ncntrlfa and pcntrlfa are the fractional responses observed in the wells containing test compound, negative controls and positive controls, respectively. Note that SynScreen assumes that the data will be normalized such that responses will increase with increasing compound concentration. If compounds are expected to inhibit the assay response then:

$$\text{normalized fa} = 1 - [(\text{DRUGXfa} - \text{ncntrlfa}) / (\text{pcntrlfa} - \text{ncntrlfa})]$$

Normalized responses < 0 were recoded as 0 prior to curve fitting.

Curves were fitted with MATLAB software using non-linear least squares regression in a sigmoidal dose-response model, the four parameter logistic equation, in which the top, bottom and slope of the fitted curve were allowed to vary.

5.3.1.2 Bliss Independence model calculations

The Bliss Independence model assumes that the effects of compounds are probabilistic processes in which the activity of each compound is independent of the other, but each contributes to a common result. The additive effects of two compounds are thus predicted by the equation:

$$\text{Blissfa} = \text{DRUG1fa} + \text{DRUG2fa} - \text{DRUG1fa} * \text{DRUG2fa}$$

in which DRUG1fa and DRUG2fa are the normalized fractional responses produced by compounds 1 and 2 acting as single agents (determined from curve fit equations) and Blissfa is the observed fractional response resulting from the two in combination. MATLAB software was used to create a three-dimensional surface representing the response predicted for each combination as if it was additive according to the Bliss Independence model. Responses to individual combinations projecting above the surface were considered greater than additive (potential synergy) and below the surface less than additive (potential antagonism). A global combination response parameter, the Bliss Beta coefficient, was also calculated as the slope of a linear least squares fit to the predicted (x-axis) vs. observed (y-axis) responses for all combinations. Data normalized as described above (response increasing with increasing compound concentration) will result in a Beta coefficient > 1 indicative of synergy, < 1 indicative of antagonism and equal to 1 indicative of additive effects. Curve fit statistics were also used to estimate a 95% confidence interval for the Bliss Beta coefficient.

5.3.1.3 Loewe Additivity model

The Loewe Additivity model assumes the dose equivalence principle in which, for a given response produced by a dose of compound 1, there is a dose of compound 2

that can produce the equivalent response. The model predicts the following relationship if the effects of two compounds are additive:

$$\text{DRUG1uM} / \text{DRUG1uMfa} + \text{DRUG2uM} / \text{DRUG2uMfa} = 1$$

in which DRUG1uM and DRUG2uM are the actual doses (uM) of compounds 1 and 2 used in combination, and DRUG1uMfa and DRUG2uMfa are the doses of compounds 1 and 2, when applied as single agents, that are required to attain the response produced by the combination. The latter two dose parameters are calculated using coefficients from the single agent dose-response curve fits. The sum of the two dose ratios is referred to as the combination index (CI). A CI < 1 is indicative of synergy and CI > 1 of antagonism. A CI = 1 is considered additive.

The Loewe Additivity model is best applied to compounds that produce dose-response curves with parallel slopes and equal individual response maxima. However, it is often the case that there will be a regime of combinations in which the response produced by the combination cannot be reproduced by the compounds when applied as single agents (e.g., when response maxima of either or both of the compounds are limiting). In such a case, a CI cannot be calculated and is designated as out of range (OOR). SynScreen displays the CI, as well as components of the CI calculation in the results table including doses used (DRUG1uM, DRUG2uM), single agent doses required to produce the observed combination response (DRUG1uMfa, DRUG2uMfa), and the dose ratio of each compound (DRUG1uMratio =

DRUG1uM/DRUG1uMfa, DRUG2uMratio = DRUG2uM/DRUG2uMfa) (**Appendix C, Table 5.1**). If any of these elements involves a value of DRUGXfa that is out of range it is given the OOR designation.

5.3.2 HTFC Assays and Data Collection

Unless otherwise noted, compounds and reagents were purchased from Sigma-Aldrich (St. Louis, MO). The leukemia cell lines U937 and RS4;11 were acquired from ATCC (Manassas, VA). These cell lines were cultured in RPMI-1640 medium supplemented with 2 mM L-glutamine, 100 U/mL penicillin-streptomycin and 10% heat-inactivated fetal bovine serum and incubated in a humidified atmosphere with 5% CO₂ at 37°C. Freshly-washed cells were resuspended in medium at 5x10⁵ cells/mL and used in 10 µL 384-well assays (final cell density = 5000/well). The HTFC cytotoxicity screen consisted of twenty-five drug combinations, composed of five previously-identified repurposed drugs [6] paired with five known chemotherapeutic agents, tested in 64-well matrix arrays. The apoptosis assay consisted of drug pairs tested in 9-point 1:1 and 1:2 fixed ratio dose responses. The drugs were added with the Echo® 555 Liquid Handler (Labcyte, San Jose, CA) into 384-well plates (Greiner Bio-One 784201, Monroe, NC) to a final DMSO concentration of 1%. To prevent excess evaporation and to optimize conditions, the assay plates were flushed with ambient air and sealed with a PlateLoc Thermal Microplate Sealer (Agilent, Santa Clara, CA) prior to incubation. The cytotoxicity plates were incubated for 48 h, and the apoptosis plates were incubated 2-24 h. The propidium iodide (PI) cell viability assay was

performed as previously described [11], and the MultiCyt Apoptosis Kit (IntelliCyt, Albuquerque, NM) was used according to the manufacturer's protocol. HTFC data were collected with a HyperCyt® platform (IntelliCyt) configured to an Accuri C6 Plus flow cytometer (BD Biosciences, Franklin Lakes, NJ). The .fcs data were resolved and annotated with HyperView software (IntelliCyt).

5.3.3 Preparation of Data for SynScreen Analysis

The preparation of data files for import into SynScreen is similar to methods used by most HTFC laboratories. After an HTFC assay, the data are exported in Flow Cytometry Standard (FCS) format and analyzed on the basis of air gap-dependent interruptions in the temporal flow of cells to identify the wells from which the cells were sampled [264]. Once the data are annotated for the contents and concentrations in each well, the observed response values are then normalized in comparison to responses recorded from cells in control wells. We generally normalize our data such that the mean %viability of cells in wells containing diluent alone (e.g., DMSO) for each assay plate = 100% viability for the compound-treated samples. The normalized data are organized in a Microsoft Excel spreadsheet containing four columns that describe the nature of the drugs and concentrations tested: 1) agent/combo IDs, 2) concentrations tested for DRUG1, 3) concentrations tested for DRUG2, and 4) response (*see Appendix C, Figure S5.1*). The spreadsheets were then imported into SynScreen and the data were analyzed as described below.

5.3.4 SynScreen Software Determination of Drug-Drug Interactions in HTFC Data

SynScreen analysis begins with entering the range of data within the spreadsheet file that is then imported into the software (**Appendix C, Figure S5.1**). The single agent data are automatically fit by nonlinear regression and analyzed, although the user should manually evaluate the dose-response curves to exclude outliers and ensure goodness of fits (**Figure 5.1A**). The dose-responses from single agents are visualized individually, and metrics for the data (total points), fit (r^2 value, slope, top, bottom), and EC_{50} are determined by the software and the tables are automatically exported (**Appendix C, Table S5.2**). Outliers may be selected and excluded from further analysis and the data output can be updated by the “UpdateSingles” button. The minFahit (%) box allows for a minimum response threshold to be set for the determination of synergy “hits” from the combination data, e.g., only data points in which 20% or more of cells respond to the drug combination are considered for the summaries of synergistic hits.

For each drug combination, a three-dimensional surface is generated based on the Bliss prediction of additivity from the single agent dose-responses (left panels of **Figure 5.1B,C**). Observed data for a combination are plotted, and either the average from repeated measures or all points from each run may be displayed. The three-dimensional graphs may be rotated within the application interface to allow for better viewing of the observed data. This is especially helpful for the visualization of data with efficacies below the Bliss surface. Moreover, SynScreen mathematically determines a global combination response parameter, the Bliss Beta coefficient,

calculated as the slope of a linear least squares fit to the predicted (x-axis) vs. observed (y-axis) responses for all combinations (right panels of **Figure 5.1B,C**). A Bliss Beta coefficient > 1 is indicative of synergy, < 1 indicative of antagonism and equal to 1 (black line in **Figure 5.1B,C**) indicative of additive effects. Curve fit statistics were also used to estimate a 95% confidence interval for the Bliss Beta coefficient (right panels of **Figure 5.1B,C**). Data points for single drugs and drug combinations can be reversibly excluded from the analysis in real time to evaluate, for example, effects of removing statistical outliers.

The analyzed data are automatically saved and exported by SynScreen. The images for each combination's three-dimensional response data and Bliss/ non-interaction threshold evaluations are exported as individual files. A summary .docx file is generated that contains statistics for all screened drug combinations contained in the imported data file, providing a basic overview of the number of synergistic data points determined by Bliss independence and combination index analyses (**Appendix C, Table S5.3**). This table provides an overview of all combinations analyzed in a data set, and facilitates the identification and ranking of drug pairs and their resultant interactions from a screen. Furthermore, for each drug combination, SynScreen tabulates metrics for all potentially synergistic data points, and it annotates: 1) the method(s) by which synergism was determined (Bliss and/or combination index); 2) the doses of each agent which interacted synergistically; 3) the differences between the observed effects and theoretical values for Bliss additivity; 4) the ratio of the concentration used in a combination relative to the single

agent concentration that elicited the same response; and 5) indications of combinations for which the Loewe Additivity model CI is not applicable due to combination responses out of range (OOR) relative to single agent dose-response curve fits (see *Methods*, **Table 5.1**, **Appendix C**, **Table S5.4**). For each drug pair, SynScreen automatically creates .docx files containing the data response graph and a table with the aforementioned metrics for each data point tested, as well as .jpg files of the three-dimensional and Bliss threshold plots.

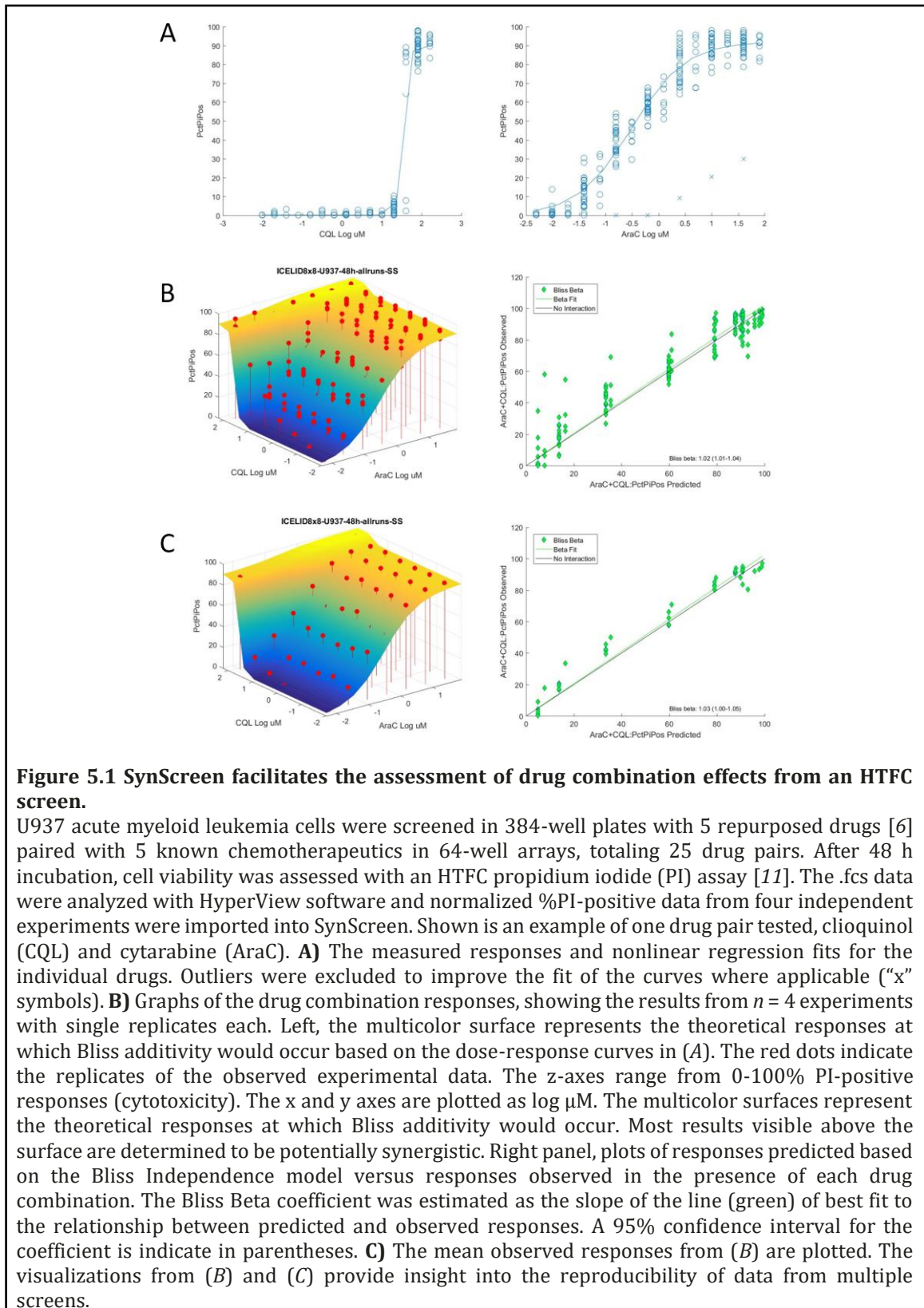


Table 5.1 Synergistic effects of the repurposed compound, clioquinol, with a conventional cytotoxic drug, cytarabine.

Shown are the hit synergistic data points from the data in **Figure 5.1**. See **Appendix C, Table S5.1** for an explanation of the reported metrics. CQL, clioquinol, AraC, cytarabine.

BlissHit	CIHit	AraCuM	CQLuM	fa	CI	AraCfa	CQLfa	Blissfa	fa>Blissfa	AraCumfa	CQLuMfa	AraCuMratio	CQLuMratio
TRUE	TRUE	0.0391	20	33.5	0.872	13.6	3.3	16.4	17.0	0.2	32.0	0.2465	0.6258
TRUE	TRUE	0.1563	0.0195	45.5	0.525	33.2	0.3	33.4	12.1	0.3	35.0	0.5244	0.0006
TRUE	TRUE	0.1563	0.0781	42.4	0.619	33.2	0.3	33.4	9.0	0.3	34.2	0.6163	0.0023
TRUE	TRUE	0.1563	0.3125	39.5	0.724	33.2	0.3	33.4	6.1	0.2	33.5	0.7142	0.0093
TRUE	TRUE	0.1563	1.25	41.6	0.677	33.2	0.3	33.4	8.2	0.2	34.0	0.6403	0.0368
TRUE	TRUE	0.1563	5	42.2	0.767	33.2	0.3	33.4	8.8	0.3	34.2	0.6202	0.1463
TRUE	TRUE	0.1563	20	50.1	0.967	33.2	3.3	35.4	14.7	0.4	36.2	0.4145	0.5521
TRUE	TRUE	0.625	0.3125	66.3	0.684	59.6	0.3	59.8	6.5	0.9	41.3	0.6764	0.0076
TRUE	TRUE	0.625	1.25	62.4	0.887	59.6	0.3	59.8	2.6	0.7	39.9	0.8557	0.0313
TRUE	TRUE	0.625	20	71.0	0.954	59.6	3.3	61.0	10.0	1.3	43.4	0.4931	0.4611
TRUE	TRUE	2.5	0.0195	80.4	0.847	78.9	0.3	79.0	1.5	3.0	49.6	0.8463	0.0004
TRUE	TRUE	2.5	0.0781	83.1	0.606	78.9	0.3	79.0	4.1	4.1	52.6	0.6045	0.0015
TRUE	TRUE	2.5	0.3125	82.5	0.663	78.9	0.3	79.0	3.5	3.8	51.9	0.6571	0.0060
TRUE	TRUE	2.5	1.25	85.2	0.451	78.9	0.3	79.0	6.2	5.8	56.2	0.4284	0.0223
TRUE	TRUE	2.5	5	80.2	0.968	78.9	0.3	79.0	1.3	2.9	49.4	0.8665	0.1011
TRUE	TRUE	2.5	20	87.8	0.545	78.9	3.3	79.6	8.2	10.7	64.4	0.2347	0.3105
TRUE	ORR	10	0.0195	90.4	ORR	87.6	0.3	87.7	2.8	33.0	160.0	0.3033	ORR
TRUE	ORR	10	0.0781	91.3	ORR	87.6	0.3	87.7	3.7	81.0	160.0	0.1235	ORR
TRUE	ORR	10	0.3125	92.1	ORR	87.6	0.3	87.7	4.4	1764.3	160.0	0.0057	ORR
TRUE	ORR	10	1.25	91.2	ORR	87.6	0.3	87.7	3.6	70.3	160.0	0.1423	ORR
TRUE	ORR	10	5	91.7	ORR	87.6	0.3	87.7	4.0	160.1	160.0	0.0625	ORR
TRUE	ORR	10	20	94.0	ORR	87.6	3.3	88.0	6.0	80.0	160.0	ORR	ORR
TRUE	ORR	40	0.0195	91.7	ORR	90.7	0.3	90.7	1.0	169.0	160.0	0.2366	ORR
TRUE	ORR	40	0.0781	93.2	ORR	90.7	0.3	90.7	2.5	80.0	160.0	ORR	ORR
TRUE	ORR	40	0.3125	92.8	ORR	90.7	0.3	90.7	2.1	80.0	160.0	ORR	ORR
TRUE	ORR	40	1.25	93.2	ORR	90.7	0.3	90.7	2.5	80.0	160.0	ORR	ORR
TRUE	ORR	40	5	94.9	ORR	90.7	0.3	90.7	4.2	80.0	160.0	ORR	ORR
TRUE	ORR	40	20	94.1	ORR	90.7	3.3	91.0	3.2	80.0	160.0	ORR	ORR

5.3.5 Validation of Synscreen and Application to Other Screening Platforms.

Normalized dose-response and combination data were obtained from the drug combination study published by Borisy, *et al.* [1]. There, compounds were tested in 10 x 10 matrices in 384-well plates and analyzed for inhibition of cell proliferation. For integration into SynScreen, the data were organized into a Microsoft Excel spreadsheet with columns (see above; **Appendix C, Figure S5.1**).

5.4 Results and Discussion

5.4.1 Validation of SynScreen Analysis for HTFC Assays

We previously identified a set of repurposed drugs with activity against leukemia cells [6]. To progress the research forward, we elected to test these drugs pairwise with known leukemia therapeutics. Hence, we adapted a HTFC viability assay [11] to quantify the effects of the 25 drug pairs tested in 64-well matrix arrays. The normalized data from four independent experiments were combined and imported into SynScreen for analysis. Data from one drug combination, clioquinol and cytarabine, are shown in **Figure 5.1**. The dose-response data for the individual drugs were fit by nonlinear regression, and outliers were removed to improve the fits (**Figure 5.1A**). Furthermore, the reproducibility of the data from multiple biological replicates was evaluated by the proximity of observed responses to one another (**Figure 5.1B**) or by visualization of the means from all replicates (**Figure 5.1C**). Synergy was evident for most paired concentrations below the maximal single agent concentrations, in the effect ranges 10-90%. Table 1 describes the synergistic data

points from this drug combination. A summary of the combination synergy statistics from the full screen can be seen in **Appendix C, Table S5.3**. All the combinations tested indicated hits for synergy, and twelve drug pairs scored with Bliss Beta > 1. Furthermore, over half the tested drug combinations produced CI values < 0.1. These metrics served to guide the compositions that should be further investigated. To further validate our findings, we processed the HTFC data from the drug pair with Combenefit [259] software. Those analyses determined similar concentration regions as synergistic that were identified with SynScreen. The discrepancies between software results are likely due to fact that the Combenefit software demonstrated poor goodness of fit for the dose responses of the individual agents. Combenefit did not allow for extended dose response data, including replicates, for the single agents to be imported for analysis. For a comparison of SynScreen to Combenefit and CompuSyn applications see the discussion in *SynScreen Facilitates Drug Combination Analysis*.

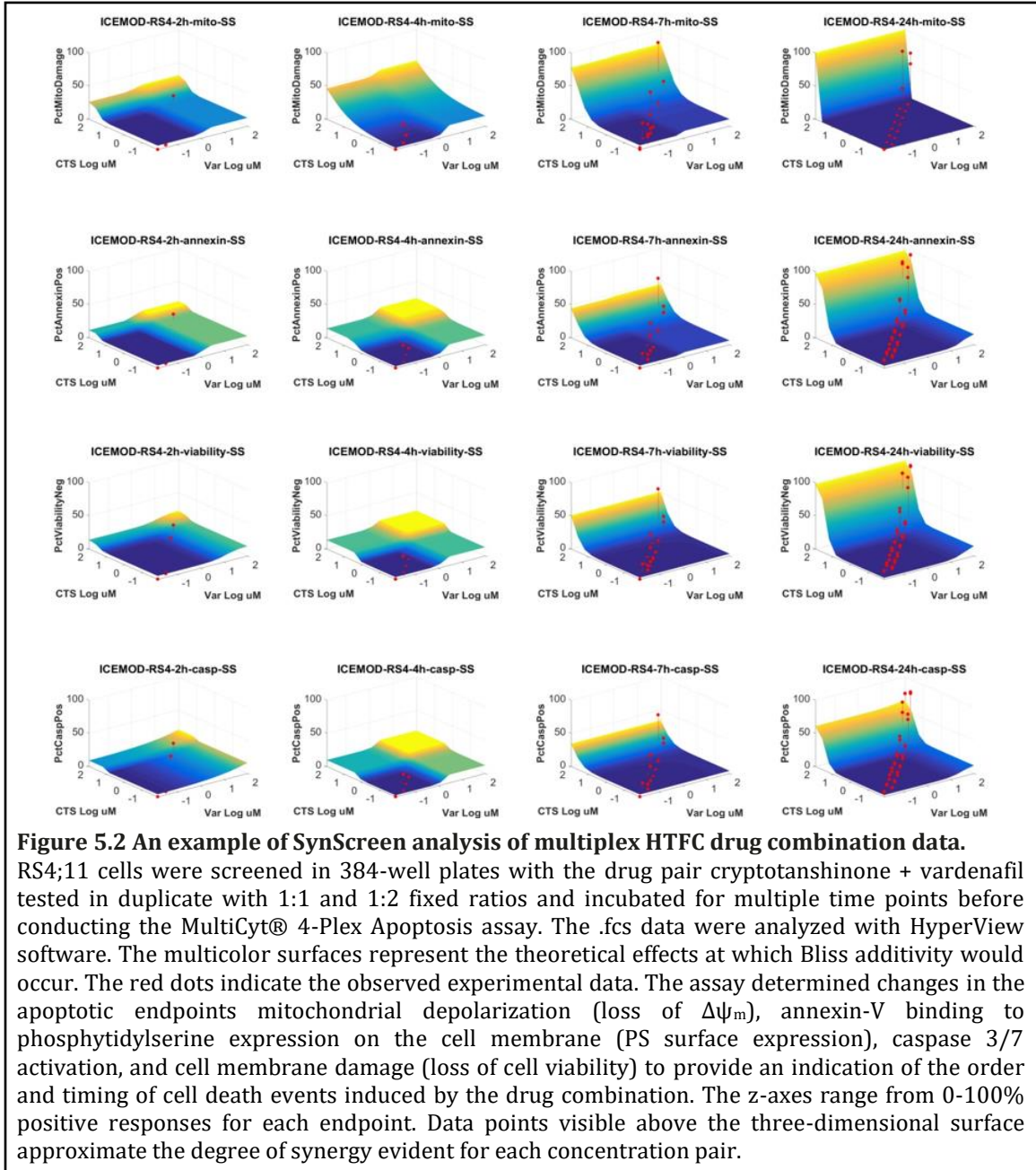
The utility of SynScreen for the analysis for multiplex HTFC drug combination assays was also tested with data from an assay wherein drug pairs were tested in fixed concentration ratio dose-responses to identify the outset and order of cell death responses induced by the compound interaction. SynScreen analysis was able to determine synergism between the repurposed agents cryptotanshinone and vardenafil within the four apoptosis endpoints collected by flow cytometry data (**Figure 5.2**). Hence, the use of SynScreen for the evaluation of drug combinations tested via HTFC by multiple assay approaches (fixed ratio, matrix, and multiplex) was

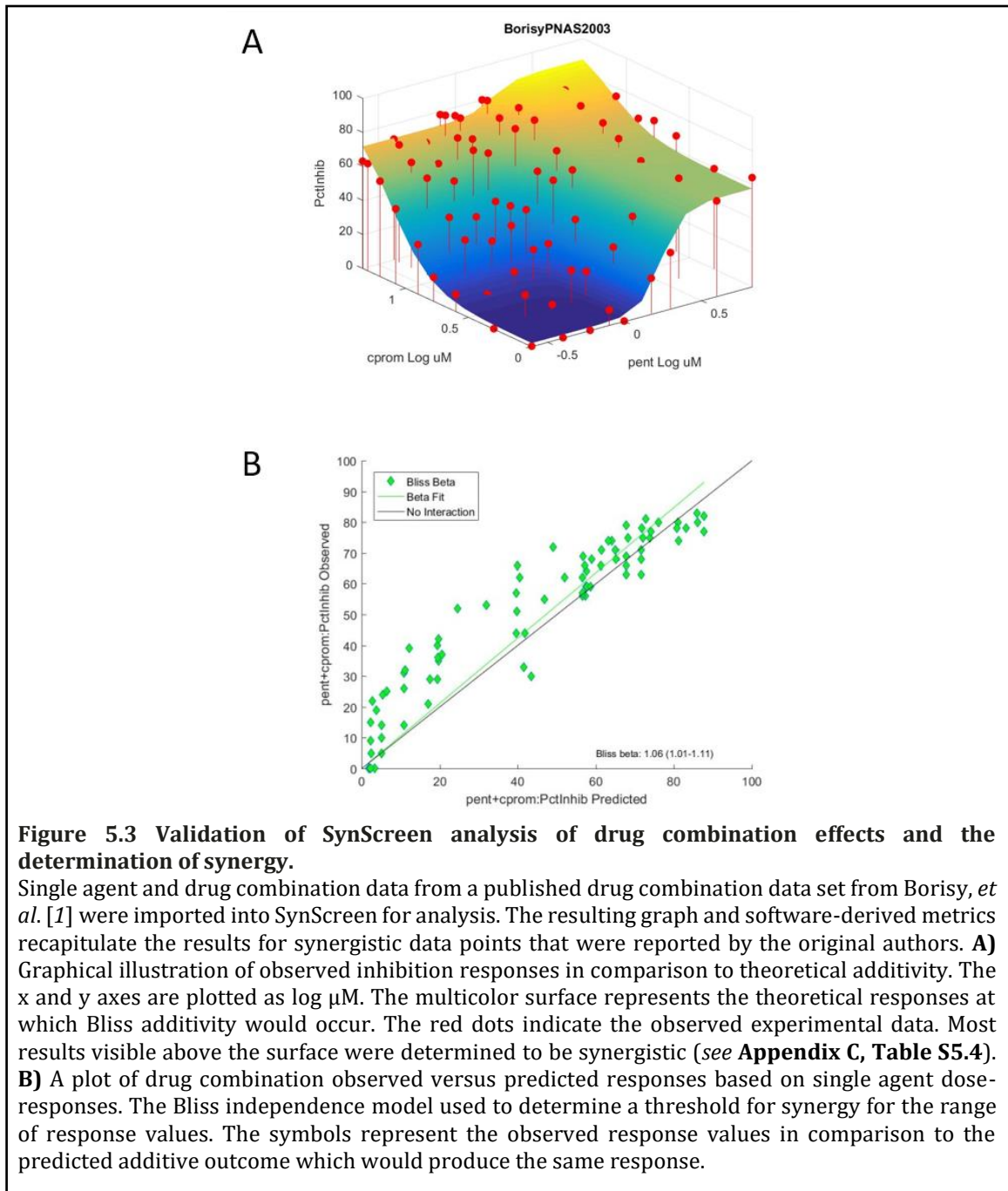
validated. The results allowed for an effective visual assessment of the tested combinations and the identification of efficacious drug pairs and concentrations. This feat would not have been easily accomplished through analysis by other software applications, which would have required considerable reformatting of HTFC data prior to analyses. While we report here the use of SynScreen for phenotypic flow cytometry assays, the analysis capabilities should be applicable for functional assays as well.

5.4.2 Application of SynScreen Analysis to Other Screening Platforms

The utility of the SynScreen application was further evaluated by analyzing a published set of drug combination data wherein synergistic interactions were identified. Data published from a screen for antiproliferative drug combinations by Borisy, *et al.* [1] were imported into SynScreen and analyzed to determine synergistic interactions. We additionally analyzed the data set with Combenefit [259]. The original publication identified 63 responses over Bliss additivism, whereas SynScreen identified 56 points and Combenefit identified 59 points. The sum of the differences between the responses and the predicted thresholds determined by Borisy, *et al.* [1] was 801, and the totals from SynScreen were 522 and 577, respectively. The results of the analyses are shown in **Appendix C, Figure S5.2**. These variations in data between applications are most likely due to the fact that some of the observed response data (percent inhibition) were negative values, and SynScreen converts negative response values to zero prior to analyses. Although SynScreen analysis did

not produce results identical to those published, it identified the same drug combination regions in which responses exceeded Bliss additivity (compare **Figure 5.3** here to Figure 4 in the original study [1]). Nonetheless, SynScreen analysis recapitulated the findings of established drug combination data, confirming its general applicability for the determination of synergistic drug interactions.





5.4.3 SynScreen Facilitates Drug Combination Analysis

A considerable benefit of HTFC is the ability to concurrently assess multiple parameters. Therefore, it is vital that software applications for HTFC data analysis be compatible with data from a variety of assay types and formats. Unfortunately, few adequate applications are amenable for HTFC drug combination data, which must be processed to isolate specific population(s) and responses for each parameter measured. The annotated data are typically tabulated in list formats which are not readily suitable for drug combination software packages specifying that data be arrayed in matrices [259], with responses from each drug positioned in rows and columns. The need to reorganize HTFC drug combination data to use such applications would limit the throughput of data generated from HTFC experiments. Additionally, some drug combination analysis programs stipulate that only data from fixed concentration ratios be entered [261]. This restricts the breadth of data that can be collected from robust methods such as HTFC. Furthermore, results from drug combination analyses are often presented in two-dimensional diagrams, such as heatmaps, dose-response x,y graphs for each concentration ratio tested, or tables of synergy statistics [1, 262], and therefore quick interpretation of the data may not be straightforward.

Using the open-source combination analysis software Combenefit [259] and CompuSyn [260], we analyzed a selection of our HTFC data from a cytotoxicity assay. The use of both applications required extensive reformatting of the HTFC data. CompuSyn has no limits on the numbers of data points entered for each drug and

combination, but requires that the response data be converted into fractional form 0-1 before each data point was entered into the software manually. CompuSyn uses linear fits in the median effect plots for individual dose responses, which are not amenable to data with various slopes without the deletion of several data points. Conversely to SynScreen, where normalized data from negative controls are set to the minimum response (e.g., 0%), Combenefit requires that normalized negative control values equal the maximum response (e.g., 100%). The application also necessitates that data be positioned in matrices, and is an ideal application for use with plate reader-based data. Because HTFC data often exists in columns and data from specific drug combinations do not necessarily appear sequentially, it took a considerable effort to reconfigure the data into such matrices. Furthermore, the data from each combination and replicate had to be saved into separate .xls files prior to import into Combenefit. Because synergy analyses rely heavily upon comparison of combination vs single agent data, we collected robust dose responses (more doses and smaller dilution factors) for single agents, in replicate, in our screen. We were unable to enter the replicate data or values from the extended dose response ranges of the single agents in our data, as the Combenefit software constrains data from individual drugs to match the tested concentrations used in combinations. Neither CompuSyn nor Combenefit allowed for real-time editing of data through their interfaces.

The utility of SynScreen overcomes some of the aforementioned limitations encountered by some drug combination analysis software packages. There is no limitation on the quantity of data imported for analysis, and data from multiple

replicates can be incorporated into a single analysis. Furthermore, HTFC data are compatible with a columnar output configuration that can be directly loaded into Excel (or CSV) files to facilitate SynScreen analysis. To expedite data processing, the application interface was developed to enable all aspects of drug combination analyses to be visualized in real-time. Because synergism can only reliably be determined by comparison of combination responses to those of each compound alone, it is imperative that researchers use dependable dose-response curves for single agent responses. Therefore, SynScreen automatically displays single agent dose-responses and nonlinear regression curve fits so that aberrant data points can be excluded to improve the fit of the data (**Figure 5.1A**). The application produces visualizations of the data in three dimensions to allow for simultaneous assessment of the combination responses in relation to the individual drug responses and the theoretical threshold of additive interactions (**Figure 5.1B, C**). The combination data are analyzed by the Bliss independence and Loewe additivity combination index models to validate data points that produce synergy. These metrics, as well as graphical representations of the data, are automatically output into common file formats, and can easily be adapted for further data processing and prioritization.

5.4.4 Limitations of the SynScreen Software Application

Like many drug combination analysis applications, SynScreen is currently designed for the analysis of drug pair interactions. The annotated drug concentrations are required to be in micromolar units. Likewise, the imported

normalized response data should be recorded in values from 0-100% (or 0-1 in fractional form) in which the normalized response increases with drug concentration. Due to this normalization, single agent dose-responses must be tested with enough data points to provide robust curves. The software does allow for data with normalized responses of less than 0% to be present in the source file, although these values are automatically set to equal zero, and thus some dose-responses may appear with reduced efficacy ranges. Moreover, the artificial weighting of all negative values to zero may mask noise in these data. One additional limitation of both SynScreen and other commonly-used drug combination analysis platforms that determine synergy by classical models is that they do not readily incorporate the influence of potential adverse effects between drugs, and thus the identification of synergistic interactions may not reflect realistic therapeutic windows [265]. However, it should be noted that incorporating these effects also requires extensive testing and validation of reference samples. For the purposes of HT screening, the pragmatic approach would be to identify potential hit drug combinations and ranges, and parse these with confirmatory secondary assays.

5.4.5 SynScreen is an Optimal Application for HTFC Drug Combination Analysis

Here, we have described the development of a novel application for drug combination analysis that is especially utile for HTFC screening data. SynScreen is particularly useful for HTFC drug combination studies because it is amenable to facile analysis of data sets of almost unlimited size. The properties of the drug

concentration ratios tested and the quantity of tested wells are unrestricted, permitting that there are sufficient data from the single compounds to produce reliable dose-response curves and fits. A minimum response threshold can be set to filter hits with specific activities. The application generates summary tables that provide an overview of the imported dose-response combination data. These serve to simplify the collation of multiple experimental runs and conditions for comparison analyses. Furthermore, the capacity to import files with screening data from multiple runs allows for a qualitative assessment of reproducibility of assays (**Figure 5.1**). Additionally, the drug combination graphs generated by SynScreen also provide a visual approximation of the regions where synergistic drug interactions have occurred. Most data points visible above the surface of the theoretical additivity threshold are mathematically identified as synergistic by Bliss and/or combination index models. Hence, HTFC drug combination data may be rapidly evaluated, thus expediting the triage process for screening campaigns.

5.5 Acknowledgements

This work was supported by funding from: NIH Minority Institutional Research Training Program Award # T32 HL007736 (D.R.P.) and NIH Cancer Center Support Grant CCSG P30 CA118100.

5.6 Conflicts of Interest

B.S.E. and L.A.S. are co-inventors of HyperCyt, and co-founders of IntelliCyt. D.R.P. and A.C. declare no conflicts of interest.

CHAPTER 6: Drug combination screen of cyclic AMP efflux inhibitors with leukemia chemotherapeutics elicits synergy in acute leukemia cells

Dominique R. Perez^{1,2,4}, Nitesh D. Sharma^{3,4}, Bruce Edwards^{1,2,4}, Anna Waller^{1,2,4},
Ksenia Matlawska-Wasowska^{3,4}, Larry A. Sklar^{1,2,4}, Alexandre Chigaev^{1,2,4}

¹ Department of Pathology, ² Center for Molecular Discovery, ³ Department of Pediatrics, Division of Pediatric Research, Health Sciences Center, University of New Mexico, Albuquerque, NM, USA

⁴ University of New Mexico Comprehensive Cancer Center, Albuquerque, NM, USA

6.1 Abstract

Acute myeloid leukemia (AML) and B-cell lineage acute lymphoblastic leukemia (B-ALL) are debilitating malignancies that affect elderly and pediatric populations, respectively. Predictably, the poor rates of survival are partially due to refractory and resistant responses to current treatment regimens. Therefore, the development of novel therapeutics for administration in combination with existing drugs is vital to improve patient outcomes. A promising target toward this advancement is the second messenger 3',5'-cyclic adenosine monophosphate (cAMP), as the expression of pathway-related proteins and downstream effectors is abnormal in many cancers. Previously, we proposed that malignant cells evade apoptosis and promote survival by active efflux of cAMP. To target this process, we identified several repurposed

drugs termed inhibitors of cAMP efflux (ICE). When used alone, ICE were capable of triggering cell death, thus targeting leukemia through a novel mechanism. Drug resistance in acute leukemias is often attributed to increased activity and expression of ATP-binding cassette transporters. Remarkably, the same transporters are also associated with cAMP efflux. Because numerous first-line leukemia drugs are known to be substrates of cAMP transporters, we hypothesized that the ICE compounds could increase sensitivity to leukemia chemotherapeutic agents (LCA). We tested AML and B-ALL cell lines, as well as primary B-ALL patient samples, with pairwise ICE+LCA combinations to identify their potential synergistic effects in reducing viability and proliferation. While sensitivities varied across cell lines, most combinations produced some degree of synergy, indicating a beneficial effect of ICE with LCAs. ICE combinations with cytarabine, methotrexate, or topotecan consistently indicated the most synergism. Future studies will explore mechanisms of action to determine whether the synergistic effects produced by ICE/LCA combinations are due to transporter inhibition and/or modulation of multiple cellular pathways. Because ICE are clinically actionable repurposed drugs, this provides the possibility for additional testing of these drugs in combination with chemotherapeutics in *in vivo* xenograft models.

6.2 Introduction

Leukemias rank amongst the top 10 cancers in the United States, in terms of both morbidity and mortality. Acute myeloid leukemia (AML) primarily affects the elderly,

and has an abysmal five-year survival rate of only 28.3% [8]. B-cell lineage acute lymphoblastic leukemia (B-ALL) is now >85% curable [19, 30]. While the lineage of the two acute leukemias may differ, both diseases involve the unregulated proliferation of immature blood cells, blasts. Due to this fact, there is significant overlap in the treatment regimens for both malignancies. Typically, induction and consolidation leukemia chemotherapeutic agents (LCA) for AML consist of a combination of cytarabine (AraC) with an anthracycline [31]. B-ALL is first treated with a combination of a glucocorticoid, anthracycline, vincristine, and asparaginase [19]. Maintenance therapy for B-ALL generally employs methotrexate and nucleotide analogs, such as mercaptopurine [19].

Despite improvements in treatment regimens over the last few decades, the long term responses from leukemia chemotherapies are poor, primarily due to the development of resistance [30, 266]. Leukemia multidrug resistance (MDR) can be attributed to many mechanisms, primarily the overexpression and activity of ATP-binding cassette (ABC) transporters [102, 103, 226] that can actively remove LCA from cells, reducing their ability to take effect. As such, one potential means to reduce MDR is to inhibit ABC transporters and thus increase cell retention of cytotoxic agents. Consequently, the development of novel therapeutics for use in combination with existing drugs is vital to improve patient outcomes.

Based on its role in physiological processes that modulate cell death and survival, cyclic AMP (cAMP) represents a promising target in cancer. The expression of cAMP pathway-related proteins is abnormal in many malignancies, including leukemias [61,

62, 65, 78, 82, 267]. Moreover, elevation of intracellular cAMP has been shown to reduce the viability of malignant hematopoietic cells [2, 3, 74, 75, 118]. In our previous work, we hypothesized that one mechanism that may be utilized by acute leukemia cells to evade cell death is by the efflux of cAMP through the ABC transporters ABCC4, ABCC5, and ABCC11 [6]. To target this process, we identified several repurposed drugs termed inhibitors of cAMP efflux (ICE). When used alone, ICE were capable of selectively reducing leukemia cell viability, and our data suggested that these effects were largely independent of leukemia genotype [6].

Due to their nucleotide-like structures, many LCA are substrates of cAMP transporters [102, 103, 133, 268-271]. Not surprisingly, the expression levels of ABCC4, ABCC5, and ABCC11 have been reported to be prognostic for clinical responses [102, 103, 226, 269]. On this basis, we propose to test ICE+LCA combinations for synergism against leukemia cells. We postulate that ICE can reduce LCA efflux, thus enhancing their cytotoxic effects. Synergistic interactions could reduce the concentrations of individual agents needed for efficacy. This is especially attractive because many LCA lack specificity for malignant cells and can be damaging to normal tissues. In support of our hypothesis, several studies have shown that cAMP-modulating agents can reverse resistance and/or enhance the effects of LCA [226, 272-274]. In preparation for these studies, we developed high throughput flow cytometry (HTFC) approaches for testing and analyzing drug combinations in leukemia cell lines and primary samples [275, 276].

The objective of this work was to assess and optimize ICE combinations to move toward clinical translation. We hypothesized that cAMP efflux mechanisms are related to drug resistance, and therefore that ICE should improve leukemia cell sensitivity to first-line leukemia therapeutics. We established the utility of ICE used in conjunction with LCA that are known substrates of cAMP transporters. In order to validate cAMP efflux as both a prognostic trait and a favorable target for acute leukemia therapeutics, we attempted to determine potential relationships between retention of a fluorescent cAMP analog (F-cAMP) and drug sensitivity. Our findings provide a basis for the development of a new class of agents, ICE, that when combined with current leukemia treatment modalities, could enhance the killing of malignant hematologic cells.

6.3 Results

6.3.1 HTFC assays were designed to test ICE+LCA combinations

We designed HTFC assays comprising drug pairs from ICE and LCA to determine whether interactions between the two classes of drugs would potentially elicit synergistic inhibition of leukemic cell viability. We proceeded with the four ICE that had the most translational potential, as well as MK-571 as a positive control. We tested LCAs that are both commonly used in leukemia chemotherapeutic protocols, as well as having been found to be substrates of the cAMP efflux transporters. **Table 6.1** summarizes the drugs tested for these combination studies.

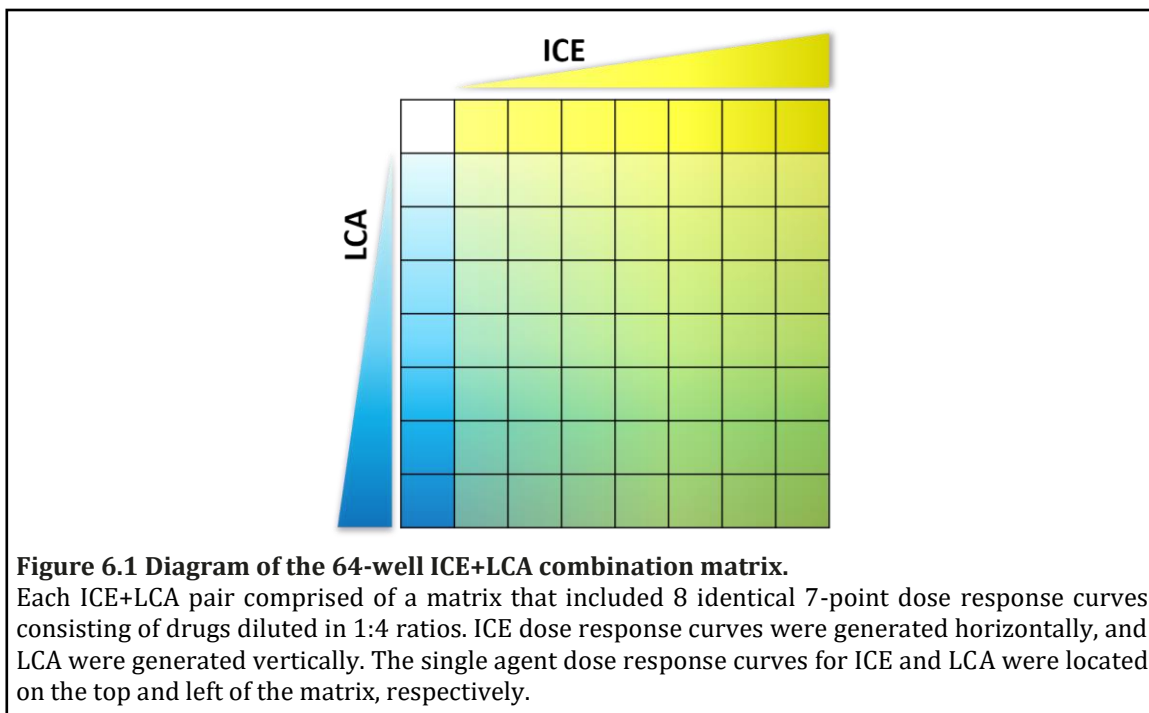
Table 6.1 Compounds used in drug combination assays.

*Indicate drugs that we identified as ICE in ref [6], but are not clinically actionable enough to pursue in drug combination assays. ‡ This drug was used only with AML cell lines.

	COMPOUND	NOTES
ICE (Inhibitor of cAMP Efflux)	Artesunate (ART)	Sesquiterpene lactone from <i>Artemisia annua</i> ; FDA-approved antimalarial
	Clioquinol (CQL)	FDA-approved antimicrobial
	Cryptotanshinone (CTS)	A tanshinone isolated from <i>Salvia miltiorrhiza</i>
	Dihydroartemisinin (DHA)	Sesquiterpene lactone; Active metabolite of artesunate
	MK-571 (571)	Positive control for cAMP efflux inhibition; blocks multiple ABC-C family transporters
	Parthenolide (PTH)*	Sesquiterpene lactone from <i>Tanacetum parthenium</i>
	Patulin (PLN)*	Mycotoxin produced by <i>Penicillium</i> and <i>Aspergillus</i>
LCA (Leukemia Chemotherapeutic Agent)	5-fluorouracil (5FU)	Substrate of ABCC5, ABCC11 [268]
	6-mercaptopurine (6MP)‡	Substrate of ABCC4, ABCC5 [269]
	Cytarabine (AraC)	Substrate of ABCB1 [103], ABCCC10 [270], ABCC11 [102]
	Methotrexate (MTX)	Substrate of ABCC4 [133]
	Topotecan (TPT)	Substrate of ABCC4 [271]

Due to the potential complex interactions that may occur between drugs used in tandem, it is important that appropriate concentration ratios are tested to encompass conditions wherein interactions might occur. With this in mind, we elected to test ICE+LCA combinations in matrices comprised of 48 different drug concentration ratios, along with 8-point dose responses for individual drugs (**Figure 6.1**). Because the responses of individual agents are critical for analyses of drug interactions, our HTFC assays also included extended dose response curves that were separate from

the matrices. The compound concentrations tested were based on previous characterization of drug efficacies [6, 275].



6.3.2 AML cell lines show enhanced sensitivity to ICE+LCA combinations

To test our hypothesis that ICE can increase sensitivity to LCAs, we analyzed combinations on AML cell line viability and determined whether such mixtures exhibit synergy. Here, we chose to test U937 cells, as we had previously extensively determined ICE effects on this cell line [6]. We also used MV-411 and KG-1a cell lines, as they represent mature and immature AML phenotypes, respectively [277, 278].

Table 6.2 describes the AML cell lines chosen for this study, as well as their characteristics.

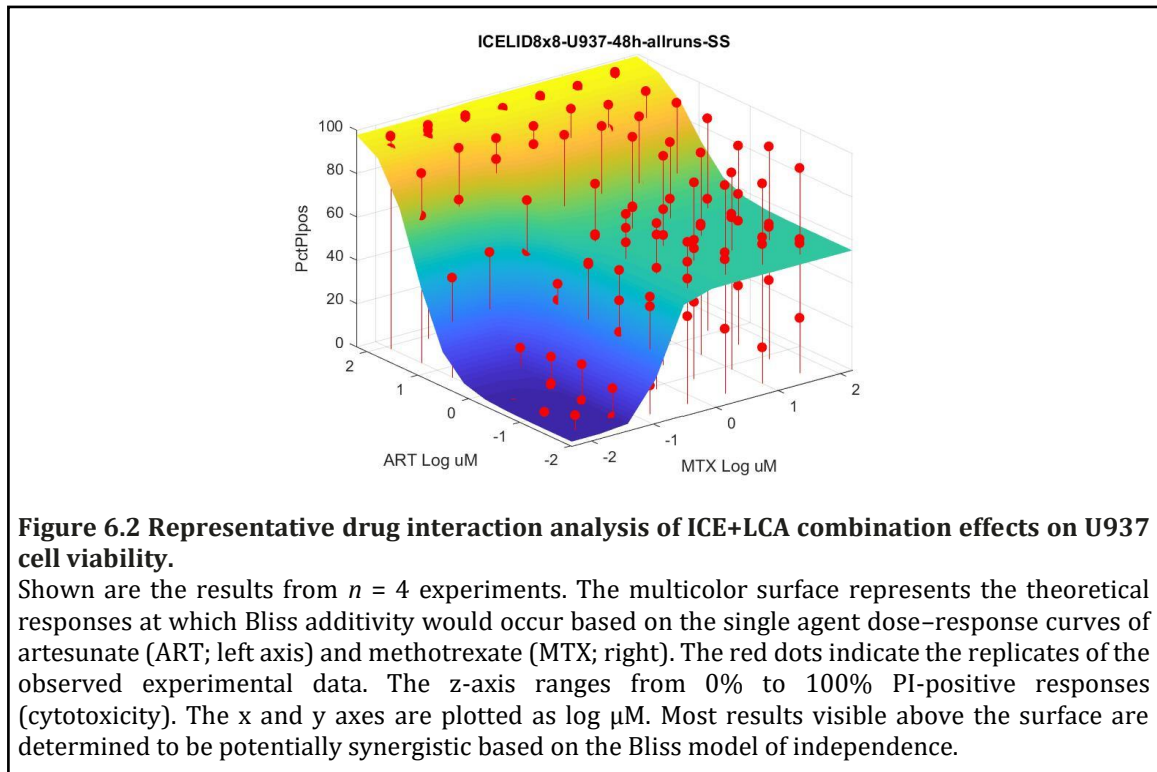
Table 6.2 The AML cell lines used in these studies and their characteristics.

AF = ALL1-fused gene from chromosome *n*; CALM = clathrin assembly lymphoid myeloid; FGFR1 = fibroblast growth factor receptor 1; FLT3-ITD = fms like tyrosine kinase 3 internal tandem duplication; MLL = mixed lineage leukemia; OP2 = oncogene partner 2; M, male.

Cell line	FAB Subtype	Source	Fusion protein	Other Characteristics
KG-1a	M0	M age 59	FGFR1OP2-FGFR1	CD34 ⁺ ;stem cell phenotype; differentiation resistant
U937	M5	M age 37	CALM-AF10	Facile differentiation
MV4-11	M5	M age 10	MLL-AF4	FLT3-ITD

We treated the AML cell lines with ICE+LCA combinations for 24 and 48 h and then determined cell viability with a propidium iodide (PI) assay. These time points were chosen based on the fact that ICE have been able to reduce cell viability within 24 h at similar concentrations [6]. We analyzed the viability data with SynScreen software, which both facilitates the analysis of drug combination data, and also provides simple 3D visualizations of data to allow for quick assessment of each drug pair [275]. We identified several drug combinations that synergistically reduced AML cell line viability. In **Figure 6.2**, we show data from the combination of artesunate and methotrexate, both to demonstrate the evidence of this synergism, as well as to provide an example of how to best interpret SynScreen data. We were able to compare the data from all the drug combinations tested to assess potential patterns. **Figure 6.3** shows the data from 4 replicate experiments of U937 cells treated with ICE+LCA combinations for 48 hours. The data on the right exhibit more observed instances of synergism, coinciding with ICE combinations with AraC, methotrexate, or topotecan which exhibit potent activity against AML cells as single agents. These drugs have also been shown to have multiple mechanisms of action, so it is plausible that these ICE+LCA combinations may be affecting pathways beyond cAMP and cell

proliferation. The data from 24 h incubation was not striking and may reflect latency on killing (**Appendix D**). **Table 6.3** provides a summary of the data for the three AML cell lines, indicating the total number of ICE+LCA combination data points that were determined to be synergistic according to the Bliss model of independence [254]. While the combination index model [256] is considered to be one of the most comprehensive methods to use for drug interaction analysis, it is inappropriate to use when the responses of drugs used in combination exceed the responses achievable by one drug alone.



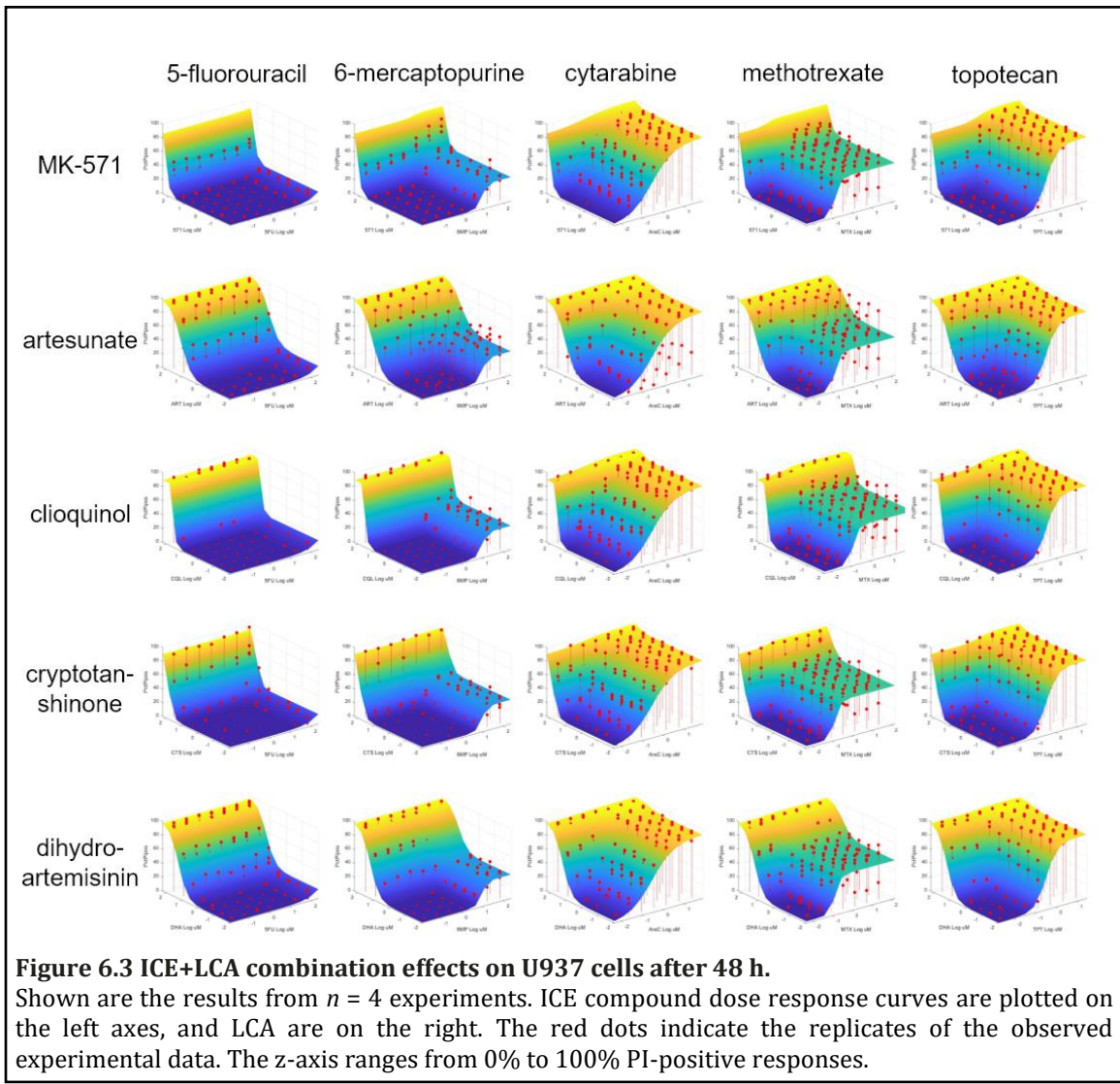


Figure 6.3 ICE+LCA combination effects on U937 cells after 48 h. Shown are the results from $n = 4$ experiments. ICE compound dose response curves are plotted on the left axes, and LCA are on the right. The red dots indicate the replicates of the observed experimental data. The z-axis ranges from 0% to 100% PI-positive responses.

Table 6.3 Summary of synergistic data points from ICE+LCA combination viability assays in AML cell lines.

Shown are the total number of data points that were identified by SynScreen software to be synergistic by the Bliss model of drug interaction analysis. Incubation times are indicated on the left. Cell lines are listed on the bottom. The LCA are listed horizontally, and ICE are listed vertically. The data from 4 replicate experiments was analyzed together. The maximum number of synergistic data points is 196 per condition. Darker colors on the heatmap indicate more identified synergistic data points.

	5FU					6MP					AraC					MTX					TPT																																																												
24 h	1	0	0	24	10	7	0	18	35	50	0	0	30	0	42	571	16	14	10	28	22	40	35	39	60	67	19	20	55	23	58	ART	14	17	18	26	13	19	12	29	43	49	8	14	37	13	48	CQL	2	2	2	30	10	30	21	33	46	61	8	7	48	14	55	CTS	19	16	19	35	26	48	44	52	66	71	10	7	39	37	44	DHA	
	48 h	0	6	0	56	48	30	47	56	59	81	14	37	79	93	74	571	16	17	14	64	62	44	49	75	67	81	41	67	71	82	86	ART	14	20	15	66	45	60	66	76	83	80	12	34	97	93	73	CQL	13	17	12	62	54	72	67	87	89	94	14	26	90	89	69	CTS	29	27	25	69	54	75	68	97	80	91	36	35	84	83	69	DHA
		KG-1a					MV4-11					U937																																																																					

6.3.3 B-ALL cell lines exhibit sensitivity to some ICE+LCA combinations

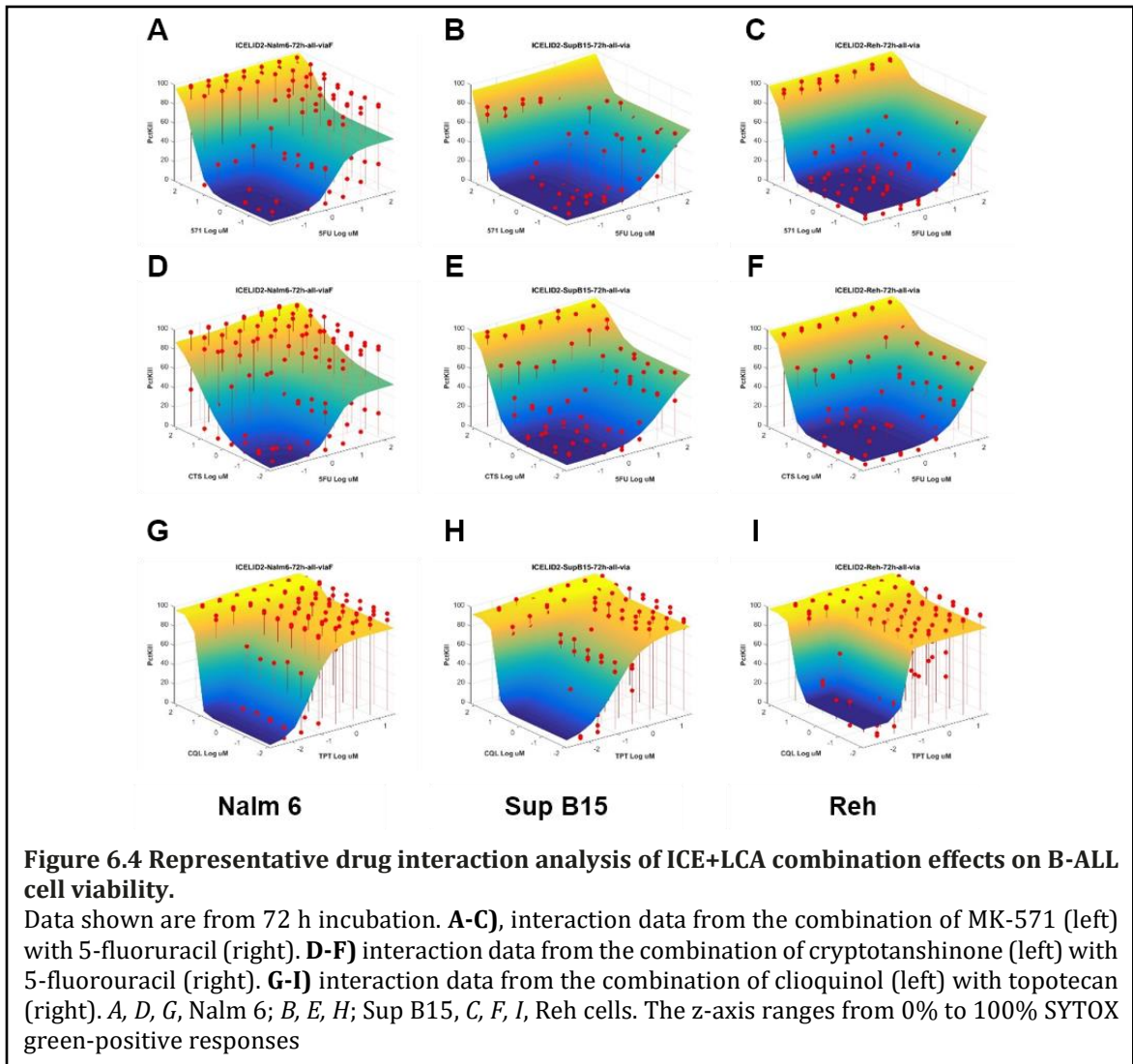
Because our work is focused on elucidating the potential utility of using ICE for treatment of acute leukemias, we proceeded to test ICE+LCA combinations on B-ALL cell lines (**Table 6.4**). Here, we chose to use three cell lines that exhibited different capacities for F-cAMP efflux, and inhibition by the positive control MK-571: Nalm 6, Sup B15, and Reh (see **Figure 3.9B** in **Chapter 3**). In contrast to the work done with AML cell lines, the B-ALL cell lines were unable to thrive under the same incubation conditions. Hence, we adapted our methods to allow these B-ALL cell lines to have access to circulating air during the incubation period. Furthermore, as we moved forward to optimize our HTFC combination assays, we opted to eliminate the LCA 6-mercaptopurine from our drug panel for efficiency, since it elicited similar results to 5-fluorouracil in the AML studies. For this stage of the work, we also wanted to expand the breadth of information that could be obtained from ICE+LCA combinations, and included proliferation as another factor for drug sensitivity.

Table 6.4 The B-ALL cell lines used in these studies and their characteristics.

Cell line	Source	Genetic	
		rearrangement	Fusion gene
Nalm 6	M, age 19	t(5;12)(q33;p13)	ETV6/PDGRFB
Reh	F, age 15	t(12;21)(q13;q22)	ETV6(TEL)/RUNX1(AML1)
Sup B15	M, age 8	t(12;21)(q13;q22)	P190 BCR/ABL1

We predicted that since Nalm 6 has the highest cAMP efflux ability, and the lowest ability for efflux to be inhibited by MK-571, that the viability of this cell line would be the most resistant to ICE+LCA combinations. Surprisingly, Nalm 6 cells exhibited the

most ICE+LCA synergistic effects. Sup B15 cells, which previously exhibited the lowest F-cAMP efflux capacity of our tested B-ALL cell lines [6], were the least sensitive to ICE+LCA combinations (**Figure 6.4**).



The B-ALL cell line behavior was further unexpected by exhibiting different sensitivities to ICE+LCA combinations in comparison to the AML cell lines. In our previous work [6], while the EC₅₀ values for single drugs tested on AML and B-ALL cell lines varied, the efficacious drugs ranked in the same order. In our ICE+LCA combination studies here, we found that combinations that included 5-fluorouracil produced strong synergism in the B-ALL cell lines, whereas these drug interactions were modest in the AML cell lines. Furthermore, we determined that combinations with our identified ICE elicited similar effects as the positive control, MK-571 (**Figure 6.4, A-F; Appendix D**). Nonetheless, akin to the AML cell line data, ICE+LCA combinations involving AraC, methotrexate, or topotecan produced synergy in the context of B-ALL cell line viability (**Figure 6.4, G-I**). We also observed that synergism was stronger in B-ALL cells incubated 72 h in comparison to those treated for 48 h. We summarize the ICE+LCA combination synergistic points in **Table 6.5**. As previously mentioned, we also sought to determine how ICE+LCA combinations might affect cell proliferation. This metric was assessed because one primary goal of cancer treatment is to limit cell growth, and clinicians are interested in treatments that are cytostatic just as much as they are interested in therapies that are cytotoxic. While the proliferation results were not as profound as that from the viability studies, some ICE+LCA combinations did synergistically limit cell replication. Of note, the combination of topotecan with clioquinol demonstrated several concentration ratios that prevented proliferation (**Figure 6.5**). It should also be noted that for the majority of drug combinations, most synergistic inhibitions of B-ALL cell line proliferation

occurred with Sup B15 cells incubated 48 h and Nalm 6 cells treated 72 h (**Appendix D**). **Table 6.6** provides a summary of the number of synergistic data points identified from the B-ALL cell line proliferation assays.

Table 6.5 Summary of synergistic data points from ICE+LCA combination viability assays in B-ALL cell lines.

Shown are the total number of data points that were identified by SynScreen software to be synergistic by the Bliss model of drug interaction analysis. Incubation times are indicated on the left. Cell lines are listed on the bottom. The LCA are listed horizontally, and ICE are listed vertically. The data from 3 replicate experiments was analyzed together. The maximum number of synergistic data points is 147 per condition. Darker colors on the heatmap indicate more identified synergistic data points.

		Nalm 6				Sup B15				Reh				
		5FU	AraC	MTX	TPT	5FU	AraC	MTX	TPT	5FU	AraC	MTX	TPT	
48 h		51	81	70	58	15	67	33	56	16	64	66	60	571
		62	88	73	76	21	40	34	38	13	58	51	54	ART
		56	87	77	79	19	87	39	63	25	49	48	51	CQL
		62	89	71	81	19	63	34	60	24	56	49	60	CTS
		57	85	69	63	26	70	51	59	17	48	50	52	DHA
72 h		60	98	83	77	20	84	35	62	20	79	67	63	571
		73	97	83	77	19	88	36	58	29	79	69	69	ART
		61	96	76	87	40	89	71	62	32	70	62	62	CQL
		74	97	88	83	41	78	64	62	36	73	69	67	CTS
		62	93	64	88	31	75	51	53	44	41	72	62	DHA

6.3.4 Primary B-ALL samples have limited sensitivity to ICE, LCA, or ICE+LCA combinations

To test the realistic potential of ICE+LCA combinations to be effective against acute leukemias, we sought to determine drug interactions against primary B-ALL samples *ex vivo*. For these samples, we assessed combination effects on cell viability. Due to the fragile nature of primary samples, we were reluctant to load these cells with a proliferation marker. In order to potentially support our hypothesis by relating cAMP efflux ability to drug sensitivity, we also measured primary B-ALL sample retention of a fluorescent cAMP analog, F-cAMP.

We tested primary B-ALL samples that were obtained at the time of diagnosis and cryogenically banked. Matched vials were previously assessed with for mRNA expression. From the genes that were analyzed, eleven related to the cAMP pathway, including three adenylyl cyclases (ADCY6, 7, 9), two phosphodiesterases (PDE7A, PDE4D), RAPGEF3 (EPAC1), PRKAR1A (protein kinase A-1 α), cAMP efflux transporters ABCC1 and ABCC5, NTPDase1 (CD39) and ecto-5'-nucleotidase (CD73). The normalized data from twenty-three primary B-ALL samples were log₂-transformed followed by unsupervised hierarchical clustering gene cluster analysis based on expression of the aforementioned genes. The samples formed two distinct clusters. We selected four representative samples from Cluster 1, and five samples from Cluster 2 for analysis in F-cAMP retention and ICE+LCA viability assays (**Figure 6.6** and **Table 6.7**).

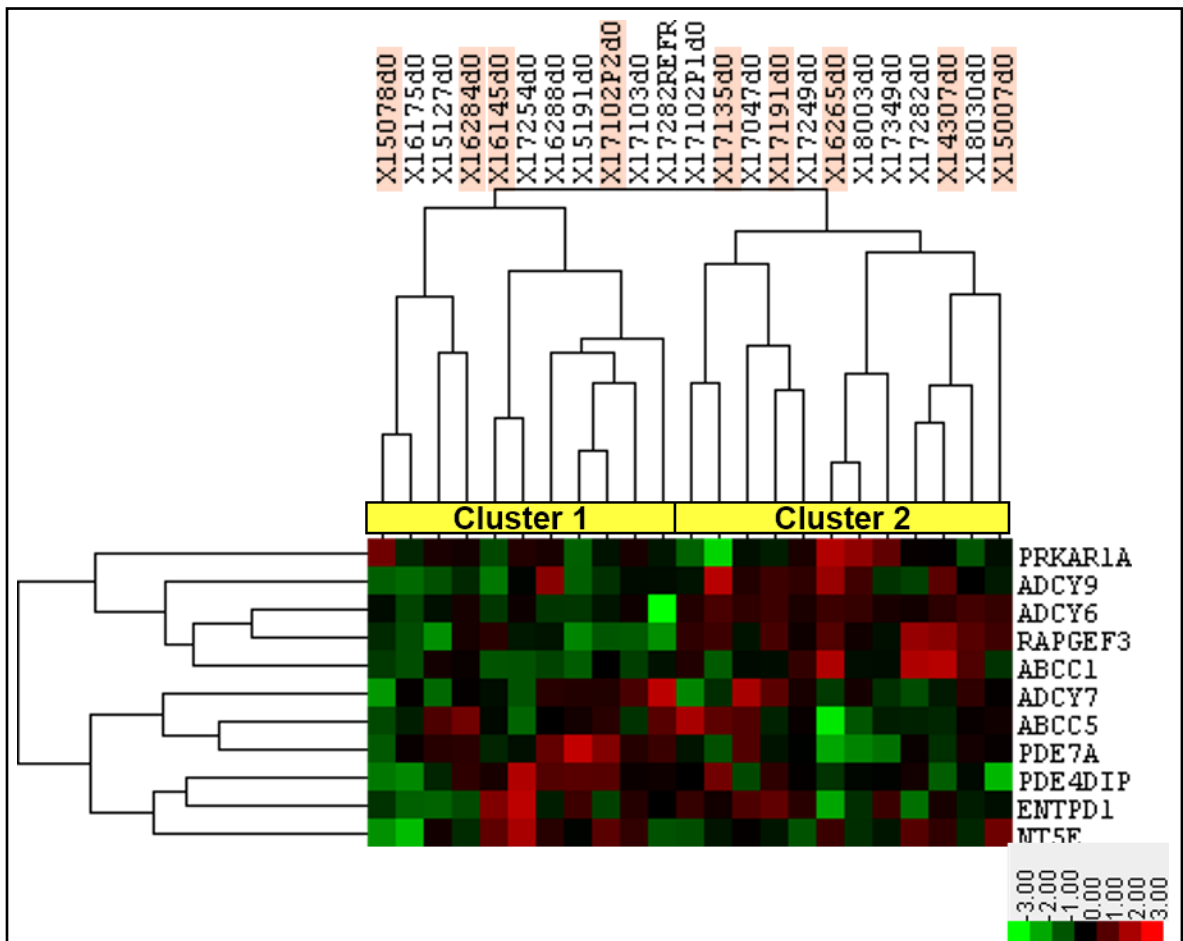


Figure 6.6 Representative drug interaction analysis of ICE+LCA combination effects on U937 cell viability.

Shown are the 23 banked B-ALL primary samples (top) that were previously analyzed and clustered based on their expression of genes related to the cAMP pathway (right). The heatmap is log₂ scale, with red indicating increased expression and green indicating reduced expression. The two identified clusters are indicated in yellow. The primary samples that were selected for our studies are highlighted with peach boxes.

Table 6.7 Characteristics of the tested primary B-ALL cell lines.

WBC, white blood count (representative of blasts in the bone marrow). MRD, minimal residual disease evident in bone marrow (BM) 29 days after diagnosis and induction therapy.

Sample ID	Initial WBC (x10 ³)/μl	Gender	Age at diagnosis	Ploidy DNA index	Karyotype	FISH	Day 29 MRD (%) BM
14-307	340.3	M	23		48,XY,+6,+21 [18]/46XY[2]		0
15-007	14.3	F	17	1.0 diploid	46,XX,t(7;22)(q32;q11.2), add(9)(p13) [10]/48,idem,i(7)(q10),+14, +22[2]/49,idem,+6,+10,+22 [1]/46,XX[9]		1.2
15-078	12	F	4		46,XX,t(1;19) (q23;p13.3),inc[2]/46,XX[6]	TCF3- PBX1	0
16-145	26.5	M	13	0.81 hypodiploid	38,XY,-3,-4,-7,-12,-13,-15,- 16,-17[6]/76,idemx2[1] 46,XY[19]		0.01
16-265	365.5	F	13		46,XX,t(9;22) (q34;q11.2)[1]/46,XX[2]	BCR- ABL	0
16-284	15.6	F	5	1.0 diploid	46,XX[7]	ETV6- RUNX1	0
17-102-P2	6	F	9	1.0 diploid	46,XX[20]	ETV6- RUNX1	0
17-135	69.1	F	8		47,XX,- 13,i(20)(p10),+21,+mar[18] /46,XX[2]		0
17-191	10.2	F	4	1.19 aneuploid	56,XX,+X,dup(1)(q21q42),+ 4,+6,+10,?add(13)(q34),+1 4,+17,+18,+21,+22[9]/46,X X[2]		0

We were only able to determine the primary B-ALL samples' ability to retain F-cAMP because there were no differences between the negative control and MK-571-treated condition. We later determined that this lack of distinction was most likely due to the inclusion of 0.5% amphotericin B in the culture media, an oversight on our part. Because amphotericin B can affect cation transport, it is likely that this molecule may have affected the integrities of the cell membranes or transporters. **Table 6.8** presents the retention of F-cAMP after incubation. Most samples lost over half of the loaded F-cAMP after about 20 hours. Patient sample 15-007 exhibited a high percentage of retention, although these data could be confounded by the fact that the

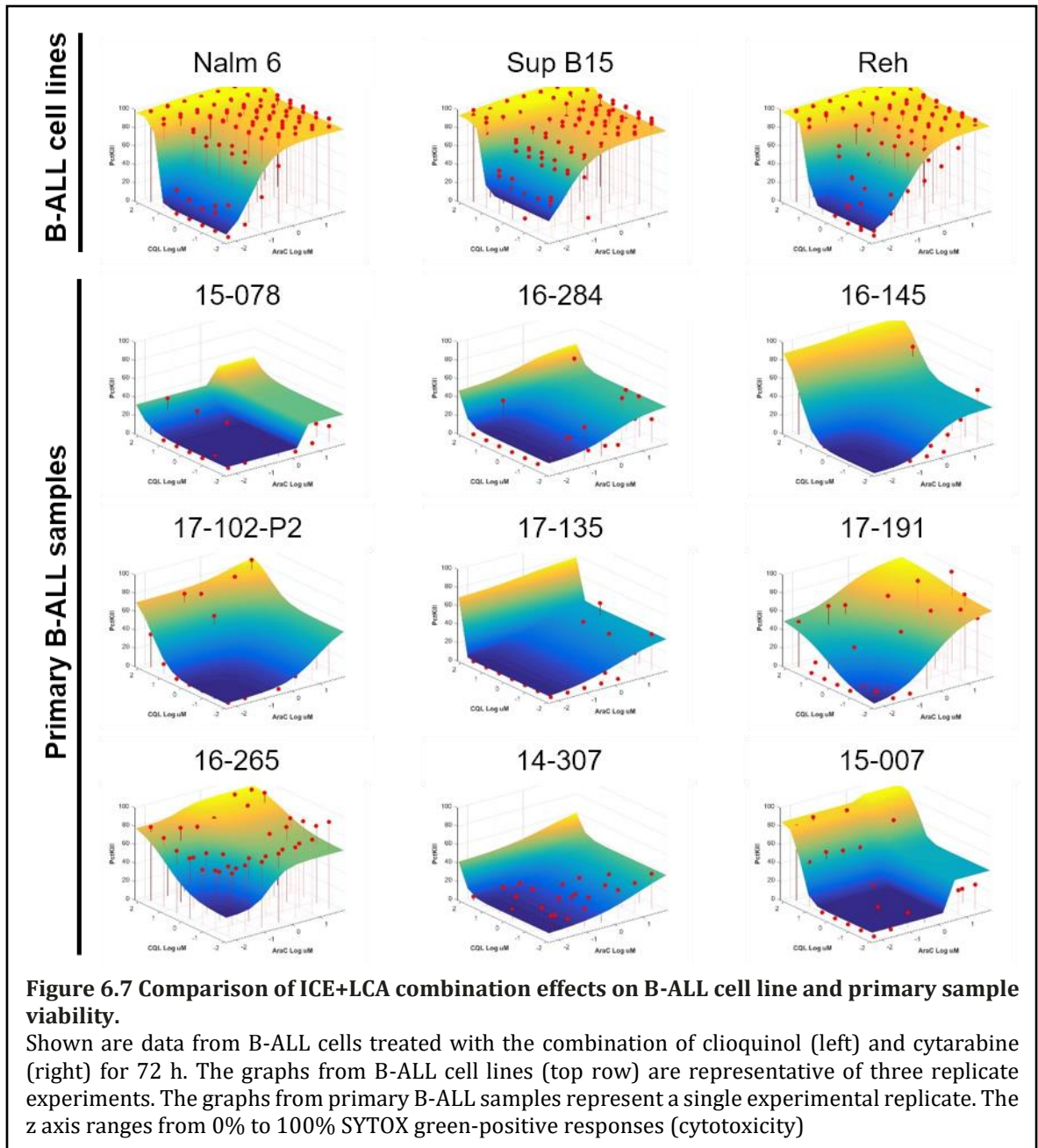
sample had low viability. Primary samples 15-078 and 17-191 had the next highest F-cAMP retention values, > 60%, and had similar diagnostic characteristics, in that both patients were young and exhibited no MRD after 29 days of treatment. However, samples 17-191 had little change, whereas 15-078 had decreased expression of most cAMP-related genes (**Tables 6.7 and 6.8, Figure 6.6**). Samples 17-102-P2, 16-265, and 14-307 exhibited the lowest F-cAMP retention values, about 30%, but were representative of different gene clusters, and thus had disparate expression of cAMP-related genes. These samples also represented patients with drastically different ages, DNA ploidy, and karyotypes. Therefore, it is difficult to associate any one trait with F-cAMP retention ability. Future studies will need to optimize the F-cAMP efflux assay without amphotericin B in order to resolve whether F-cAMP efflux ability, and its potential inhibition by MK-571, are associated with any specific patient sample traits.

Table 6.8 Summary of primary B-ALL sample F-cAMP retention and viability.

Shown are the primary B-ALL samples selected for our studies and the cAMP gene cluster from which they were identified. The incubation time and % retention of F-cAMP are indicated. Also provided are the average % viability of the negative controls (DMSO-only) that were used for data normalization.

Primary Sample	cAMP gene cluster	F-cAMP incub. (h)	% F-cAMP retention	Avg. %viability neg. ctrl	
				48 h	72 h
15-078	1	23	61.30	43.5	71.2
16-284	1	23	48.43	57.9	46.3
16-145	1	22.5	49.59	33.9	22.8
17-102-P2	1	22	29.35	70.7	65.5
17-135	2	22.5	48.01	50.6	33.4
17-191	2	23	66.38	51.9	37.2
16-265	2	21	30.51	44.6	31.1
14-307	2	21	29.71	46.9	65.7
15-007	2	22	96.15	38.2	26.5

While it has been often reported that the drug sensitivities determined for cell lines *in vitro* are similar to those observed for primary samples *ex vivo*, our ICE+LCA combination data do not necessarily fall within that paradigm. Whereas the drug combinations elicited multiple synergistic interactions in the B-ALL cell lines, the responses of the primary B-ALL samples were poor. The primary samples were not only resistant to the ICE+LCA combinations, but to the drugs as single agents as well. Note the difference in the single agent dose responses at the edges of the graphs in **Figure 6.7**. Nonetheless, the primary B-ALL samples did exhibit a variety of responses. Surprisingly, the two samples that exhibited the lowest F-cAMP retention, 17-102-P2 and 16-265, appeared to be the most sensitive to ICE+LCA combinations, and synergistic interactions therein. However, sample 14-307, which exhibited similar F-cAMP retention, but also represented poor diagnostic traits (older age, high initial WBC), was poorly responsive to treatment. Remarkably, the two primary samples that displayed MRD after treatment, a significant marker of poor prognosis, 15-007 and 16-145 (**Table 6.7**), showed dose-dependent responses to the ICE compound clioquinol (CQL) that resulted in nearly total loss of cell viability (**Figure 6.7**).



Given the heterogeneity of the sample characteristics, cAMP-related gene expression, and ability to retain F-cAMP, these variations were expected. A summary of the total synergistic ICE+LCA interactions that were identified for the primary B-ALL samples is provided in **Table 6.9** and the graphs for these data are in **Appendix**

D. These data underscore both the fact that the responses of individual patients are unique, and additionally support the premise that personalized medicine approaches, such as those developed in these studies, are necessary to maximize the potency of a treatment regimen [279].

Table 6.9 Summary of synergistic data points from ICE+LCA combination viability assays in primary B-ALL samples.

Shown are the total number of data points that were identified by SynScreen software to be synergistic by the Bliss model of drug interaction analysis. Incubation times are indicated on the bottom. Patient sample identifiers are listed on the left. The LCA are listed horizontally, and ICE are listed vertically. The maximum number of synergistic data points is 49 per condition. Darker colors on the heatmap indicate more identified synergistic data points.

	48 h				72 h				
	5FU	AraC	MTX	TPT	5FU	AraC	MTX	TPT	
15-078	1	7	0	5	0	0	0	5	571
	0	5	0	4	0	0	0	0	ART
	0	6	0	3	1	1	0	1	CQL
	0	4	1	0	0	0	0	2	CTS
	5	3	3	1	2	3	1	7	DHA
16-284	2	11	1	4	1	7	0	5	571
	3	10	0	8	0	5	0	3	ART
	7	8	3	5	2	7	0	3	CQL
	2	13	1	9	0	4	1	0	CTS
	3	12	4	4	6	5	5	2	DHA
16-145	1	7	4	11	1	7	1	8	571
	1	9	8	5	2	5	4	7	ART
	3	4	4	3	1	2	4	15	CQL
	2	0	2	2	2	4	1	10	CTS
	2	10	0	14	1	2	0	5	DHA
17-102-P2	6	10	3	6	4	7	3	5	571
	11	2	7	2	3	14	1	12	ART
	8	8	10	3	9	5	3	2	CQL
	8	8	7	1	0	11	1	6	CTS
	1	11	0	0	3	8	1	5	DHA
17-135	1	5	2	8	0	3	1	2	571
	3	7	5	7	0	9	1	5	ART
	6	6	6	3	3	4	0	7	CQL
	3	14	1	7	1	11	0	5	CTS
	2	5	1	4	0	6	3	1	DHA
17-191	1	14	0	4	8	16	7	11	571
	4	20	3	3	10	18	6	3	ART
	11	23	5	10	3	11	4	13	CQL
	2	13	0	9	11	19	13	10	CTS
	4	15	0	4	8	10	7	6	DHA
16-265	3	1	2	1	0	4	0	4	571
	0	8	0	4	0	2	0	5	ART
	1	0	0	0	0	34	0	29	CQL
	8	18	0	9	0	10	1	10	CTS
	1	4	1	4	0	2	1	7	DHA
14-307	2	5	2	6	0	3	1	2	571
	1	3	1	0	0	1	0	0	ART
	2	6	0	8	0	3	0	2	CQL
	0	14	0	11	1	4	0	6	CTS
	0	2	0	1	0	31	0	13	DHA
15-007	3	2	28	21	2	2	1	7	571
	17	0	14	1	12	7	6	10	ART
	6	1	12	4	17	7	4	10	CQL
	1	0	1	6	13	2	2	0	CTS
	0	0	0	7	26	4	8	2	DHA

6.4 Discussion

We previously identified several compounds capable of reducing the efflux of a fluorescent cAMP analog from drug repurposing libraries, which we termed inhibitors of cAMP efflux (ICE). We validated the fact that ICE appropriately modulated downstream cAMP pathway activity [6] in acute leukemia cells, and hypothesized that these molecules might be capable of reducing the activity of the cyclic nucleotide effluxing transporters ABCC4, ABCC5, and ABCC11. Due to the fact that many leukemia chemotherapeutic agents (LCA) are nucleotide analogs, the expression of ABCC4, ABCC5, and ABCC11 is associated with drug resistance [102, 103, 226, 269]. Considering that the expression of these transporters is related to prognosis, we hypothesized that the combination of ICE with LCA may interact synergistically. Since both ICE and LCA are capable of independently inducing apoptosis, the combination of the two classes of agents should increase the efficacy of reducing leukemia cell viability. As such, we determined the effects of ICE+LCA combinations on AML and B-ALL cell lines and primary B-ALL samples.

We identified several drug pairs that resulted in synergism at several concentration ratios. Generally, combinations that included the LCA AraC, methotrexate, or topotecan exhibited the most potency. The effects of ICE+LCA combinations were more effective in reducing acute leukemia cell viability, although some drug pairs were able to also decrease proliferation. It is plausible that the incubation times in which proliferation was assessed, 48 and 72 h, were not long enough to allow for several cell divisions. However, for most of our proliferation data,

the ICE+LCA combinations were less potent than what was observed for the agents used alone. Two possibilities may account for these observations. First, because we determined that the ICE+LCA drug pairs were able to synergistically reduce cell viability at the same time points, perhaps too few viable cells remained to significantly influence proliferation. Second, it has been noted that under conditions of cellular stress, modest elevation in intracellular cAMP can stimulate cell growth [83, 85]. Further studies would be needed to elucidate the effects of specific ICE+LCA combinations on cell replication mechanisms.

We observed that the sensitivity of AML cell lines was related to phenotype. The stem-like cell line KG-1a was fairly resistant to ICE+LCA combinations, whereas MV-411 cells, representing a more mature phenotype, were more sensitive to the tested drug pairs (**Table 6.3**). Other researchers have indicated that less-differentiated hematopoietic cells have higher expression of ABC transporters [96]. In our past work, we found that cells that had higher F-cAMP efflux ability were not as sensitive to efflux inhibition by our positive control MK-571 [6] (**Figure 3.9**). Hence, it is plausible that the KG-1a cells were resistant to the effects of ICE, LCA, and combinations since these cells likely express a multitude of transporters that are not as easily affected by our tested drugs. However, in striking contrast to our observations with AML cell lines, our results from B-ALL cell lines indicate that the cell line that we previously identified as having high F-cAMP efflux activity, Nalm 6, was most sensitive to ICE+LCA combinations (**Figure 6.4** and **Table 6.4**). These results are in contrast to Shabestari, *et al.*, wherein the combination of cAMP-

elevating agents with the anthracycline doxorubicin reduced Nalm 6 cell apoptosis [87]. It should be also be noted that Nalm 6 cells had the lowest overall viability at the measured time points, indicating that these cells generally had the lowest capacity for survival under our experimental conditions. Our data for Sup B15 cells, which have lower F-cAMP efflux activity, were the least sensitive to the tested compounds. The differences in our data for AML and B-ALL cell lines may be attributed to lineage specific mechanisms, or to potential differences in intracellular signaling and metabolism. We observed that B-ALL cells required free air exchange during incubation, while AML cells had higher viability if the plates were sealed with ambient air. Therefore, the differences in oxygen sensitivity of these two hematopoietic lineages may be a result of different metabolic dependencies [280].

The data from this work also demonstrated that the primary B-ALL samples were much less sensitive to the tested compounds, to the extent that some conditions did not even induce dose dependent responses (**Appendix D**). We obtained similar results in a previous study wherein we tested tyrosine kinase inhibitors on primary T-cell lineage ALL cells [276]. Because primary cells have been developed in a complex microenvironment, enriched in pro-survival chemokines, it makes sense that these cells have likely employed different survival mechanisms than cell lines. One potential limitation of our experimental approach may be the fact that we incubated the primary cells in media containing serum. While some researchers have used similar approaches [281], others have focused on the use of serum-free culturing conditions [244]. The ability to appropriately mimic the leukemia microenvironment

for the development of personalized medicine approaches will be difficult to resolve, and much more work needs to be done to determine the optimal conditions (serum, oxygen content, growth factors) to culture primary samples.

While the data from the current study were promising, it should be noted that the development of drug combinations for translation to treatment regimens is complex. Here, we tested drug pairs administered to leukemia cells concomitantly. Others have reported that some drug combinations are more efficacious when the individual drugs are used sequentially [282]. Lee, *et al.* noted that erlotinib administered for 24 h prior to the addition of doxorubicin significantly reduced triple negative breast cancer cell viability more than when the drugs were used simultaneously [283]. Given that ICE potentially reduce the transport of LCA out of cells, it is possible that incubation of leukemia cells with ICE prior to the addition of LCA might produce stronger apoptotic effects.

We should also note that our approach was simplistic in the sense that we limited our combinations to pairs. This approach was used both to facilitate the mathematical determinations of drug interactions, but also to limit the potential mechanistic variables that could be involved in the cell responses. However, our work shows that we are on the right track, as recent work by Drenberg, *et al.* determined that combinations of artesunate or dihydroartemisinin with cytarabine synergistically reduced AML burden in three murine *in vivo* models [284]. Realistically, current cancer treatment paradigms involve the use of multiple chemotherapeutics, and future work would need to be done to test ICE in combination with these drug

cocktails to determine both efficacy and potential contraindications. Because efflux transporters are expressed in many organs, we should also be wary of the potential of any compounds targeting these proteins to cause damage to these tissues. Belinsky, *et al.* showed that the administration of the nucleotide analog PMEA to ABCC4 knockout mice induced damage to the bone marrow, spleen, thymus, and intestine [285]. Another study showed that single nucleotide polymorphisms that rendered the transporters ABCB1, ABCC1, or ABCG2 non-functional caused AML patients to develop hepatic, lung, and cardiac toxicities after treatment with induction chemotherapy [286]. The testing of ICE+LCA combinations *in vivo* could help identify these potential issues. Nonetheless, because the transporters that may be responsible for apoptotic evasion by cAMP efflux can also potentially support the removal of structurally related chemotherapy drugs, and thus may contribute to multidrug resistance [226-228, 268], this work may lead to the development of new treatment regimens with increased efficacy against acute leukemia cells.

6.5 Materials and Methods

6.5.1 Reagents and compounds

The positive control for F-cAMP efflux, MK-571, was purchased from Cayman Chemical (Ann Arbor, MI). The remaining ICE and LCA compounds were purchased from Sigma-Aldrich (St. Louis, MO). All ICE and LCA compounds were dissolved in DMSO. Other reagents were purchased from Thermo Fisher Scientific (Waltham, MA) unless specified otherwise.

6.5.2 Cell lines

The human AML (U937, MV-411, KG-1a) and B-ALL (Nalm 6, Sup B15, Reh), and stromal (HS-5) cell lines were acquired from ATCC (Manassas, VA). These cell lines were cultured in complete RPMI (cRPMI; RPMI-1640 medium supplemented with 2 mM L-glutamine, 100 U/mL penicillin-streptomycin and 10% heat-inactivated fetal bovine serum; VWR, Radnor, PA) and incubated in a humidified atmosphere with 5% CO₂ at 37°C. However, it should be noted that the B-ALL and stromal cell line culture cRPMI media additionally contained 1% amphotericin B (cRPMI+B; Sigma-Aldrich).

Conditioned media from HS-5 stromal cells were collected after 3-4 days of growth, with cells at 70-90% confluency. The conditioned media were centrifuged 5 min at 400 rcf to remove cellular debris. The supernatant was collected and frozen until use.

6.5.3 B-ALL patient samples

Primary B-ALL bone marrow samples were acquired at diagnosis from pediatric patients with written, informed consent (HRPO-05-435). All patients or their parent(s)/guardian(s) provided written, informed consent for future research in accordance with the Declaration of Helsinki and local institutional guidelines. Leukemia blasts were enriched by Ficoll-Paque centrifugation and the RNA was extracted using Direct-zol RNA Kit (Zymo Research). RNA libraries were sequenced on P1v2 chips using the Ion Proton™ System (Thermo Fisher Scientific). Sequencing and data processing was completed by the Analytical and Translational Genomics

Shared Resource at the University of New Mexico Comprehensive Cancer Center as described before [287]. The normalized data were log₂-transformed followed by unsupervised hierarchical clustering. Java Tree View was used to create the heatmaps [288].

Only cryopreserved patient samples that had a combined total of at least 20 million cells were used for our studies. The primary cryopreserved cells were thawed, centrifuged at 1300 rpm, and rested for ~2 h in a 5% CO₂ incubator at 37 °C in cRPMI without penicillin or streptomycin. Prior to use, for assays, the rested primary cells were centrifuged at 400 rcf, and resuspended in 27 mL cRPMI+B.

6.5.4 HTFC drug combination setup

All HTFC assays were conducted in 384-well plates (Greiner Bio-One 784201, Monroe, NC). Media were added to all wells with a BioTek MultiFlo (Winooski, VT) liquid dispenser, 5 µL for sample wells and 10 µL for wash wells. For cell lines, the media was that used for tissue culture. For primary B-ALL samples, the conditioned media from HS-5 cells was used for this step. The compounds were then added with the Echo® 555 Acoustic Liquid Handler (Labcyte, San Jose, CA) into to a final DMSO concentration of 1%. Freshly washed cells were resuspended in media (cell lines: 10⁶ cells/mL; primary cells: 0.7-1 x 10⁶ cells/mL, based on the above description). Then, 5 µL of cells were added to sample wells, resulting in a final density of 5000 cells/well for cell lines, and 3500-5000 cells/well for primary B-ALL samples). According to our previous methods[6, 275], the AML cell line assay plates were flushed with ambient

air and sealed with a PlateLoc Thermal Microplate Sealer (Agilent, Santa Clara, CA) prior to incubation. The B-ALL cell lines and primary samples were sealed with Breathe-Easy® sealing membranes according to the manufacturer's protocol (Diversified Biotech, Dedham, MA), and covered with polystyrene plate lids prior to incubation. The AML cell lines were incubated with ICE+LCA combinations for 24 and 48 h, whereas B-ALL cell lines and primary samples were incubated for 48 and 72 h.

6.5.5 HTFC viability assays

6.5.5.1 Propidium iodide (PI) viability assay

The propidium iodide (PI) assay to determine cell viability was performed as previously described [11, 276]. Briefly, PI (Sigma-Aldrich, St. Louis, MO) was added to all wells of the assay plates with a BioTek MultiFlo to a final concentration of 1 µg/mL. The plates were then incubated on rotators at 4°C for 20-45 min.

6.5.5.2 SYTOX green viability assay

The SYTOX green nucleic acid stain (Thermo Fisher Scientific) was used to determine B-ALL cell viability. The dye was diluted with Dulbecco's phosphate-buffered saline (DPBS) to a working concentration of 1.5 µM. The Echo® 555 Acoustic Liquid Handler was used to dispense 20 nL of this solution into assay plates, resulting in a final concentration of 3 nM. The plates were incubated on rotators at 4°C for 15-40 min to prevent potential efflux of the dye at room temperature.

6.5.5.3 Viability data collection and analysis

The HTFC viability data were collected and analyzed as previously described [275, 276]. The assay plates were vortexed on an Eppendorf MixMate® (Hauppauge, NY) at 2000 rpm for 15-30 sec prior to flow cytometry. The data were collected with a HyperCyt® platform (IntelliCyt, Albuquerque, NM) configured to an Accuri C6 Plus flow cytometer (BD Biosciences, Franklin Lakes, NJ). The data were exported in Flow Cytometry Standard (FCS) format and analyzed based on events collected from individual wells [264]. The data were analyzed with ForeCyt® software (IntelliCyt). The samples were gated on forward and side scatter to isolate the cell populations, and a binary gate was used on the fluorescence histograms (PI, FL-3; SYTOX green, FL-1) to distinguish negative (viable) and positive (non-viable) populations.

The data were annotated for the contents and concentrations in each well, and the observed response values were normalized in comparison to responses recorded from cells in control wells. Generally, the mean %viability of cells in negative control wells (containing diluent alone, e.g., DMSO) for each assay plate = 100% viability for the compound-treated samples. The negative control data from individual assay plates was used for normalization, with outliers excluded. The normalized data were then imported into SynScreen software (Bruce Edwards, Albuquerque, NM) and analyzed for drug combination effects as described previously [275].

6.5.6 HTFC proliferation assay

The Multicyt FL-4 cell proliferation kit (IntelliCyt) was used to assess B-ALL cell line proliferation. The cells were loaded according to the manufacturer's protocol, with 5 μ L of dye used to stain 25.2 million cells. After loading, the cells were rested for at least 30 min prior to being added to the assay plates. Small aliquots of unstained and stained cells were analyzed with Accuri C6 Plus flow cytometers to determine the FL-4 channel autofluorescence and initial proliferation dye fluorescence intensity in the cells ($t = 0$).

For HTFC proliferation assay data analysis, the median fluorescence intensity (MFI) from unstained cells was subtracted from the $t = 0$ MFI value, generating the $\Delta t = 0$ MFI value used for normalization. The FL-4 MFI values were obtained for each sample well in the assay. The data were normalized to determine the %retention of the FL-4 fluor. %retention = (sample FL-4 MFI - autofluorescence MFI) / $\Delta t = 0$. Higher %retention values are indicative of reduced proliferation. These %retention values were imported into SynScreen software and analyzed for drug interactions.

6.5.7 Primary cell F-cAMP assay

The F-cAMP assay that we previously reported [6, 101, 124] was adapted to load small batches of primary B-ALL cells with the analog. The F-cAMP was purchased from BIOLOG Life Science Institute (cat. no. F002, via AXXORA, LLC, Farmingdale, NY). DPBS was used to dissolve the probe, resulting in a 500 μ M F-cAMP solution. From the prepared B-ALL samples described above, 1 mL was harvested, centrifuged at 300

rcf for 3 min, and resuspended in NF-RPMI (cRPMI without FBS), then washed once more. The cells were then suspended in the F-cAMP loading solution, consisting of 100 μ L hypertonic solution (10% w/v polyethylene glycol (PEG), 500 mM sucrose in NF-RPMI) with 10 μ L of 500 μ M F-cAMP. The samples were incubated in F-cAMP loading solution for 10 min at room temperature, then centrifuged. The samples were resuspended in 500 μ L hypotonic solution (40% purified, deionized water, 60% cRPMI) and incubated for 2 min at room temperature. The cells were again centrifuged, then resuspended in 1 mL cRPMI. In a 12-well plate (Corning® Costar® TC-treated, 3513, Corning, NY), 500 μ L of HS-5 conditioned medium was added to three wells. Unstained primary cells (500 μ L) were added to one well, and 500 μ L of F-cAMP-loaded primary cells were added to the remaining two wells. One F-cAMP-loaded well was treated with 2.5 μ L 20 mM MK-571 (50 μ M final), while the remaining two wells were treated with 2.5 μ L DMSO alone. 300 μ L was collected from each well to determine initial fluorescence intensities. The remaining samples were incubated under tissue culture conditions for 20-24 h.

The fluorescence intensities for F-cAMP (FL-1) were obtained via flow cytometric analysis of 10,000 cells. The samples were gated on forward and side scatter to identify live cells. These gates were kept consistent for both time 0 (t0) and after incubation. To determine F-cAMP retention, the FL-1 MFI values were first baseline-corrected: A, (t0 F-cAMP loaded MFI – t0 autofluorescence MFI) = t0*; B, (incubated F-cAMP loaded – incubated autofluorescence MFI) = incubated*. % F-cAMP retention = t0* / incubated*.

CHAPTER 7: Clioquinol: to harm or heal

Dominique R. Perez^{1,3}, Larry A. Sklar¹⁻³, and Alexandre Chigaev^{1-3*}

¹ Center for Molecular Discovery, ² Comprehensive Cancer Center, ³ Department of Pathology, University of New Mexico Health Sciences Center, Albuquerque, NM, USA

Pharmacology & Therapeutics. 2019 July 01 (199): 155-163.

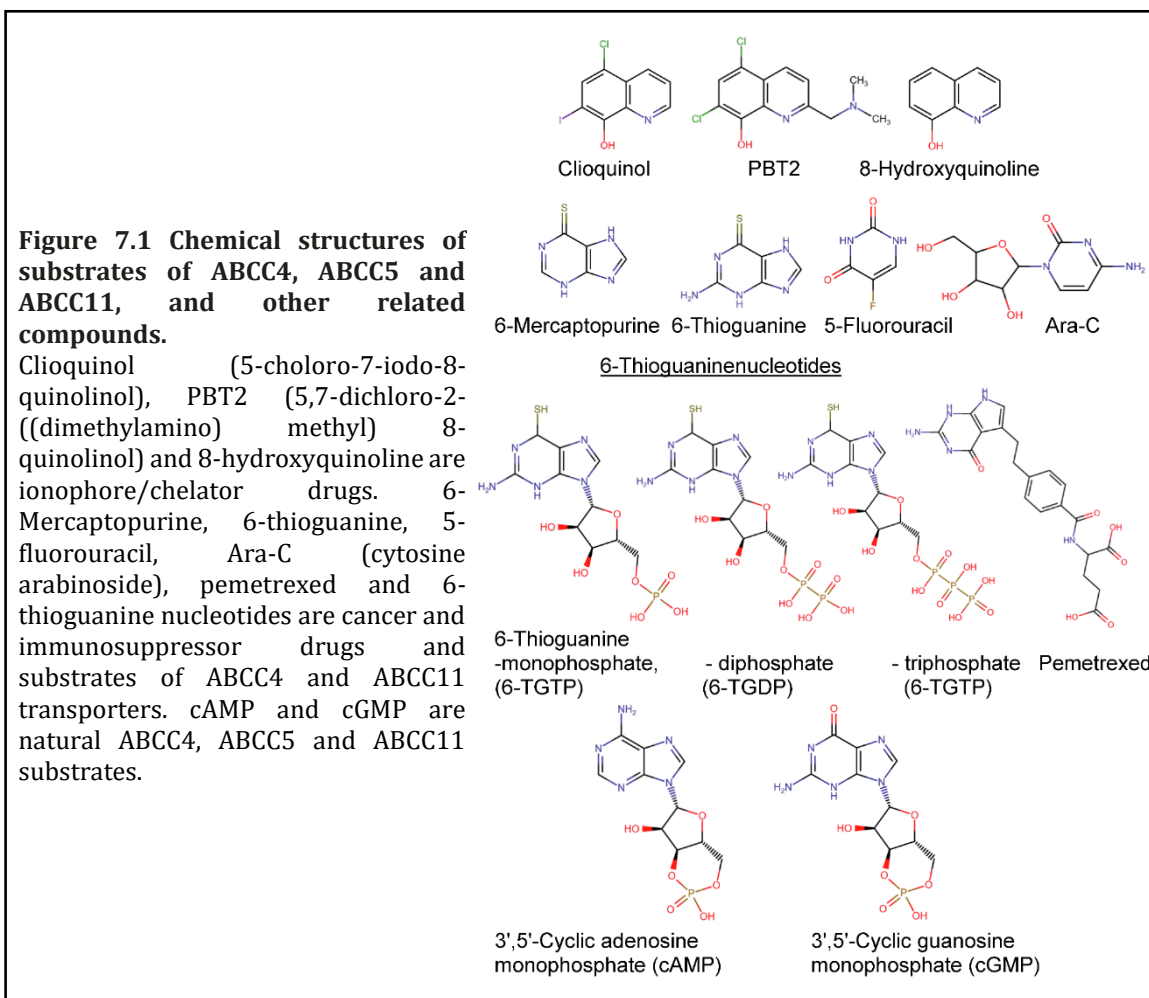
<https://doi.org/10.1016/j.pharmthera.2019.03.009> PMID: 30898518

7.1 Abstract

Clioquinol, one of the first mass-produced drugs, was considered safe and efficacious for many years. It was used as an antifungal and an antiprotozoal drug until it was linked to an outbreak of subacute myelo-optic neuropathy (SMON), a debilitating disease almost exclusively confined to Japan. Today, new information regarding clioquinol targets and its mechanism of action, as well as genetic variation (SNPs) in efflux transporters in the Japanese population, provide a unique interpretation of the existing phenomena. Further understanding of clioquinol's role in the inhibition of cAMP efflux and promoting apoptosis might offer promise for the treatment of cancer and/or neurodegenerative diseases. Here, we highlight recent developments in the field and discuss possible connections, hypotheses and perspectives in clioquinol-related research.

7.2 Introduction

Clioquinol (5-chloro-7-iodo-quinolin-8-ol) (**Figure 7.1**) was first developed in 1899 as a topical antiseptic. It was subsequently repurposed to treat traveler's diarrhea, as well as certain fungal and protozoal infections of the gastrointestinal tract [289]. For many years, it was considered safe, and in the 1930s clioquinol became available over-the-counter in Europe, the US and Asia.



7.3 Subacute myelo-optic neuropathy: clioquinol's fall from grace

While versatile and used worldwide, clioquinol became associated with a mysterious illness primarily confined to Japan. Between 1958-1970, Japanese physicians observed a number of cases that, at first, were characterized by mild abdominal pain and/or diarrhea [290]. These symptoms were often followed by a myelitis-like illness that exhibited an array of neuropathological changes consisting of “pseudosystemic degeneration involving the peripheral nerves, post-lateral columns of the spinal cord and retrobulbar optic nerves” [290]. The new illness was designated as subacute myelo-optic neuropathy or SMON, with unknown etiology. It affected thousands of people who were blinded, paralyzed or confined to wheelchairs for the rest of their lives [289]. 10,000 diagnoses were made and nearly 5 % of cases were fatal [291]. Multiple hypotheses on the etiology of SMON were considered: intoxication by industrial waste or pesticides; a metabolic disorder or vitamin deficiency, and involvement of viral or bacterial infections [290], none of which were confirmed by subsequent studies. SMON patients presented with a green “fur” on their tongues, and green-pigmented urine and feces. Surprisingly, this green pigment was identified as the Fe (III) chelate of clioquinol [290]. Moreover, the number of SMON monthly cases closely correlated with the number of clioquinol tablets consumed, and only patients that took clioquinol exhibited symptoms of the disease [290]. This necessitated a ban of clioquinol sales in September 1970. As a result, the monthly SMON incidence went from ~ 150 in July to 1 in October [290]. However, one mystery that remained was that SMON was primarily endemic to Japan.

Internationally, the 1969 sales of clioquinol per capita in 15 studied countries were higher than in Japan, yet there were no reports of SMON [291]. Some researchers speculated that familial (genetic) factors could account for the higher incidence of SMON in Japanese clioquinol users [290].

7.4 Clioquinol makes a comeback against neurodegenerative diseases

One of clioquinol's first-identified mechanisms of action relates to its ability to interact with metals. The idea that the accumulation of the "wrong" metals in the human brain can cause Alzheimer's disease (AD) dates back to the late 1970s [292]. In a more recent study, researchers found a significant decrease in serum manganese level in AD subjects vs. healthy individuals but concluded that neither lead nor manganese levels represented biomarkers in the studied cohort [293]. Another study found that the copper content was increased in AD platelets. The patient stratification using MMSE score (*see glossary*, section 7.12) revealed a larger copper increase in the group with more significant impairment. They detected a 1700% copper increase in severe cognitive impaired patients and only a 112% increase in the mild-to-moderate cognitively impaired group. As a result, platelet copper was envisioned as a potential diagnostic biomarker for AD [294]. Specific roles for rubidium and potassium in AD were also proposed, since both metal ions are decreased across all intracellular compartments in the AD brain [295]. Nevertheless, these and other data motivated studies to assess metals as markers in AD pathogenesis.

In an effort to develop a novel therapeutic options for AD, Ashley Bush and collaborators reported results from a drug repurposing screen aimed at identifying efficient metal chelators among existing antibiotics and anti-inflammatory drugs [296]. In 2001, clioquinol was reported to dissolve β -amyloid deposits in postmortem human tissues [297]. In a mouse AD model, clioquinol was also reported to inhibit plaque formation [296]. Subsequently, Dr. Bush's group introduced the novel concept of metallostasis, a dysfunction of metal trafficking in the brain, where metals are redistributed into inappropriate compartments [298]. This hypothesis, originating from early clioquinol-related findings, is based upon a triad of transition metals: Fe, Cu and Zn [299-301]. Today, several groups are attempting to improve clioquinol-based structures (**Figure 7.1**) [302, 303]. Clioquinol and its next generation metal chelator derivative, PBT2 (5,7-dichloro-2-((dimethylamino)methyl) 8-quinolinol; **Figure 7.1**), have shown "cognitive and plasma biomarker effect[s]" for 36 patients in a Phase II clinical trial in AD. However, a subsequent Phase II/III trial was terminated because of a toxic impurity, an unwanted by-product of the drug synthesis (see <http://www.alzforum.org/therapeutics/cliouquinol>). The following trials showed satisfactory safety and tolerability of PBT2 in AD and Huntington's disease patients, with the conclusion that larger and longer future trials will be required to establish any potential therapeutic benefits [303, 304]. Hence, future "large-scale phase 3 trials of [metal based therapeutic approaches] are warranted" [305]. More recent reports indicate that clioquinol was also capable of preventing the loss of *substantia nigra* cells in the Parkinsonian human A53T transgenic mouse model, as

the accumulation of nigral iron (Fe) in aggregates containing α -synuclein represents an important feature of Parkinson's disease pathogenesis [306]. The effect of clioquinol upon cognitive and motor function in this mouse model was attributed to its ability to prevent a Fe-synuclein interaction as a moderate-affinity metal chelator [307].

Nonetheless, the mechanism of clioquinol's action, at first thought to be related to Cu/Zn or other metal chelating properties, is still debated and considered important [289]. Alternative theories have suggested that the accumulation of aggregated proteins in neurodegenerative diseases like AD could be attributed to defective clearance of misfolded or aggregated proteins in astrocytes and neurons. Autophagy, a cellular degradation process that targets unnecessary cytosolic proteins to the lysosomal compartment, seemed a plausible candidate for the pathogenesis of AD. In fact, it was found that clioquinol induces autophagy [308], or that it can reverse arrested autophagy [309]. At micromolar concentrations, clioquinol up-regulated phosphatidylethanolamine conjugated to the protein LC3-I, a marker of autophagy. The microtubule-associated protein 1A/1B-light chain 3 (LC3) cytosolic form is referenced as LC3-I, and the phosphatidylethanolamine conjugate as LC3-II [310]. This effect appears to be related to the ionophore properties of clioquinol rather than its zinc chelation properties, as an alternative zinc chelator was shown to reduce LC3-II accumulation. Moreover, the addition of zinc increased the accumulation of LC3-II, confirming the role of zinc in the induction of autophagy [308]. While "arrested autophagy" could contribute to AD [309], data relating clioquinol and autophagy are

limited. Because targeting the autophagic pathway is envisioned as a promising approach in cancer therapy [311], it is not surprising that clioquinol is under study in cancer-related fields.

Nonetheless, several reports indicate that autophagy induction by clioquinol is model-dependent. For example, in human hepatoma cells, clioquinol induced neither autophagy nor apoptosis, although it triggered cell cycle arrest in the S-phase. This effect was accompanied by down-modulation of cell cycle proteins, including Cdk2 and cyclins D1 and A2, as well as up-regulation of p21 and p27 [312]. As transition metals are unlikely to be unique targets of clioquinol, other potential clioquinol targets were later identified. ABC transporters represent one class of potential targets.

7.5 Clioquinol may be a rising star against cancer too

Due to multiple reported cellular effects, clioquinol has also been studied for use against cancer, where modulating membrane transport is of interest. Originally, ATP binding cassette (ABC) transporters (*see glossary*, section 7.12) attracted attention because of their abilities to efflux the nucleoside-like drugs that are used for chemotherapy in cancer or immunosuppression in autoimmune diseases (**Figure 7.1**). The idea that ABC transporters have normal physiological functions, that include active transport of metabolites and signaling molecules, was later accepted [105]. Given their altered metabolism, cancer cells rely upon membrane transport more than normal cells. Moreover, up-regulated expression of membrane transporters was

associated with poor overall survival and a high degree of resistant disease in acute myeloid leukemia [313]. Another concept links aberrant membrane transport in cancer with evasion of programmed cell death. The efflux of the pro-apoptotic second messenger, 3',5'-cyclic adenosine monophosphate (cAMP, **Figure 7.1**), is proposed as one such cell survival mechanism [6, 314]. Three transporters from the ABCC family, ABCC4, ABCC5 and ABCC11, are reported to efflux cyclic nucleotides. Furthermore, the increased expression of these transport proteins is known to be associated with worse prognosis in leukemia [102, 314].

To test the hypothesis that blocking cAMP efflux triggers the accumulation of cAMP and stimulates cAMP-dependent downstream signaling, we developed a screen using a fluorescent cAMP analog to identify compounds that block active cAMP efflux [315]. Surprisingly, one of the identified drugs was clioquinol. In support of our hypothesis, treatment with clioquinol or other Inhibitors of cAMP Efflux (ICE) resulted in increased phosphorylation of the cAMP-responsive element-binding protein (CREB; Ser133), a classical cAMP downstream effector that activates target genes. Furthermore, it triggered dose-dependent hallmarks of the cAMP-dependent intrinsic apoptotic pathway. While no apparent correlation between ABCC4 (MRP4) expression and cAMP efflux was found, we concluded that alternate ABC transporters capable of cAMP efflux, such as ABCC5 (MRP5) and ABCC11 (MRP8), could contribute to the removal of cAMP from different cells [6]. These studies suggest that clioquinol and other ICE can target cAMP efflux in cancer via ABC transporters. A recent report showed the effect of clioquinol on another ABC transporter, ABCB1 (MDR1 or P-gp)

[316]. A combination of clioquinol with zinc and copper significantly increased the expression of the ABCB1 protein. This was accompanied by a change in the ability of cells to efflux the ABCB1 substrate [316]. Thus, there could be an underappreciated connection between ABC transporters, efflux substrates and clioquinol.

7.6 ATP-binding cassette transporters, potential culprits in clioquinol-associated subacute myelo-optic neuropathy?

Clioquinol's potential involvement with ABC transporters brings us back to SMON. Could transporter inhibition contribute to its neuropathological symptoms? We propose that a natural (genetic) impairment of normal transporter function or capacity, combined with increased transport inhibition by clioquinol, could trigger the etiology of SMON. Toward this end, we focus on the fact that SMON was almost completely confined to the Japanese population and was seldom reported in other countries [290, 291]. While high doses of clioquinol were sufficient to partially recapitulate human pathology in several animal models, only a few cases of the disease were reported outside of Japan.

The familial aggregation of the SMON cases, previously interpreted in terms of the infectious nature of SMON etiology [290], could reflect a genetic component related to single-nucleotide polymorphisms (SNPs; *see glossary*, section 7.12) in cAMP-transporting ABC pumps. Multiple non-synonymous SNPs that can potentially affect a transporter's function have been identified, and surprisingly, ABCC4 and ABCC11 SNPs are elevated in the Japanese population.

7.7 Single nucleotide polymorphisms in ABCC4 and ABCC11 in Japanese population dramatically increase sensitivity to nucleotide-like drugs

7.7.1 ABCC4

The ABCC4 SNP rs3765534 (G2269A, E857K) dramatically reduces transporter function by interfering with protein membrane localization [317]. This SNP is widespread in the Japanese population (> 18 % allelic frequency) but is significantly less in all other studied groups: Ashkenazi Jews, Africans north of the Sahara, Pacific Islanders, European Americans, African Americans, Middle Easterners and Chinese Americans [317]. In Japanese patients with inflammatory bowel disease, the allelic frequency of ABCC4 G2269A was 14.7%, with levels of the substrate 6-thioguanine significantly higher in patients with the ABCC4 variant alone than in patients with the WT allelotype. This result, together with experiments in murine models, suggests that the decreased ability to efflux 6-thioguanine nucleotides (**Figure 7.1**) accounts for thiopurine-induced hematopoietic toxicity in patients with the ABCC4 G2269A SNP [317]. In another study, the relationship between ABCC4 G2269A, increased thiopurine sensitivity and leukopenia was also reported [318].

Additional SNPs in ABCC4 with a high frequency in the Japanese population are C912A and C559T (compare 0.3 and 0.14 respectively in the Japanese population vs. 0.02 and 0 in the Caucasian population), and these have been shown to affect 6-mercaptopurine (**Figure 7.1**) sensitivity in childhood ALL [319]. The variant G559T correlated with diminished ABCC4 protein expression in human liver samples [320] and reduced drug efflux function [321]. ABCC4 expression in the livers of patients

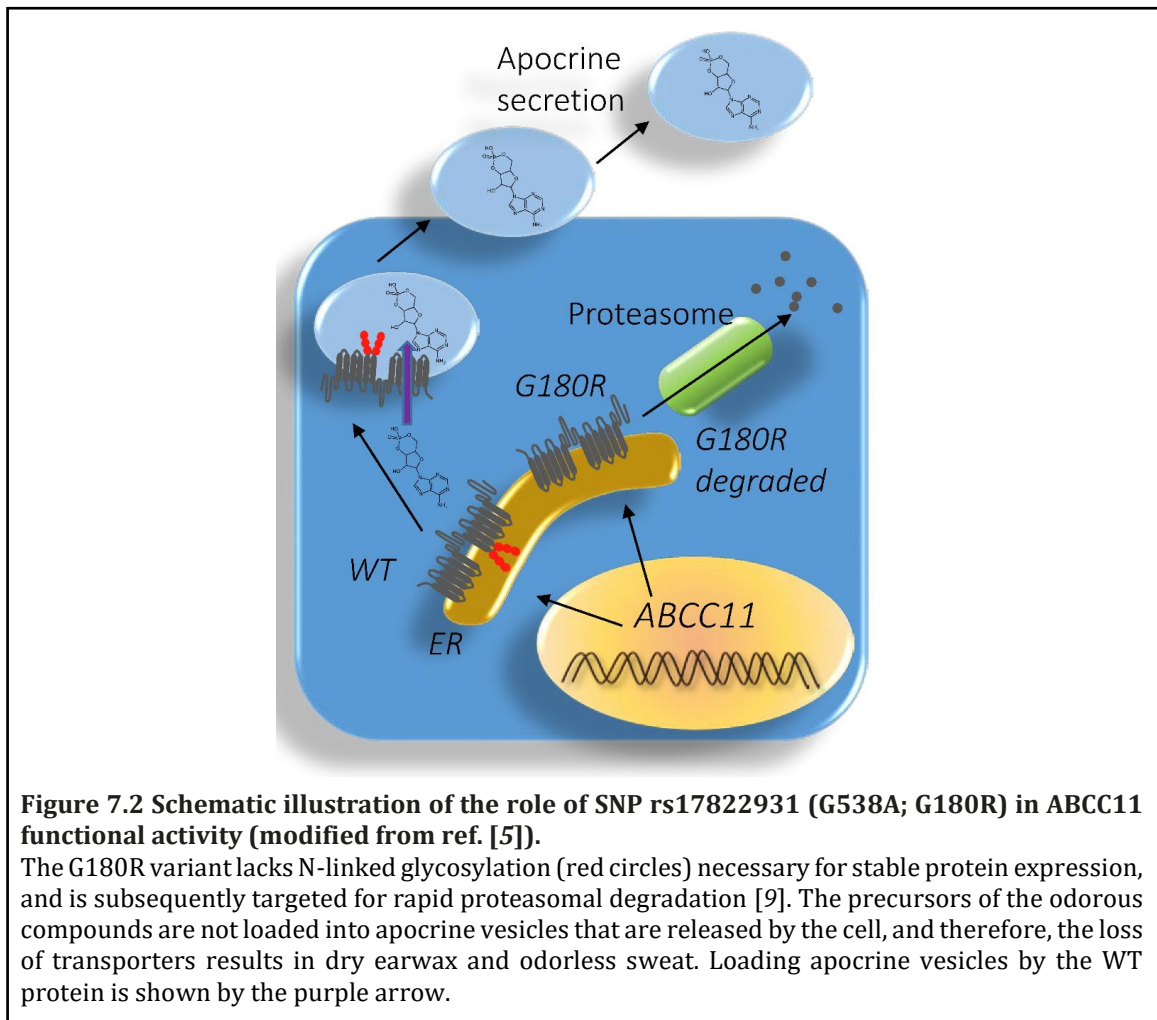
carrying the non-synonymous C912A variant was only ~54 % of control expression. Hence, ABCC4 SNPs that negatively affect expression or efflux function of the transporter and thus, increase patient sensitivity to nucleotide-like drugs are enriched in the Japanese population.

7.7.2 ABCC11

The SNP rs17822931 (G538A; G180R) in ABCC11 was first discovered as a genetic variant that determines earwax type in humans [322]. WT ABCC11 is associated with brownish, sticky, wet-type earwax and axillary osmidrosis (*see glossary, section 7.12*) [9, 323]. The G180R is related to the formation of dry-type earwax [322]. The G180R variant lacks N-linked glycosylation necessary for stable protein expression, and therefore, undergoes rapid proteasomal degradation [9]. As a result, the secretion of earwax is dramatically changed (**Figure 7.2**).

In the Japanese population, the frequency of the G538A allele is very high. Accordingly, it varies from 0.71-0.99 in different prefectures of Japan [324]. In populations of European or African origin, it is extremely rare (0.00-0.03). The geographical distribution of this allele is believed to be related to the migration of the Yayoi people, who came to Japan 3000–1800 years ago [324]. It worth noting that this distribution is somewhat similar to the distribution of the annual incidence or prevalence rates of SMON, with the highest rates in the southwestern part of Japan, especially in the Kinki or Kansai and Shikoku prefectures (compare maps in references [324] and [290]).

Similar to ABCC4, several studies also indicated the importance of this SNP in nucleotide-like drug sensitivity. Uemura et al., 2010 analyzed the effect of the ABCC11 SNP genotype (G538A, G/G, G/A, and A/A) in a set of 13 adenocarcinoma cell lines. They found that A/A homozygotes were significantly more sensitive to pemetrexed (**Figure 7.1**), as compared to the combined G/G and G/A groups. The authors concluded that SNP (G538A) in the ABCC11 gene represents an important determinant of pemetrexed sensitivity [325].



Thus, an increased sensitivity to nucleotide-like drugs directly related to ABCC protein polymorphisms has been reported in Japanese patients [318, 320]. The cyclic nucleotides, cAMP and cGMP, are well known natural substrates of ABCC transporters that exhibit significant structural similarity with anticancer drugs, including pemetrexed, methotrexate, cytosine arabinoside, and 9'-(2'-phosphonyl-methoxyethyl)adenine, as well as 5-fluoro-2'-deoxyuridine 5'-monophosphate, an active metabolite of 5-FU (5-fluorouracil) (**Figure 7.1**) [326]. Is it plausible that the decreased function of the ABC transporter in patients carrying SNPs, in a manner similar to cancer drugs, also diminishes cAMP efflux? Would patients with SNPs in ABCC4 and ABCC11 transporters be vulnerable to clioquinol, while patients carrying wild type alleles would be resistant? While testing these hypotheses would require additional studies, if true, clioquinol could be safe for a large fraction of the world's population and could allow broad repurposing. Tests for detecting mutant ABCC4 and ABCC11 alleles have already been developed and validated in large human populations [324], thus allowing for easy identification of good candidates for clioquinol treatment.

7.8 Possible beneficial effects of single nucleotide polymorphisms in ABCC transporters

It noteworthy that SNPs in cAMP transporters are not entirely harmful. They may provide benefits for other conditions, like cancer. While the physiological function of ABCC11 beyond earwax and axillary glands is unclear, a role in cancer is possible.

Caucasians and African-Americans showed approximately four-fold higher rates of breast cancer mortality as compared to women of Japanese and Taiwanese origin. The international mortality and frequency rates for breast cancer were reported to be associated with the frequency of the allele for wet-type earwax [327]. A direct study of ABCC11 G538A association with breast cancer conducted in Japanese women revealed that the WT (538G) allele frequency in cancer patients was higher than in the control group and moderately associated with the risk of breast cancer [328]. Since WT ABCC11 has the ability to efflux cyclic nucleotides (cAMP and cGMP), the finding that a functionally “defective” transporter allele has a protective effect against cancer supports the idea that cAMP efflux transporters can contribute to the evasion of apoptosis and that impaired cAMP removal helps to eliminate cancer cells [6]. In Caucasian women, no significant relationship between breast cancer risk and G538A allele has been found [329] [330]. One explanation for this phenomenon could be that the presence of fully functional ABCC11 paralogs (such as ABCC4, for example) in the Caucasians population compensates for the function of the mutated transporter. Since the Japanese population is enriched in SNPs that can also down modulate ABCC4 function, it is plausible that a specific set of SNPs in ABCC transporters (rather than a single SNP) is required to provide a cancer-protective function.

If down-modulation of transporter function is beneficial for cancer patients, then transporter up-regulation should have the opposite effect. Indeed, a high level of ABCC11 expression in breast tumor tissue was associated with worse disease-free

survival [331]. Typically, such data are interpreted as though an increased expression of the transporter causes efflux of the chemotherapy drug, providing a survival benefit for malignant cells. However, the authors argued that only a fraction of the patient cohort used in this study (~ 30.9%) had received 5-fluorouracil (**Figure 7.1**), a known substrate of ABCC11 used for breast cancer therapy. Therefore, they posited that drug “efflux alone cannot explain the association” between transporter overexpression and poor disease-free survival. The authors concluded that “some other function of ABCC11 may contribute to the phenomenon” [332]. Thus, the efflux of another substrate, possibly of a nucleotide nature, may provide a plausible explanation. The recent discovery that type 10 soluble adenylyl cyclase (sAC; *see glossary, section 7.12*) produces cAMP as a result of oncogenic stress and functions as a tumor suppressor protein may also provide indirect support for the notion of a specific role of cAMP in cancerogenesis [333].

Furthermore, it is well established that in Japan, the rates of AD are lower than in other developed countries. This difference is usually attributed to differences in diet, low in cholesterol and saturated fat [334]. However, since the SNPs in cAMP transporters seem to lower, or at least negatively correlate, with the risk of breast cancer, is it possible that a similar relationship exists in AD?

7.9 Could clioquinol's effect on cAMP be relevant to clioquinol's action in Alzheimer's disease?

The ability to modify the efficacy of synaptic transmission in response to neural activity is termed synaptic plasticity. It underlies the capacity of neuronal networks to adjust to external stimuli, and to process information. Long-term plasticity, occurring over tens of minutes to years, appears to impact memory and learning. Experimentally studied as long-term potentiation (LTP; *see glossary*, section 7.12), it may represent the measurable cellular correlate of learning and memory. Consequently, the etiology of AD pathology is shifting from β -amyloid deposits and neuronal death toward synaptic dysfunction as an early cause of the disease. LTP impairment was one of the first quantifiable outcomes supporting this idea [335]. However, the molecular mechanisms of this process are unclear.

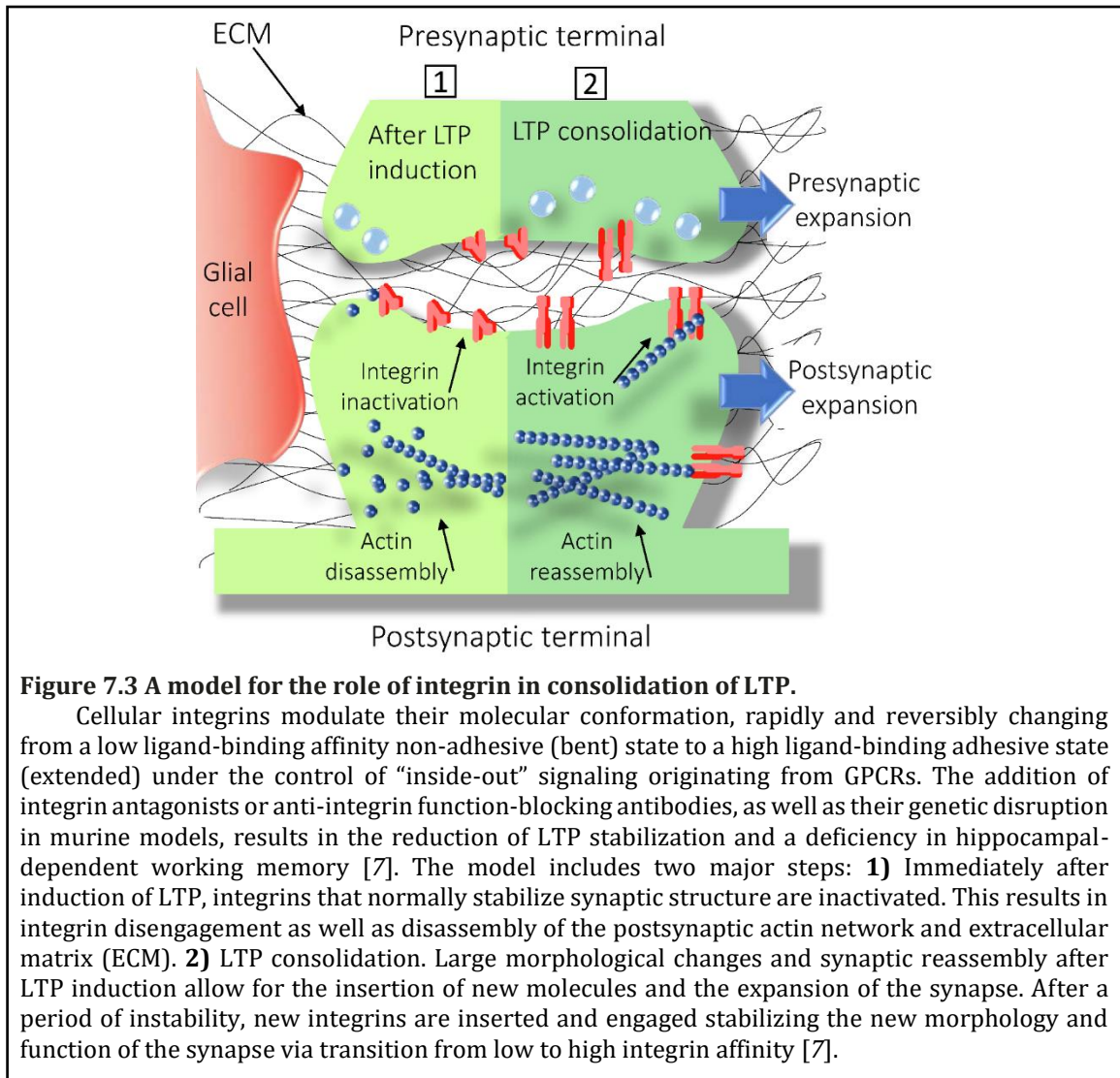


Figure 7.3 A model for the role of integrin in consolidation of LTP.

Cellular integrins modulate their molecular conformation, rapidly and reversibly changing from a low ligand-binding affinity non-adhesive (bent) state to a high ligand-binding adhesive state (extended) under the control of “inside-out” signaling originating from GPCRs. The addition of integrin antagonists or anti-integrin function-blocking antibodies, as well as their genetic disruption in murine models, results in the reduction of LTP stabilization and a deficiency in hippocampal-dependent working memory [7]. The model includes two major steps: **1)** Immediately after induction of LTP, integrins that normally stabilize synaptic structure are inactivated. This results in integrin disengagement as well as disassembly of the postsynaptic actin network and extracellular matrix (ECM). **2)** LTP consolidation. Large morphological changes and synaptic reassembly after LTP induction allow for the insertion of new molecules and the expansion of the synapse. After a period of instability, new integrins are inserted and engaged stabilizing the new morphology and function of the synapse via transition from low to high integrin affinity [7].

Because the consolidation of LTP requires a series of transitions between engaged and disengaged cell adhesion molecules, like integrins (**Figure 7.3; see glossary, section 7.12**), it is possible that the stabilization of one state due to a signaling dysfunction would significantly perturb the outcome of the entire process. As integrin function depends upon the cAMP/PKA/CREB pathway [336-339], clioquinol and other ICE compounds shown to up-regulate the cAMP-signaling

pathway were also able to deactivate integrins [6]. The observation that anti-integrin antibodies or antagonists that inhibit adhesive interactions were capable of preventing the β -amyloid peptide-induced inhibition of LTP [340], suggests that the de-adhesion or integrin deactivation step of the LTP consolidation sequence (step #1, **Figure 7.3**) is likely affected in AD. The fact that pharmacologically-increased intracellular cAMP was also capable of preventing the inhibition of LTP induced by β -amyloid peptides [341] additionally supports this idea. Thus, cAMP regulation of cell adhesion through integrin receptors provides an unexpected link between clioquinol and synaptic plasticity (**Figure 7.4**).

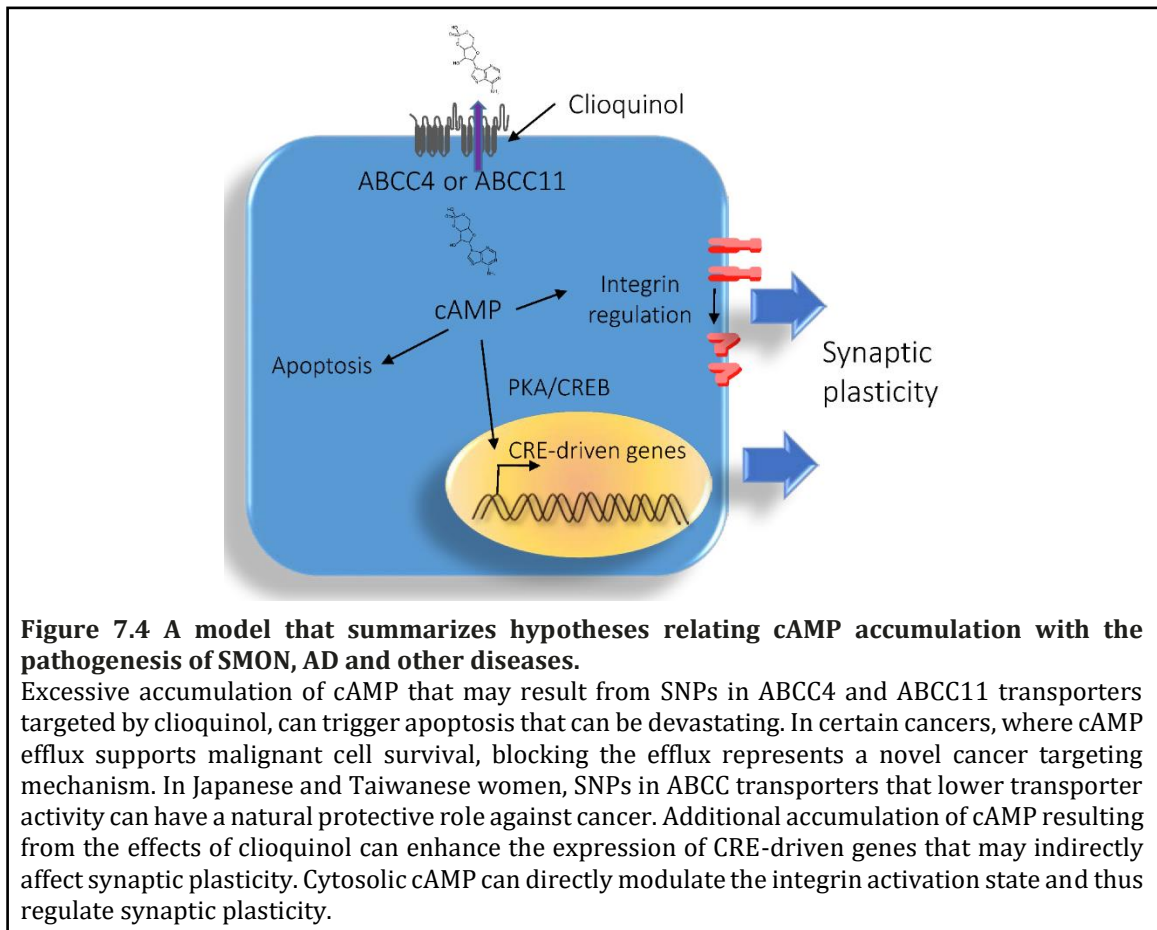


Figure 7.4 A model that summarizes hypotheses relating cAMP accumulation with the pathogenesis of SMON, AD and other diseases.

Excessive accumulation of cAMP that may result from SNPs in ABCC4 and ABCC11 transporters targeted by clioquinol, can trigger apoptosis that can be devastating. In certain cancers, where cAMP efflux supports malignant cell survival, blocking the efflux represents a novel cancer targeting mechanism. In Japanese and Taiwanese women, SNPs in ABCC transporters that lower transporter activity can have a natural protective role against cancer. Additional accumulation of cAMP resulting from the effects of clioquinol can enhance the expression of CRE-driven genes that may indirectly affect synaptic plasticity. Cytosolic cAMP can directly modulate the integrin activation state and thus regulate synaptic plasticity.

7.10 The cAMP/PKA/CREB signaling pathway as a possible target in Alzheimer's disease

Discovered in a screen designed to identify compounds that block the efflux of a cAMP fluorescent derivative, clioquinol was reported to up-regulate CREB Ser133 phosphorylation (see Figure 3 in reference [6]). It was also shown that mice expressing a constitutively active form of CREB (VP16-CREB) in hippocampal neurons facilitated LTP [342]. The enhanced expression of CRE-driven genes facilitated the priming of synapses leading to the stimulation of synaptic capture [343]. Thus, increased cAMP signaling, via administration of caffeine [344], or environmental enrichment (*see glossary*, section 7.12) by means of β 2 adrenergic receptor/adenylyl cyclase stimulation, can be beneficial in animal models of AD [342]. Moreover, because impaired CREB phosphorylation represents an essential pathological component of AD, the induction of CREB phosphorylation (Ser133) in response to different classes of drugs/compounds has been proposed as a mechanistic marker for identifying compounds potentially beneficial for treating AD [345]. However, the cause of the cAMP-dependent pathway dysfunction in AD remains unknown.

Earlier models for AD pathology proposed PKA dysfunction, where oxidative stress mediated by the β -amyloid peptide, ROS and mitochondrial dysfunction were envisioned to contribute to AD pathogenesis [346]. Alternative β -amyloid peptide-independent models have also been considered [347-349]. Nevertheless, the role of cAMP efflux and cAMP-efflux transporters in AD has never been considered despite:

1. cAMP-efflux transporter expression on neurons [350],
2. elevated ABCC4 expression in AD brains [351],
3. increased cerebrospinal fluid cAMP levels in AD patients [352],
4. increased cAMP immunostaining in cerebral cortical and meningeal vessels correlated with β -amyloid immunostaining localized in the “selectively vulnerable targets of neurodegeneration” [353]. Furthermore, ABC transporters are generally considered good drug targets in neurological diseases [354].

Extracellular deposits of β -amyloid peptides and neurofibrillary tangles (aggregates of hyper-phosphorylated tau protein) are two pathological hallmarks of AD. However, it is difficult to correlate the severity of clinical manifestations of the disease, such as dementia, and these pathological features [355]. We propose that dysregulation of neuronal cAMP signaling, and specifically cAMP efflux, contributes to the pathology of AD. The idea that these protein assemblies can cause synaptic dysfunction and impair LTP has gotten more attention from the scientific community. One of the first breakthrough findings here was the observation that β -amyloid peptides were capable of inhibiting the cAMP/PKA/CREB pathway and LTP. Elevation of the cAMP content in neurons was sufficient to reverse this inhibition [356]. Today, a large body of literature supports the notion that additional stimulation of the cAMP/PKA/CREB pathway leads to subsequent CREB phosphorylation in AD (Figure 7.4).

The cAMP-dependent signaling pathway and multiple cAMP-downstream effectors also play significant roles in triggering neuronal apoptosis [357-359]. Numerous stress factors, including ischemia and reperfusion, traumatic brain injury, etc., are reported to stimulate cAMP-dependent signaling. Surprisingly, the signaling pathway that activates apoptosis in neurons is very similar to the pathway that induces the death of cancer cells. In neurons, apoptosis induced by reperfusion after simulated ischemia results in increased cAMP accumulation, mitochondrial depolarization, and effector caspase activation [360]. These steps parallel the apoptosis induced in leukemic cells by clioquinol and other ICE [6]. In both cases, apoptosis was prevented with KH7, a specific inhibitor of the cAMP-producing enzyme sAC. Moreover, the three transporters reported to actively efflux cAMP from cells were detected on the protein level in neurons (ABCC5 and ABCC11), astrocytes and microglia (ABCC4 and ABCC5), and endothelia (ABCC4 and ABCC5) [350], providing a target for clioquinol and other ICE in the CNS. Given the potential relationship of CNS transporters, neuronal function, and clioquinol, is it possible that clioquinol's capacity to inhibit cAMP efflux, rather than its chelator/ionophore activity, provides any of the speculated benefits that were reported in AD? If true, could other ICE compounds provide similar potential benefits? Indeed, two ICE compounds, cryptotanshinone and parthenolide, were claimed to prevent, alleviate or treat AD or AD symptoms ([361-364] and patent applications US 2004/0039050 A1, US 2015/0164858 A1). Thus, it is plausible that ICE may restore activation of downstream cAMP signaling. Hence, a story that started with clioquinol and a

mysterious disease confined to Japan, leads to novel questions and hypotheses about AD pathogenesis.

7.11 Concluding remarks and future perspectives

The public health impact of AD is expected to increase in the next 30-50 years, yet there is no effective preventative strategy or treatment that will dramatically reverse its debilitating effects. The main difficulty is our lack of understanding of the disease pathogenesis. A deeper understanding of the AD pathological process will help us to identify better therapeutic targets and will facilitate the development of new therapeutic strategies and drugs aimed at overcoming the disease progression and burden.

Here, we have briefly reviewed the history of the drug clioquinol and highlighted multiple mechanisms of action that have been attributed to the beneficial effects of the drug, as well as its severe side effects during different historical periods. Further interest in the use of clioquinol was aroused by the finding that it inhibited plaque formation in AD mouse models, possibly by its ionophore properties. A key concept here is the ability of clioquinol to block cAMP efflux from cells and thus, to trigger the phosphorylation of CREB Ser133, a classical cAMP effector that activates target genes. This finding provided a connection to possible targets of clioquinol: ABCC4 and ABCC11, transporters that normally efflux numerous endogenous substrates, including cAMP. A further analysis revealed the presence of SNPs in both ABCC4 and ABCC11, capable of reducing transporter function and at the same time present with

a high frequency in the Japanese population. Modern studies showed that these SNPs are critical for patient sensitivity to cancer and immunosuppressor nucleotide-like drugs, substrates of ABCC4 and ABCC11 transporters. Thus, this line of research provides a plausible explanation for the SMON phenomenon: patients that carry SNPs in ABC transporters that dramatically affect nucleotide efflux are expected to be more sensitive to clioquinol. Since these SNPs are geographically restricted to Japan, this also accounts for the specific distribution of the disease. Today, these hypotheses can be experimentally verified, and as a result, might offer a path to the safer use of clioquinol in clinical practice.

Several alternative ideas about clioquinol's mechanism of action were explored by others, however, they did not result in significant breakthroughs. One exciting new concept presented here describes clioquinol's role in blocking cAMP efflux and increasing CREB phosphorylation. Because the dysregulation of the cAMP/PKA/CREB pathway is a hallmark of several diseases, it is plausible that the beneficial effects of clioquinol are due to its influence on this pathway. Moreover, the specific role of cAMP-related signaling in integrin inside-out deactivation provides an unexpected molecular mechanism that could link clioquinol effects with synaptic plasticity. This leads to a number of questions that can all be addressed using modern technologies. For example, it is important to know how blocking cAMP efflux affects LTP consolidation. Very limited data about the efflux of signaling mediators, including cyclic nucleotides, from the tetrapartite synapse elements are available. In addition, it is necessary to understand conformational and ligand-binding affinity changes in

synaptic and glial integrins that occur under different conditions, and how changes in the extracellular environment affect the synapse. On a macro scale, studies of the signaling partners of the cAMP/PKA/CREB pathway and their alterations in aging, health and disease are also required. And finally, will it be possible to develop novel therapeutic strategies for AD by targeting active cyclic nucleotide efflux?

Today we still have much to learn about the pathological processes underlying neurodegenerative diseases. As the human population ages, the overall impact of AD is expected to grow. Recent research, surprisingly originating from studies of an old drug, clioquinol, and implicating cAMP-related signaling in the pathogenesis of AD, represent a promising approach that may lead to a better future for generations to come.

7.12 Glossary

ATP-binding cassette (ABC) transporter: A superfamily of active transporters that use energy from ATP hydrolysis to pump substrates across cell membranes. Certain ABC pumps participate in drug efflux from cancer cells, thus contributing to drug resistance. Defects in transport function may lead to drug sensitivity and adverse drug reactions. ABCC (subfamily C) members are also known as multidrug resistance proteins (MRPs). ABCC4 (MRP4), ABCC5 (MRP5) and ABCC11 (MRP8) are reported to efflux cyclic nucleotides (cAMP and cGMP).

Axillary osmidrosis: A condition characterized by increased foul odor in the underarm region. Specific SNPs in ABCC11 result in a loss of transporter activity, and therefore dramatically reduce body odor.

Environmental enrichment: Manipulations administered to laboratory animals, including expanded living space, physical exercise and engagement with novel objects that stimulate sensory perception and cognition.

Integrin: Integrins, cell adhesion molecules expressed on the majority of cells, are known to be critical for cell adhesion to endothelium, extravasation, homing and mobilization. They are also vital for the tetrapartite structure of neuronal synapses, where impairing integrin adhesion has been shown to damage synaptic transmission and the induction of LTP. Rapid changes in cell adhesion are controlled by integrin conformational changes rather than by changes in expression or trafficking. Cyclic AMP accumulation has been shown to down-modulate integrin-dependent adhesion.

Long-term potentiation (LTP): A sustained strengthening of neurological synapses resulting from recent synaptic activity. This particular type of synaptic plasticity is believed to underlie short-term memory and learning in mammals. LTP and other types of synaptic plasticity are controlled at least in part by integrins.

Mini-mental state examination (MMSE): A test administered by a health-care professional to evaluate a patient's mental skills (cognitive state). It includes a series of questions, and the score interprets the degree of mental state impairment. MMSE is one of the tests used to assess dementia.

Single nucleotide polymorphism (SNP): A common type of genetic variability wherein a single DNA nucleotide is changed. Two major types of SNPs exist: synonymous and non-synonymous substitutions. Non-synonymous SNPs alter the amino acid encoded, which may or may not result in a change of a protein function.

Soluble adenylyl cyclase (sAC): The protein encoded by the ADCY10 gene catalyzes the formation of the second messenger cAMP from ATP. Its activity is stimulated by low pH, bicarbonate ion and CO₂. Also, sAC has been implicated as a tumor suppressor protein whose expression is down-modulated in several cancers. Decreased sAC expression promotes cellular transformation *in vitro* and stimulates cancer progression *in vivo*.

7.13 Acknowledgments

This work was supported by the National Institutes of Health (USA) grants: UNM Comprehensive Cancer Center CCSG P30 CA118100 grant, the UNM Autophagy Inflammation and Metabolism CoBRE P20 GM121176 grant, the UNM Clinical and Translational Science Center grant UL1TR001449 and NIH Minority Institutional Research Training Program Award T32 HL007736.

7.14 Conflict of interest statement

The authors declare that there are no conflicts of interest.

CHAPTER 8: Discussion and future directions

8.1 Discussion

Since we hypothesized that cAMP efflux is an adaptation for apoptotic evasion in malignant cells, this dissertation is aimed at documenting the ability of ICE to modulate survival responses in acute leukemia cells. These relationships were explored in **Chapter 3** and **Chapter 6**, and they will be discussed further below. The remaining chapters describe the development of methods used to support the analysis and characterization of ICE effects on AML and B-ALL cells. Published as a method **Chapter 2** provides details of a novel assay to assess cellular efflux of a fluorescent cAMP analog. Published as a technical note, **Chapter 4** describes a high throughput flow cytometry (HTFC) approach to assess the chemotherapeutic impact on the viability of primary leukemia samples, in the context of hypoxia and normoxia. Finding little difference in cell responses related to oxygen exposure, we opted to continue subsequent work in normoxia. Published as an application note, **Chapter 5** introduces SynScreen software, which we developed to facilitate the analysis of drug interactions and to determine the potential synergism of tested combinations. Providing benefits for the analysis of large data sets, SynScreen allows for multiple experimental replicates to be compared simultaneously (see the *Results and Discussion* section of **Chapter 5** for a detailed comparison of SynScreen with other drug combination analysis software). Published as a review, **Chapter 7** explores: 1) how the detrimental effects of an ICE compound, clioquinol, in subacute myelo-optic

neuropathy may be related to SNPs in cyclic nucleotide transporters; and 2) the potential association of cAMP efflux with disease states, such as Alzheimer's disease.

In **Chapter 3**, we established that acute leukemia cell lines efflux F-cAMP, whereas normal PBMCs do not. These results both support our hypothesis that cAMP efflux is a malignancy-specific adaptation, and the fact that hematopoietic progenitor cells have increased expression of ABC transporters [96], a phenotype that is shared by the blast cells associated with acute leukemias. We also determined relationships between ICE and the cAMP pathway by validating the ability of ICE compounds to appropriately modulate downstream signaling that affected CREB activation and integrin deactivation. We further demonstrated that the ability of ICE to reduce cell viability was partially dependent on the activity of soluble adenylyl cyclase, a source for cytosolic, mitochondrial, and nuclear cAMP production [13]. In terms of cAMP efflux transporters, we assessed ABCC4 expression for cell lines. We determined that there was no relationship between quantity of ABCC4 transporters per cell, as determined by antibody binding to the protein, and F-cAMP efflux ability (compare **Figures 3.9** and **3.10**). This leads to the possibility that protein expression was disassociated from efflux activity, or that ICE act by alternative mechanism(s) unrelated to transporter inhibition. Because flow cytometry compatible monoclonal antibodies were not available during the course of the project, we did not determine ABCC5 or ABCC11 expression on our tested cells. Work by Guo, *et al.* previously showed that, of the known cAMP efflux transporters, only the expression of ABCC11 was prognostically relevant in leukemia [102]. Other studies have indicated the

possibility for the ABCC1 and ABCG2 transporters to efflux cyclic nucleotides [99, 365]. It is therefore plausible that acute leukemia cells may reduce intracellular cAMP by ABCC5, ABCC11, or other MRP transporters.

In **Chapter 6**, our approach for ICE+LCA combinations had the rationale of increasing cellular retention of drugs that are known substrates of cyclic nucleotide transporters in order to increase leukemic cell death. While our results showed synergism for multiple combinations, especially those including AraC, methotrexate, or topotecan, the ability for this work to be translated would not be simple. We addressed several limitations of our approach in **Chapter 6**. One other factor that needs to be considered regarding ICE+LCA combinations for translational development is that transporter inhibitors combined with therapeutics in hopes of reducing drug resistance failed to produce any clinically beneficial results [366]. However, because ICE were potent and selective against leukemia cells when used alone, it is possible that the ‘two-hit’ approach to treatment could be beneficial because the cells would be killed by mechanisms related to the cAMP pathway and to cell replication. As such, it is plausible that ICE+LCA combinations may also to improve response *in vivo*. In fact, synergism for some ICE compounds with LCA has already demonstrated efficacy *in vivo* [284].

Aside from our assay development work in **Chapter 4**, we chose not to study T-cell lineage ALL (T-ALL) in the context of cAMP efflux and ICE for several reasons. First, T-ALL is a rarer disease than AML or B-ALL, and primary samples are difficult to acquire. Second, to our knowledge, aside from instances of acquired drug

resistance, T lineage cells have not been reported to have aberrancies in cAMP efflux proteins in relation to prognosis or treatment response. Lastly, in several studies, T cells were not subject to cAMP-induced apoptotic induction [55, 56, 367]. It has been proposed that this may be because T cells preferentially express PDE3 isoforms, which have 5-10 times greater affinity for cGMP in comparison to cAMP [368].

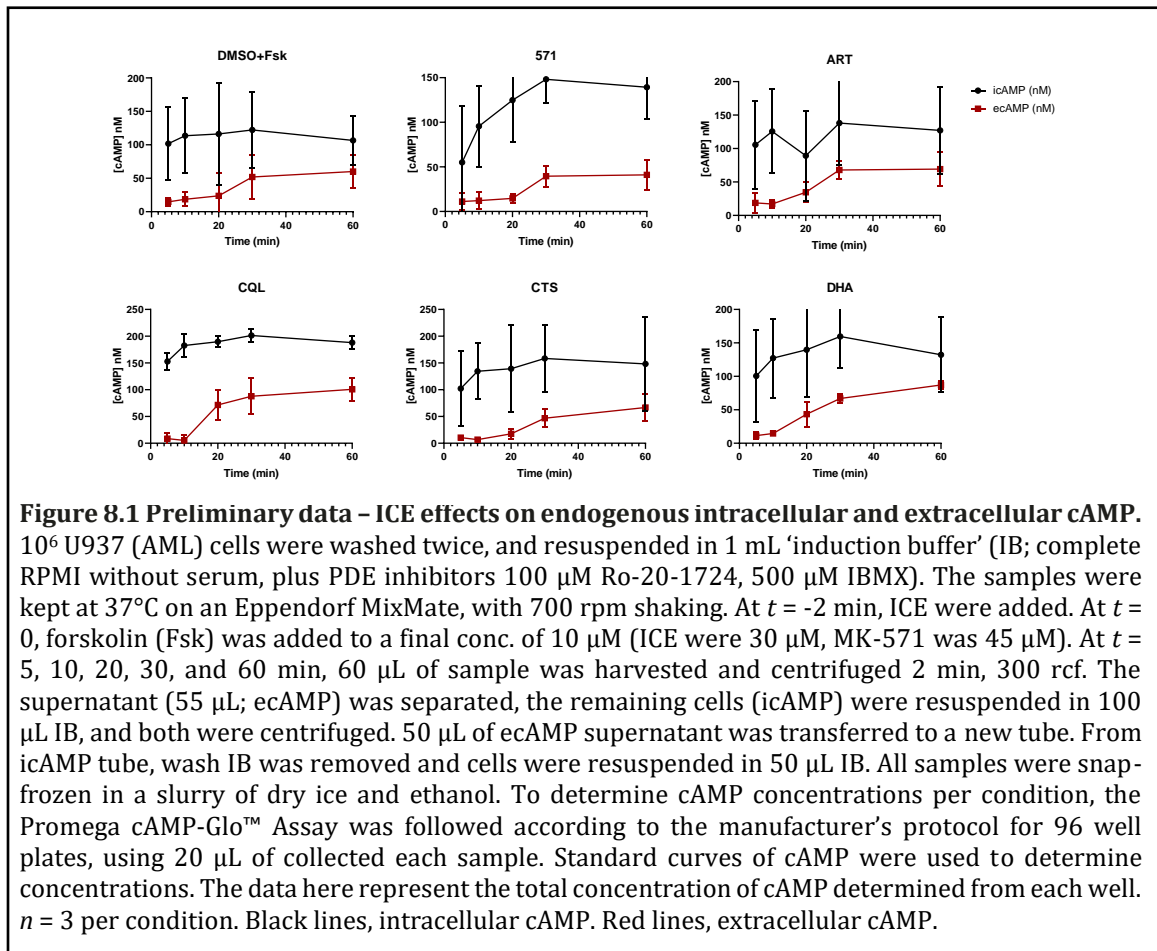
Nonetheless, the work described in this dissertation, with the exception of **Chapter 6**, has been peer-reviewed and accepted by the scientific community. Therefore, further work with ICE to explore their potential for clinical development is justified.

8.2 Future Directions

8.2.1 Determine the effects of ICE on endogenous cAMP signaling

One important future direction for this work would be to determine how ICE modulate endogenous cAMP concentrations. While we have demonstrated that ICE increase cAMP pathway activity (**Chapter 3**), the mechanism of action of ICE on efflux transporters has not been verified. If ICE are shown to increase accumulation of icAMP, while also slowing the increase of ecAMP over time, then that would support the notion that ICE compounds antagonize transporter activity. We have conducted a preliminary study to assess cAMP concentrations in the presence of ICE (**Figure 8.1**). In the presence of PDE4 inhibitors, U937 (AML) cells were pre-treated with ICE for 2 min, and then cAMP production was stimulated with the AC agonist forskolin. Samples were collected after 5-60 min, and cells and supernatant were separated and

washed. The cAMP concentrations from each condition were determined with the Promega cAMP-Glo™ assay. The levels of icAMP plateau after 20 min for all conditions. All samples treated with ICE appear to have higher icAMP concentrations than the negative control. However, the ecAMP concentrations appear to increase over time in a manner similar to the negative control.



Nevertheless, definitive conclusions should not be drawn from this preliminary data, as the experimental approach may not have been optimized with respect to reagent concentrations, timing, and method of sample acquisition. It should also be

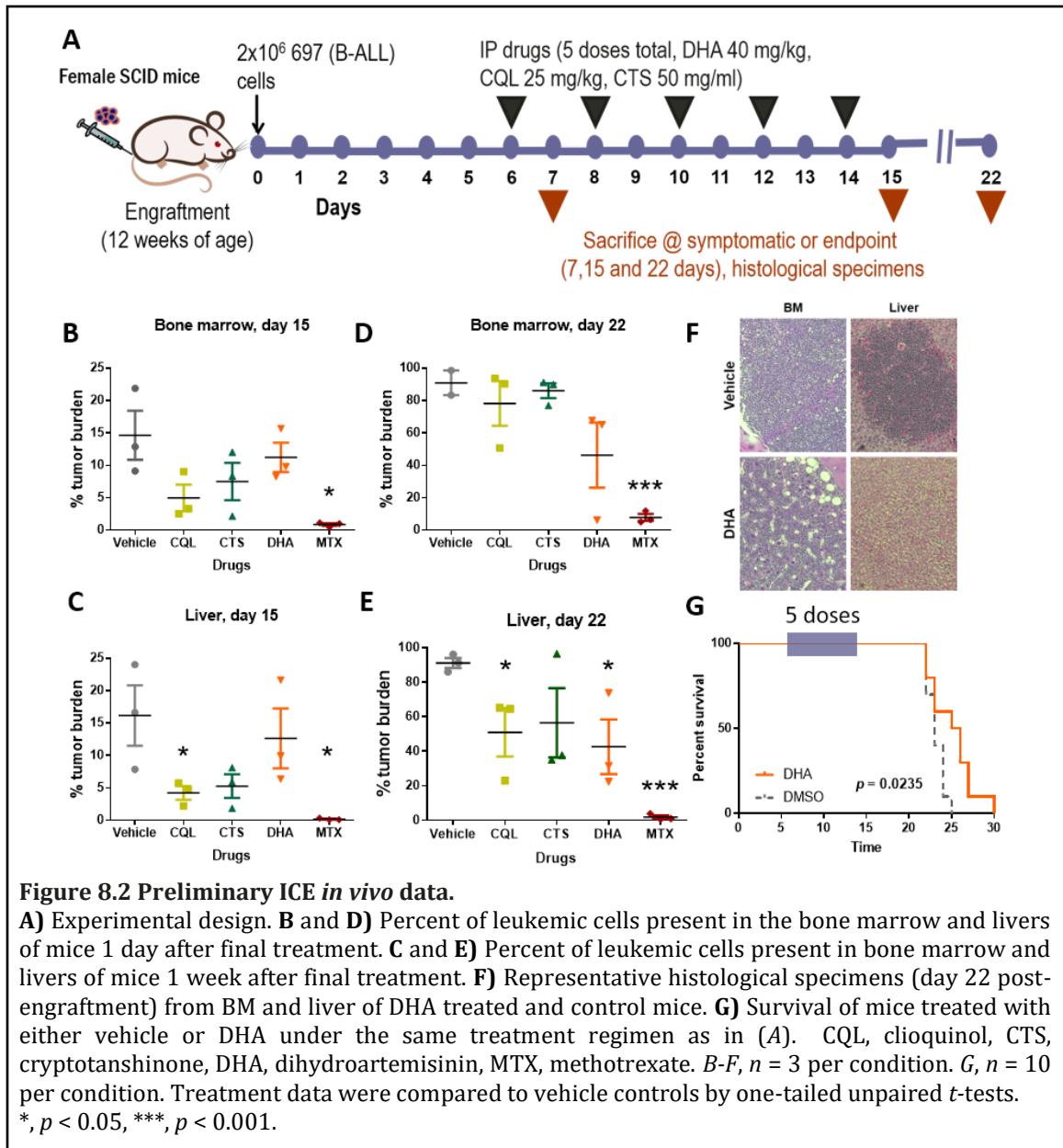
noted that MK-571, the most commonly-used positive control for cAMP efflux inhibition, failed to reduce the accumulation of extracellular cAMP. Hence, this unexpected response could be an artifact. Alternatively, Wang, *et al.* indicated that in triple negative breast cancer cell lines, MK-571 was less effective at reducing cAMP efflux in comparison to probenecid [99]. However, the fact that MK-571 previously worked in our experiments with U937 cells makes this interpretation less likely. Accordingly, future studies need to optimize methods to analyze ICE-induced changes in malignant cell icAMP and ecAMP over time. This may require the use of alternative approaches, such as ELISA, radioimmunoassays, or homogeneous time resolved fluorescence (HTRF) assays.

8.2.2 Evaluate ICE effects *in vivo*

The natural next step in determining the potential of ICE to be clinically translated is to determine the efficacy of these compounds *in vivo*. We conducted a pilot study to test small cohorts of mice in a B-ALL xenograft model. Female SCID mice (12 week-old) were housed in the UNM Animal Resource Facility. The mice were engrafted with 2×10^6 697 (B-ALL) cells by tail vein injection on day zero [369]. After five days, mice received IP injections of vehicle, ICE, or MTX (positive control). The treatments were administered twice weekly for a total of five doses. Next, mice were sacrificed, organs were digested and disease burden was assessed using flow cytometry [370]. Slides were prepared from formalin-fixed, paraffin embedded liver and BM utilizing Wright and H&E stains (**Figure 8.2A**). There were no differences in

tumor burden evident in the bone marrow either one day or one week after the last ICE injection (**Figure 8.2B, D**). However, one day after the last treatment, clioquinol significantly reduced tumor burden in the liver (**Figure 8.2C**). One week after the last treatment, both clioquinol and dihydroartemisinin significantly reduced tumor burden in the liver (**Figure 8.2E-F**). Using the same xenograft model and dosing schedule, we also determined that dihydroartemisinin significantly improved overall survival in comparison to untreated mice (**Figure 8.2G**). Hence, there is some promise for additional *in vivo* studies with ICE.

It should be emphasized that the data in **Figure 8.2** are preliminary. One of the first issues that we encountered with this pilot study was that ICE had limited solubility in water-based media. For the data presented, ICE were dissolved in HBSS (Gibco™) supplemented with 3% DMSO and 0.4 % Tween 20. This formulation was empirically based on laboratory tests of drug solubility. We anticipate that better drug formulations will contribute to improved drug efficacy. It was also evident that both the doses of ICE used, as well as the treatment schedule, were not optimal. In a recent AML mouse xenograft study, efficacy was achieved with 120 mg/kg artesunate administered twice daily for five days, followed by five days of 100 mg/kg twice daily [284]. We administered the artesunate metabolite, dihydroartemisinin, at 40 mg/kg once every other day for five days. Because this dose was so much lower than others have used, it is remarkable that we were able find any significant differences between conditions. Future studies will need to further assess the effects of metabolically relevant ICE concentrations on AML and B-ALL burden *in vivo*.



8.3 Concluding remarks

A common characteristic among many cancers is dysregulation of cAMP pathway activity. Therefore, we propose that the active removal of cAMP represents a novel mechanism that can be exploited by cancer cells for evasion of apoptosis. Accordingly, we suggest that inhibition of cAMP efflux by small molecules, especially by repurposed drugs, could expedite the translation of cAMP pathway-targeted therapeutics. Hence, the objective of this dissertation work was to identify compounds that increase cAMP pathway activity and reduce the viability of acute leukemia cells. We identified several agents that fit these criteria. In agreement with our hypothesis that elevated cAMP efflux activity is a malignant adaptation, we demonstrated that normal peripheral blood cells lack this trait. Furthermore, the drugs that we identified demonstrated selectivity against AML and B-ALL cells. When our cAMP modulatory agents were combined with leukemia chemotherapeutics, leukemia cell sensitivity was increased. This research is expected to provide a foundation toward the development of novel therapeutic options for leukemia and other diseases associated with aberrant cAMP signaling.

APPENDICES

APPENDIX A: Abbreviations used

- 571 – MK-571 (MRP inhibitor); ICE compound positive control
- 5FU – 5-fluorouracil; a LCA
- 6MP – 6-mercaptopurine; a LCA
- ABC – ATP-binding cassette
- ABCC4 – MRP4; cyclic nucleotide transporter
- ABCC5 – MRP5; cyclic nucleotide transporter
- ABCC11 – MRP8; cyclic nucleotide transporter
- AD – Alzheimer’s disease
- ALL – acute lymphoblastic leukemia
- AML – acute myeloid leukemia
- AraC – cytarabine, cytosine arabinoside; a LCA
- ART – artesunate; ICE compound
- ATP – adenosine triphosphate
- B-ALL – B-cell lineage acute lymphoblastic leukemia
- cAMP – 3',5'-cyclic adenosine monophosphate; cyclic AMP
- Cdk2 – cyclin-dependent kinase 2
- cGMP – cyclic guanosine monophosphate
- CRE – cAMP response elements
- CREB – cyclic AMP responsive element-binding protein
- CQL – clioquinol; ICE compound
- CTS – cryptotanshinone; ICE compound
- DHA – dihydroartemisinin; ICE compound
- ECM – extracellular matrix
- EPAC – exchange protein activated by cAMP; downstream effector of cAMP
- ER – endoplasmic reticulum
- GPCR – G protein-coupled receptor
- HTFC – high throughput flow cytometry

F-cAMP – fluorescent cAMP analog used in our studies
HTFC – high throughput flow cytometry
IBMX – 3-isobutyl-1-methylxanthine; PDE inhibitor
ICE – inhibitors of cAMP efflux
LC3-II – microtubule-associated protein 1 light chain 3
LCA – leukemia therapeutic agent
LTP – long-term potentiation
MDR – multidrug resistance
MDR1 – multidrug resistance protein 1, ABCB1, P-gp
MMSE – mini-mental state examination
MRD – minimal residual disease
MRP – multidrug resistance protein (members of the ABC-C family of transporters)
MTX – methotrexate; a LCA
P-gp – P-glycoprotein 1, MDR1, ABCB1
PBT2 – (5,7-dichloro-2-((dimethylamino)methyl) 8-quinolinol
PI – propidium iodide
PKA – protein kinase A; cAMP-dependent protein kinase; downstream effector of cAMP
Ro-20-1724 – 4-(3-Butoxy-4-methoxyphenyl)methyl-2-imidazolidone; PDE4 inhibitor
ROS – reactive oxygen species
sAC – soluble adenylyl cyclase; generates cAMP
SMON – subacute myelo-optic neuropathy
SNP – single nucleotide polymorphism
T-ALL – T-cell lineage acute lymphoblastic leukemia
tmAC – transmembrane-associated adenylyl cyclase; generates cAMP
TPT – topotecan; a LCA
VLA-4 – very late antigen-4
WT – wild type

APPENDIX B: Supplemental material for Chapter 4

Table S4.1 Karyotypic and molecular classification of primary T-ALL samples used for the development of PDX.

primary T-ALL samples used in this study; ND, not determined; R, rearrangements;

* reported by Matlawska-Wasowska et al. (2016) Leukemia [371].

Patient ID	PDX ID	Origin Patient	Karyotype	Lesion	ETP
15-093#	15-093	UNM	46,XY[20]	ND	Not ETP
12-089#	12-089	UNM	46,XY,t(?;11)(?;q23). Ish (MLL x 2), (5'MLL sep 3'MLL x 1)	KMT2A-R	ND
ALL82*	PATZZM	COG	46,XY,t(5;14)(q35;q32)[3]/47,idem,+mar[3]/46,XY[19]	ND	not ETP
ALL68*	PATRAP	COG	46,X,add(X)(q26),del(5)(q31),t(10;11)(p12;q21)[13]/46,XX[7]	MLLT10-R	ETP
ALL27*	PASNXS	COG	46,XX,del(2)(q33),del(12)(p12)[20]	CCDC91-R	near ETP
ALL16*	PASGJG	COG	46,Y,t(X;10)(p10;p10)[18]/46,XY[2]	MLLT10-R	ND
ALL31*	PASSPP	COG	46,XY,t(11;19)(q23;p13.3)[20]/46,XY[3]	KMT2A-R	not ETP

Table S4.2 List of the tested inhibitors and their clinical relevance.

Compound	Inhibitor type	Tested Concentration range	FDA approved	Clinical dosage			Steady state plasma concentration (Cmax)					References
				Dose	unit	route	PlasmaConc (µM)	PlasmaConc (M)	MW	Cmax	Unit	
Afatinib	TKI	0.005-100 µM	yes	40 mg		O	0.16	1.58E-07	485			https://www.ncbi.nlm.nih.gov/pmc/articles/PMC5315739/
Alvociclib	CDK	0.05-1000 nM	no	60 mg		P	2.24	2.24E-06	401			https://www.ncbi.nlm.nih.gov/pmc/articles/PMC3618599/#SD2
Axitinib	TKI	0.005-100 µM	yes	10 mg		O	0.10	9.59E-08	386	37	nanog/millil	https://www.ncbi.nlm.nih.gov/pmc/articles/PMC3425526/
Bortezomib	proteasome	0.05-1000 nM	yes	2.6 mg		P	0.23	2.25E-07	384.24	86.5	nanog/millil	http://drugcentral.org/label/1521d321-e724-4ffc-adad-34bf444fac7/view
Bosutinib	TKI	0.005-100 µM	yes	500 mg		O	0.38	3.77E-07	530	200	nanog/millil	https://www.drugbank.ca/drugs/DB06616
Cabozantinib	TKI	0.005-100 µM	yes	140 mg		O	0.61	6.11E-07	501	306	nanog/millil	https://www.ncbi.nlm.nih.gov/pmc/articles/PMC3646303/
Carfilzomib	proteasome	0.05-1000 nM	yes	40 mg		P	1.93	1.93E-06	719	1389	nanog/millil	https://www.ncbi.nlm.nih.gov/pmc/articles/PMC5438822/
Celecoxib	TKI	0.005-100 µM	yes	200 mg		O	1.80	1.80E-06	381	686	nanog/millil	https://www.ncbi.nlm.nih.gov/pubmed/16149679
Ceritinib	TKI	0.005-100 µM	yes	750 mg		O	1.43	1.43E-06	558	800	nanog/millil	https://www.ncbi.nlm.nih.gov/pmc/articles/PMC4079055/#SD1
Crizotinib	TKI	0.005-100 µM	yes	500 mg		O	0.82	8.18E-07	450	368	nanog/millil	https://www.ncbi.nlm.nih.gov/pmc/articles/PMC4982581/
Dabrafenib	TKI	0.005-100 µM	yes	300 mg		O	1.55	1.55E-06	519	806	nanog/millil	https://www.ncbi.nlm.nih.gov/pmc/articles/PMC3859275/
Dasatinib	TKI	0.005-100 µM	yes	100 mg		O	0.23	2.29E-07	488	111.6	nanog/millil	https://www.ncbi.nlm.nih.gov/pubmed/22587422
Erlotinib	TKI	0.005-100 µM	yes	150 mg		O	4.40	4.40E-06	393	1.73	microg/millil	https://bmccancer.biomedcentral.com/articles/10.1186/1471-2407-11-284
Gefitinib	TKI	0.005-100 µM	yes	250 mg		O	0.19	1.91E-07	446	85	nanog/millil	https://www.ncbi.nlm.nih.gov/pubmed/16231967
Ibrutinib	TKI	0.005-100 µM	yes	560 mg		O	0.12	1.18E-07	440	51.7	nanog/millil	https://www.ncbi.nlm.nih.gov/pmc/articles/PMC4419161/
Imatinib	TKI	0.005-100 µM	yes	400 mg		O	3.24	3.24E-06	493.6	1.6	millig/L	https://pdfs.semanticscholar.org/b9b0/5b7fc6cc9065ef1809e9cbde1752a6c4870.pdf
Lapatinib	TKI	0.005-100 µM	yes	1250 mg		O	6.06	6.06E-06	581	3.52	microg/millil	https://www.ncbi.nlm.nih.gov/pmc/articles/PMC4331616/
Nilotinib	TKI	0.005-100 µM	yes	400 mg		O	4.08	4.08E-06	529.5	2160.7	nanog/millil	https://www.ncbi.nlm.nih.gov/pubmed/19895406
Palbociclib	CDK	0.005-100 µM	yes	125 mg		O	0.41	4.15E-07	447.5	185.5	nanog/millil	https://www.ncbi.nlm.nih.gov/pmc/articles/PMC4968609/
Ponatinib	TKI	0.005-100 µM	yes	45 mg		O	0.15	1.45E-07	532.5			https://www.ncbi.nlm.nih.gov/pmc/articles/PMC5344956/
Regorafenib	TKI	0.005-100 µM	yes	160 mg		O	7.15	7.15E-06	482.8	3.45	millig/L	https://www.ncbi.nlm.nih.gov/pmc/articles/PMC3364125/
Ruxolitinib	TKI	0.005-100 µM	yes	20 mg		O	1.32	1.32E-06	306	1320	nanomol/L	http://www.bloodjournal.org/content/118/2/1516278s0-checked=true
Saracatinib	TKI	0.005-100 µM	yes	175 mg			0.82	8.19E-07	542	444	nanog/millil	http://clincancerres.aacrjournals.org/content/clinres/16/19/4876.full.pdf
Selumetinib	TKI	0.005-100 µM	yes	75 mg			1.22	1.22E-06	457.68	557	nanog/millil	https://www.ncbi.nlm.nih.gov/pubmed/21953275
Sorafenib	TKI	0.005-100 µM	yes	400 mg		O	7.90	7.90E-06	464.8	3.67	millig/L	https://link.springer.com/article/10.1007%2Fs00280-010-1423-9
Sunitinib	TKI	0.005-100 µM	yes	50 mg		O	0.06	6.27E-08	398.5	25	nanog/millil	https://onlinelibrary.wiley.com/doi/pdf/10.1002/encr.28554
Tofacitinib	TKI	0.005-100 µM	yes	10 mg		O	1.26	1.26E-06	312.3	392	nanog/millil	http://dmd.aspetjournals.org/content/dmd/42/4/759.full.pdf
Trametinib	TKI	0.005-100 µM	yes	2 mg		O	0.04	3.61E-08	615.4	22.2	nanog/millil	https://www.drugbank.ca/drugs/DB08911
Vandetanib	TKI	0.005-100 µM	yes	300 mg		O	0.36	3.58E-07	475.35	170	nanog/millil	https://www.ncbi.nlm.nih.gov/pmc/articles/PMC3586143/
Vemurafenib	TKI	0.005-100 µM	yes	960 mg		O	9.80	9.80E-06	489.92	4.8	microg/millil	https://link.springer.com/article/10.1007%2Fs00280-013-2324-5
Vismodegib	Hedgehog	0.005-100 µM	yes	150 mg		O	3.58	3.58E-06	421	3.58	micromol/L	https://www.ncbi.nlm.nih.gov/pmc/articles/PMC3703823/

Table S4.3 Ex vivo drug response profiling of T-ALL cell lines.

The cells were incubated for 72 hr with the tested agents and the EC₅₀ values were calculated from three independent experiments. EC₅₀ values were reported for inhibitors that yielded maximum response values of 20% or greater. For EC₅₀ values calculated to be beyond the concentration range tested, they were reported as >100 µM. This indicate the cells that were insensitive to the inhibitors at tested concentration range.

Compound	CUTLL1	ALL-SIL	CCRF-CEM	Jurkat	Loucy
Afatinib	3.30	4.44	2.57	2.13	1.91
Alvocidib	0.02	0.03	0.08	0.01	0.01
Axitinib	0.63	1.37	0.07	0.42	0.45
Bortezomib	0.17	0.18	0.01	0.14	0.15
Bosutinib	14.91	7.58	0.03	1.17	1.42
Cabozantinib	10.61	11.27	5.73	6.22	4.10
Carfilzomib	0.03	0.03	0.00	0.02	0.02
Celecoxib	>100	>100	36.29	>100	>100
Ceritinib	45.46	7.62	6.32	3.24	3.03
Crizotinib	2.26	6.79	1.91	2.23	1.90
Dabrafenib	nd	>100	45.75	>100	>100
Dasatinib	>100	7.99	14.96	5.84	6.87
Erlotinib	>100	8.93	>100	6.25	9.18
Gefitinib	21.57	16.42	30.91	19.35	8.87
Ibrutinib	>100	>100	21.59	18.65	14.75
Imatinib	25.85	29.11	39.10	11.55	9.80
Lapatinib	15.51	7.57	7.25	4.15	3.46
Nilotinib	>100	>100	>100	52.12	>100
Palbociclib	>100	>100	>100	>100	>100
Ponatinib	5.66	3.34	4.68	1.12	1.46
Regorafenib	36.34	14.96	10.36	11.95	11.66
Ruxolitinib	12.71	42.56	39.39	55.91	33.10
Saracatinib	>100	60.16	25.49	9.81	8.18
Selumetinib	>100	>100	>100	>100	35.49
Sorafenib	26.66	12.15	11.54	10.72	10.93
Sunitinib	1.71	1.33	4.02	1.62	1.58
Tofacitinib	>100	>100	>100	>100	>100
Trametinib	>100	>100	22.71	29.56	38.18
Vandetanib	>100	>100	13.51	9.21	3.37
Vemurafenib	18.55	9.63	10.31	8.66	9.32
Vismodegib	>100	>100	nd	>100	>100

Table S4.4 Cell viability (%) of T-ALL cell lines, primary samples, PDX models and PBMC at indicated time points after incubation with DMSO (<1%).

* Mean values obtained from three independent experiments. ND, not determined.

	15-093	12-089	PATZZM	PATRAP	PASNXS	PASGJG	PASSPP	CUTTTL1	ALL-SIL	CCRF-CEM	Jurkat	Loucy	PBMC
48 h	82.2	74.8	87.6	76.6	66.4	90.9	89.1	ND	ND	ND	ND	ND	96.2
72 h	77.2	71.5	85.9	72.4	75.3	94.7	92.4	78.3*	85.7*	86.1*	87.9*	83.1*	94.2

Table S4.5 Response of T-ALL patient samples and patient derived xenografts to 31 FDA-approved inhibitors.

Response of T-ALL patient samples and patient derived xenografts to 31 small molecule inhibitors. The cells were incubated for 48 hrs with the tested agents. EC₅₀ values were reported for inhibitors that yielded maximum response values of 20% or greater. The EC₅₀ values that were beyond the concentration range tested are reported as >100 µM. This indicates the cells that were insensitive to the inhibitors at tested concentrations.

Compound	15-093	12-089	PATZZM	PATRAP	PASNXS	PASGJG	PASSPP
Afatinib	10.12	11.09	9.00	6.76	4.47	>100	>100
Alvocidib	0.25	1.19	>100	>100	48.71	>100	>100
Axitinib	>100	>100	>100	>100	>100	>100	>100
Bortezomib	>100	>100	>100	>100	>100	>100	>100
Bosutinib	48.20	18.73	15.14	1.95	11.85	>100	>100
Cabozantinib	>100	>100	>100	>100	>100	>100	>100
Carfilzomib	0.01	0.005	0.006	0.004	0.012	>100	>100
Celecoxib	>100	>100	>100	>100	>100	>100	>100
Ceritinib	13.38	>100	30.21	>100	>100	>100	>100
Crizotinib	12.21	12.43	6.75	9.62	0.07	>100	>100
Dabrafenib	>100	>100	>100	>100	>100	>100	>100
Dasatinib	>100	>100	>100	2.43	>100	>100	>100
Erlotinib	>100	>100	>100	>100	>100	>100	>100
Gefitinib	>100	>100	>100	20.0	>100	>100	>100
Ibrutinib	>100	54.46	>100	>100	>100	>100	>100
Imatinib	>100	>100	>100	>100	>100	>100	>100
Lapatinib	>100	57.11	>100	13.87	>100	>100	>100
Nilotinib	>100	>100	>100	>100	>100	>100	>100
Palbociclib	>100	>100	>100	>100	>100	>100	>100
Ponatinib	11.21	22.35	5.63	6.98	1.92	>100	>100
Regorafenib	>100	40.4	>100	>100	>100	>100	>100
Ruxolitinib	>100	>100	>100	>100	>100	>100	>100
Saracatinib	>100	>100	>100	>100	>100	>100	>100
Selumetinib	>100	>100	>100	>100	2.71	>100	>100
Sorafenib	>100	>100	96.24	>100	>100	>100	>100
Sunitinib	1.38	5.57	1.35	3.23	1.40	>100	>100
Tofacitinib	>100	>100	>100	>100	>100	>100	>100
Trametinib	>100	>100	>100	>100	>100	>100	>100
Vandetanib	45.71	29.11	26.43	11.57	>100	>100	>100
Vemurafenib	>100	>100	>100	>100	>100	>100	>100
Vismodegib	>100	>100	>100	>100	>100	>100	>100

Figure S4.1. Hypoxia Cytotoxicity Ratio (HCR) for a panel of T-ALL cell lines treated with 31 inhibitors under normoxia and hypoxia conditions, respectively (72 hr).

HCR was determined for each drug and cell line as $EC_{50}^{normoxia}/EC_{50}^{hypoxia}$. Each HCR was calculated from mean EC_{50} values for three independent experiments. (paired Student's *t*-test, * $p < 0.05$; # $p < 0.07$).

	CUTLL1	ALL-SIL	CCRF-CEM	Jurkat	Loucy
Afatinib	0.514	0.895*	0.940	0.563	0.729
Alvocidib	0.478	1.011	1.394	0.890*	1.032
Axitinib	0.464	0.782	2.118	1.306	0.627
Bortezomib	0.630	0.974	1.261	0.945	
Bosutinib	0.989	1.484	0.780	0.604	0.544
Cabozantinib	1.619	0.975	0.856	2.019	1.063
Carfilzomib	0.798	1.367*	1.040	1.231	1.356#
Celecoxib			0.902		
Ceritinib		1.032	1.092	0.849	0.860
Crizotinib	0.293	0.562	0.799	0.536	0.959
Dabrafenib					
Dasatinib		0.859	0.977	0.807	1.219
Erlotinib		0.848		0.837	1.103
Gefitinib	1.092	0.844	1.170	1.916	0.863*
Ibrutinib			0.840	0.856	0.563
Imatinib	1.528	1.591	1.473	1.638	1.338
Lapatinib	0.854#	0.812	0.851	1.026	0.686
Nilotinib					
Palbociclib					
Ponatinib	0.801	0.834	0.972	0.936	1.205
Regorafenib	0.392	0.770	0.809	0.897	0.926
Ruxolitinib	1.081	1.122	1.401	1.373	1.003
Saracatinib		1.376	1.071	1.080	0.369
Selumetinib					
Sorafenib	0.537*	0.837	0.903	0.854	0.890
Sunitinib	1.406	1.080	1.329#	1.306	1.216
Tofacitinib					
Trametinib			0.849	0.380	
Vandetanib			1.117	1.022	0.695
Vemurafenib		0.829		0.534	0.658
Vismodegib					

Figure S4.2. Response of T-ALL cell lines to the highest tested dose of each inhibitor under hypoxia.

(100 μ M for each drug with the exception of *alvociclib, *bortezomib and *carfilzomib, for which the highest tested dose was 1 μ M). Heatmap indicates the percentage of dead cells (0 -100%).

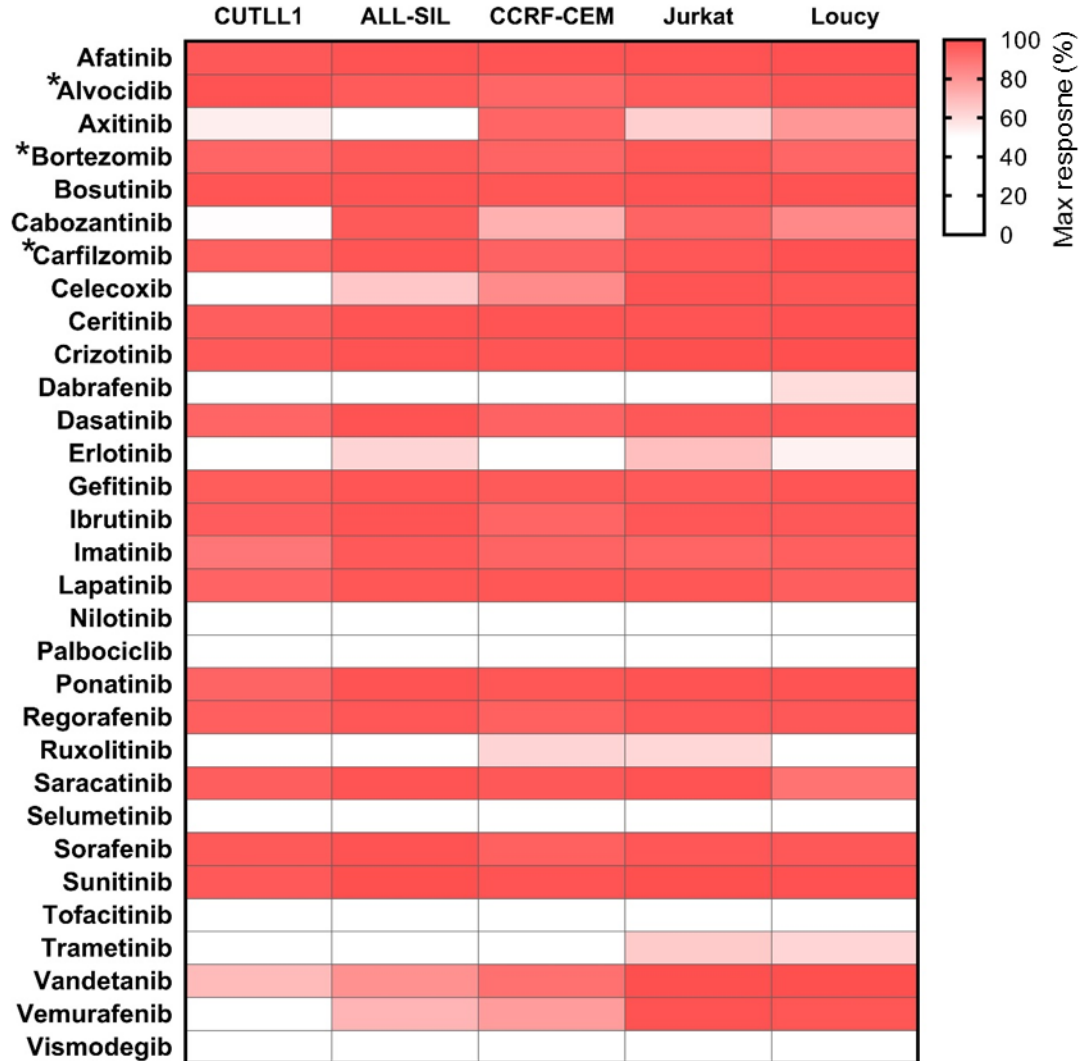


Figure S4.3.

A) The heatmap represents the mean EC_{50} values obtained for the samples treated with the drugs for 72 hr under normoxic conditions. The columns indicate T-ALL samples and the rows indicate the tested drugs. The darkest red indicates the most sensitivity (lowest EC_{50} values) of the cells to the tested inhibitors. EC_{50} values are only reported for compounds that yielded maximum response values of 20% or greater. For those samples which yielded maximal responses < 20% and/or had EC_{50} values greater than 100 μM , we report those EC_{50} values as “>100 μM ” (light grey). **B)** Response of T-ALL patient samples and PDX to the highest tested dose of each inhibitor (100 μM for each drug with the exception of *alvociclib, *bortezomib and *carfilzomib for which the highest tested dose was 1 μM). Heatmap indicates the percentage of dead cells after 72 hr incubation.

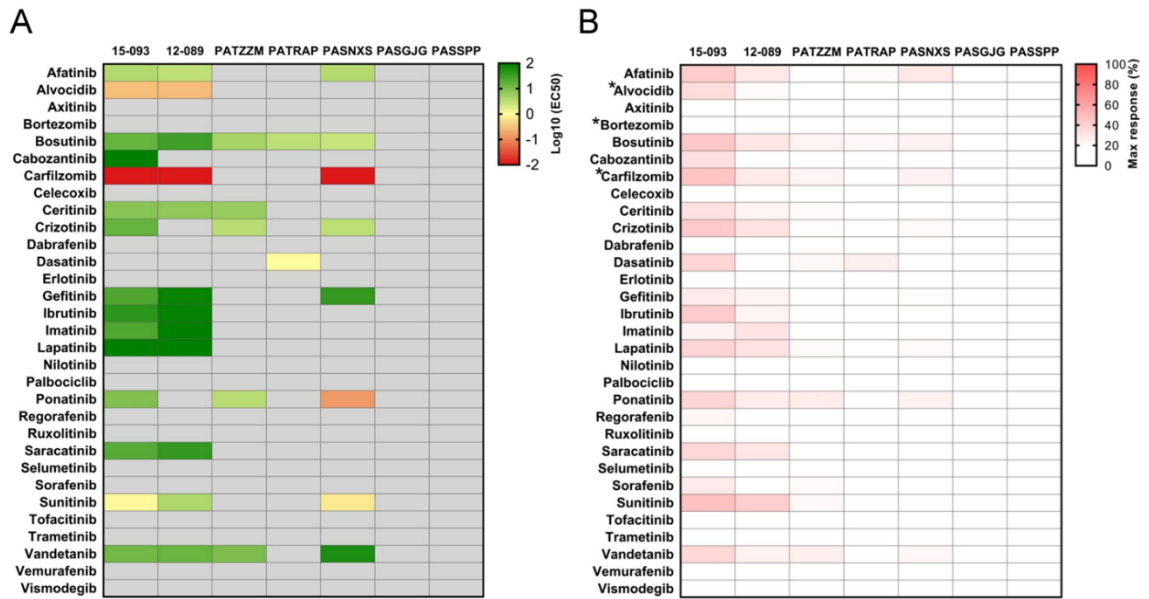


Figure S4.4. The HTFC PI assay provides information on the morphological shift that occurs in cells treated with the tested inhibitors.

Shown are data from one replicate experiment of CUTLL1 cells incubated with vehicle or TKIs for 72 h in normoxia or hypoxia conditions, then interrogated with the HTFC PI assay. **A)** Forward- and side-scatter plots of CUTLL1 cells from individual wells in the assay at different conditions. Gated cells that were PI-positive cells are shown in green. Top panels, vehicle-only negative control. Bottom panels, wells treated with 3.6 μ M crizotinib. Left panels, wells from the assay plate incubated at normoxia. Right panels, wells from the assay plate incubated in hypoxia. **B-C)** PI stain histograms from the wells shown in (A). The gated % PI-positive values are shown on the upper right. Grey, negative control well for that oxygen incubation condition. **B)** Wells incubated in normoxia. Blue, well treated with 3.6 μ M crizotinib. **C)** Wells incubated in hypoxia. Red, well treated with 3.6 μ M crizotinib.

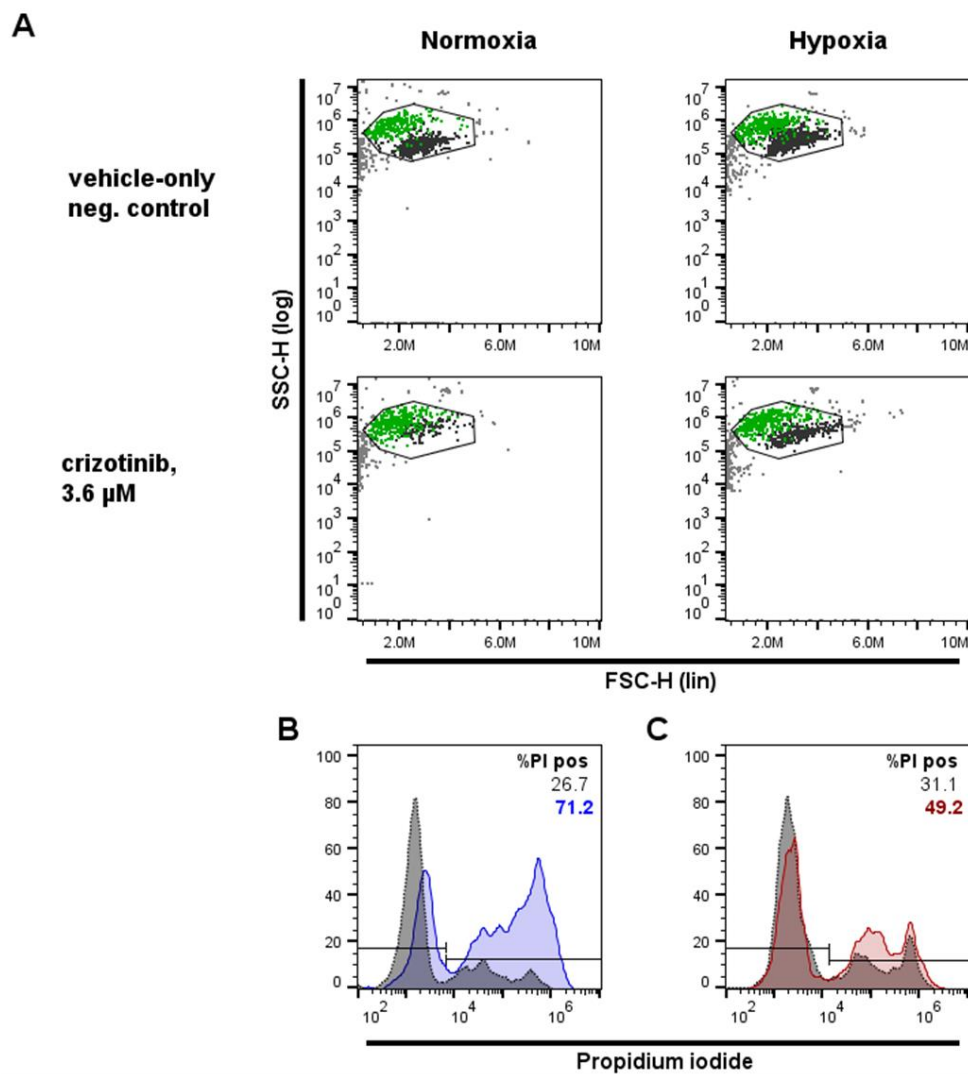
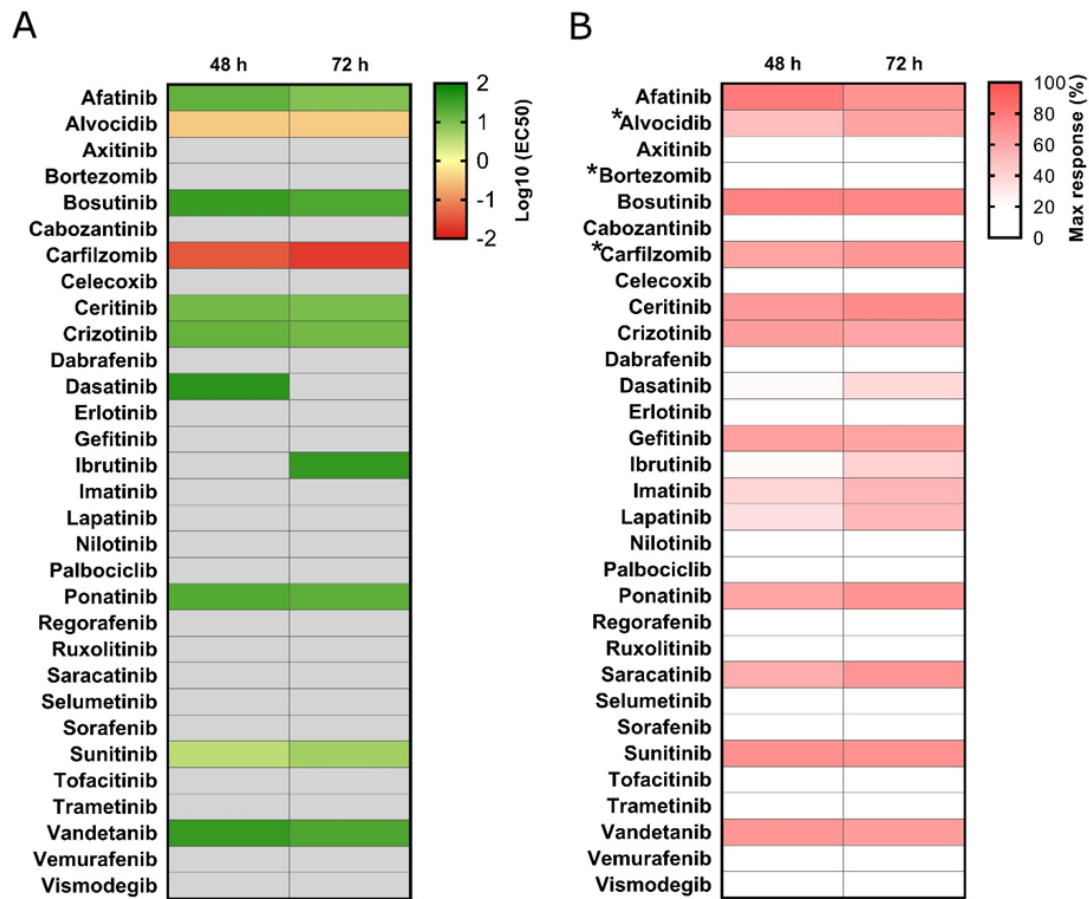


Figure S4.5. Sensitivity of peripheral blood mononuclear cells (PBMC) to 31 small molecule inhibitors.

A) The heatmap represents the mean EC₅₀ values obtained for normal PBMC treated with the drugs for 42 and 72 hr under normoxic conditions. The columns indicate time points and the rows indicate the tested drugs. The darkest red indicates the most sensitivity (lowest EC₅₀ values) of the cells to the tested inhibitors. Light grey, the dose responses indicated EC₅₀ > 100 μM indicating limited/lack of response to the tested compounds. **B)** Response to the highest tested dose of each inhibitor (100 μM for each drug with the exception of *alvocidib, *bortezomib and *carfilzomib for which the highest tested dose was 1 μM). Heatmap indicates the percentage of dead cells after 48 and 72 hr incubation.



APPENDIX C: Supplemental material for Chapter 5

Figure S5.1. Example of spreadsheet formatting needed for files that are imported into SynScreen. Shown are the mean response values for the plate DMSO control wells that were used to normalize the PctKill responses listed in column H. For import into SynScreen, the import range E1:H37 was used.

	A	B	C	D	E	F	G	H
1		DMSO %Pos	DMSO %Neg	ID	VERTuM	HORIZuM	PctKill	
2	Mean	5.39	94.61	DHA	0	0.009766	0.349	
3	SD	2.28	2.28	DHA	0	0.019531	-0.175	
4	CV	42.39	2.41	DHA	0	0.039063	-2.061	
5				DHA	0	0.078125	-0.384	
6				DHA	0	0.15625	0.559	
7				DHA	0	0.3125	0.664	
8				DHA	0	0.625	-1.013	
9				DHA	0	1.25	1.292	
10				DHA	0	2.5	4.750	
11				DHA	0	5	13.762	
12				DHA	0	10	32.518	
13				DHA	0	20	65.107	
14				DHA	0	40	68.879	
15				DHA	0	80	94.446	
16				DHA	0	160	96.018	
17				MTX	0.004882813	0	1.083	
18				MTX	0.009765625	0	4.960	
19				MTX	0.01953125	0	7.579	
20				MTX	0.0390625	0	7.999	
21				MTX	0.078125	0	8.103	
22				MTX	0.15625	0	12.819	
23				MTX	0.3125	0	23.716	
24				MTX	0.625	0	14.390	
25				MTX	2.5	0	14.914	
26				MTX	5	0	24.240	
27				MTX	10	0	17.115	
28				MTX	20	0	21.411	
29				MTX	40	0	25.288	
30				MTX	80	0	39.434	
31				MTX+DHA	0.009765625	1.25	1.083	
32				MTX+DHA	0.0390625	1.25	8.942	
33				MTX+DHA	0.15625	1.25	33.252	
34				MTX+DHA	0.625	1.25	41.844	
35				MTX+DHA	2.5	1.25	24.240	
36				MTX+DHA	10	1.25	47.188	
37				MTX+DHA	40	1.25	43.416	

Figure S5.2. A comparison of the synergy data analysis from the data set of Borisy, *et al.* 2003. Plotted are the observed responses in comparison to the predicted Bliss values determined by each source. **A)** The original observed values compared to predicted Bliss additivity from Figure 4 in Borisy, 2003. **B)** The observed data in comparison to predicted Bliss values from SynScreen. **C)** The observed data in comparison to predicted Bliss values from Combenefit.

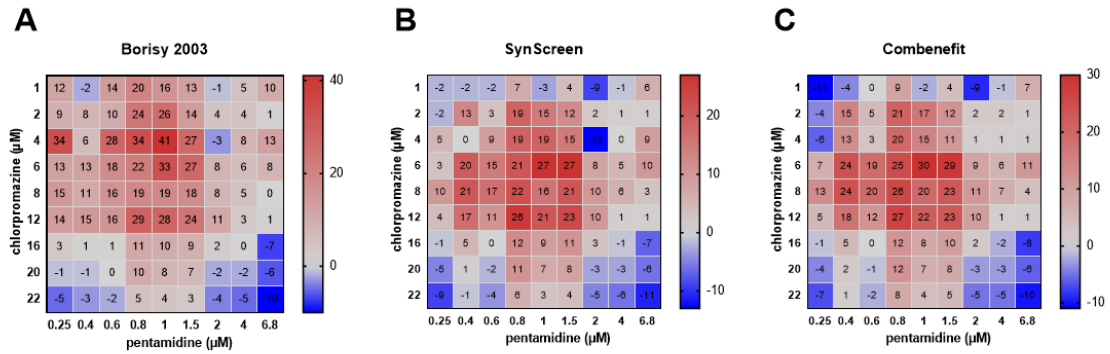


Table S5.1. Metrics determined by SynScreen and their definitions. DR, dose response.

Annotation	Meaning
Single agent DR stats	<i>cpd</i> Compound or drug identifier
	<i>npts</i> Total number of points used in curve fit to data (non-linear regression)
	<i>bottom</i> Bottom effect value estimated from curve fit to data
	<i>top</i> Top effect value estimated from curve fit to data
	<i>slope</i> Hill slope estimated from curve fit to data
	<i>ec50_uM</i> Concentration determined by data fit to elicit 50% response (uM)
	<i>rsqr</i> Data goodness of fit (correlation coefficient)
	<i>max_uM</i> Maximum concentration of a compound used in the assay (uM)
	<i>fa_max</i> Maximum measured response for each compound (expressed as %)
	<i>min_uM</i> Minimum concentration of a compound used in data fit (uM)
<i>fa_min</i> Minimum measured response for each compound (expressed as %)	
Combo Hit stats	<i>Combod</i> Compound or drug combination identifier
	<i>minfaHit (%)</i> Threshold set for minimum response considered for synergy hits
	<i>#BlissHits</i> Total number of combinations producing effects in excess of that predicted from the Bliss independence model
	<i>#CIHits</i> Total number of synergistic hits determined by combination index based on Loewe additivity model, i.e., $CI < 1$
	<i>#CI<0.5</i> Total number of combinations that have CI values < 0.5
	<i>#CI<0.1</i> Total number of combinations that have CI values < 0.1
	<i>Bliss beta</i> A characterization of the deviation of observed data from the additive response predicted from the Bliss independence model
	<i>BlissHit</i> True/false indication of whether an observed response is greater than additive as predicted by Bliss Independence model
	<i>CIHit</i> True/false indication of whether an observed response is considered synergistic as predicted by the Loewe additivity model ($CI < 1$)
	<i>DRUGuM</i> Concentration of a compound used (uM)
	<i>fa</i> Fraction affected; observed normalized response (expressed as %)
	<i>CI</i> Combination index value determined by Loewe additivity model analysis
	<i>DRUGfa</i> Dose of drug, when applied as a single agent, that is required to attain the response produced by the combination of two drugs
	<i>BlissFa</i> Based on the single agent dose responses, this is the theoretical additive response in which those drugs used in combination would produce by the Bliss independence model (expressed as %)
<i>fa>BlissFa</i> Difference between the observed response and the Bliss theoretical response value for additivity, i.e., distance of observed response from the 3D Bliss surface in SynScreen 3D graphs (expressed as %)	
<i>DRUGuMratio</i> The ratio of DRUGuM to DRUGuMfa	

Table S5.2. Example of single agent metrics determined by SynScreen. These are the metrics from the single agent dose responses used for a 5 x 5 drug combination screen. Ten drugs were tested in 15-point, two-fold dilution dose responses in duplicate for each screening run. Additionally, the drugs were tested with each combination matrix for 7-point four-fold dilution dose responses, totaling five replicates per run. The data provided here are from a combination of four experimental replicates. Outliers were removed based on dose response curves generated in the SynScreen interface. See Appendix C, Table S5.1 for an explanation of the reported metrics.

cpd	npts	bottom	top	slope	ec50_uM	rsqr	max_uM	fa_max	min_uM	fa_min
Cpd1	257	0.549	100.000	1.090	>1000	0.632	240.000	13.3	0.015	0.5
Cpd2	254	0.546	34.065	3.429	9.912	0.924	240.000	34.1	0.015	0.5
Cpd3	260	0.000	90.674	0.835	0.316	0.904	80.000	89.8	0.005	2.7
Cpd4	249	1.906	55.514	2.897	0.137	0.707	160.000	55.5	0.005	1.9
Cpd5	252	0.319	91.349	1.728	0.348	0.922	30.720	91.3	0.002	0.3
CpdA	257	0.409	95.575	4.254	142.852	0.954	240.000	86.1	0.015	0.4
CpdB	260	0.000	100.000	1.404	11.867	0.956	160.000	97.5	0.010	0.1
CpdC	257	0.288	89.533	9.260	28.860	0.995	160.000	89.5	0.010	0.3
CpdD	256	1.068	95.905	3.452	71.559	0.894	160.000	90.4	0.010	1.1
CpdE	258	0.000	100.000	1.620	16.862	0.964	160.000	97.5	0.010	0.1

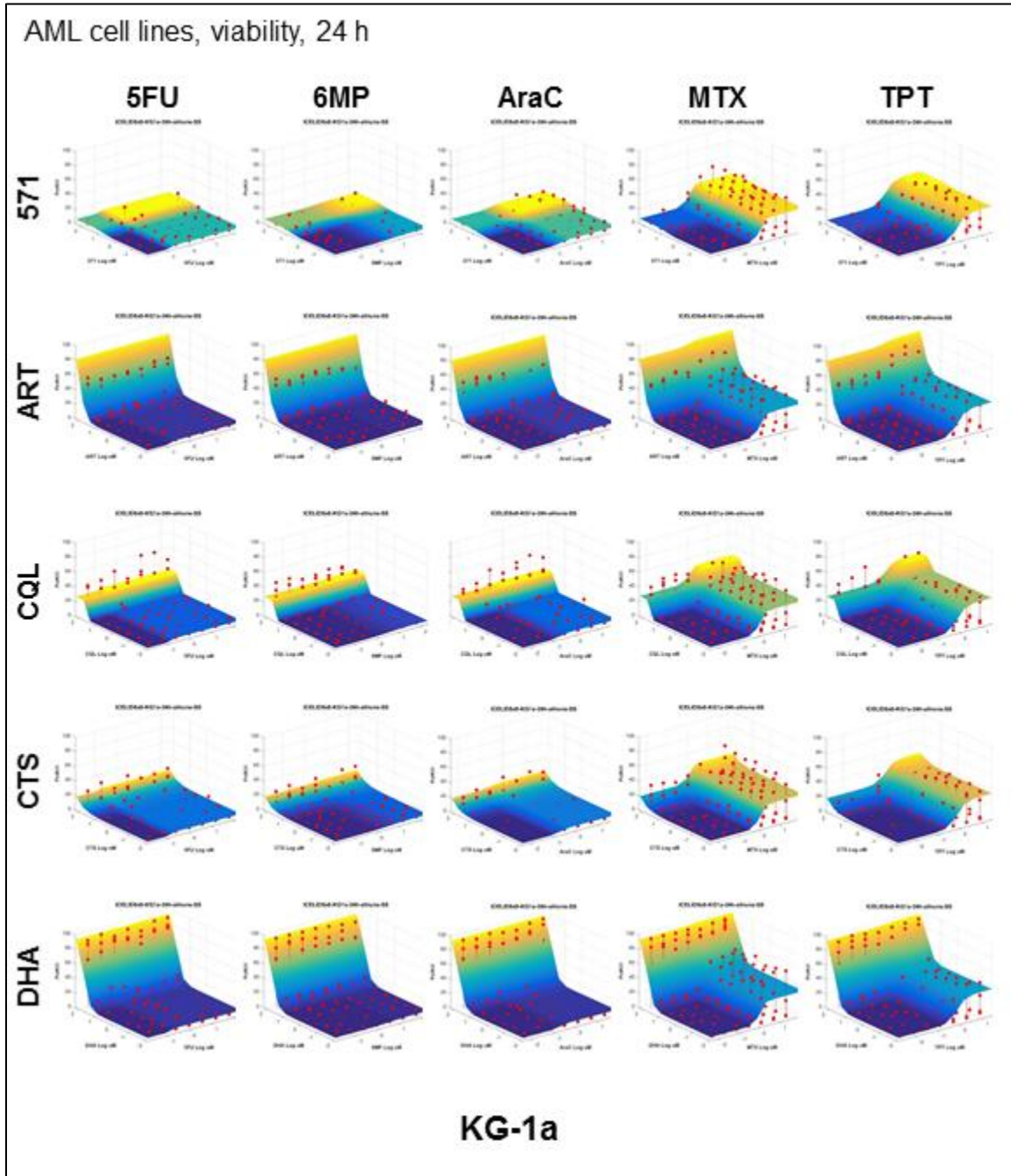
Table S5.3. Example of combination screen summary metrics determined by SynScreen. These are the quantification of synergistic hits determined from the data presented in Figure 1. Twenty-five drug pairs were tested in matrix dose responses and repeated $n = 4$. The user set a threshold such that synergy was only determined for data points that elicited responses $\geq 30\%$. See Appendix C, Table S5.1 for an explanation of the reported metrics.

ComboID	minfaHit (%)	#BlissHits	#CIHits	#CI<0.5	#CI<0.1	beta
Cpd1+CpdA	30	14	12	0	0	1.01
Cpd1+CpdB	30	41	41	20	0	1.00
Cpd1+CpdC	30	12	12	0	0	0.96
Cpd1+CpdD	30	14	14	6	0	1.03
Cpd1+CpdE	30	36	36	12	1	1.01
Cpd2+CpdA	30	37	37	9	0	1.01
Cpd2+CpdB	30	67	66	41	9	0.98
Cpd2+CpdC	30	34	36	11	0	0.99
Cpd2+CpdD	30	26	28	12	0	0.92
Cpd2+CpdE	30	35	40	14	0	0.92
Cpd3+CpdA	30	79	79	34	6	1.00
Cpd3+CpdB	30	71	77	37	3	0.89
Cpd3+CpdC	30	97	105	36	5	1.02
Cpd3+CpdD	30	90	98	35	6	1.01
Cpd3+CpdE	30	84	94	40	7	0.99
Cpd4+CpdA	30	93	94	81	48	1.01
Cpd4+CpdB	30	82	92	74	39	0.99
Cpd4+CpdC	30	93	103	69	35	1.04
Cpd4+CpdD	30	89	97	79	40	1.01
Cpd4+CpdE	30	83	96	69	36	0.96
Cpd5+CpdA	30	74	73	38	8	1.01
Cpd5+CpdB	30	86	101	55	12	1.01
Cpd5+CpdC	30	73	77	34	7	1.01
Cpd5+CpdD	30	69	70	35	8	1.02
Cpd5+CpdE	30	69	77	44	8	0.99

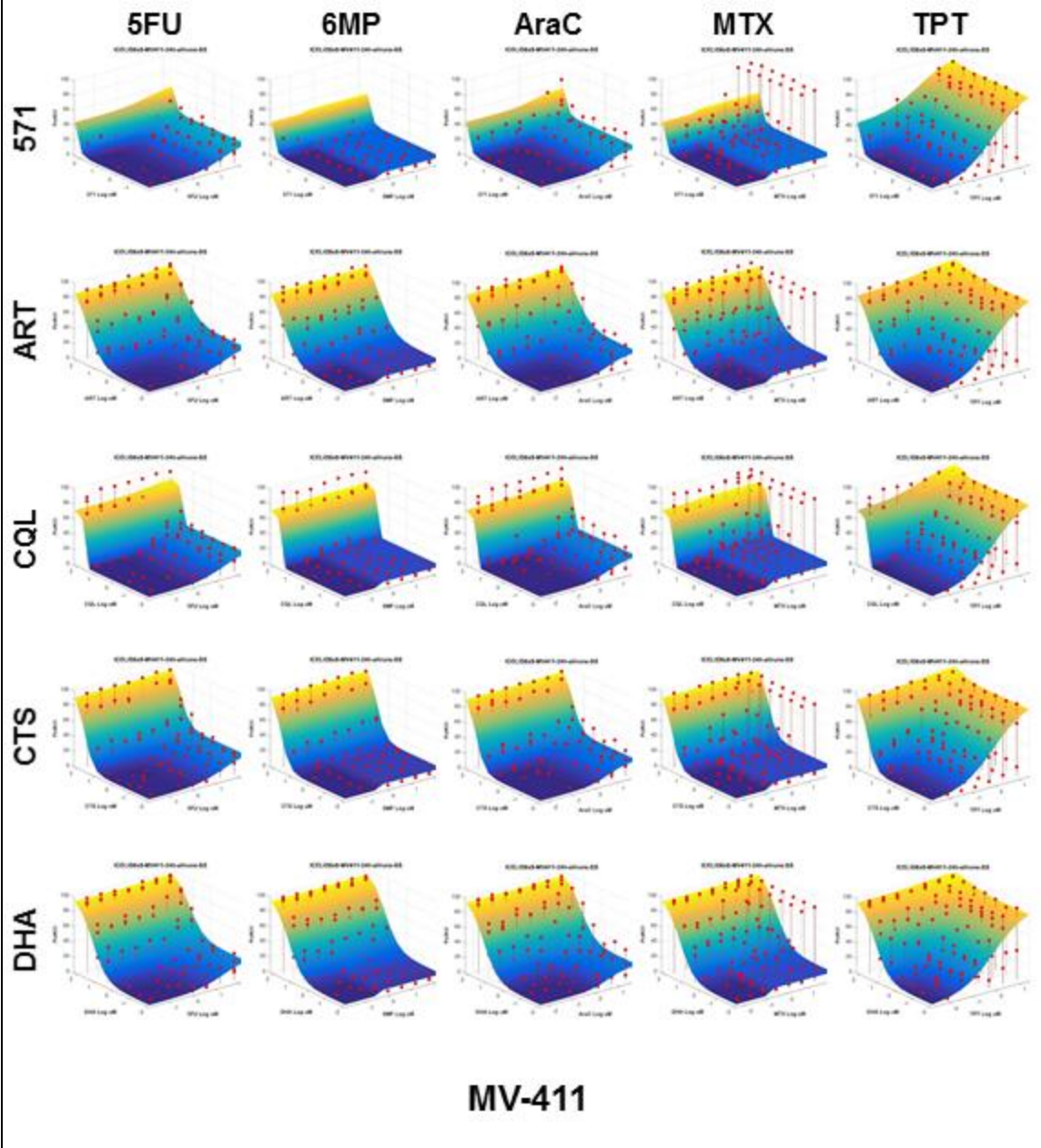
Table S5.4. Synergistic data points identified from the data presented in Figure 5.3. To remain consistent with the original study, no minFahit (%) was used. See Appendix C, Table S5.1 for an explanation of the reported metrics.

BlissHit	CIHit	pentCuM	cpromuM	fa	CI	Flag	pentfa	cpromfa	Blissfa	fa>Blissfa	pentumfa	cpromuMfa	pentuMratio	cpromuMratio
TRUE	FALSE	0.25	1	0.1	1.315	0	0.0	0.1	0.1	0.0	0.6	1.1	0.4099	0.9048
TRUE	FALSE	0.25	4	10.0	0.831	0	0.0	3.3	3.3	6.7	1.3	6.2	0.1875	0.6435
TRUE	FALSE	0.25	6	14.0	1.012	0	0.0	9.2	9.2	4.8	1.4	7.2	0.1750	0.8374
TRUE	FALSE	0.25	8	29.0	0.933	0	0.0	17.9	17.9	11.1	1.7	10.1	0.1451	0.7883
TRUE	FALSE	0.25	12	44.0	1.034	0	0.0	38.5	38.5	5.5	2.1	13.1	0.1201	0.9135
TRUE	FALSE	0.25	16	56.0	1.077	0	0.0	55.7	55.7	0.3	3.1	16.1	0.0816	0.9949
TRUE	FALSE	0.4	1	0.1	1.561	0	0.0	0.1	0.1	0.0	0.6	1.1	0.6559	0.9048
TRUE	FALSE	0.4	2	15.0	0.547	0	0.0	0.5	0.5	14.5	1.5	7.4	0.2758	0.2708
TRUE	FALSE	0.4	4	5.0	1.190	0	0.0	3.3	3.3	1.7	1.2	4.7	0.3415	0.8480
TRUE	TRUE	0.4	6	31.0	0.797	0	0.0	9.2	9.2	21.8	1.8	10.5	0.2269	0.5698
TRUE	TRUE	0.4	8	40.0	0.854	0	0.0	17.9	17.9	22.1	2.0	12.3	0.2035	0.6506
TRUE	TRUE	0.4	12	57.0	0.845	0	0.0	38.5	38.5	18.5	3.6	16.4	0.1115	0.7330
TRUE	OOOR	0.4	16	62.0	OOOR	1	0.0	55.7	55.7	6.3	6.8	18.0	OOOR	0.8903
TRUE	OOOR	0.4	20	69.0	OOOR	1	0.0	67.1	67.1	1.9	6.8	20.9	OOOR	0.9579
TRUE	FALSE	0.6	2	5.0	0.936	0	0.1	0.5	0.6	4.4	1.2	4.7	0.5123	0.4240
TRUE	FALSE	0.6	4	14.0	0.978	0	0.1	3.3	3.3	10.7	1.4	7.2	0.4200	0.5583
TRUE	FALSE	0.6	6	26.0	0.987	0	0.1	9.2	9.3	16.7	1.7	9.6	0.3603	0.6264
TRUE	FALSE	0.6	8	36.0	1.017	0	0.1	17.9	18.0	18.0	1.9	11.5	0.3211	0.6959
TRUE	FALSE	0.6	12	51.0	1.064	0	0.1	38.5	38.6	12.4	2.4	14.8	0.2502	0.8133
TRUE	FALSE	0.6	16	57.0	1.145	0	0.1	55.7	55.8	1.2	3.6	16.4	0.1673	0.9774
TRUE	FALSE	0.8	1	9.0	0.781	0	0.5	0.1	0.6	8.4	1.3	6.0	0.6126	0.1680
TRUE	FALSE	0.8	2	22.0	0.730	0	0.5	0.5	1.0	21.0	1.6	8.8	0.5033	0.2270
TRUE	FALSE	0.8	4	24.0	0.927	0	0.5	3.3	3.8	20.2	1.6	9.2	0.4916	0.4350
TRUE	FALSE	0.8	6	32.0	1.008	0	0.5	9.2	9.6	22.4	1.8	10.7	0.4487	0.5597
TRUE	FALSE	0.8	8	42.0	1.025	0	0.5	17.9	18.4	23.6	2.0	12.7	0.3960	0.6294
TRUE	OOOR	0.8	12	66.0	OOOR	1	0.5	38.5	38.9	27.1	6.8	19.5	OOOR	0.6151
TRUE	OOOR	0.8	16	69.0	OOOR	1	0.5	55.7	55.9	13.1	6.8	20.9	OOOR	0.7663
TRUE	OOOR	0.8	20	79.0	OOOR	1	0.5	67.1	67.3	11.7	6.8	28.4	OOOR	0.7046
TRUE	OOOR	0.8	22	78.0	OOOR	1	0.5	71.1	71.3	6.7	6.8	27.3	OOOR	0.8069
TRUE	FALSE	1	2	19.0	0.896	0	2.0	0.5	2.5	16.5	1.5	8.2	0.6529	0.2434
TRUE	FALSE	1	4	25.0	1.034	0	2.0	3.3	5.2	19.8	1.6	9.4	0.6074	0.4261
TRUE	FALSE	1	6	39.0	1.012	0	2.0	9.2	11.0	28.0	1.9	12.1	0.5155	0.4962
TRUE	FALSE	1	8	37.0	1.213	0	2.0	17.9	19.6	17.4	1.9	11.7	0.5287	0.6842
TRUE	OOOR	1	12	62.0	OOOR	1	2.0	38.5	39.8	22.2	6.8	18.0	OOOR	0.6677
TRUE	OOOR	1	16	66.0	OOOR	1	2.0	55.7	56.6	9.4	6.8	19.5	OOOR	0.8202
TRUE	OOOR	1	20	75.0	OOOR	1	2.0	67.1	67.8	7.2	6.8	24.6	OOOR	0.8141
TRUE	OOOR	1	22	75.0	OOOR	1	2.0	71.1	71.7	3.3	6.8	24.6	OOOR	0.8955
TRUE	FALSE	1.5	1	21.0	1.071	0	17.4	0.1	17.5	3.5	1.6	8.6	0.9552	0.1161
TRUE	FALSE	1.5	2	29.0	1.068	0	17.4	0.5	17.8	11.2	1.7	10.1	0.8705	0.1971
TRUE	FALSE	1.5	4	35.0	1.166	0	17.4	3.3	20.1	14.9	1.8	11.3	0.8125	0.3540
TRUE	FALSE	1.5	6	52.0	1.007	0	17.4	9.2	25.0	27.0	2.5	15.0	0.6070	0.3998
TRUE	FALSE	1.5	8	53.0	1.110	0	17.4	17.9	32.2	20.8	2.6	15.3	0.5861	0.5241
TRUE	OOOR	1.5	12	72.0	OOOR	1	17.4	38.5	49.2	22.8	6.8	22.5	OOOR	0.5328
TRUE	OOOR	1.5	16	74.0	OOOR	1	17.4	55.7	63.4	10.6	6.8	23.8	OOOR	0.6715
TRUE	OOOR	1.5	20	81.0	OOOR	1	17.4	67.1	72.9	8.1	6.8	31.1	OOOR	0.6421
TRUE	OOOR	1.5	22	80.0	OOOR	1	17.4	71.1	76.1	3.9	6.8	29.7	OOOR	0.7416
TRUE	FALSE	2	2	44.0	1.113	0	41.3	0.5	41.6	2.4	2.1	13.1	0.9607	0.1522
TRUE	FALSE	2	6	55.0	1.088	0	41.3	9.2	46.7	8.3	2.8	15.8	0.7083	0.3797
TRUE	OOOR	2	8	62.0	OOOR	1	41.3	17.9	51.8	10.2	6.8	18.0	OOOR	0.4451
TRUE	OOOR	2	12	74.0	OOOR	1	41.3	38.5	63.9	10.1	6.8	23.8	OOOR	0.5036
TRUE	OOOR	2	16	77.0	OOOR	1	41.3	55.7	74.0	3.0	6.8	26.3	OOOR	0.6091
TRUE	OOOR	4	2	59.0	OOOR	1	57.3	0.5	57.5	1.5	6.8	17.0	OOOR	0.1178
TRUE	OOOR	4	4	59.0	OOOR	1	57.3	3.3	58.7	0.3	6.8	17.0	OOOR	0.2356
TRUE	OOOR	4	6	66.0	OOOR	1	57.3	9.2	61.2	4.8	6.8	19.5	OOOR	0.3076
TRUE	OOOR	4	8	71.0	OOOR	1	57.3	17.9	65.0	6.0	6.8	21.9	OOOR	0.3647
TRUE	OOOR	4	12	75.0	OOOR	1	57.3	38.5	73.8	1.2	6.8	24.6	OOOR	0.4884
TRUE	OOOR	6.8	1	64.0	OOOR	1	57.6	0.1	57.6	6.4	6.8	18.7	OOOR	0.0535
TRUE	OOOR	6.8	2	59.0	OOOR	1	57.6	0.5	57.8	1.2	6.8	17.0	OOOR	0.1178
TRUE	OOOR	6.8	4	68.0	OOOR	1	57.6	3.3	59.0	9.0	6.8	20.4	OOOR	0.1961
TRUE	OOOR	6.8	6	71.0	OOOR	1	57.6	9.2	61.5	9.5	6.8	21.9	OOOR	0.2735
TRUE	OOOR	6.8	8	68.0	OOOR	1	57.6	17.9	65.2	2.8	6.8	20.4	OOOR	0.3922
TRUE	OOOR	6.8	12	75.0	OOOR	1	57.6	38.5	74.0	1.0	6.8	24.6	OOOR	0.4884

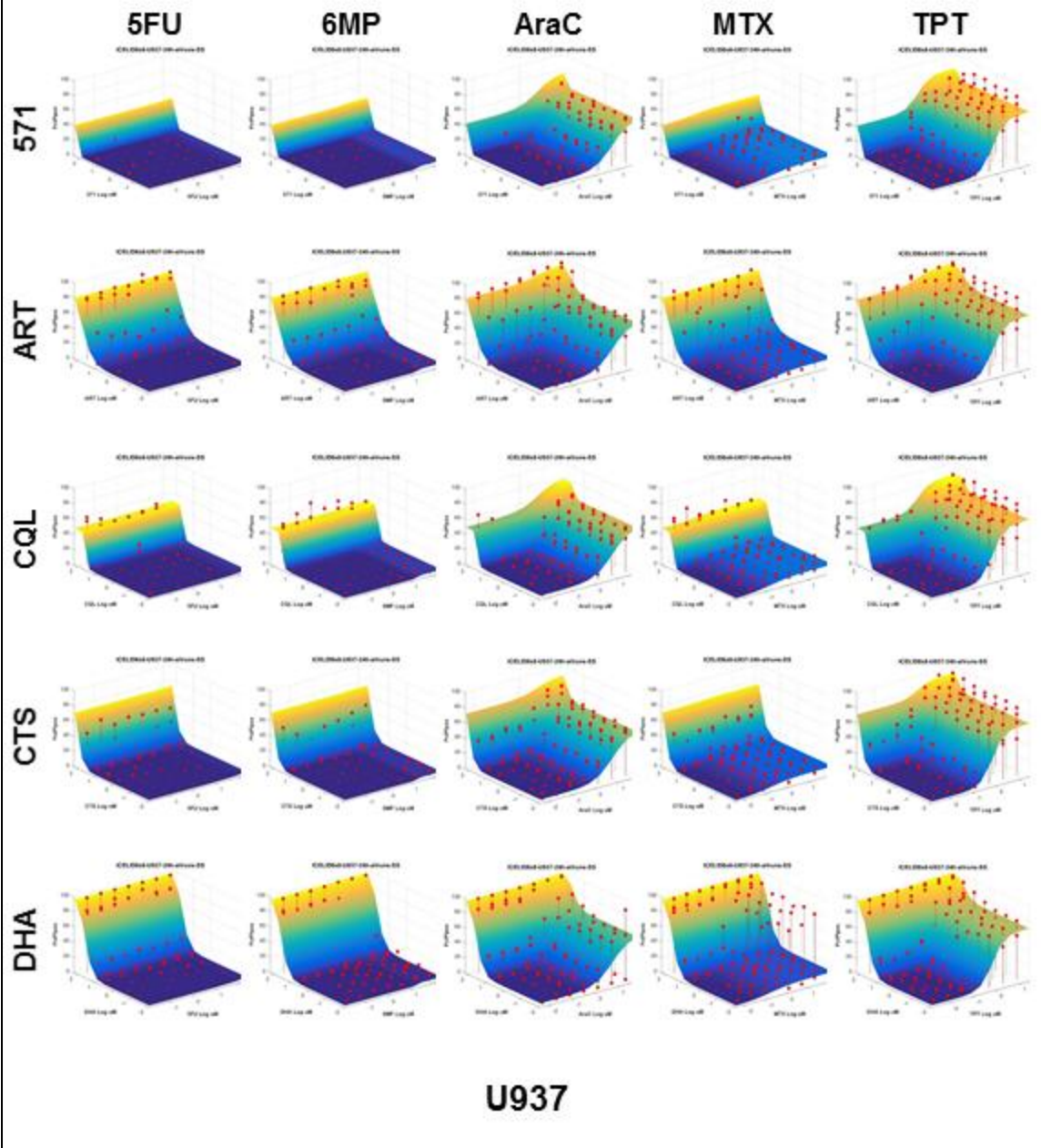
APPENDIX D: Supplementary material for Chapter 6



AML cell lines, viability, 24 h



AML cell lines, viability, 24 h

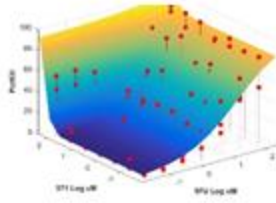


Viability, 48 h

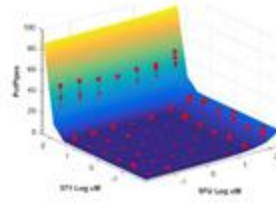
5FU+571

AML cell lines

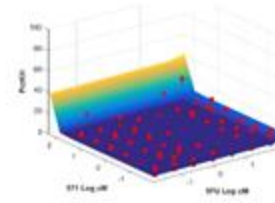
MV-411



U937

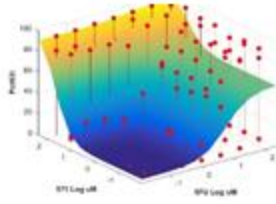


KG-1a

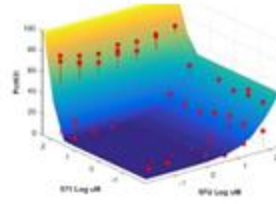


B-ALL cell lines

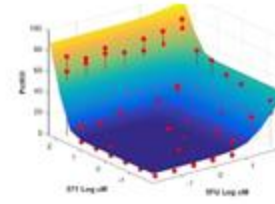
Nalm 6



Sup B15

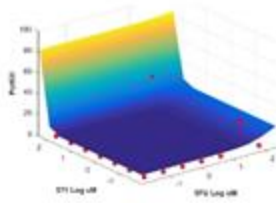


Reh

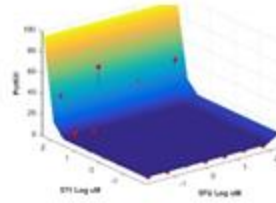


Primary B-ALL samples

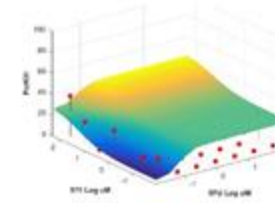
15-078



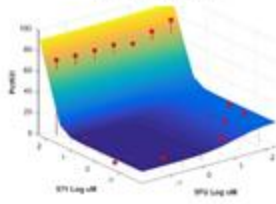
16-284



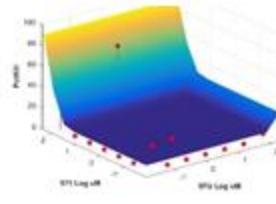
16-145



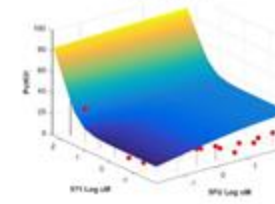
17-102-P2



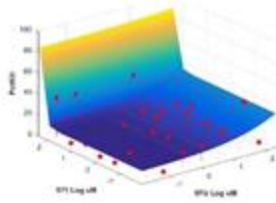
17-135



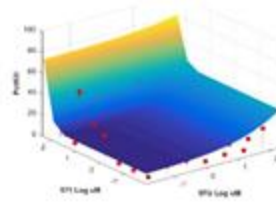
17-191



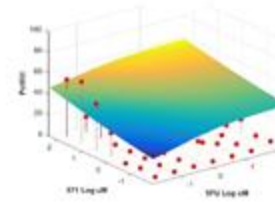
16-265



14-307



15-007

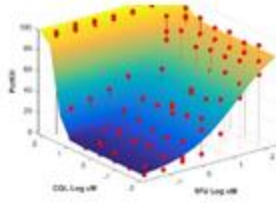


Viability, 48 h

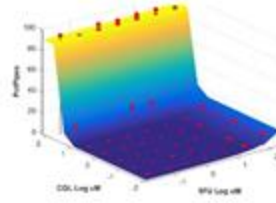
5FU+CQL

AML cell lines

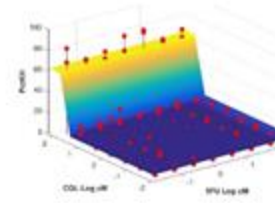
MV-411



U937

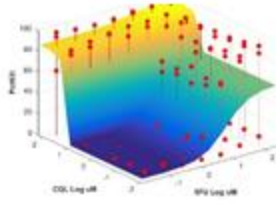


KG-1a

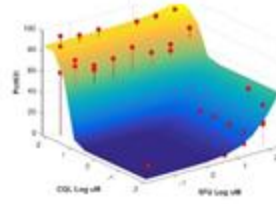


B-ALL cell lines

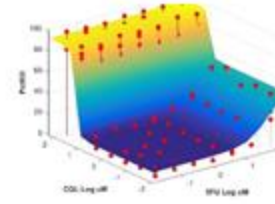
Nalm 6



Sup B15

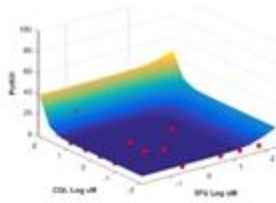


Reh

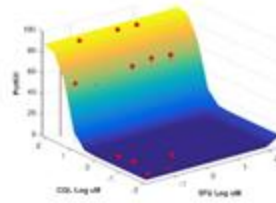


Primary B-ALL samples

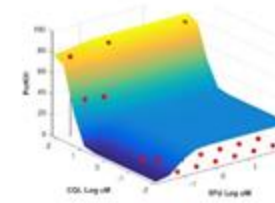
15-078



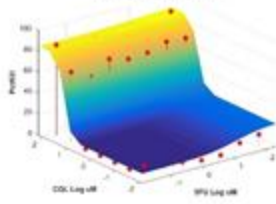
16-284



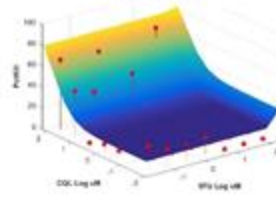
16-145



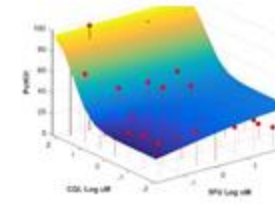
17-102-P2



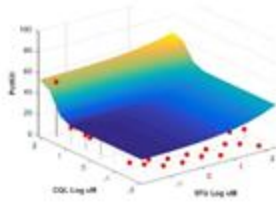
17-135



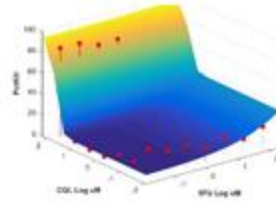
17-191



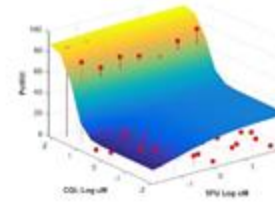
16-265



14-307



15-007

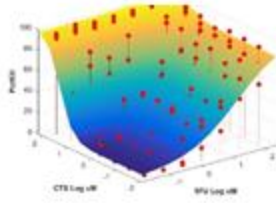


Viability, 48 h

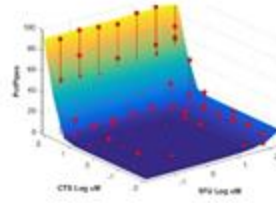
5FU+CTS

AML cell lines

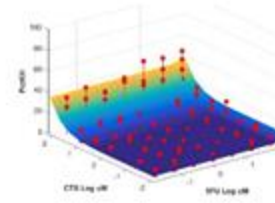
MV-411



U937

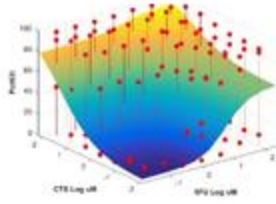


KG-1a

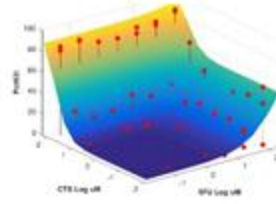


B-ALL cell lines

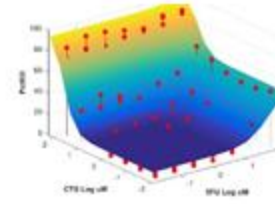
Nalm 6



Sup B15

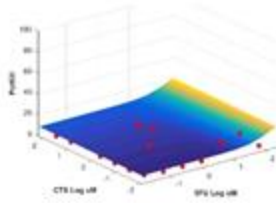


Reh

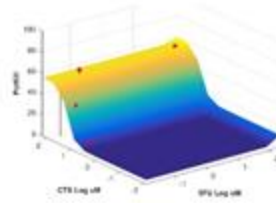


Primary B-ALL samples

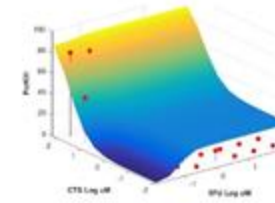
15-078



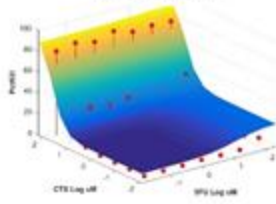
16-284



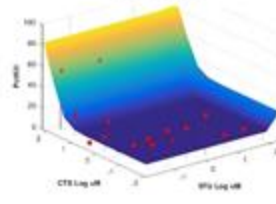
16-145



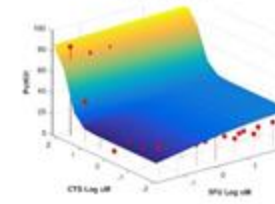
17-102-P2



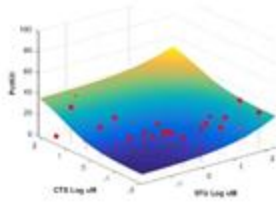
17-135



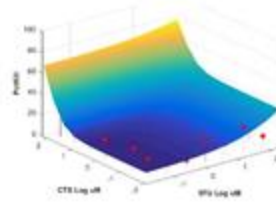
17-191



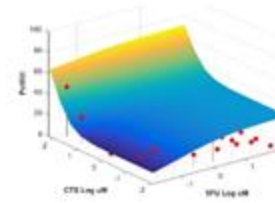
16-265



14-307



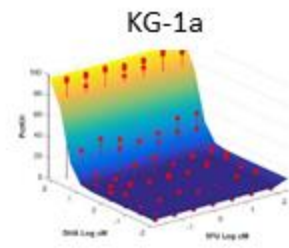
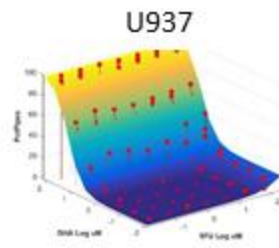
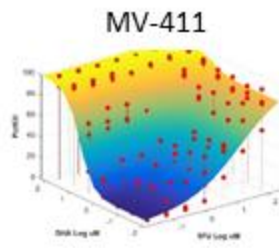
15-007



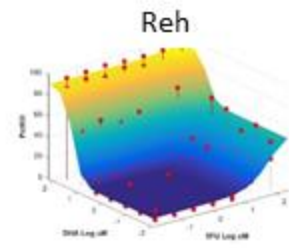
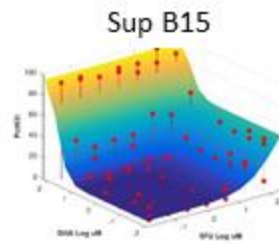
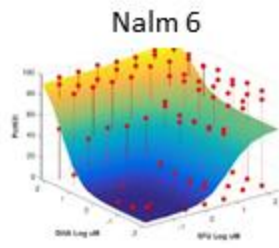
Viability, 48 h

5FU+DHA

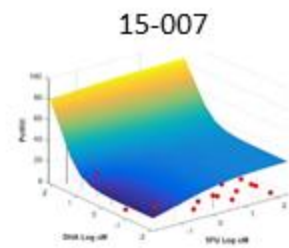
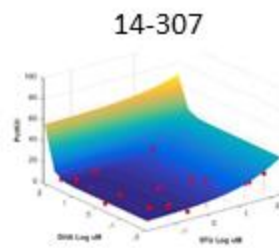
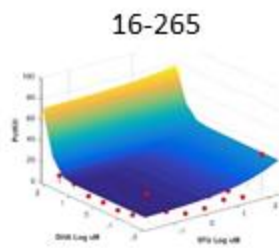
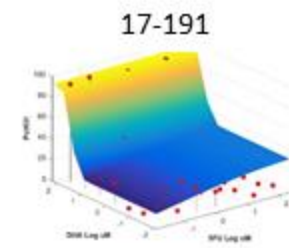
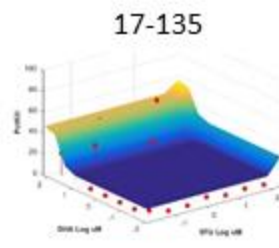
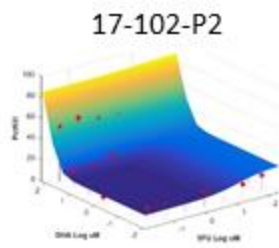
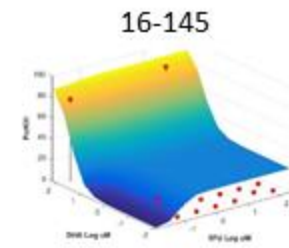
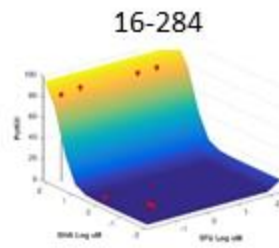
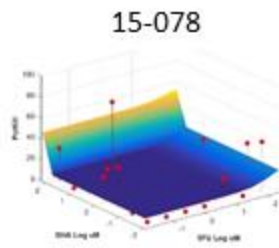
AML cell lines



B-ALL cell lines



Primary B-ALL samples

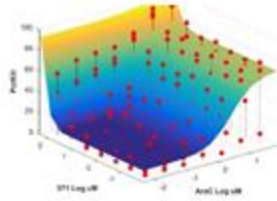


Viability, 48 h

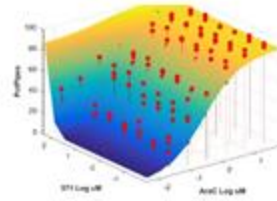
AraC+571

AML cell lines

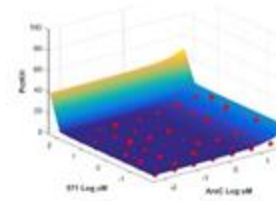
MV-411



U937

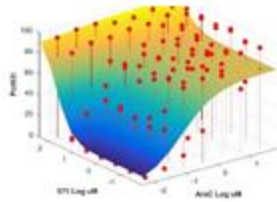


KG-1a

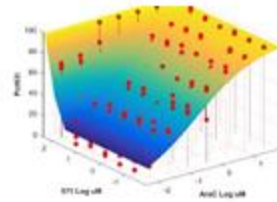


B-ALL cell lines

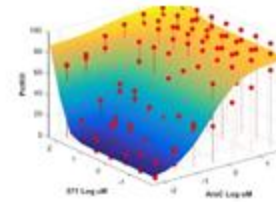
Nalm 6



Sup B15

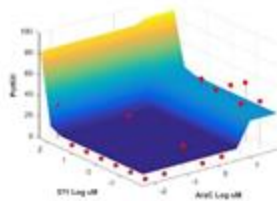


Reh

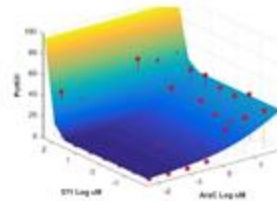


Primary B-ALL samples

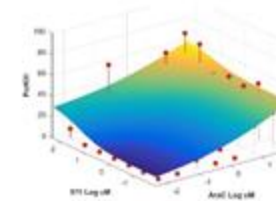
15-078



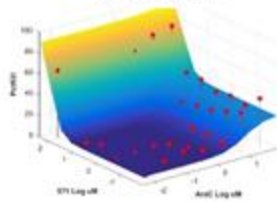
16-284



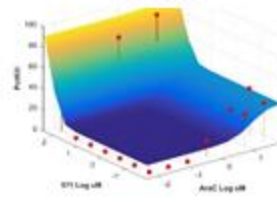
16-145



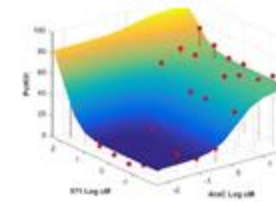
17-102-P2



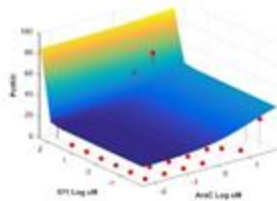
17-135



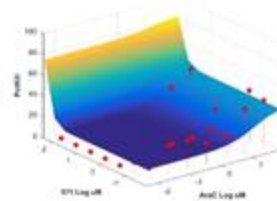
17-191



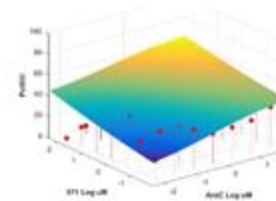
16-265



14-307



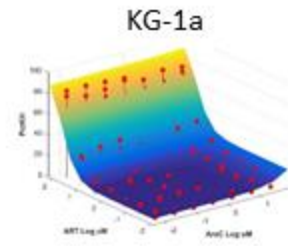
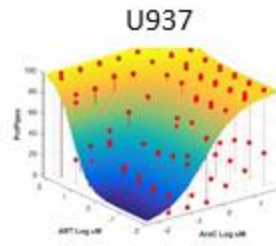
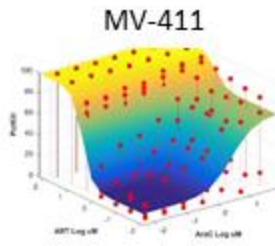
15-007



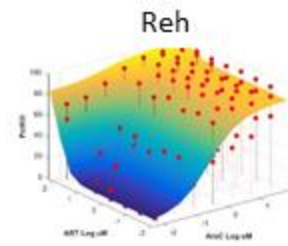
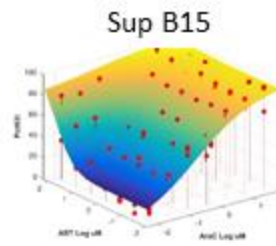
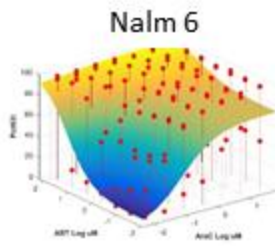
Viability, 48 h

AraC+ART

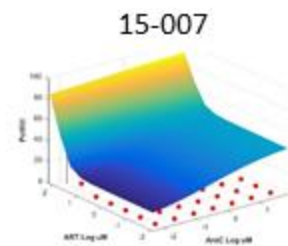
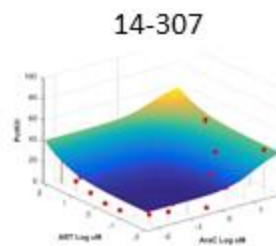
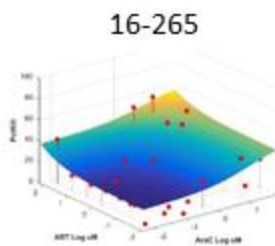
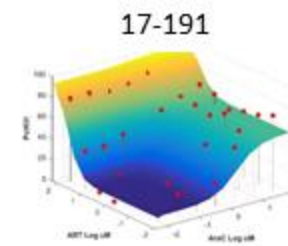
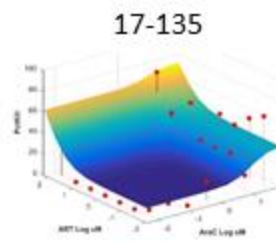
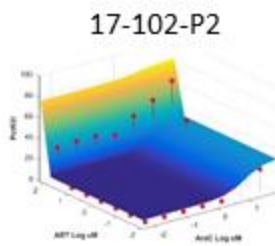
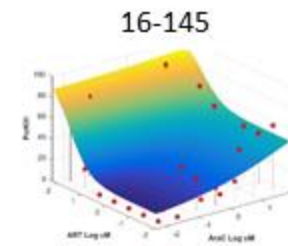
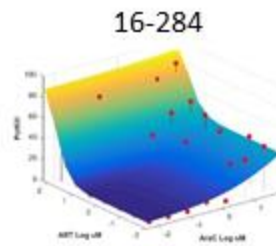
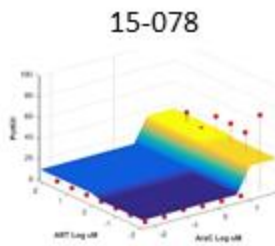
AML cell lines



B-ALL cell lines



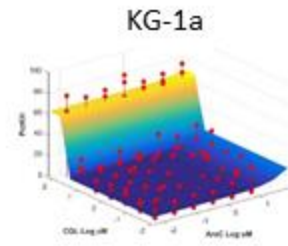
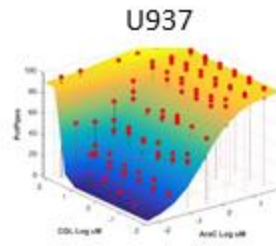
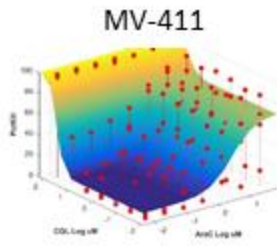
Primary B-ALL samples



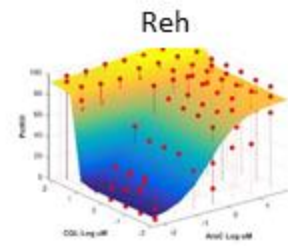
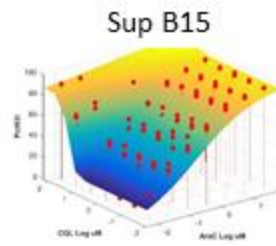
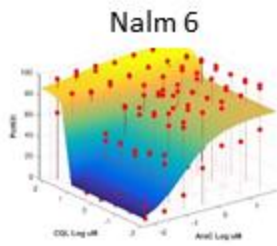
Viability, 48 h

AraC+CQL

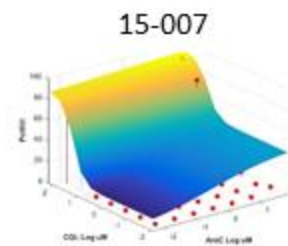
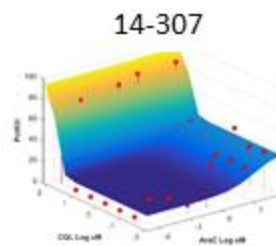
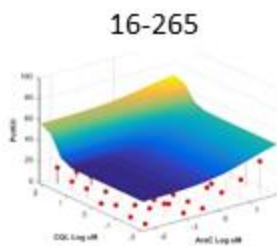
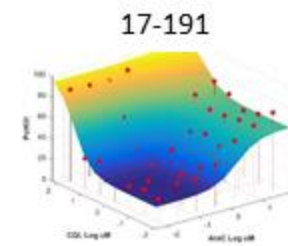
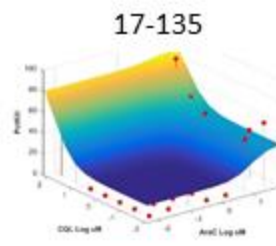
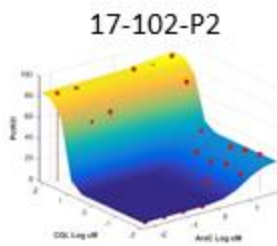
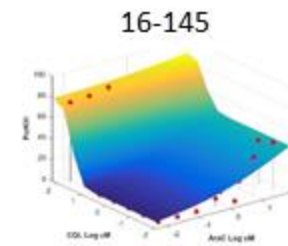
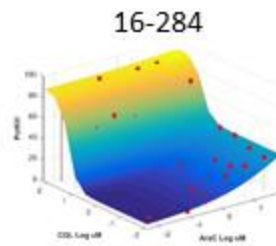
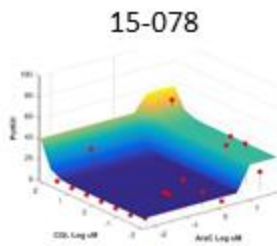
AML cell lines



B-ALL cell lines



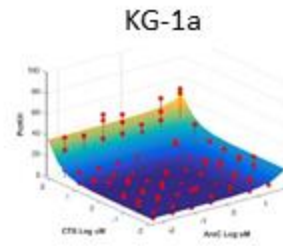
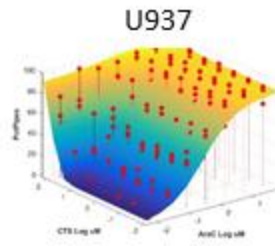
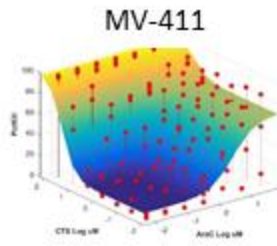
Primary B-ALL samples



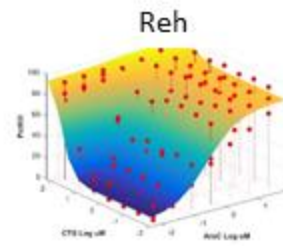
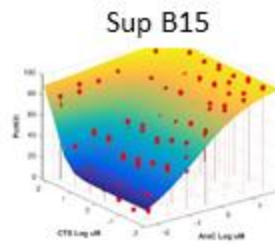
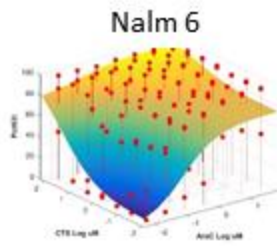
Viability, 48 h

AraC+CTS

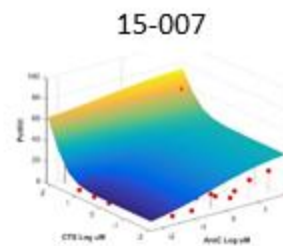
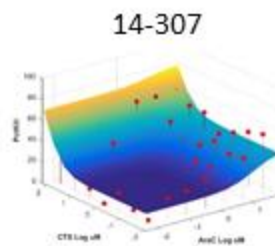
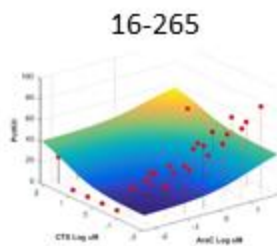
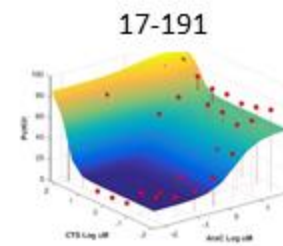
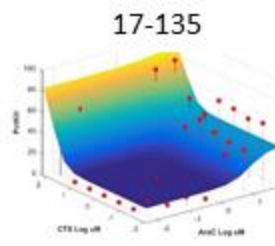
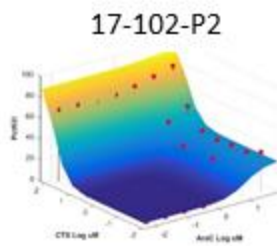
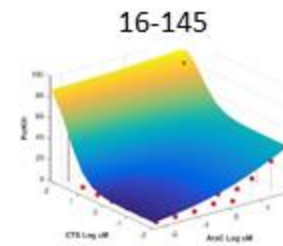
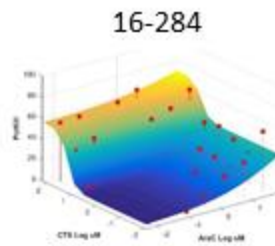
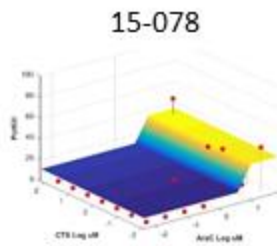
AML cell lines



B-ALL cell lines



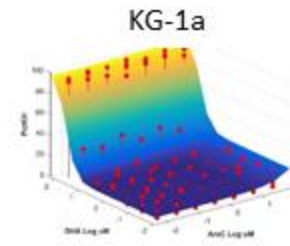
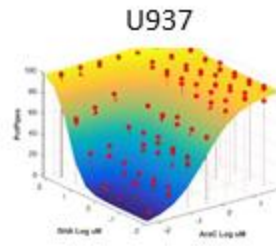
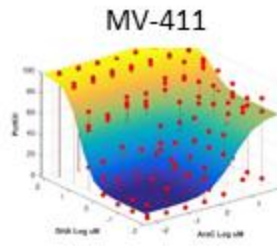
Primary B-ALL samples



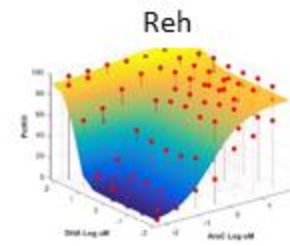
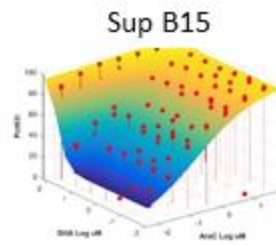
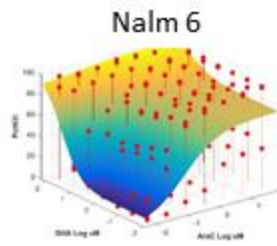
Viability, 48 h

AraC+DHA

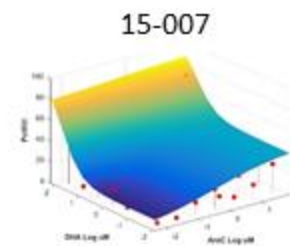
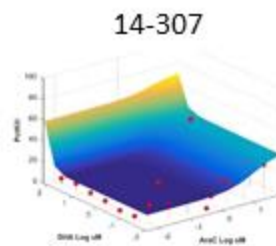
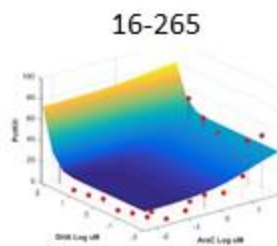
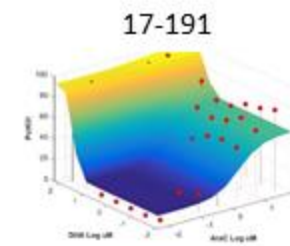
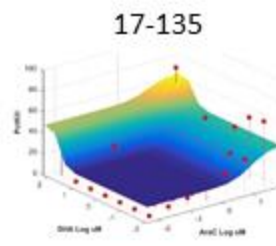
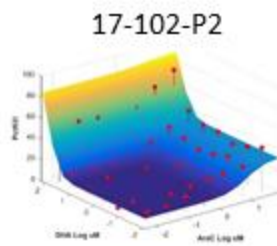
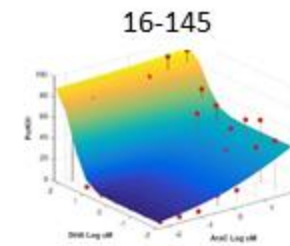
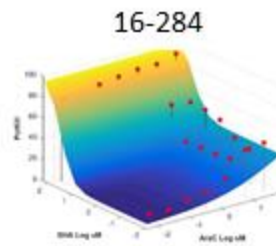
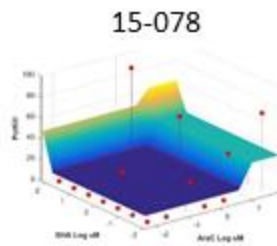
AML cell lines



B-ALL cell lines



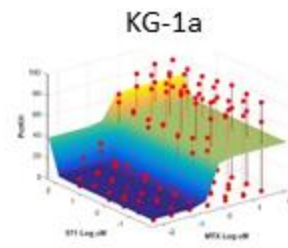
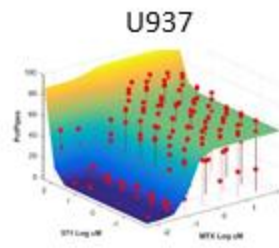
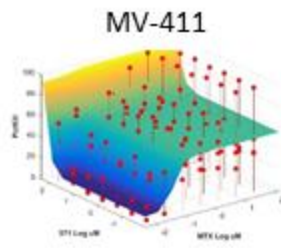
Primary B-ALL samples



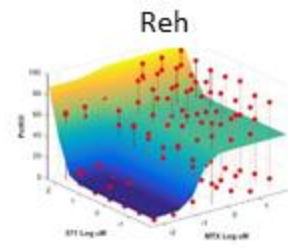
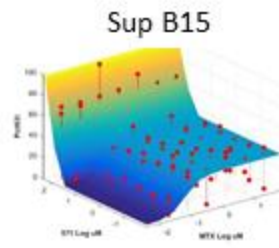
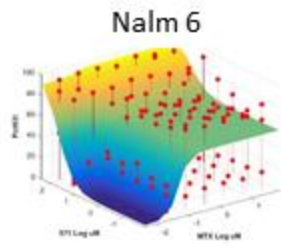
Viability, 48 h

MTX+571

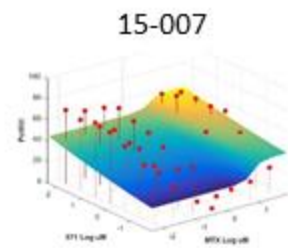
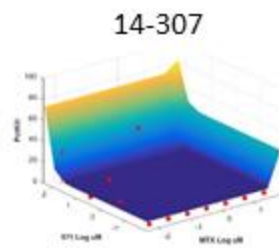
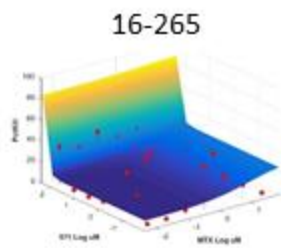
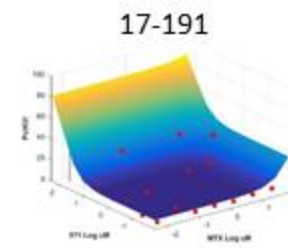
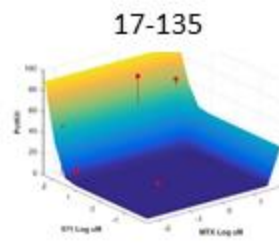
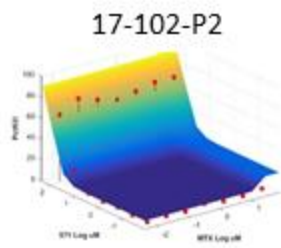
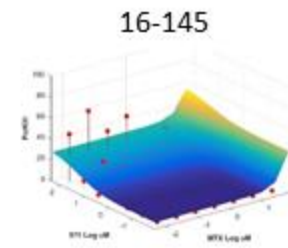
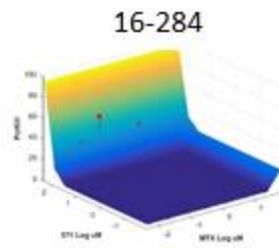
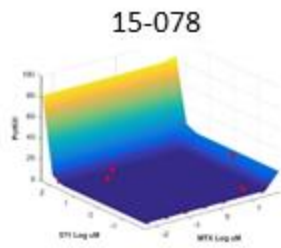
AML cell lines



B-ALL cell lines



Primary B-ALL samples

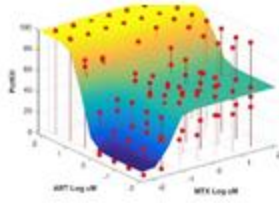


Viability, 48 h

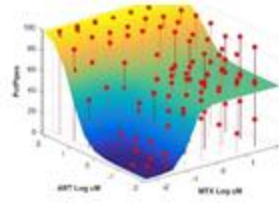
MTX+ART

AML cell lines

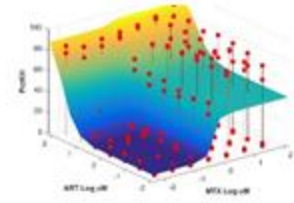
MV-411



U937

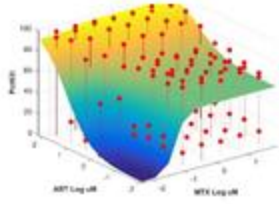


KG-1a

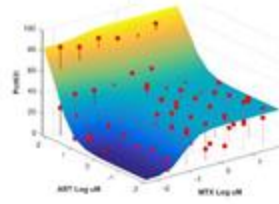


B-ALL cell lines

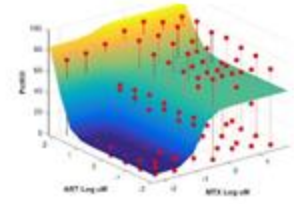
Nalm 6



Sup B15

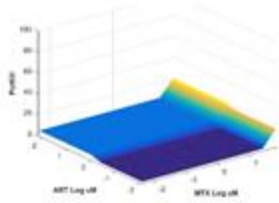


Reh

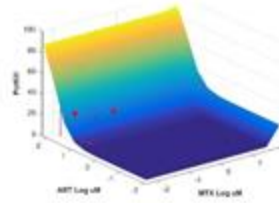


Primary B-ALL samples

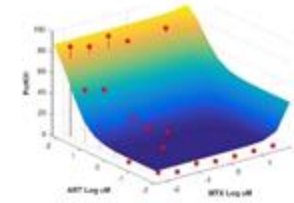
15-078



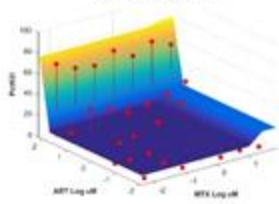
16-284



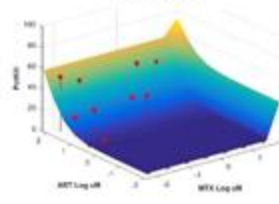
16-145



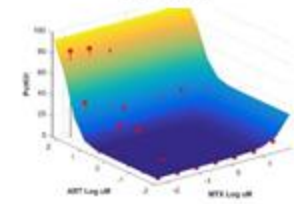
17-102-P2



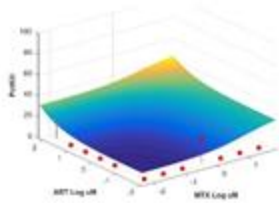
17-135



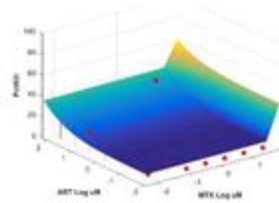
17-191



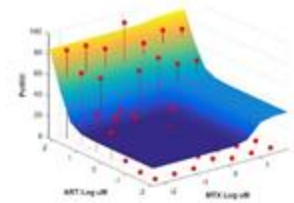
16-265



14-307



15-007

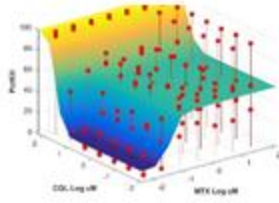


Viability, 48 h

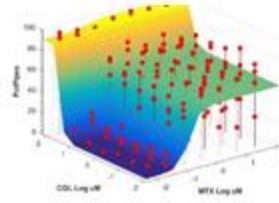
MTX+CQL

AML cell lines

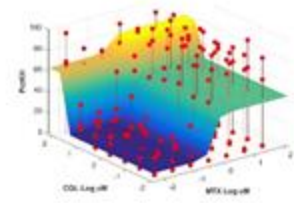
MV-411



U937

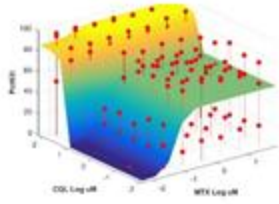


KG-1a

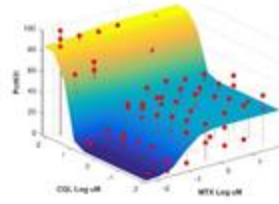


B-ALL cell lines

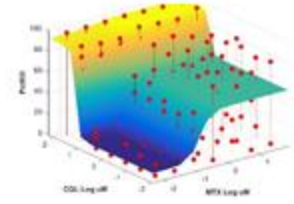
Nalm 6



Sup B15

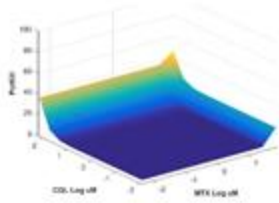


Reh

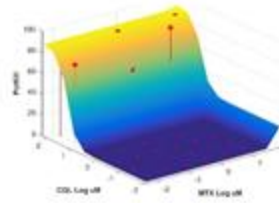


Primary B-ALL samples

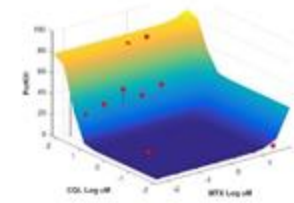
15-078



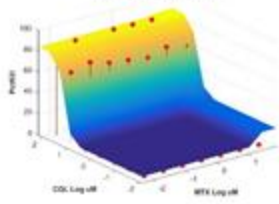
16-284



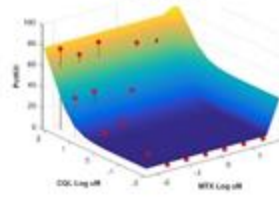
16-145



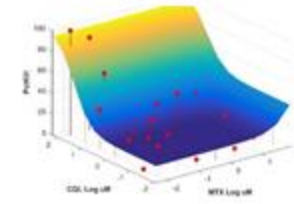
17-102-P2



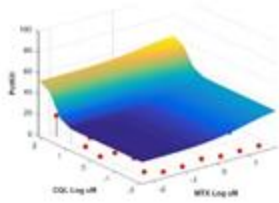
17-135



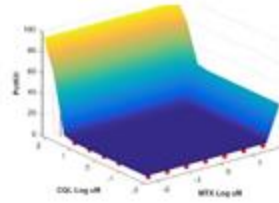
17-191



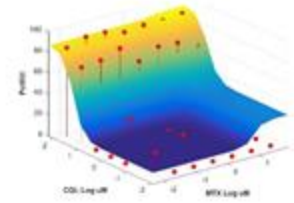
16-265



14-307



15-007

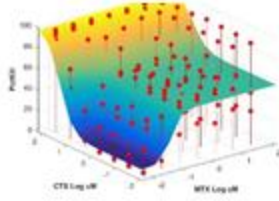


Viability, 48 h

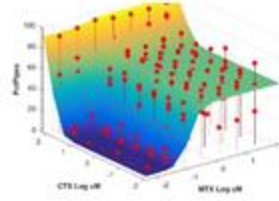
MTX+CTS

AML cell lines

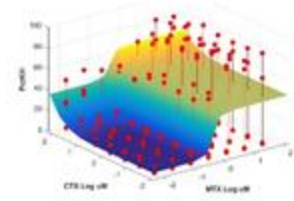
MV-411



U937

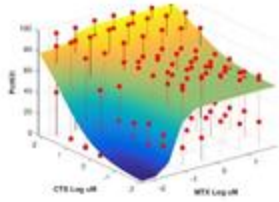


KG-1a

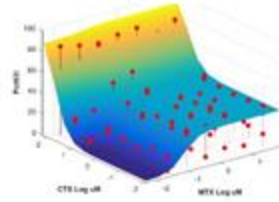


B-ALL cell lines

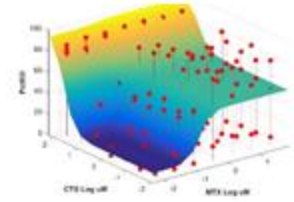
Nalm 6



Sup B15

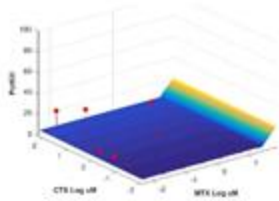


Reh

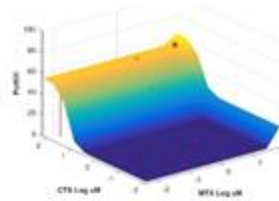


Primary B-ALL samples

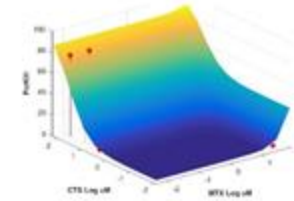
15-078



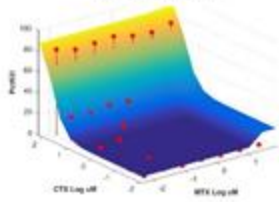
16-284



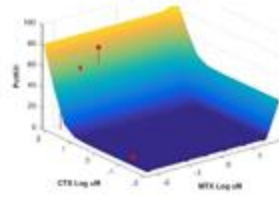
16-145



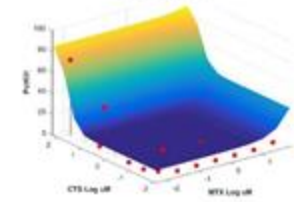
17-102-P2



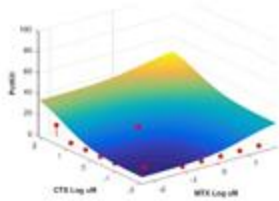
17-135



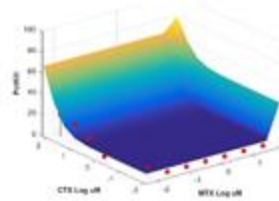
17-191



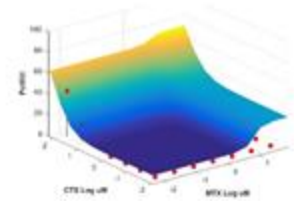
16-265



14-307



15-007

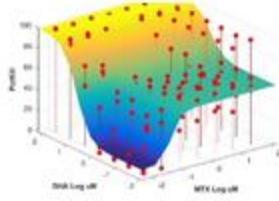


Viability, 48 h

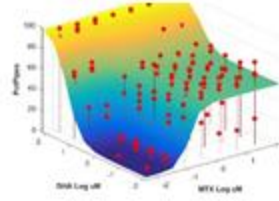
MTX+DHA

AML cell lines

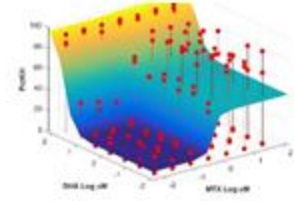
MV-411



U937

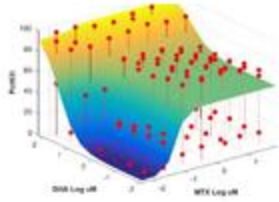


KG-1a

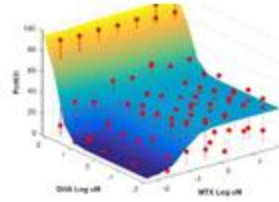


B-ALL cell lines

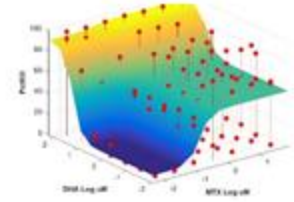
Nalm 6



Sup B15

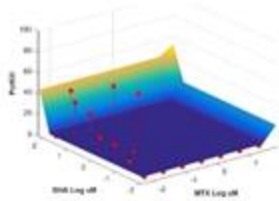


Reh

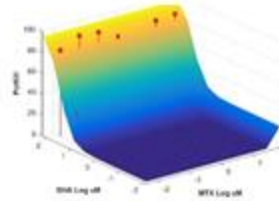


Primary B-ALL samples

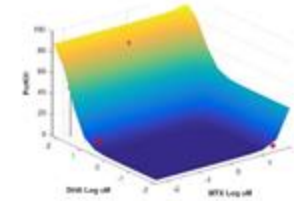
15-078



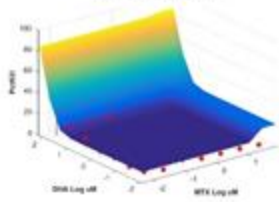
16-284



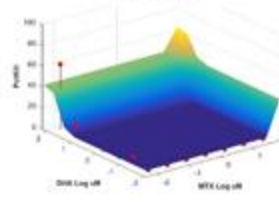
16-145



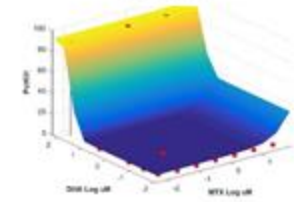
17-102-P2



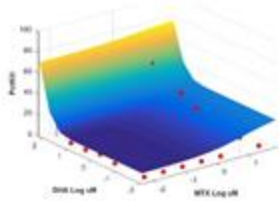
17-135



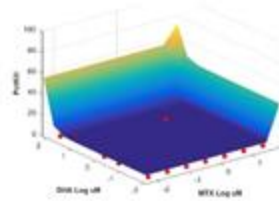
17-191



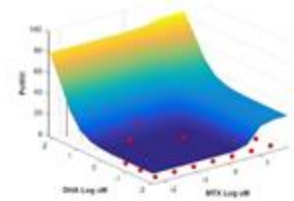
16-265



14-307



15-007

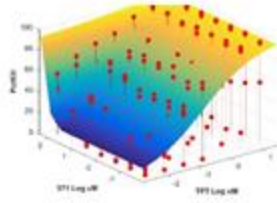


Viability, 48 h

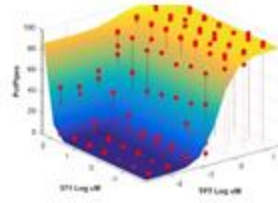
TPT+571

AML cell lines

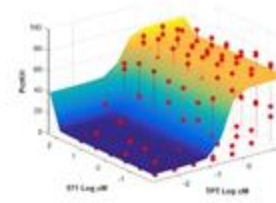
MV-411



U937

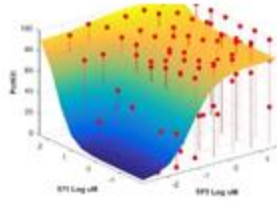


KG-1a

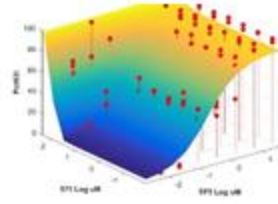


B-ALL cell lines

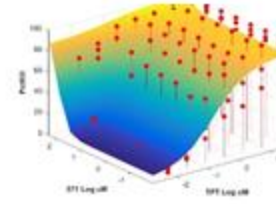
Nalm 6



Sup B15

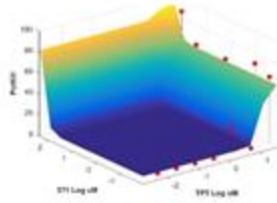


Reh

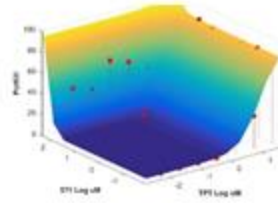


Primary B-ALL samples

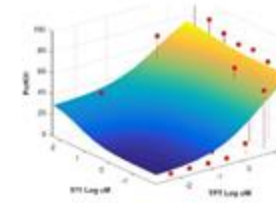
15-078



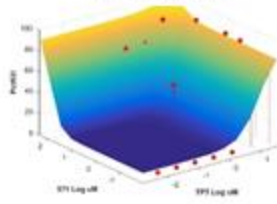
16-284



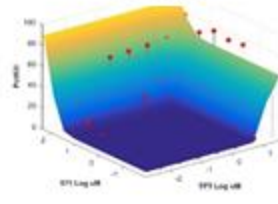
16-145



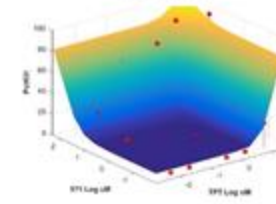
17-102-P2



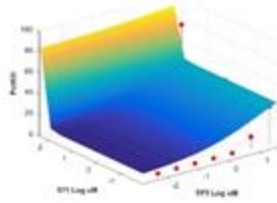
17-135



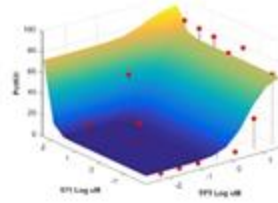
17-191



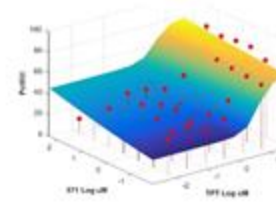
16-265



14-307



15-007

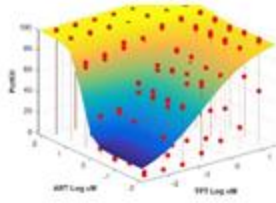


Viability, 48 h

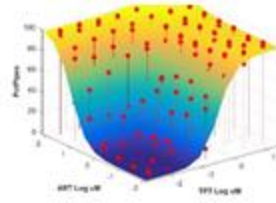
TPT+ART

AML cell lines

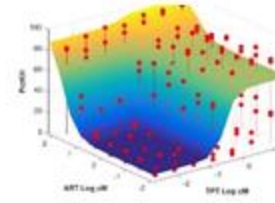
MV-411



U937

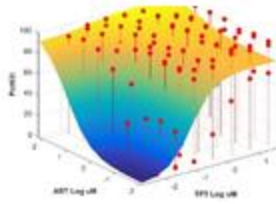


KG-1a

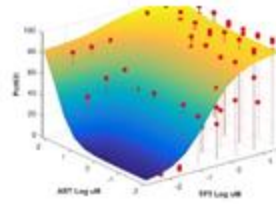


B-ALL cell lines

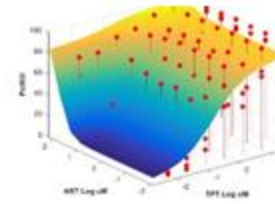
Nalm 6



Sup B15

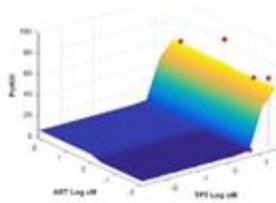


Reh

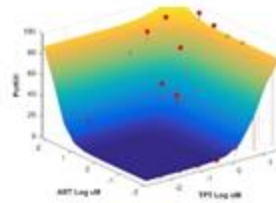


Primary B-ALL samples

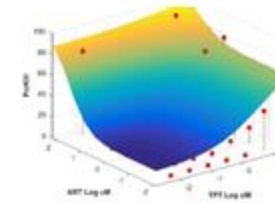
15-078



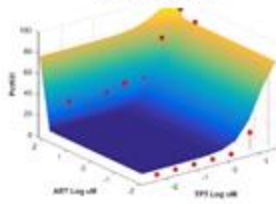
16-284



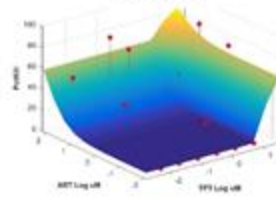
16-145



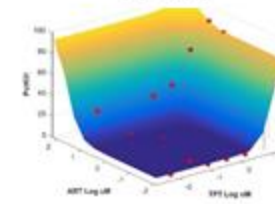
17-102-P2



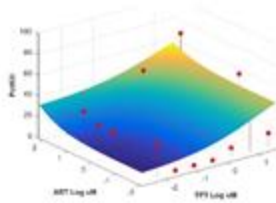
17-135



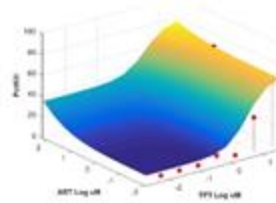
17-191



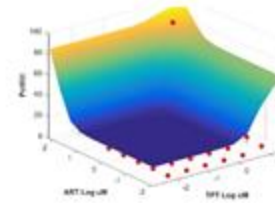
16-265



14-307



15-007

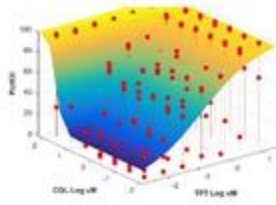


Viability, 48 h

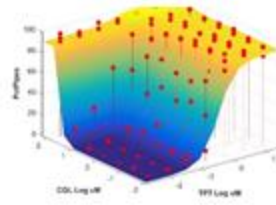
TPT+CQL

AML cell lines

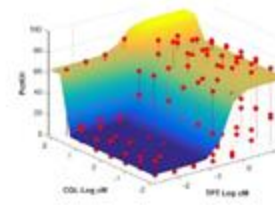
MV-411



U937

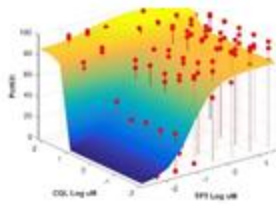


KG-1a

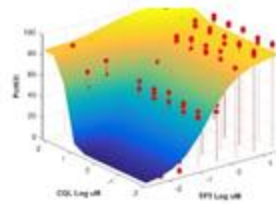


B-ALL cell lines

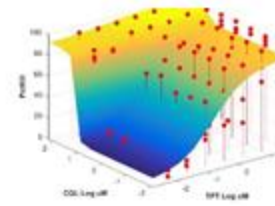
Nalm 6



Sup B15

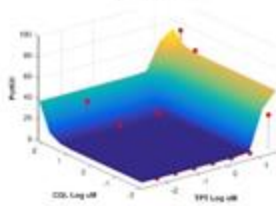


Reh

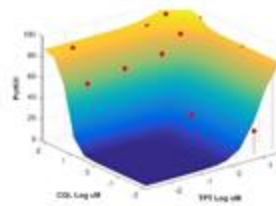


Primary B-ALL samples

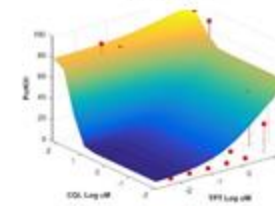
15-078



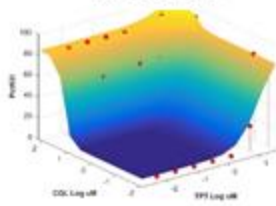
16-284



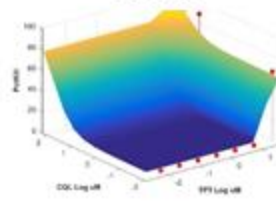
16-145



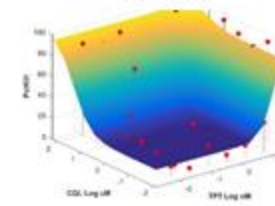
17-102-P2



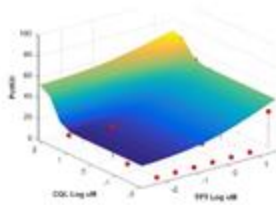
17-135



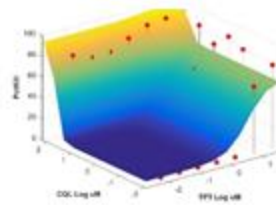
17-191



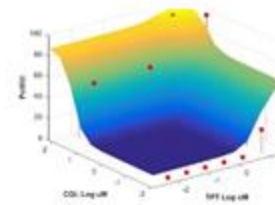
16-265



14-307



15-007

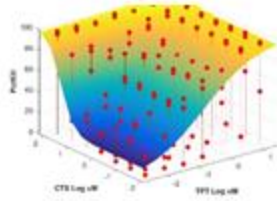


Viability, 48 h

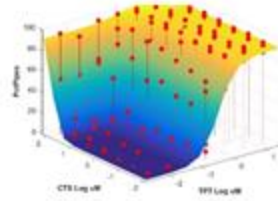
TPT+CTS

AML cell lines

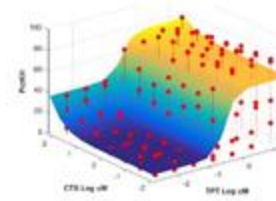
MV-411



U937

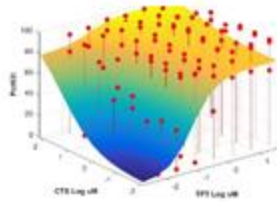


KG-1a

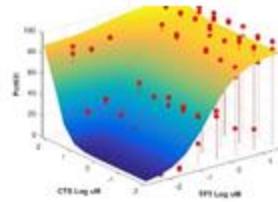


B-ALL cell lines

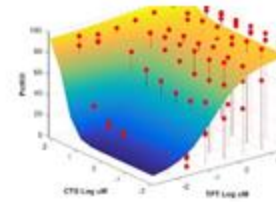
Nalm 6



Sup B15

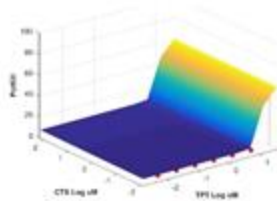


Reh

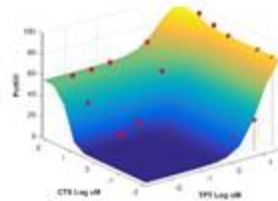


Primary B-ALL samples

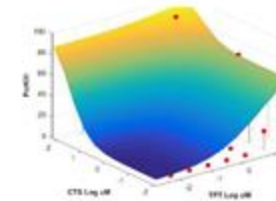
15-078



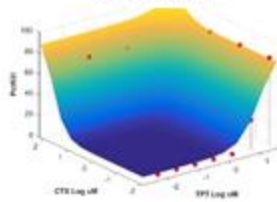
16-284



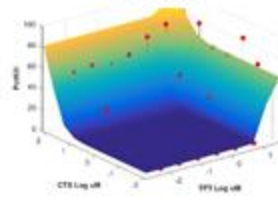
16-145



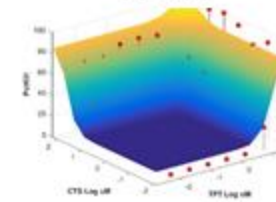
17-102-P2



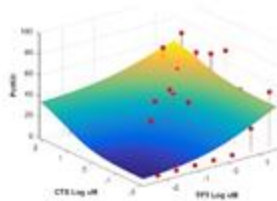
17-135



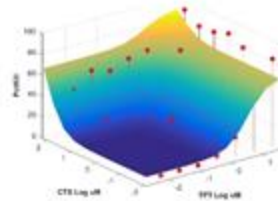
17-191



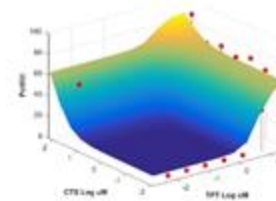
16-265



14-307



15-007

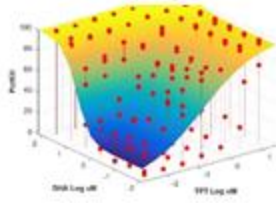


Viability, 48 h

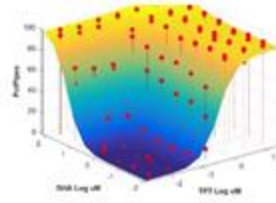
TPT+DHA

AML cell lines

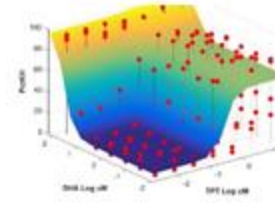
MV-411



U937

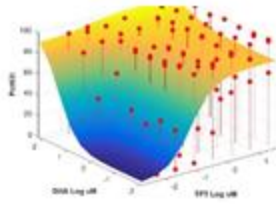


KG-1a

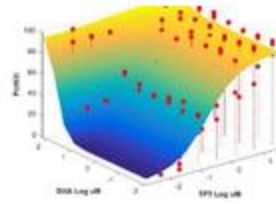


B-ALL cell lines

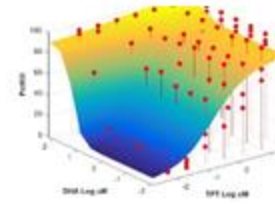
Nalm 6



Sup B15

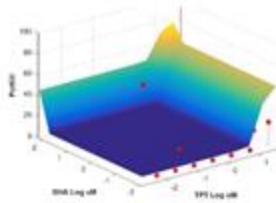


Reh

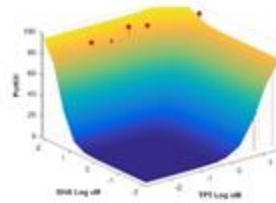


Primary B-ALL samples

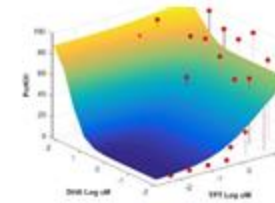
15-078



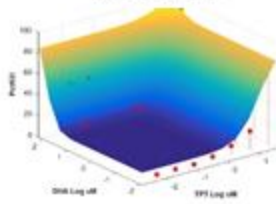
16-284



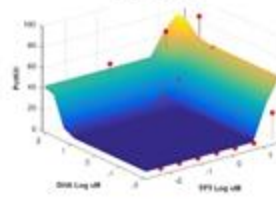
16-145



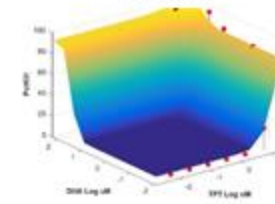
17-102-P2



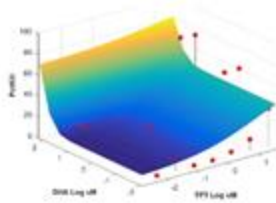
17-135



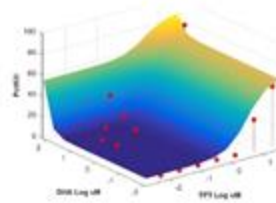
17-191



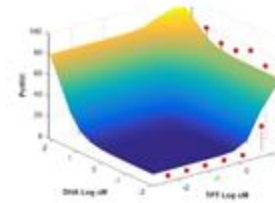
16-265



14-307



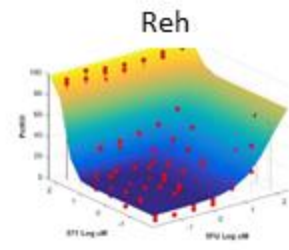
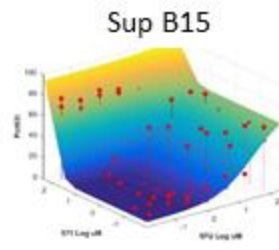
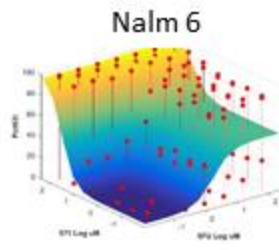
15-007



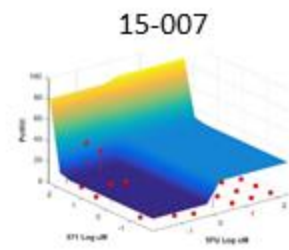
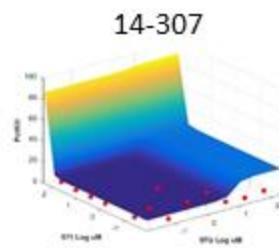
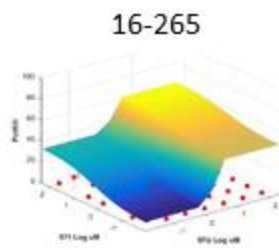
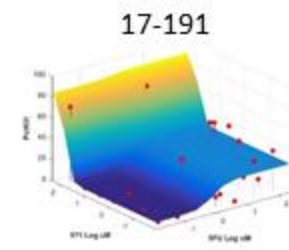
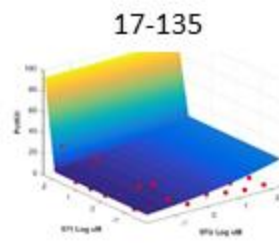
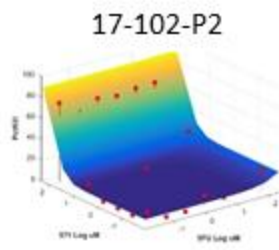
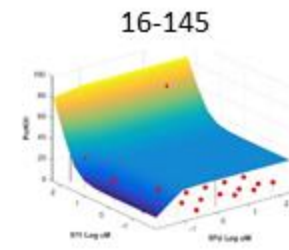
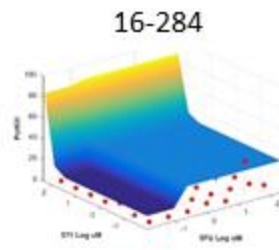
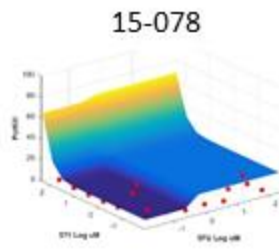
Viability, 72 h

5FU+571

B-ALL cell lines



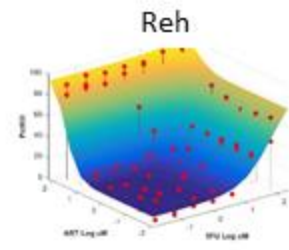
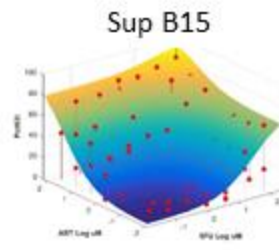
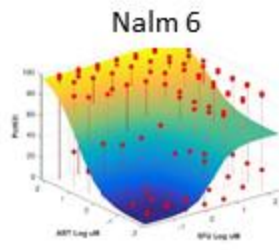
Primary B-ALL samples



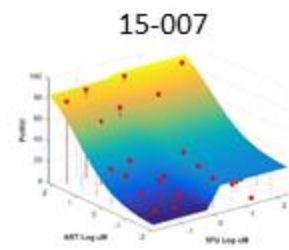
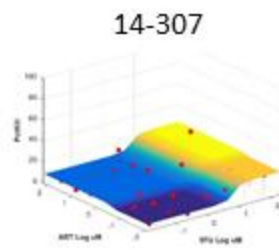
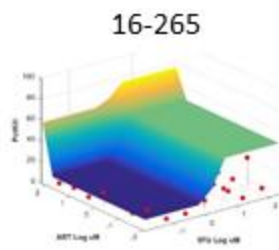
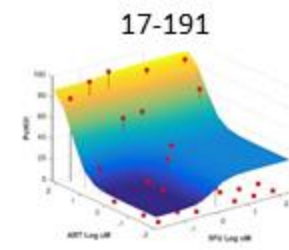
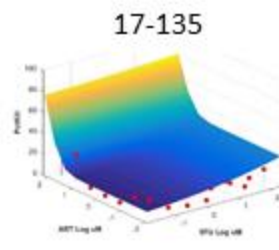
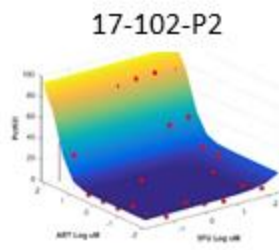
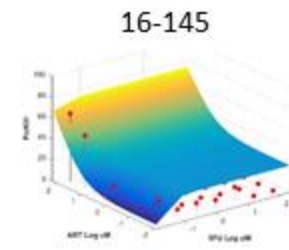
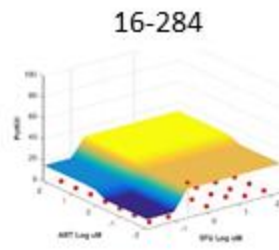
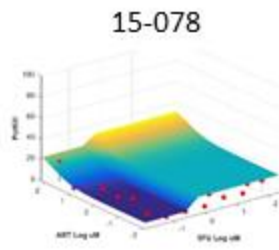
Viability, 72 h

5FU+ART

B-ALL cell lines



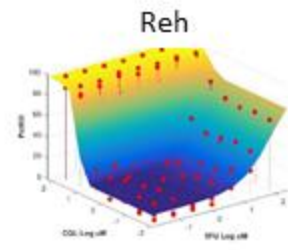
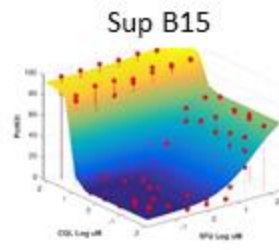
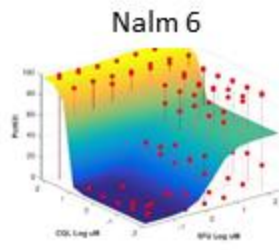
Primary B-ALL samples



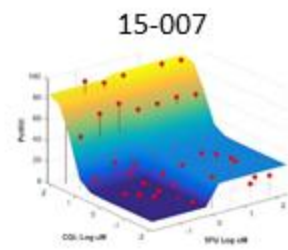
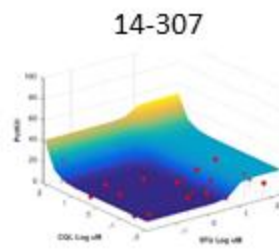
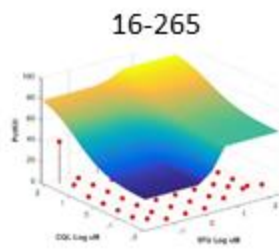
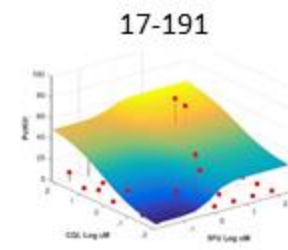
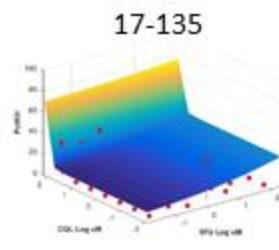
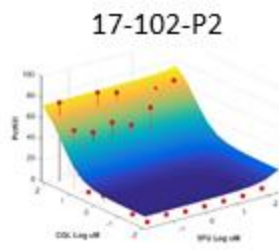
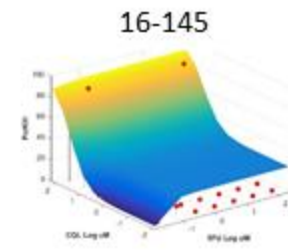
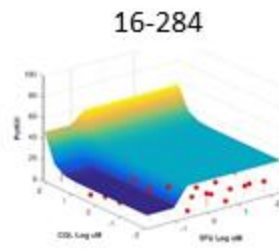
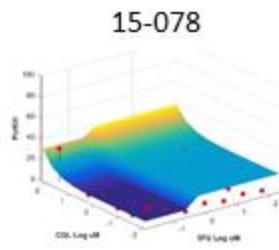
Viability, 72 h

5FU+CQL

B-ALL cell lines



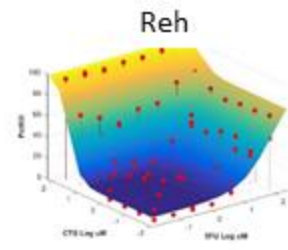
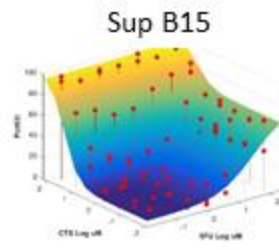
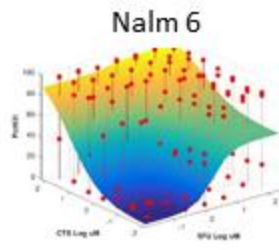
Primary B-ALL samples



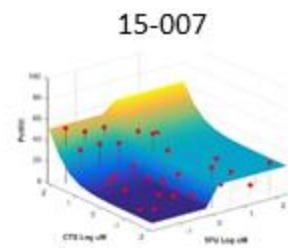
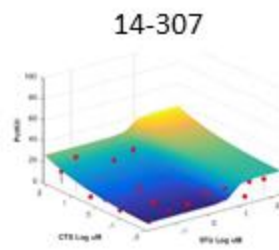
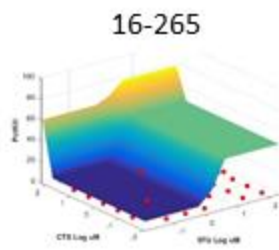
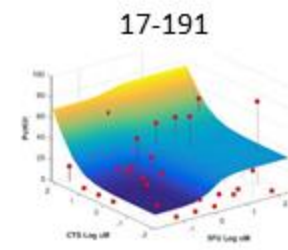
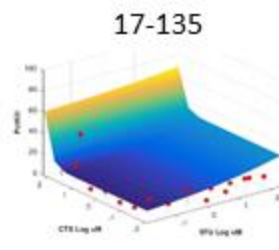
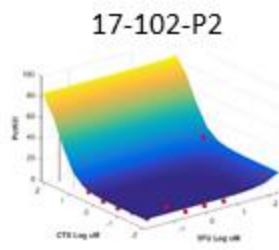
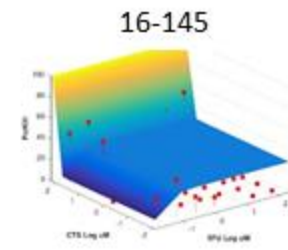
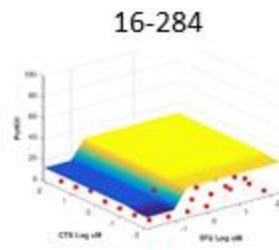
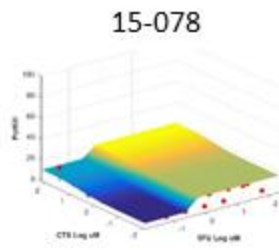
Viability, 72 h

5FU+CTS

B-ALL cell lines



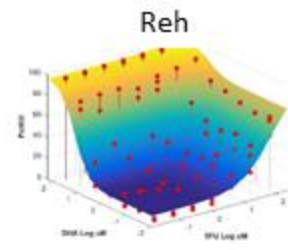
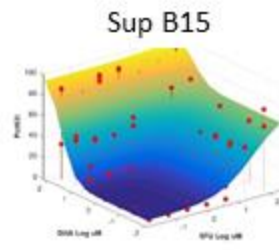
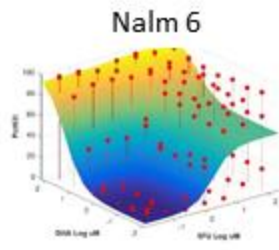
Primary B-ALL samples



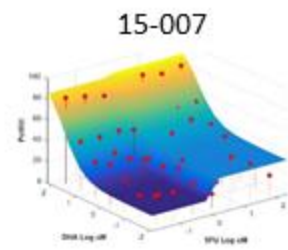
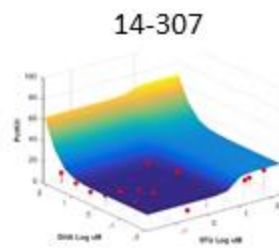
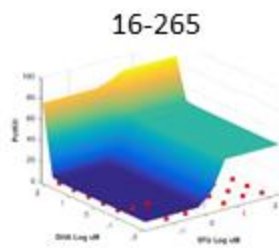
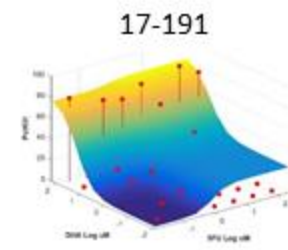
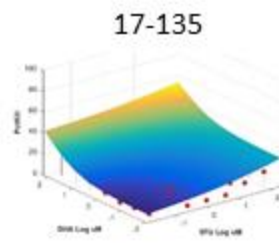
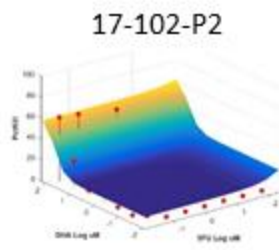
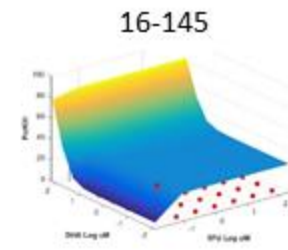
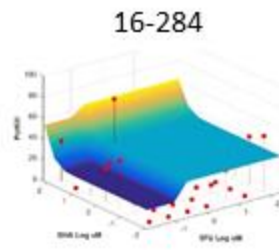
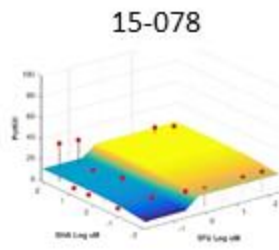
Viability, 72 h

5FU+DHA

B-ALL cell lines



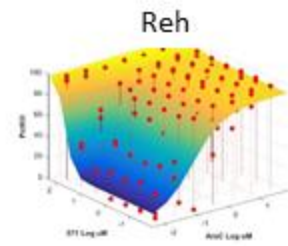
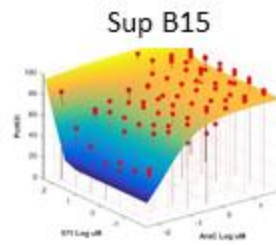
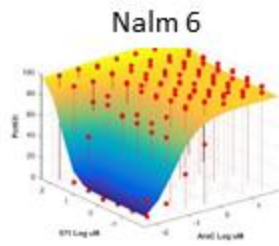
Primary B-ALL samples



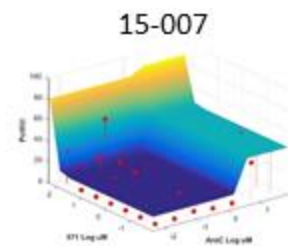
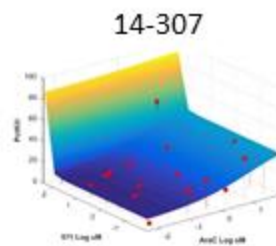
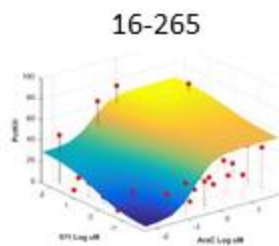
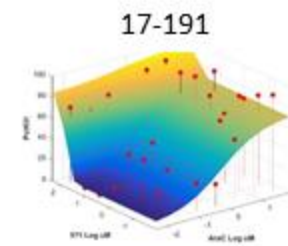
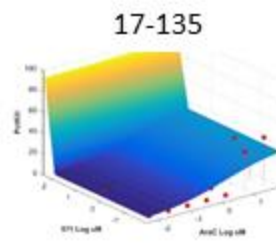
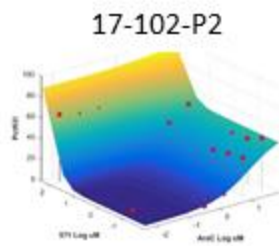
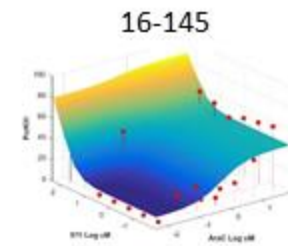
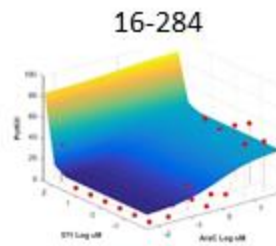
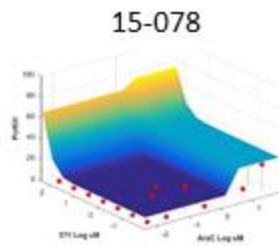
Viability, 72 h

AraC+571

B-ALL cell lines



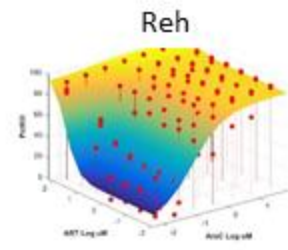
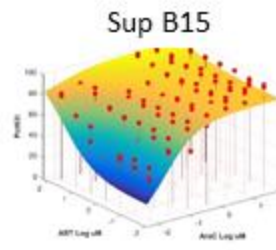
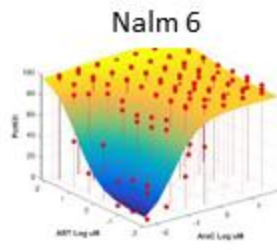
Primary B-ALL samples



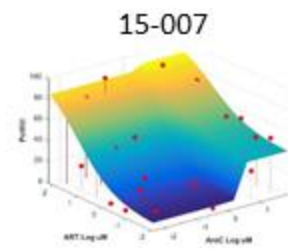
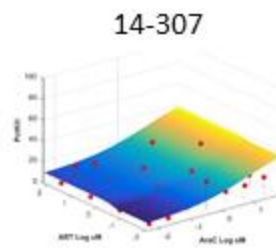
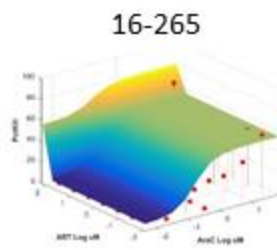
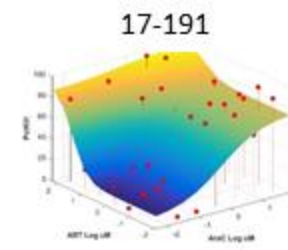
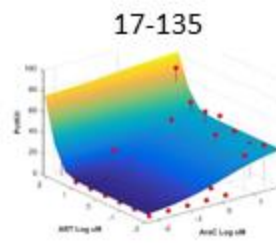
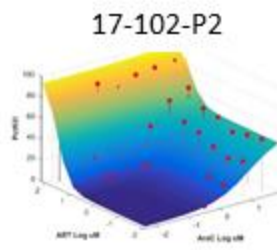
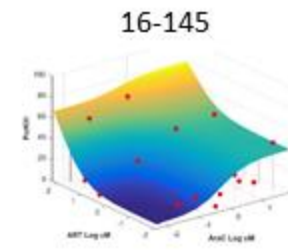
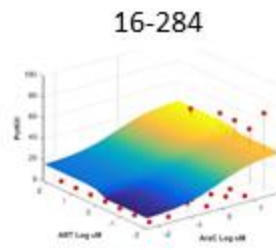
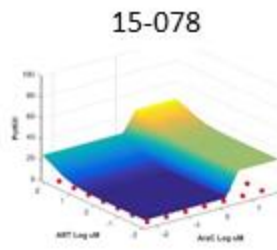
Viability, 72 h

AraC+ART

B-ALL cell lines



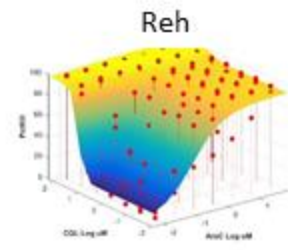
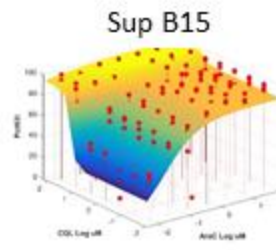
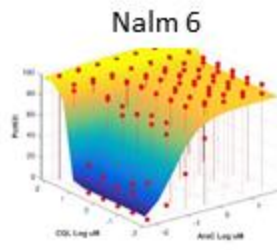
Primary B-ALL samples



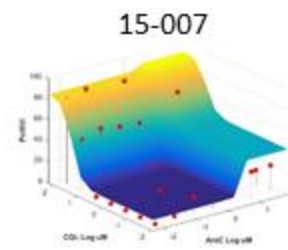
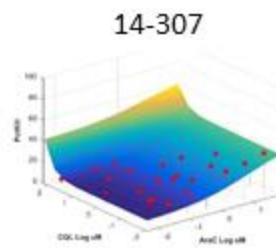
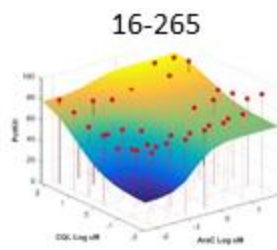
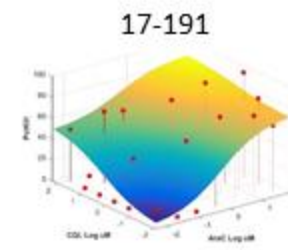
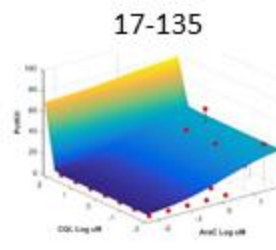
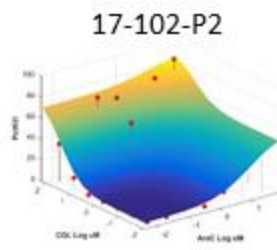
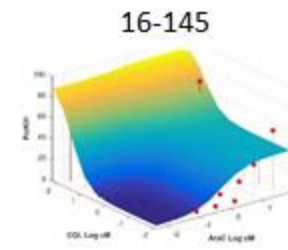
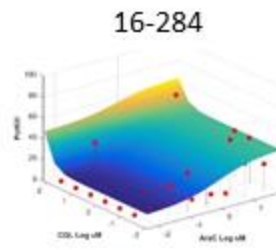
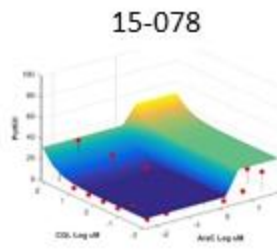
Viability, 72 h

AraC+CQL

B-ALL cell lines



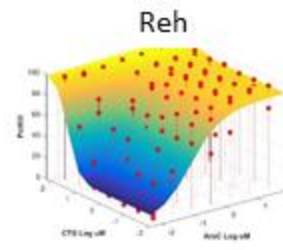
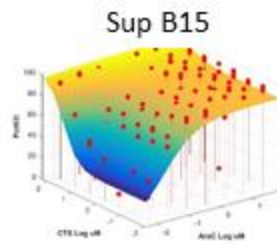
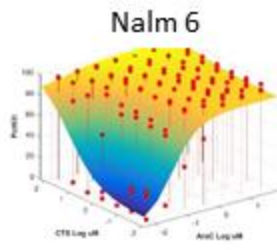
Primary B-ALL samples



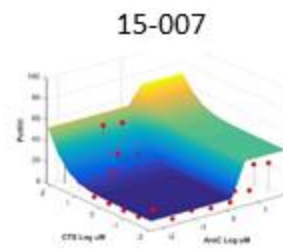
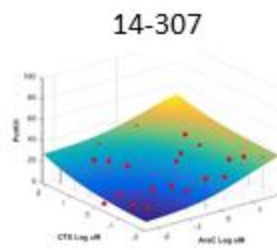
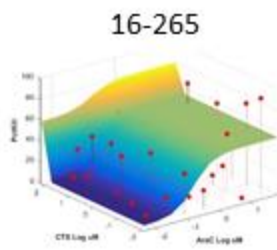
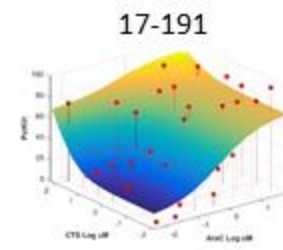
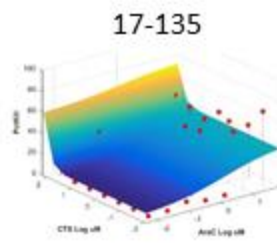
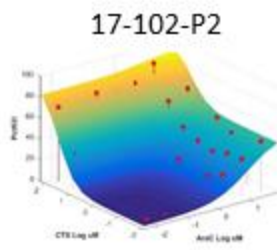
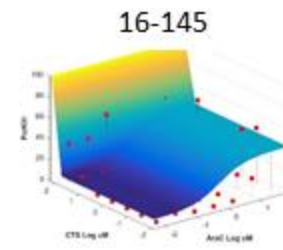
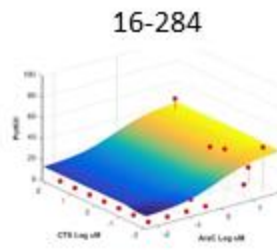
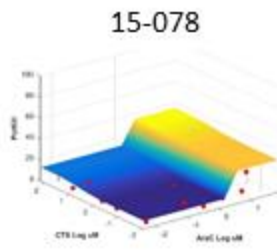
Viability, 72 h

AraC+CTS

B-ALL cell lines



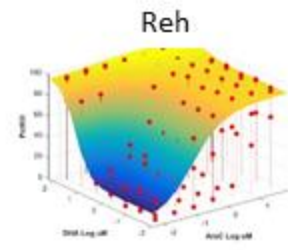
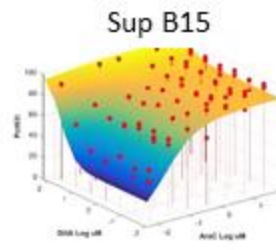
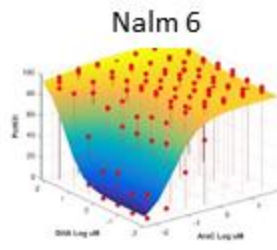
Primary B-ALL samples



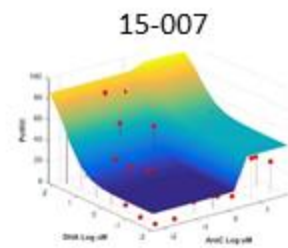
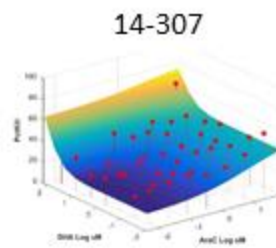
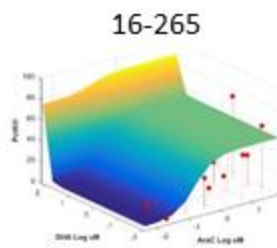
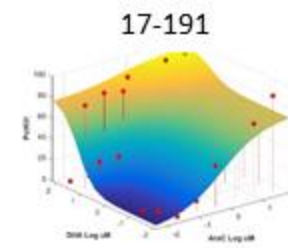
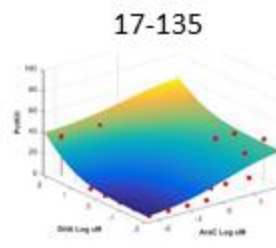
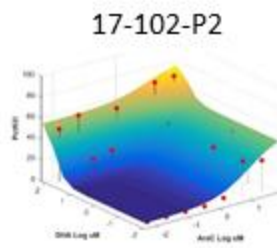
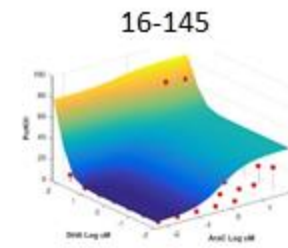
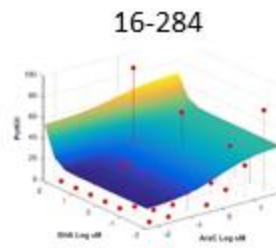
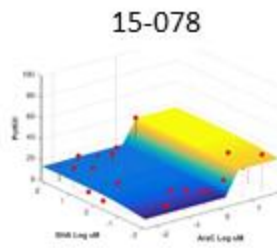
Viability, 72 h

AraC+DHA

B-ALL cell lines



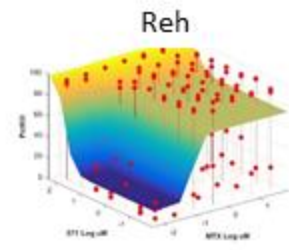
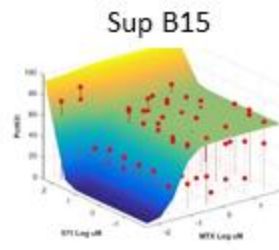
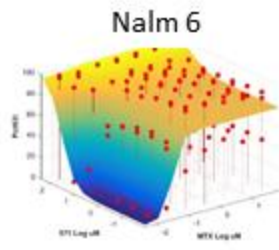
Primary B-ALL samples



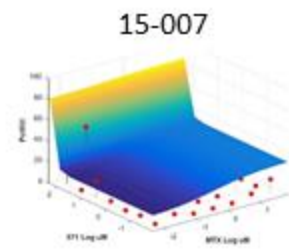
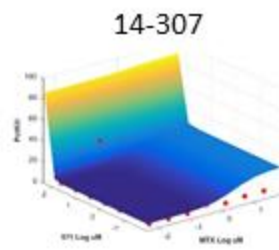
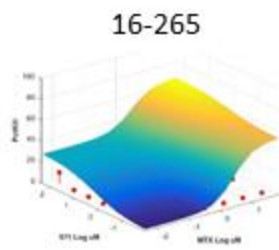
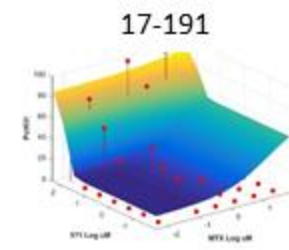
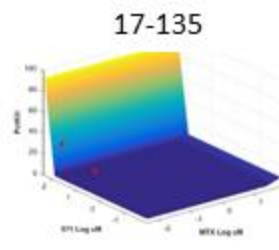
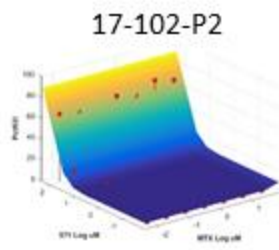
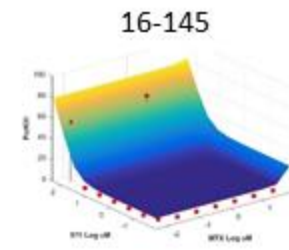
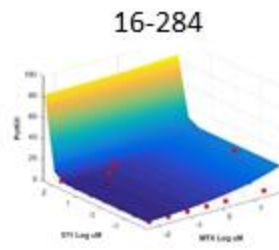
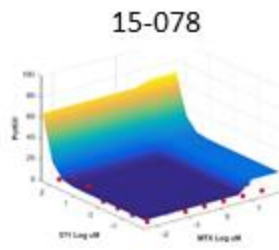
Viability, 72 h

MTX+571

B-ALL cell lines



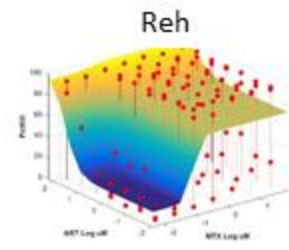
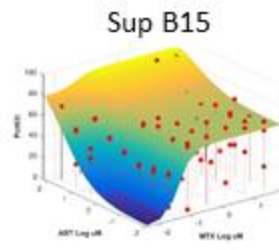
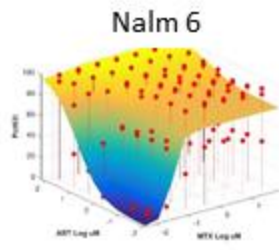
Primary B-ALL samples



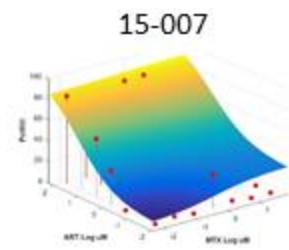
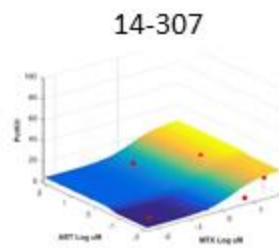
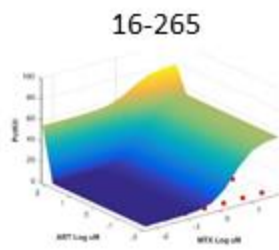
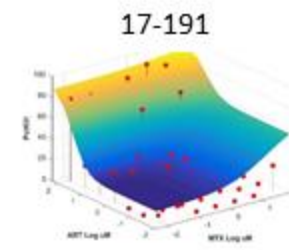
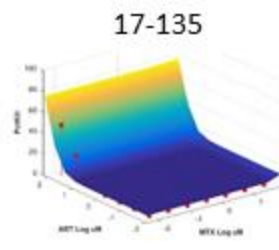
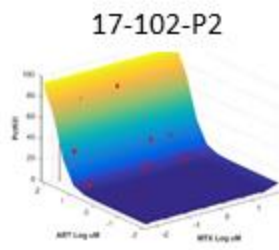
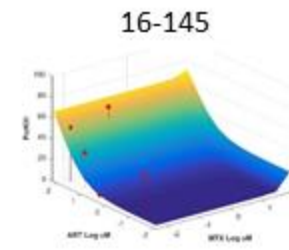
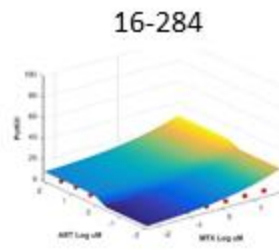
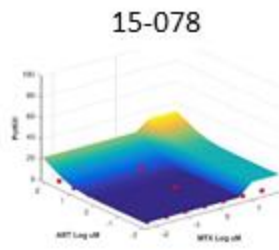
Viability, 72 h

MTX+ART

B-ALL cell lines



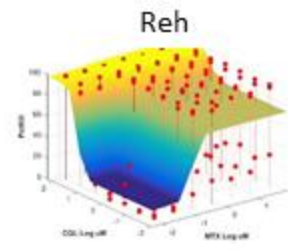
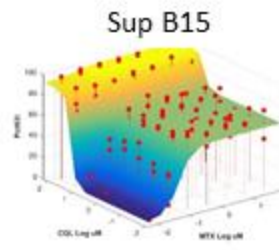
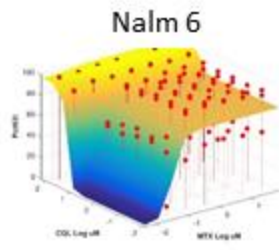
Primary B-ALL samples



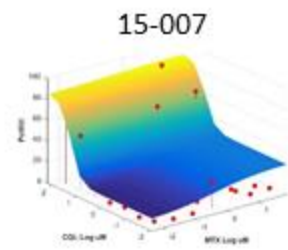
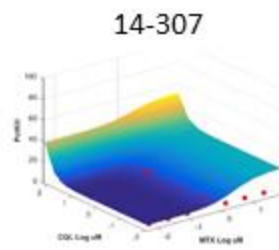
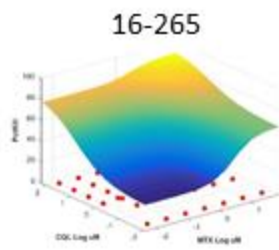
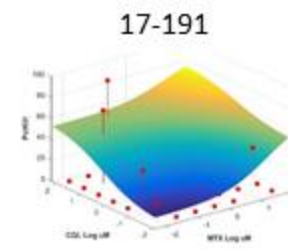
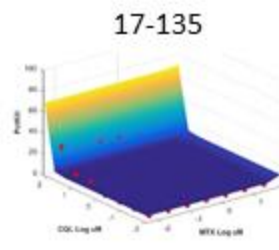
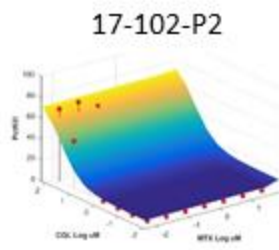
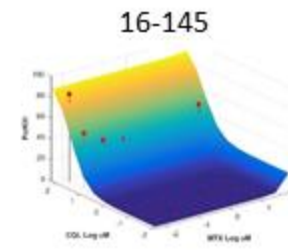
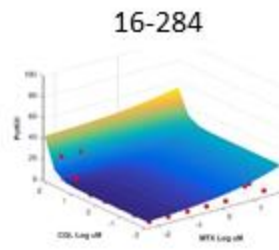
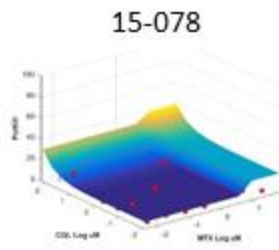
Viability, 72 h

MTX+CQL

B-ALL cell lines



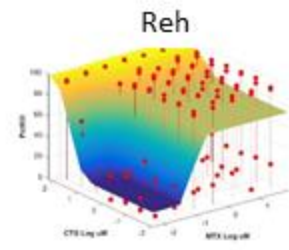
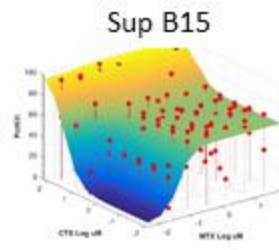
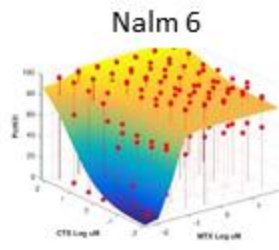
Primary B-ALL samples



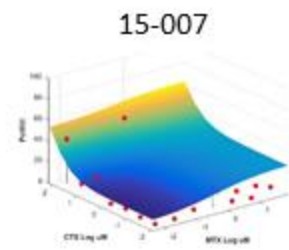
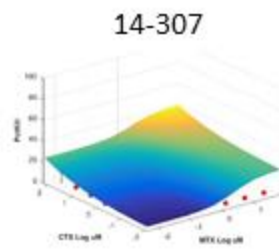
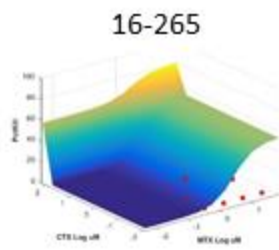
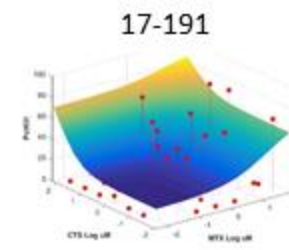
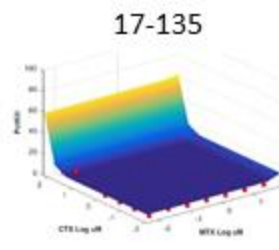
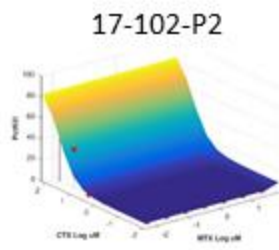
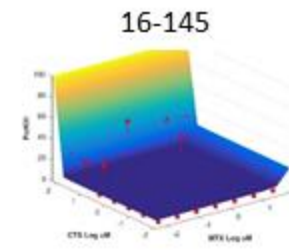
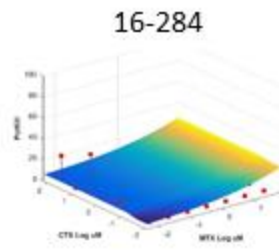
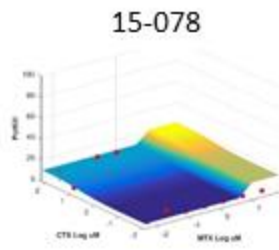
Viability, 72 h

MTX+CTS

B-ALL cell lines



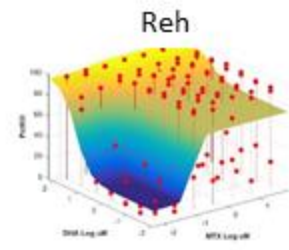
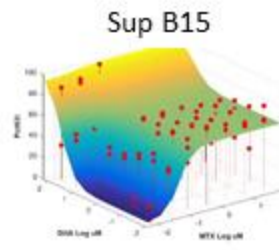
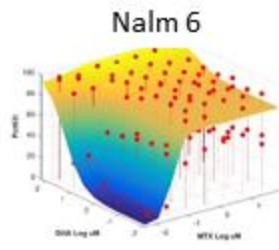
Primary B-ALL samples



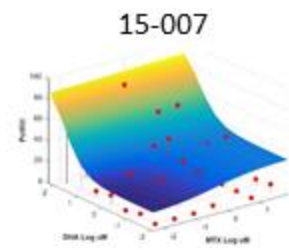
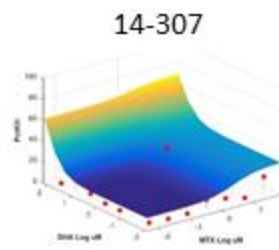
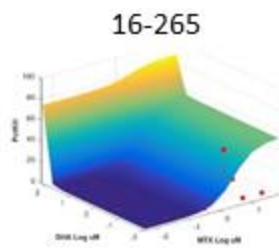
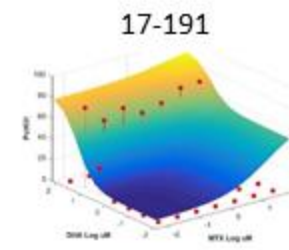
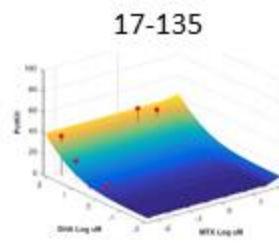
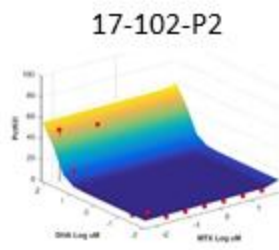
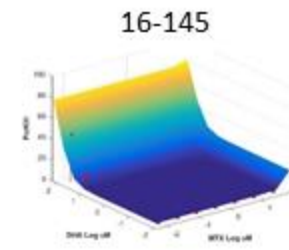
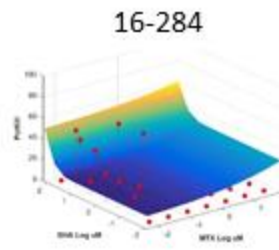
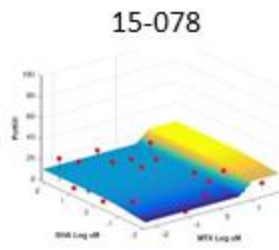
Viability, 72 h

MTX+DHA

B-ALL cell lines



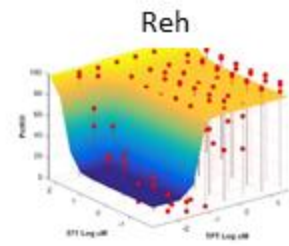
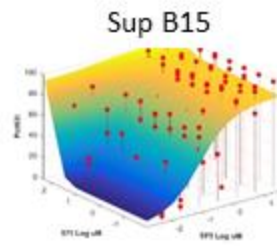
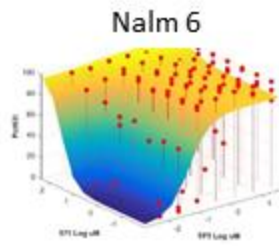
Primary B-ALL samples



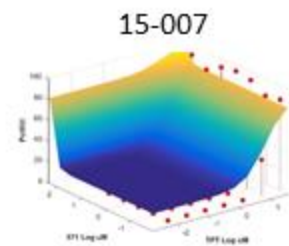
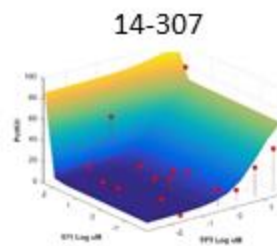
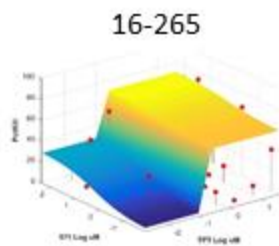
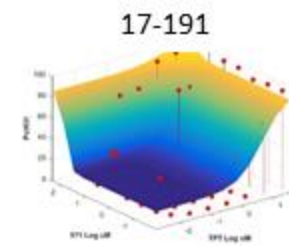
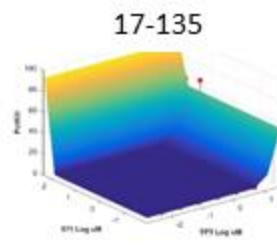
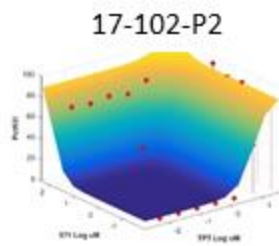
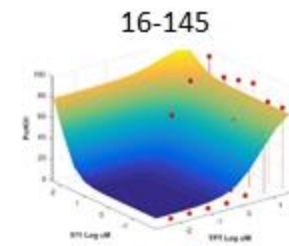
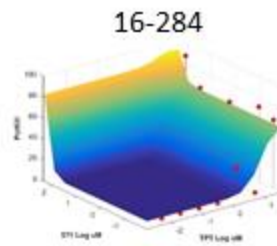
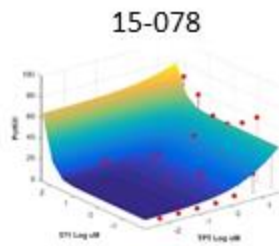
Viability, 72 h

TPT+571

B-ALL cell lines



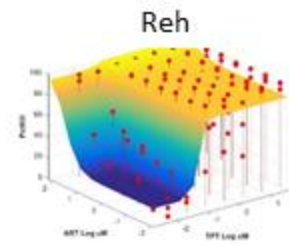
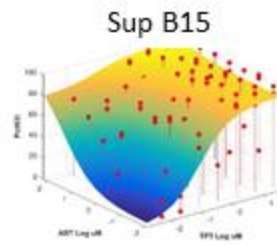
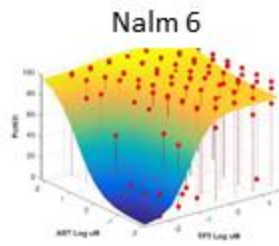
Primary B-ALL samples



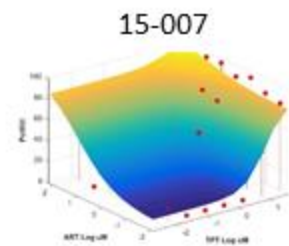
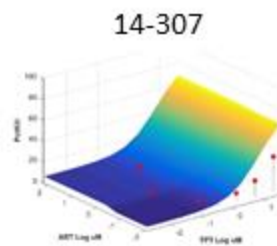
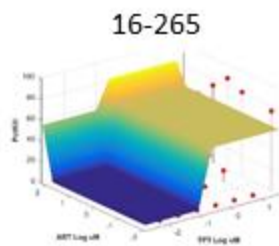
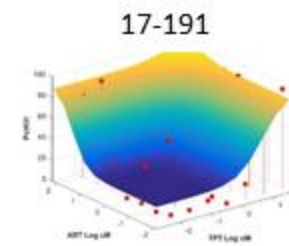
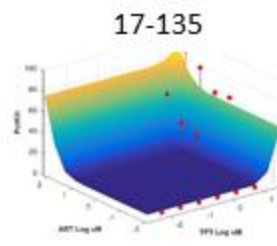
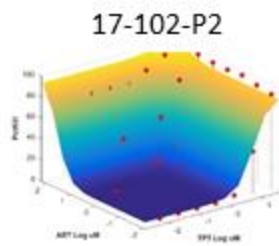
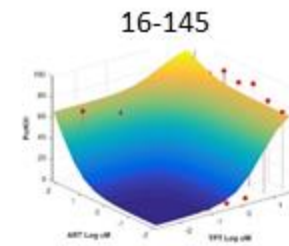
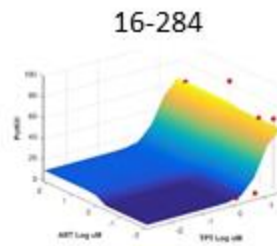
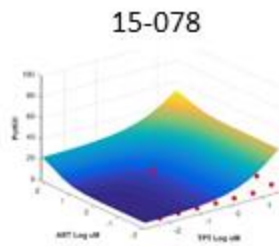
Viability, 72 h

TPT+ART

B-ALL cell lines



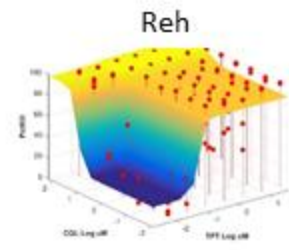
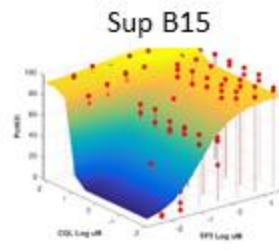
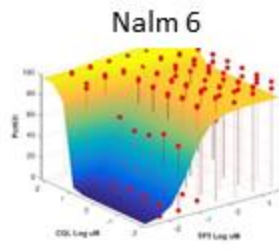
Primary B-ALL samples



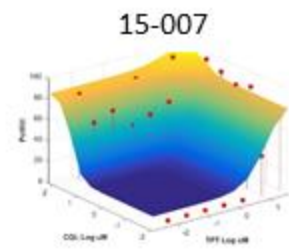
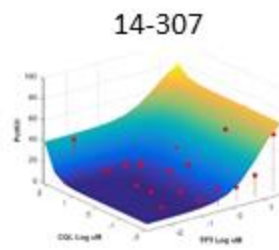
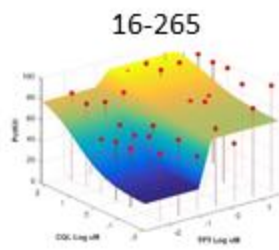
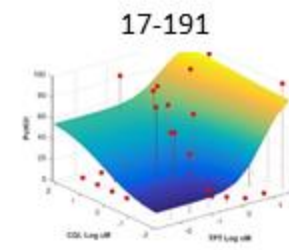
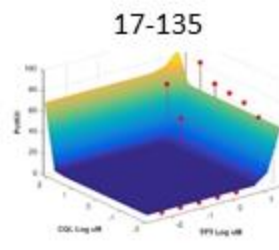
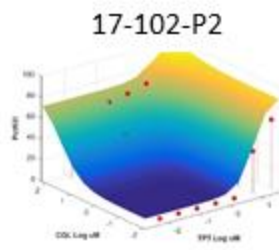
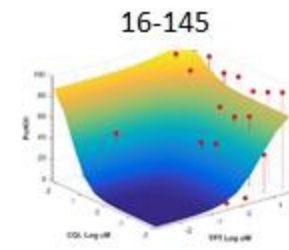
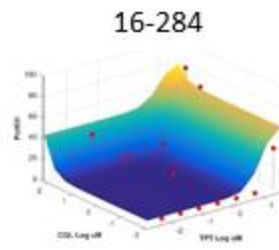
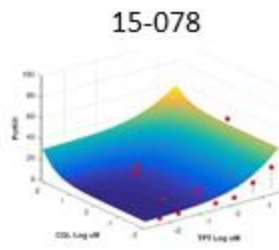
Viability, 72 h

TPT+QCL

B-ALL cell lines



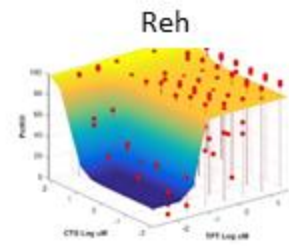
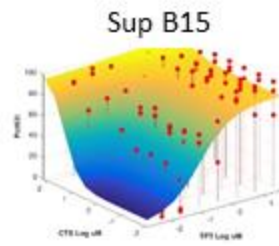
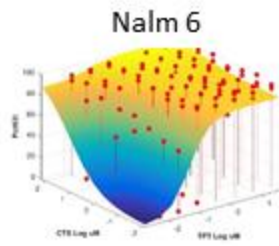
Primary B-ALL samples



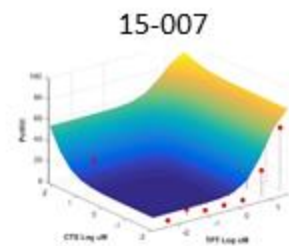
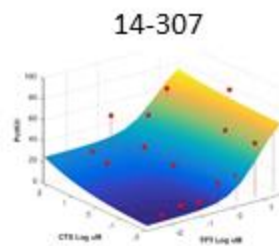
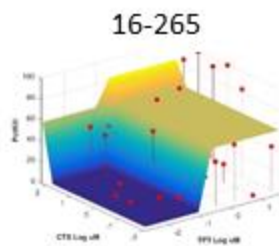
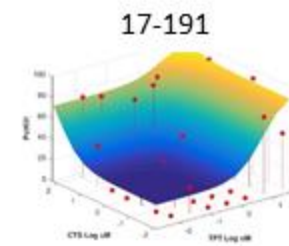
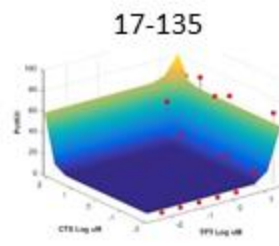
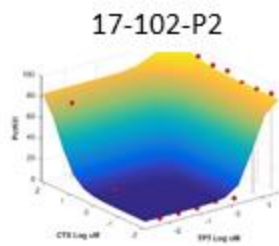
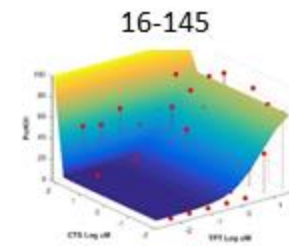
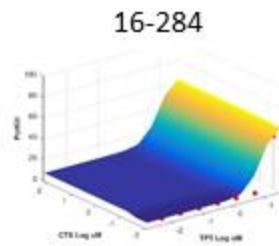
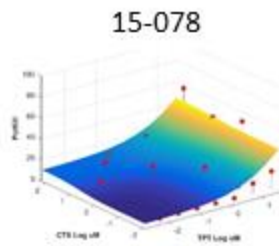
Viability, 72 h

TPT+CTS

B-ALL cell lines



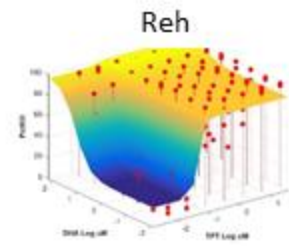
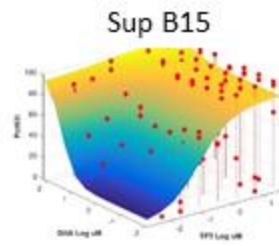
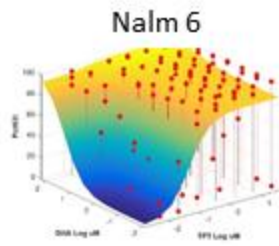
Primary B-ALL samples



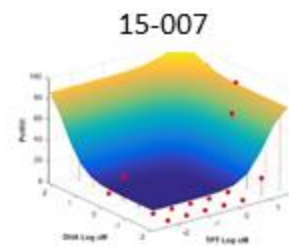
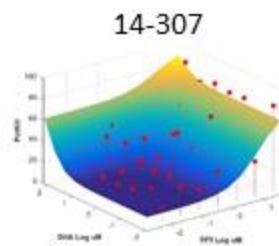
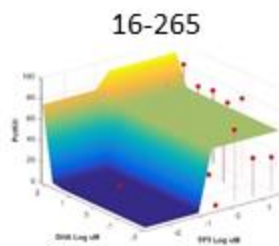
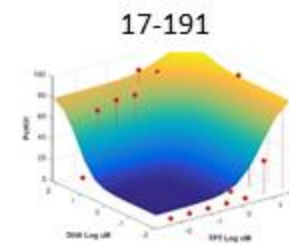
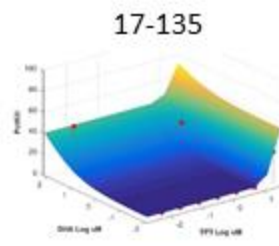
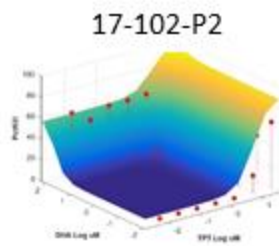
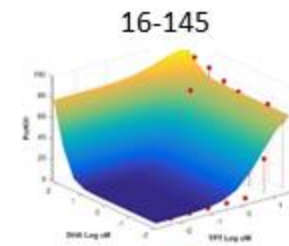
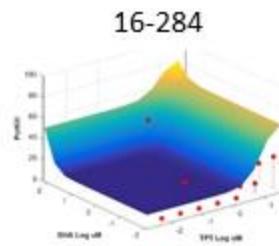
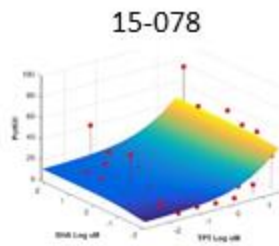
Viability, 72 h

TPT+DHA

B-ALL cell lines



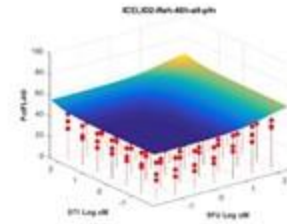
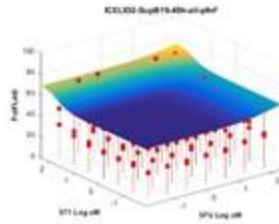
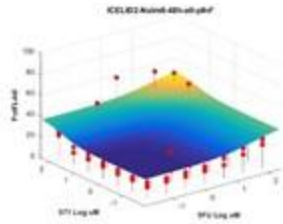
Primary B-ALL samples



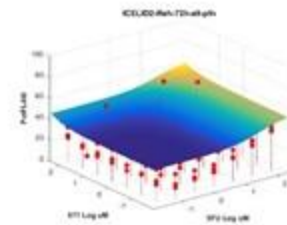
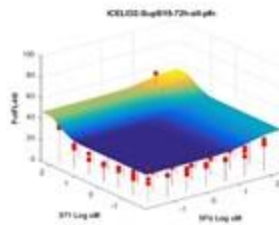
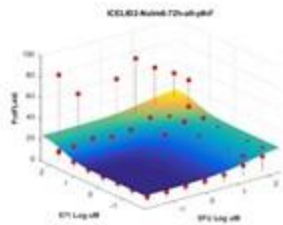
Proliferation, B-ALL cell lines

5FU+571

48 h



72 h



Nalm 6

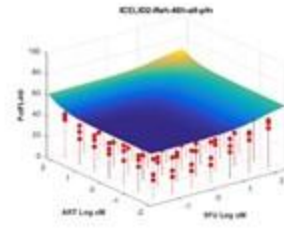
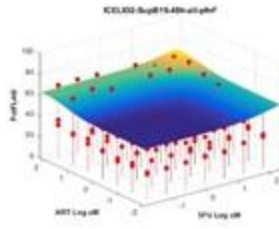
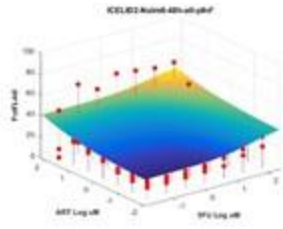
Sup B15

Reh

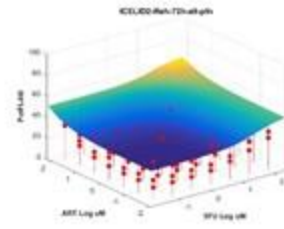
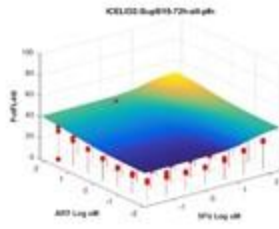
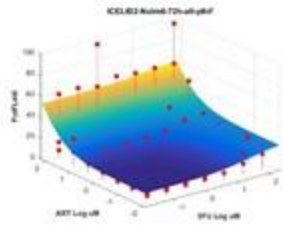
Proliferation, B-ALL cell lines

5FU+ART

48 h



72 h



Nalm 6

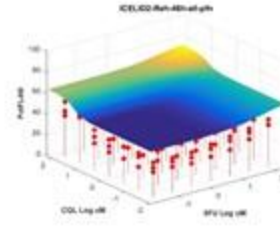
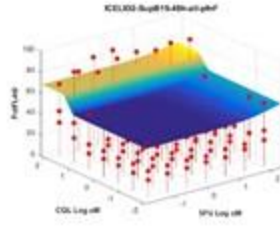
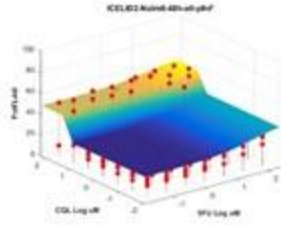
Sup B15

Reh

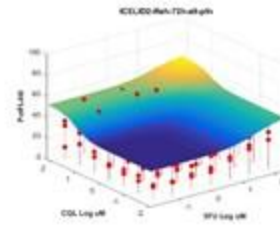
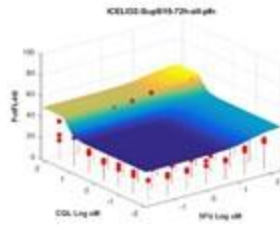
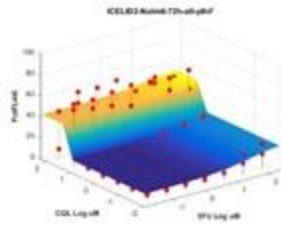
Proliferation, B-ALL cell lines

5FU+CQL

48 h



72 h



Nalm 6

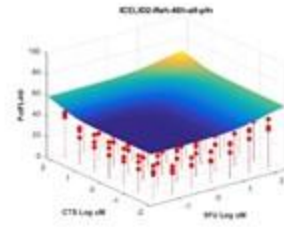
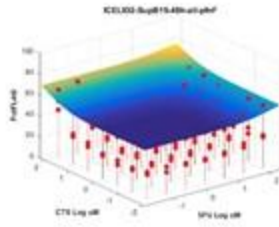
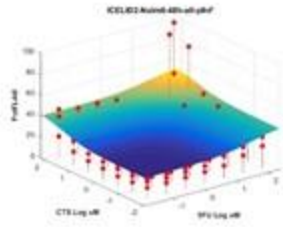
Sup B15

Reh

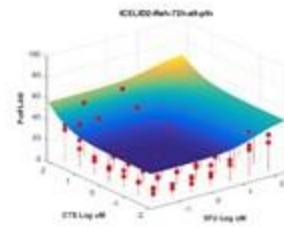
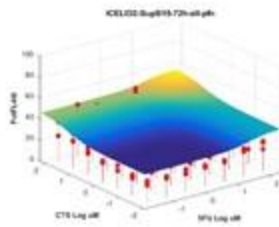
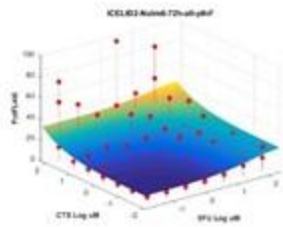
Proliferation, B-ALL cell lines

5FU+CTS

48 h



72 h



Nalm 6

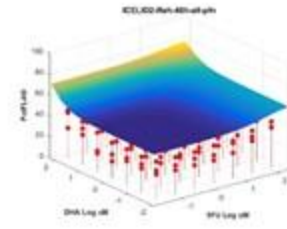
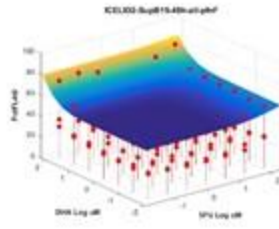
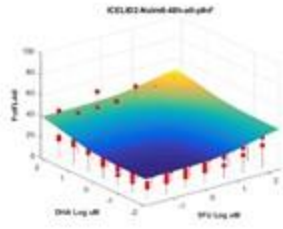
Sup B15

Reh

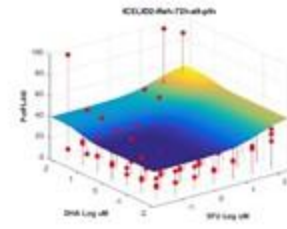
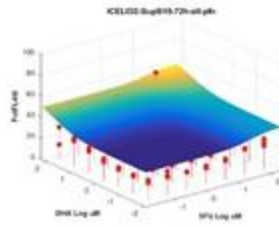
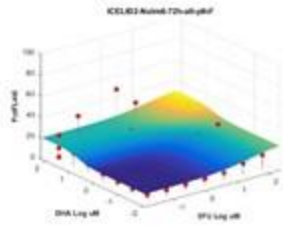
Proliferation, B-ALL cell lines

5FU+DHA

48 h



72 h



Nalm 6

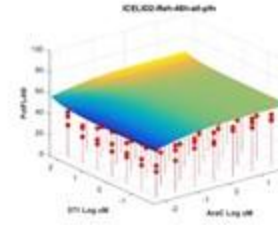
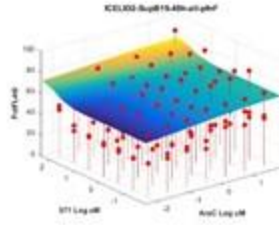
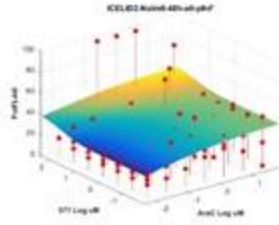
Sup B15

Reh

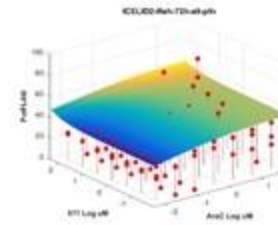
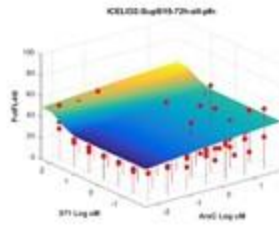
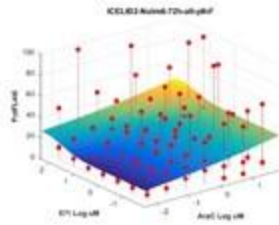
Proliferation, B-ALL cell lines

AraC+571

48 h



72 h



Nalm 6

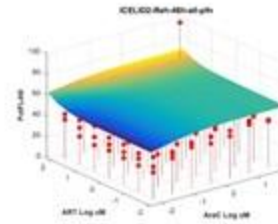
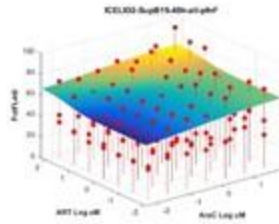
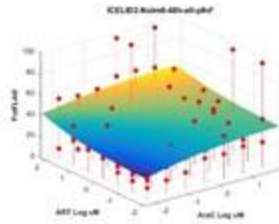
Sup B15

Reh

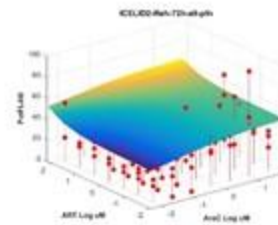
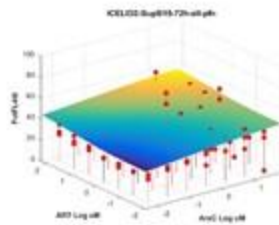
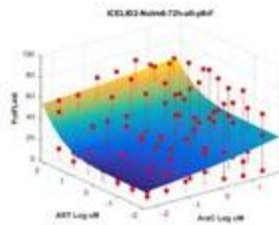
Proliferation, B-ALL cell lines

AraC+ART

48 h



72 h



Nalm 6

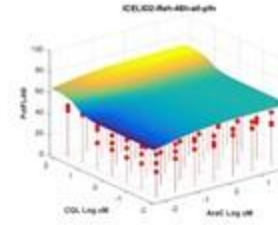
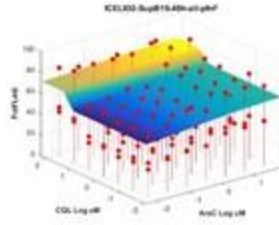
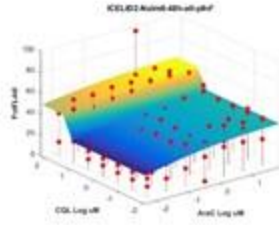
Sup B15

Reh

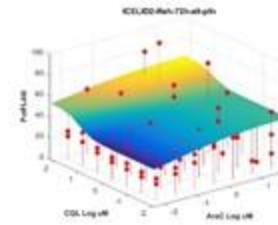
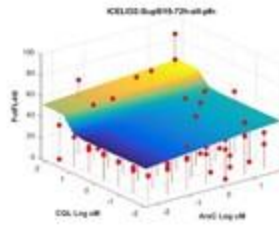
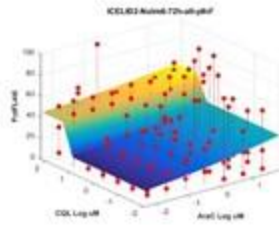
Proliferation, B-ALL cell lines

AraC+CQL

48 h



72 h



Nalm 6

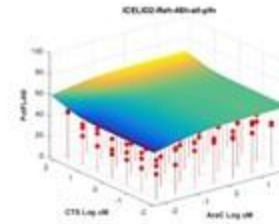
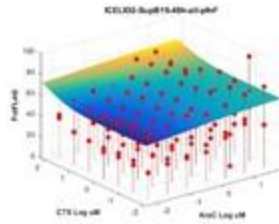
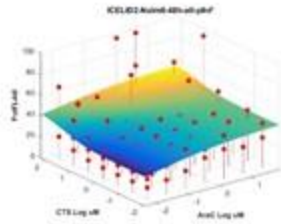
Sup B15

Reh

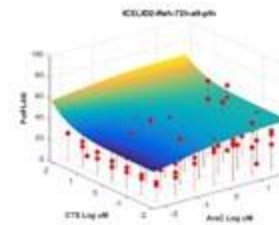
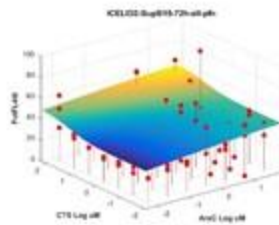
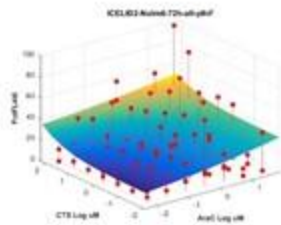
Proliferation, B-ALL cell lines

AraC+CTS

48 h



72 h



Nalm 6

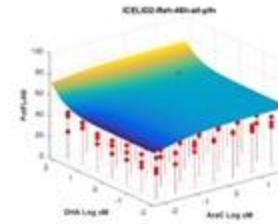
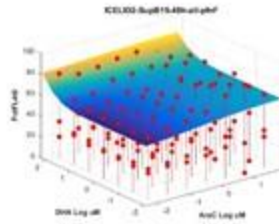
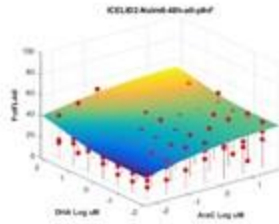
Sup B15

Reh

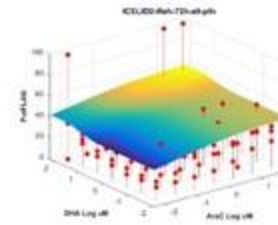
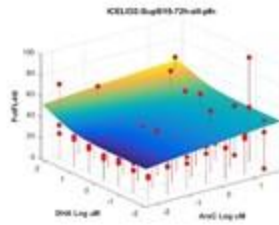
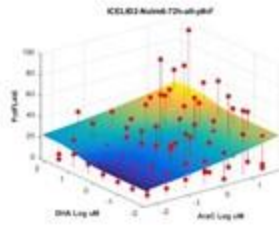
Proliferation, B-ALL cell lines

AraC+DHA

48 h



72 h



Nalm 6

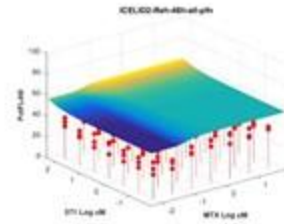
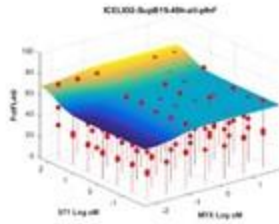
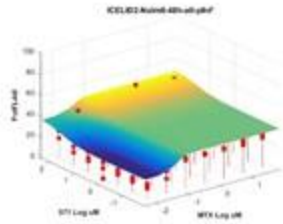
Sup B15

Reh

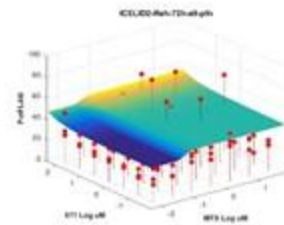
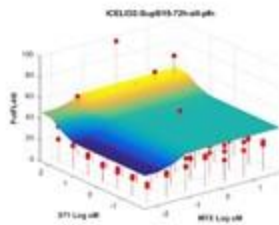
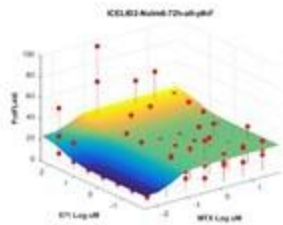
Proliferation, B-ALL cell lines

MTX+571

48 h



72 h



Nalm 6

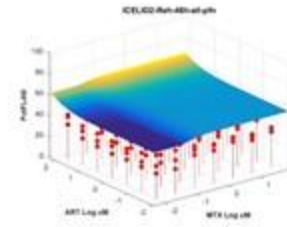
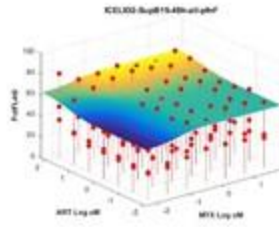
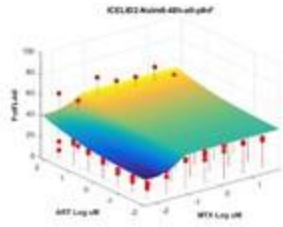
Sup B15

Reh

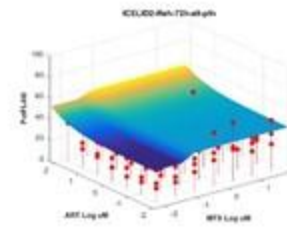
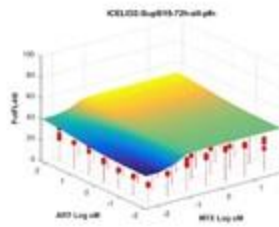
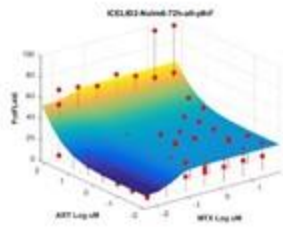
Proliferation, B-ALL cell lines

MTX+ART

48 h



72 h



Nalm 6

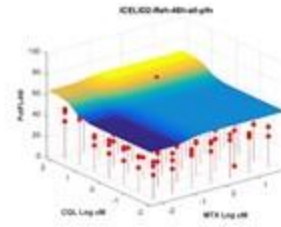
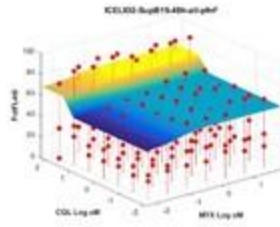
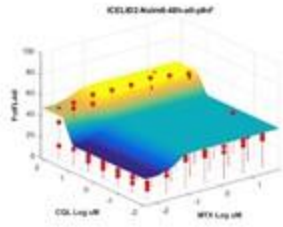
Sup B15

Reh

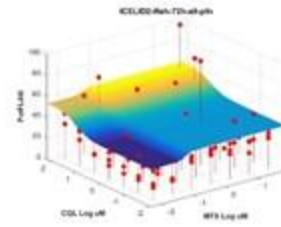
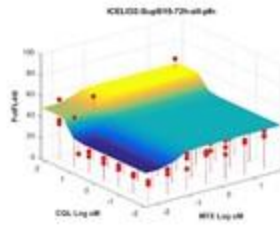
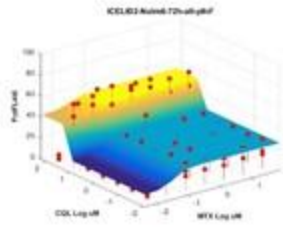
Proliferation, B-ALL cell lines

MTX+CQL

48 h



72 h



Nalm 6

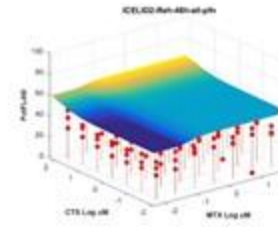
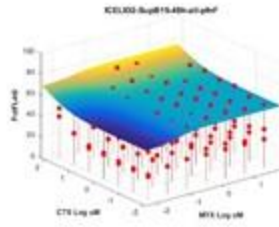
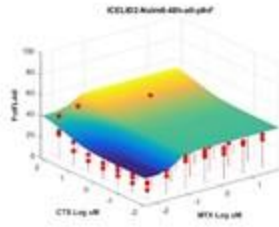
Sup B15

Reh

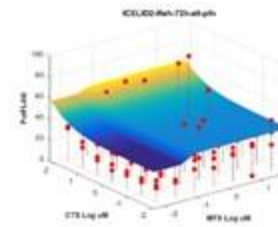
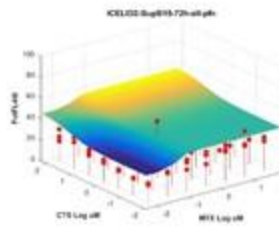
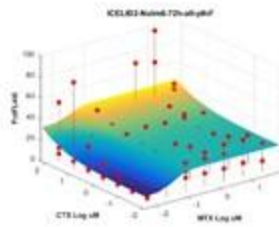
Proliferation, B-ALL cell lines

MTX+CTS

48 h



72 h



Nalm 6

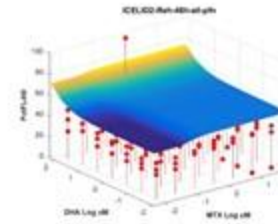
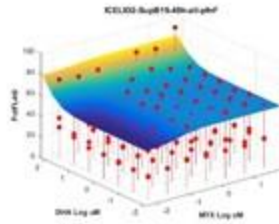
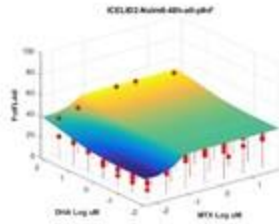
Sup B15

Reh

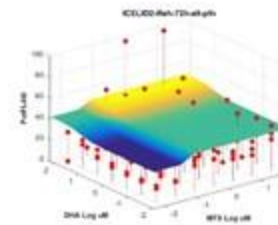
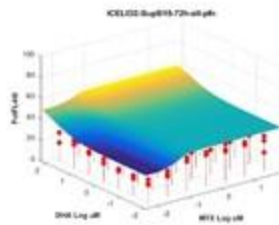
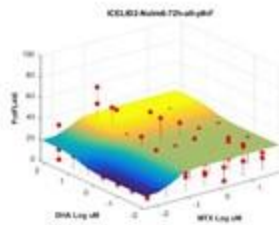
Proliferation, B-ALL cell lines

MTX+DHA

48 h



72 h



Nalm 6

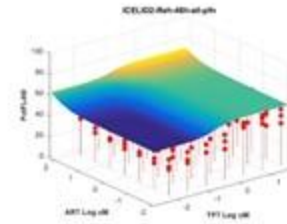
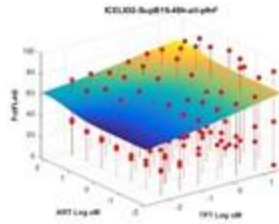
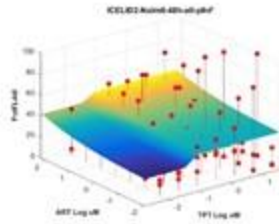
Sup B15

Reh

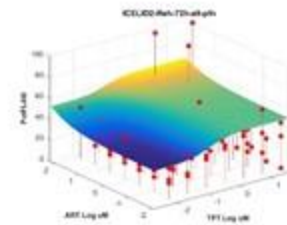
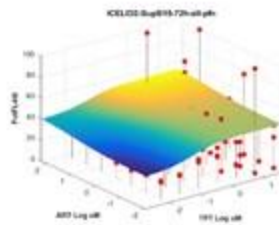
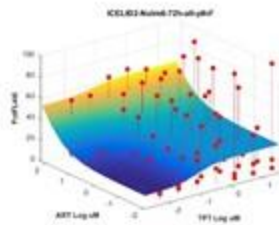
Proliferation, B-ALL cell lines

TPT+ART

48 h



72 h



Nalm 6

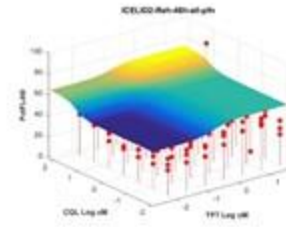
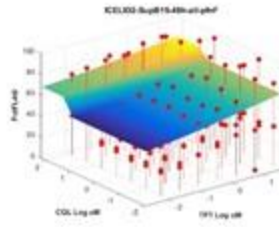
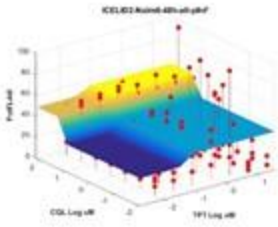
Sup B15

Reh

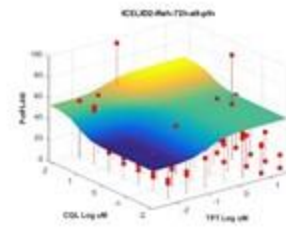
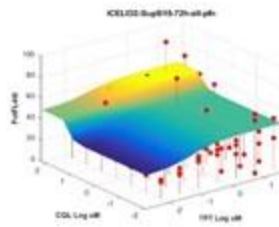
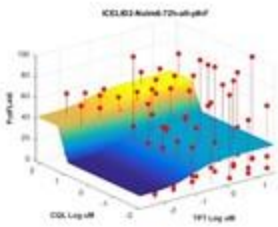
Proliferation, B-ALL cell lines

TPT+CQL

48 h



72 h



Nalm 6

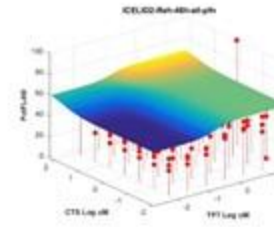
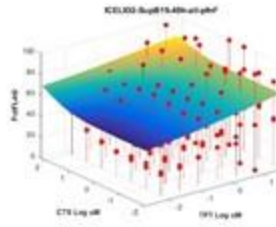
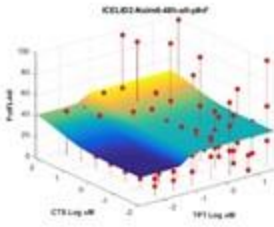
Sup B15

Reh

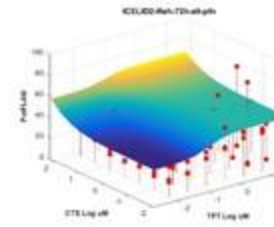
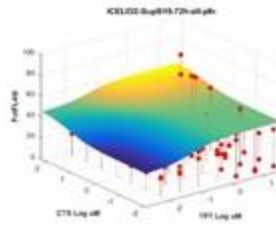
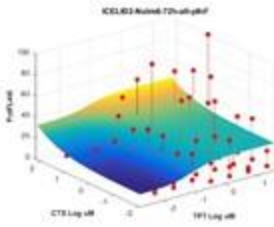
Proliferation, B-ALL cell lines

TPT+CTS

48 h



72 h



Nalm 6

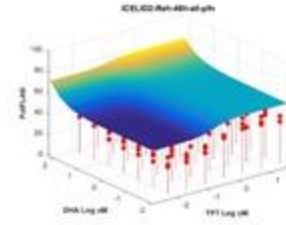
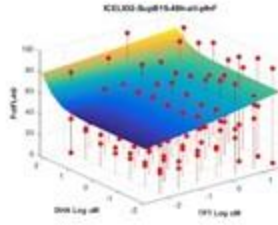
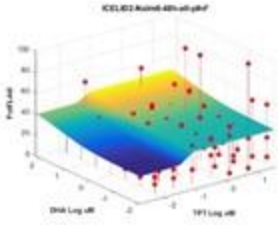
Sup B15

Reh

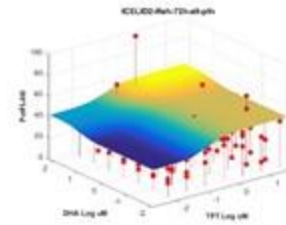
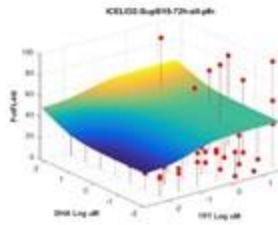
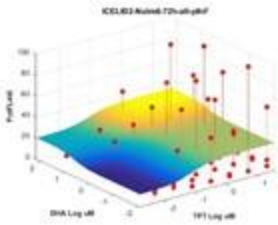
Proliferation, B-ALL cell lines

TPT+DHA

48 h



72 h



Nalm 6

Sup B15

Reh

REFERENCES

1. Borisy, A. A., Elliott, P. J., Hurst, N. W., Lee, M. S., Lehar, J., Price, E. R., *et al.* (2003) Systematic discovery of multicomponent therapeutics. *Proc Natl Acad Sci U S A* **100**, 7977-7982
2. Huseby, S., Gausdal, G., Keen, T. J., Kjaerland, E., Krakstad, C., Myhren, L., *et al.* (2011) Cyclic AMP induces IPC leukemia cell apoptosis via CRE-and CDK-dependent Bim transcription. *Cell Death Dis* **2**, e237
3. Zhang, L., and Insel, P. A. (2004) The pro-apoptotic protein Bim is a convergence point for cAMP/protein kinase A- and glucocorticoid-promoted apoptosis of lymphoid cells. *J Biol Chem* **279**, 20858-20865
4. Follin-Arbelet, V., Torgersen, M. L., Naderi, E. H., Misund, K., Sundan, A., and Blomhoff, H. K. (2013) Death of multiple myeloma cells induced by cAMP-signaling involves downregulation of Mcl-1 via the JAK/STAT pathway. *Cancer Lett* **335**, 323-331
5. Toyoda, Y., Gomi, T., Nakagawa, H., Nagakura, M., and Ishikawa, T. (2016) Diagnosis of Human Axillary Osmidrosis by Genotyping of the Human ABCC11 Gene: Clinical Practice and Basic Scientific Evidence. *Biomed Res Int* **2016**, 7670483
6. Perez, D. R., Smagley, Y., Garcia, M., Carter, M. B., Evangelisti, A., Matlawska-Wasowska, K., *et al.* (2016) Cyclic AMP efflux inhibitors as potential therapeutic agents for leukemia. *Oncotarget* **7**, 33960-33982
7. McGeachie, A. B., Cingolani, L. A., and Goda, Y. (2011) Stabilising influence: integrins in regulation of synaptic plasticity. *Neurosci Res* **70**, 24-29
8. Howlader, N., Noone, A. M., Krapcho, M., Miller, D., Brest, A., Yu, M., *et al.* (2019) SEER Cancer Statistics Review, 1975-2016. National Cancer Institute, Bethesda, MD
9. Toyoda, Y., Sakurai, A., Mitani, Y., Nakashima, M., Yoshiura, K., Nakagawa, H., *et al.* (2009) Earwax, osmidrosis, and breast cancer: why does one SNP (538G>A) in the human ABC transporter ABCC11 gene determine earwax type? *FASEB J* **23**, 2001-2013
10. Myklebust, J. H., Josefsen, D., Blomhoff, H. K., Levy, F. O., Naderi, S., Reed, J. C., *et al.* (1999) Activation of the cAMP signaling pathway increases apoptosis in

human B-precursor cells and is associated with downregulation of Mcl-1 expression. *Journal of Cellular Physiology* **180**, 71-80

11. Edwards, B. S., Ivnitski-Steele, I., Young, S. M., Salas, V. M., and Sklar, L. A. (2007) High-throughput cytotoxicity screening by propidium iodide staining. *Curr Protoc Cytom* **Chapter 9**, Unit9 24
12. Kansal, R. (2016) Acute myeloid leukemia in the era of precision medicine: recent advances in diagnostic classification and risk stratification. *Cancer Biol Med* **13**, 41-54
13. Ladilov, Y., and Appukuttan, A. (2014) Role of soluble adenylyl cyclase in cell death and growth. *Biochim Biophys Acta* **1842**, 2646-2655
14. Fiegl, M. (2016) Epidemiology, pathogenesis, and etiology of acute leukemia. 3-13
15. Gerlo, S., Kooijman, R., Beck, I. M., Kolmus, K., Spooren, A., and Haegeman, G. (2011) Cyclic AMP: a selective modulator of NF-kappaB action. *Cell Mol Life Sci* **68**, 3823-3841
16. Guzman, M. L., and Allan, J. N. (2014) Concise review: Leukemia stem cells in personalized medicine. *Stem Cells* **32**, 844-851
17. Perry, A. M., and Attar, E. C. (2014) New insights in AML biology from genomic analysis. *Semin Hematol* **51**, 282-297
18. (2019) Cancer Facts & Figures 2019. (Society, A. C., ed), American Cancer Society, Atlanta
19. Hunger, S. P., and Mullighan, C. G. (2015) Acute Lymphoblastic Leukemia in Children. *N Engl J Med* **373**, 1541-1552
20. (2013) Genomic and Epigenomic Landscapes of Adult De Novo Acute Myeloid Leukemia. *New England Journal of Medicine* **368**, 2059-2074
21. Ma, X., Edmonson, M., Yergeau, D., Muzny, D. M., Hampton, O. A., Rusch, M., *et al.* (2015) Rise and fall of subclones from diagnosis to relapse in pediatric B-acute lymphoblastic leukaemia. *Nat Commun* **6**, 6604
22. Kelly, L. M., and Gilliland, D. G. (2002) Genetics of myeloid leukemias. *Annual Review of Genomics and Human Genetics* **3**, 179-198

23. Padró, T., Bieker, R., Ruiz, S., Steins, M., Retzlaff, S., Bürger, H., *et al.* (2002) Overexpression of vascular endothelial growth factor (VEGF) and its cellular receptor KDR (VEGFR-2) in the bone marrow of patients with acute myeloid leukemia. *Leukemia* **16**, 1302-1310
24. Passaro, D., Di Tullio, A., Abarrategi, A., Rouault-Pierre, K., Foster, K., Ariza-McNaughton, L., *et al.* (2017) Increased Vascular Permeability in the Bone Marrow Microenvironment Contributes to Disease Progression and Drug Response in Acute Myeloid Leukemia. *Cancer Cell* **32**, 324-341 e326
25. Tripathi, P., Tripathi, P., Kashyap, L., and Singh, V. (2007) The role of nitric oxide in inflammatory reactions. *Pathogens and Disease* **51**, 443-452
26. Emadi, A., and Karp, J. E. (2012) The clinically relevant pharmacogenomic changes in acute myelogenous leukemia. *Pharmacogenomics* **13**, 1257-1269
27. Walter, R. B., Othus, M., Burnett, A. K., Löwenberg, B., Kantarjian, H. M., Ossenkoppele, G. J., *et al.* (2014) Resistance prediction in AML: analysis of 4601 patients from MRC/NCRI, HOVON/SAKK, SWOG and MD Anderson Cancer Center. *Leukemia* **29**, 312
28. De Kouchkovsky, I., and Abdul-Hay, M. (2016) 'Acute myeloid leukemia: a comprehensive review and 2016 update'. *Blood Cancer J* **6**, e441
29. Vora, A., Goulden, N., Wade, R., Mitchell, C., Hancock, J., Hough, R., *et al.* (2013) Treatment reduction for children and young adults with low-risk acute lymphoblastic leukaemia defined by minimal residual disease (UKALL 2003): a randomised controlled trial. *The Lancet Oncology* **14**, 199-209
30. Goto, H. (2015) Childhood relapsed acute lymphoblastic leukemia: Biology and recent treatment progress. *Pediatr Int* **57**, 1059-1066
31. Grimwade, D., Knapper, S., and Mrózek, K. (2016) Acute Myeloid Leukemia. 527-559
32. Moorman, A. V., Ensor, H. M., Richards, S. M., Chilton, L., Schwab, C., Kinsey, S. E., *et al.* (2010) Prognostic effect of chromosomal abnormalities in childhood B-cell precursor acute lymphoblastic leukaemia: results from the UK Medical Research Council ALL97/99 randomised trial. *The Lancet Oncology* **11**, 429-438
33. Printz, C. (2010) Adult survivors of childhood and adolescent cancer have more heart disease. *Cancer* **116**, 2507-2507

34. Kadan-Lottick, N. S., Dinu, I., Wasilewski-Masker, K., Kaste, S., Meacham, L. R., Mahajan, A., *et al.* (2008) Osteonecrosis in Adult Survivors of Childhood Cancer: A Report From the Childhood Cancer Survivor Study. *Journal of Clinical Oncology* **26**, 3038-3045
35. Te Winkel, M. L., Pieters, R., Wind, E. J., Bessems, J. H., and van den Heuvel-Eibrink, M. M. (2014) Management and treatment of osteonecrosis in children and adolescents with acute lymphoblastic leukemia. *Haematologica* **99**, 430-436
36. Krull, K. R., Brinkman, T. M., Li, C., Armstrong, G. T., Ness, K. K., Srivastava, D. K., *et al.* (2013) Neurocognitive outcomes decades after treatment for childhood acute lymphoblastic leukemia: a report from the St Jude lifetime cohort study. *J Clin Oncol* **31**, 4407-4415
37. Duffner, P. K., Armstrong, F. D., Chen, L., Helton, K. J., Brecher, M. L., Bell, B., *et al.* (2014) Neurocognitive and neuroradiologic central nervous system late effects in children treated on Pediatric Oncology Group (POG) P9605 (standard risk) and P9201 (lesser risk) acute lymphoblastic leukemia protocols (ACCL0131): a methotrexate consequence? A report from the Children's Oncology Group. *J Pediatr Hematol Oncol* **36**, 8-15
38. Rall, T. W., and Sutherland, E. W. (1958) Formation of a cyclic adenine ribonucleotide by tissue particles. *J Biol Chem* **232**, 1065-1076
39. Insel, P. A., Zhang, L., Murray, F., Yokouchi, H., and Zambon, A. C. (2012) Cyclic AMP is both a pro-apoptotic and anti-apoptotic second messenger. *Acta Physiol (Oxf)* **204**, 277-287
40. Cho, E. C., Mitton, B., and Sakamoto, K. M. (2011) CREB and leukemogenesis. *Crit Rev Oncog* **16**, 37-46
41. Tresguerres, M., Levin, L. R., and Buck, J. (2011) Intracellular cAMP signaling by soluble adenylyl cyclase. *Kidney Int* **79**, 1277-1288
42. Acin-Perez, R., Salazar, E., Kamenetsky, M., Buck, J., Levin, L. R., and Manfredi, G. (2009) Cyclic AMP produced inside mitochondria regulates oxidative phosphorylation. *Cell Metab* **9**, 265-276
43. Zippin, J. H., Farrell, J., Huron, D., Kamenetsky, M., Hess, K. C., Fischman, D. A., *et al.* (2004) Bicarbonate-responsive "soluble" adenylyl cyclase defines a nuclear cAMP microdomain. *J Cell Biol* **164**, 527-534

44. Steegborn, C. (2014) Structure, mechanism, and regulation of soluble adenylyl cyclases - similarities and differences to transmembrane adenylyl cyclases. *Biochim Biophys Acta* **1842**, 2535-2547
45. Kumar, S., Kostin, S., Flacke, J. P., Reusch, H. P., and Ladilov, Y. (2009) Soluble adenylyl cyclase controls mitochondria-dependent apoptosis in coronary endothelial cells. *J Biol Chem* **284**, 14760-14768
46. Appukuttan, A., Kasseckert, S. A., Kumar, S., Reusch, H. P., and Ladilov, Y. (2013) Oxysterol-induced apoptosis of smooth muscle cells is under the control of a soluble adenylyl cyclase. *Cardiovasc Res* **99**, 734-742
47. Fajardo, A. M., Piazza, G. A., and Tinsley, H. N. (2014) The role of cyclic nucleotide signaling pathways in cancer: targets for prevention and treatment. *Cancers (Basel)* **6**, 436-458
48. Davoren, P. R., and Sutherland, E. W. (1963) The Effect of L-Epinephrine and Other Agents on the Synthesis and Release of Adenosine 3',5'-Phosphate by Whole Pigeon Erythrocytes. *J Biol Chem* **238**, 3009-3015
49. Carnegie, G. K., Means, C. K., and Scott, J. D. (2009) A-kinase anchoring proteins: from protein complexes to physiology and disease. *IUBMB Life* **61**, 394-406
50. Lefkimmatis, K., and Zaccolo, M. (2014) cAMP signaling in subcellular compartments. *Pharmacol Ther* **143**, 295-304
51. Desman, G., Waintraub, C., and Zippin, J. H. (2014) Investigation of cAMP microdomains as a path to novel cancer diagnostics. *Biochim Biophys Acta* **1842**, 2636-2645
52. Arora, K., Sinha, C., Zhang, W., Ren, A., Moon, C. S., Yarlagadda, S., *et al.* (2013) Compartmentalization of cyclic nucleotide signaling: a question of when, where, and why? *Pflugers Arch* **465**, 1397-1407
53. Murray, F., and Insel, P. A. (2013) Targeting cAMP in chronic lymphocytic leukemia: a pathway-dependent approach for the treatment of leukemia and lymphoma. *Expert Opin Ther Targets* **17**, 937-949
54. Sapio, L., Di Maiolo, F., Illiano, M., Esposito, A., Chiosi, E., Spina, A., *et al.* (2014) Targeting protein kinase A in cancer therapy: an update. *EXCLI J* **13**, 843-855
55. Lerner, A., Kim, D. H., and Lee, R. (2000) The cAMP signaling pathway as a therapeutic target in lymphoid malignancies. *Leukemia Lymphoma* **37**, 39-+

56. Meyers, J. A., Su, D. W., and Lerner, A. (2009) Chronic lymphocytic leukemia and B and T cells differ in their response to cyclic nucleotide phosphodiesterase inhibitors. *J Immunol* **182**, 5400-5411
57. Li, C., Xie, J., Lu, Z., Chen, C., Yin, Y., Zhan, R., *et al.* (2015) ADCY7 supports development of acute myeloid leukemia. *Biochem Biophys Res Commun* **465**, 47-52
58. Hait, W. N., and Weiss, B. (1976) Increased cyclic nucleotide phosphodiesterase activity in leukaemic lymphocytes. *Nature* **259**, 321-323
59. Baus, E., Van Laethem, F., Andris, F., Rolin, S., Urbain, J., and Leo, O. (2001) Dexamethasone increases intracellular cyclic AMP concentration in murine T lymphocyte cell lines. *Steroids* **66**, 39-47
60. Cheng, J. C., Kinjo, K., Judelson, D. R., Chang, J., Wu, W. S., Schmid, I., *et al.* (2008) CREB is a critical regulator of normal hematopoiesis and leukemogenesis. *Blood* **111**, 1182-1192
61. Shankar, D. B., Cheng, J. C., and Sakamoto, K. M. (2005) Role of cyclic AMP response element binding protein in human leukemias. *Cancer* **104**, 1819-1824
62. van der Sligte, N. E., Kampen, K. R., ter Elst, A., Scherpen, F. J., Meeuwse-de Boer, T. G., Guryev, V., *et al.* (2015) Essential role for cyclic-AMP responsive element binding protein 1 (CREB) in the survival of acute lymphoblastic leukemia. *Oncotarget* **6**, 14970-14981
63. Crans-Vargas, H. N., Landaw, E. M., Bhatia, S., Sandusky, G., Moore, T. B., and Sakamoto, K. M. (2002) Expression of cyclic adenosine monophosphate response-element binding protein in acute leukemia. *Blood* **99**, 2617-2619
64. Petrov, I., Suntsova, M., Mutorova, O., Sorokin, M., Garazha, A., Ilnitskaya, E., *et al.* (2016) Molecular pathway activation features of pediatric acute myeloid leukemia (AML) and acute lymphoblast leukemia (ALL) cells. *Aging-Us* **8**, 2936-2947
65. Mitton, B., Chae, H. D., Hsu, K., Dutta, R., Aldana-Masangkay, G., Ferrari, R., *et al.* (2016) Small molecule inhibition of cAMP response element binding protein in human acute myeloid leukemia cells. *Leukemia* **30**, 2302-2311
66. Pigazzi, M., Manara, E., Baron, E., and Basso, G. (2008) ICER expression inhibits leukemia phenotype and controls tumor progression. *Leukemia* **22**, 2217-2225

67. Mullighan, C. G. (2011) Genomic profiling of B-progenitor acute lymphoblastic leukemia. *Best Pract Res Clin Haematol* **24**, 489-503
68. Ding, L. W., Sun, Q. Y., Tan, K. T., Chien, W., Mayakonda, A., Yeoh, A. E. J., *et al.* (2017) Mutational Landscape of Pediatric Acute Lymphoblastic Leukemia. *Cancer Res* **77**, 390-400
69. Propper, D. J., Saunders, M. P., Salisbury, A. J., Long, L., O'Byrne, K. J., Braybrooke, J. P., *et al.* (1999) Phase I study of the novel cyclic AMP (cAMP) analogue 8-chloro-cAMP in patients with cancer: toxicity, hormonal, and immunological effects. *Clin Cancer Res* **5**, 1682-1689
70. Saunders, M. P., Salisbury, A. J., O'Byrne, K. J., Long, L., Whitehouse, R. M., Talbot, D. C., *et al.* (1997) A novel cyclic adenosine monophosphate analog induces hypercalcemia via production of 1,25-dihydroxyvitamin D in patients with solid tumors. *J Clin Endocrinol Metab* **82**, 4044-4048
71. Schwede, F., Maronde, E., Genieser, H. G., and Jastorff, B. (2000) Cyclic nucleotide analogs as biochemical tools and prospective drugs. *Pharmacol Therapeut* **87**, 199-226
72. Wiernik, P. H., Paietta, E., Goloubeva, O., Lee, S. J., Makower, D., Bennett, J. M., *et al.* (2004) Phase II study of theophylline in chronic lymphocytic leukemia: a study of the Eastern Cooperative Oncology Group (E4998). *Leukemia* **18**, 1605-1610
73. Coffino, P., Bourne, H. R., and Tomkins, G. M. (1975) Mechanism of lymphoma cell death induced by cyclic AMP. *Am J Pathol* **81**, 199-204
74. Lomo, J., Blomhoff, H. K., Beiske, K., Stokke, T., and Smeland, E. B. (1995) TGF-beta 1 and cyclic AMP promote apoptosis in resting human B lymphocytes. *J Immunol* **154**, 1634-1643
75. Cheng, Y. M., Zhu, Q., Yao, Y. Y., Tang, Y., Wang, M. M., and Zou, L. F. (2012) 8-Chloroadenosine 3',5'-monophosphate induces cell cycle arrest and apoptosis in multiple myeloma cells through multiple mechanisms. *Oncol Lett* **4**, 1384-1388
76. Krett, N. L., Zell, J. L., Halgren, R. G., Pillay, S., Traynor, A. E., and Rosen, S. T. (1997) Cyclic adenosine-3',5'-monophosphate-mediated cytotoxicity in steroid sensitive and resistant myeloma. *Clin Cancer Res* **3**, 1781-1787

77. Zambon, A. C., Wilderman, A., Ho, A., and Insel, P. A. (2011) Increased expression of the pro-apoptotic protein BIM, a mechanism for cAMP/protein kinase A (PKA)-induced apoptosis of immature T cells. *J Biol Chem* **286**, 33260-33267
78. Yin, Y., Allen, P. D., Jia, L., MacEy, M. G., Kelsey, S. M., and Newland, A. C. (2000) Constitutive levels of cAMP-dependent protein kinase activity determine sensitivity of human multidrug-resistant leukaemic cell lines to growth inhibition and apoptosis by forskolin and tumour necrosis factor alpha. *Br J Haematol* **108**, 565-573
79. Naderi, S., and Blomhoff, H. K. (2008) Activation of cAMP signaling enhances Fas-mediated apoptosis and activation-induced cell death through potentiation of caspase 8 activation. *Hum Immunol* **69**, 833-836
80. Shayo, C., Legnazzi, B. L., Monczor, F., Fernández, N., Riveiro, M. a. E., Baldi, A., *et al.* (2004) The time-course of cyclic AMP signaling is critical for leukemia U-937 cell differentiation. *Biochemical and Biophysical Research Communications* **314**, 798-804
81. Yan, L., Herrmann, V., Hofer, J. K., and Insel, P. A. (2000) beta-adrenergic receptor/cAMP-mediated signaling and apoptosis of S49 lymphoma cells. *Am J Physiol Cell Physiol* **279**, C1665-1674
82. Zhang, L., Murray, F., Zahno, A., Kanter, J. R., Chou, D., Suda, R., *et al.* (2008) Cyclic nucleotide phosphodiesterase profiling reveals increased expression of phosphodiesterase 7B in chronic lymphocytic leukemia. *Proc Natl Acad Sci U S A* **105**, 19532-19537
83. Garcia-Bermejo, L., Perez, C., Vilaboa, N. E., de Blas, E., and Aller, P. (1998) cAMP increasing agents attenuate the generation of apoptosis by etoposide in promonocytic leukemia cells. *J Cell Sci* **111 (Pt 5)**, 637-644
84. Gausdal, G., Wergeland, A., Skavland, J., Nguyen, E., Pendino, F., Rouhee, N., *et al.* (2013) Cyclic AMP can promote APL progression and protect myeloid leukemia cells against anthracycline-induced apoptosis. *Cell Death Dis* **4**, e516
85. Kloster, M. M., Naderi, E. H., Carlsen, H., Blomhoff, H. K., and Naderi, S. (2011) Hyperactivation of NF-kappaB via the MEK signaling is indispensable for the inhibitory effect of cAMP on DNA damage-induced cell death. *Mol Cancer* **10**, 45
86. Naderi, E. H., Jochemsen, A. G., Blomhoff, H. K., and Naderi, S. (2011) Activation of cAMP Signaling Interferes with Stress-Induced p53 Accumulation in ALL-

Derived Cells by Promoting the Interaction between p53 and HDM2. *Neoplasia* **13**, 653-IN614

87. Shabestari, R. M., Safa, M., Banan, M., and Kazemi, A. (2016) Cyclic AMP-Induced p53 Destabilization is Independent of CREB in Pre-B Acute Lymphoblastic Leukemia Cells. *Int J Mol Cell Med* **5**, 220-228
88. Xiao, L. Y., and Kan, W. M. (2017) Cyclic AMP (cAMP) confers drug resistance against DNA damaging agents via PKAIA in CML cells. *Eur J Pharmacol* **794**, 201-208
89. Lee, K., Belinsky, M. G., Bell, D. W., Testa, J. R., and Kruh, G. D. (1998) Isolation of MOAT-B, a Widely Expressed Multidrug Resistance-associated Protein/Canalicular Multispecific Organic Anion Transporter-related Transporter. *Cancer Research* **58**, 2741-2747
90. Morrissey, K. M., Wen, C. C., Johns, S. J., Zhang, L., Huang, S. M., and Giacomini, K. M. (2012) The UCSF-FDA TransPortal: a public drug transporter database. *Clin Pharmacol Ther* **92**, 545-546
91. Kock, K., Grube, M., Jedlitschky, G., Oevermann, L., Siegmund, W., Ritter, C. A., *et al.* (2007) Expression of adenosine triphosphate-binding cassette (ABC) drug transporters in peripheral blood cells: relevance for physiology and pharmacotherapy. *Clin Pharmacokinet* **46**, 449-470
92. Lai, L., and Tan, T. M. (2002) Role of glutathione in the multidrug resistance protein 4 (MRP4/ABCC4)-mediated efflux of cAMP and resistance to purine analogues. *Biochem J* **361**, 497-503
93. Xie, M., Rich, T. C., Scheitrum, C., Conti, M., and Richter, W. (2011) Inactivation of multidrug resistance proteins disrupts both cellular extrusion and intracellular degradation of cAMP. *Mol Pharmacol* **80**, 281-293
94. Pavan, B., Capuzzo, A., and Forlani, G. (2015) Quercetin and quercetin-3-O-glucoside interact with different components of the cAMP signaling cascade in human retinal pigment epithelial cells. *Life Sci* **121**, 166-173
95. Kim, H. P., Bernard, L., Berkowitz, J., Nitta, J., and Hogge, D. E. (2012) Flow cytometry-based assessment of mitoxantrone efflux from leukemic blasts varies with response to induction chemotherapy in acute myeloid leukemia. *Cytometry B Clin Cytom* **82**, 283-294
96. Oevermann, L., Scheitz, J., Starke, K., Kock, K., Kiefer, T., Dolken, G., *et al.* (2009) Hematopoietic stem cell differentiation affects expression and function of

MRP4 (ABCC4), a transport protein for signaling molecules and drugs. *Int J Cancer* **124**, 2303-2311

97. Copsel, S., Garcia, C., Diez, F., Vermeulen, M., Baldi, A., Bianciotti, L. G., *et al.* (2011) Multidrug resistance protein 4 (MRP4/ABCC4) regulates cAMP cellular levels and controls human leukemia cell proliferation and differentiation. *J Biol Chem* **286**, 6979-6988
98. Copsel, S., Bruzzone, A., May, M., Beyrath, J., Wargon, V., Cany, J., *et al.* (2014) Multidrug resistance protein 4/ATP binding cassette transporter 4: a new potential therapeutic target for acute myeloid leukemia. *Oncotarget* **5**, 9308-9321
99. Wang, W., Li, Y., Zhu, J. Y., Fang, D. D., Ding, H. F., Dong, Z., *et al.* (2016) Triple negative breast cancer development can be selectively suppressed by sustaining an elevated level of cellular cyclic AMP through simultaneously blocking its efflux and decomposition. *Oncotarget* **7**, 87232-87245
100. Perez, D., Simons, P. C., Smagley, Y., Sklar, L. A., and Chigaev, A. (2016) A High-Throughput Flow Cytometry Assay for Identification of Inhibitors of 3',5'-Cyclic Adenosine Monophosphate Efflux. In *High Throughput Screening: Methods and Protocols* (Janzen, W. P., ed) pp. 227-244, Springer New York, New York, NY
101. Chigaev, A., Perez, D. R., and Sklar, L. A. (2016) Method for Cancer Cell Reprogramming. STC.UNM, US
102. Guo, Y., Kock, K., Ritter, C. A., Chen, Z. S., Grube, M., Jedlitschky, G., *et al.* (2009) Expression of ABCC-type nucleotide exporters in blasts of adult acute myeloid leukemia: relation to long-term survival. *Clin Cancer Res* **15**, 1762-1769
103. Fukuda, Y., and Schuetz, J. D. (2012) ABC transporters and their role in nucleoside and nucleotide drug resistance. *Biochem Pharmacol* **83**, 1073-1083
104. Cherny, R. A., Atwood, C. S., Xilinas, M. E., Gray, D. N., Jones, W. D., McLean, C. A., *et al.* (2001) Treatment with a Copper-Zinc Chelator Markedly and Rapidly Inhibits β -Amyloid Accumulation in Alzheimer's Disease Transgenic Mice. *Neuron* **30**, 665-676
105. Fletcher, J. I., Haber, M., Henderson, M. J., and Norris, M. D. (2010) ABC transporters in cancer: more than just drug efflux pumps. *Nat Rev Cancer* **10**, 147-156

106. Zinzi, L., Contino, M., Cantore, M., Capparelli, E., Leopoldo, M., and Colabufo, N. A. (2014) ABC transporters in CSCs membranes as a novel target for treating tumor relapse. *Front Pharmacol* **5**, 163
107. Aronsen, L., Orvoll, E., Lysaa, R., Ravna, A. W., and Sager, G. (2014) Modulation of high affinity ATP-dependent cyclic nucleotide transporters by specific and non-specific cyclic nucleotide phosphodiesterase inhibitors. *Eur J Pharmacol* **745**, 249-253
108. Wu, C. P., Calcagno, A. M., and Ambudkar, S. V. (2008) Reversal of ABC drug transporter-mediated multidrug resistance in cancer cells: evaluation of current strategies. *Curr Mol Pharmacol* **1**, 93-105
109. Shiozawa, K., Oka, M., Soda, H., Yoshikawa, M., Ikegami, Y., Tsurutani, J., *et al.* (2004) Reversal of breast cancer resistance protein (BCRP/ABCG2)-mediated drug resistance by novobiocin, a coumermycin antibiotic. *Int J Cancer* **108**, 146-151
110. Jekerle, V., Klinkhammer, W., Scollard, D. A., Breitbach, K., Reilly, R. M., Piquette-Miller, M., *et al.* (2006) In vitro and in vivo evaluation of WK-X-34, a novel inhibitor of P-glycoprotein and BCRP, using radio imaging techniques. *International Journal of Cancer* **119**, 414-422
111. Ozben, T. (2006) Mechanisms and strategies to overcome multiple drug resistance in cancer. *FEBS Lett* **580**, 2903-2909
112. Zarrin, A., Mehdipour, A. R., and Miri, R. (2010) Dihydropyridines and multidrug resistance: previous attempts, present state, and future trends. *Chem Biol Drug Des* **76**, 369-381
113. Nigam, S. K. (2015) What do drug transporters really do? *Nat Rev Drug Discov* **14**, 29-44
114. Dou, A. X., and Wang, X. (2010) Cyclic adenosine monophosphate signal pathway in targeted therapy of lymphoma. *Chin Med J (Engl)* **123**, 95-99
115. Zhang, J. H., Chung, T. D. Y., and Oldenburg, K. R. (1999) A simple statistical parameter for use in evaluation and validation of high throughput screening assays. *Journal of Biomolecular Screening* **4**, 67-73
116. Hanahan, D., and Weinberg, Robert A. (2011) Hallmarks of Cancer: The Next Generation. *Cell* **144**, 646-674

117. Conti, M., Mika, D., and Richter, W. (2014) Cyclic AMP compartments and signaling specificity: role of cyclic nucleotide phosphodiesterases. *J Gen Physiol* **143**, 29-38
118. Gjertsen, B. T., Cressey, L. I., Ruchaud, S., Houge, G., Lanotte, M., and Doskeland, S. O. (1994) Multiple Apoptotic Death Types Triggered through Activation of Separate Pathways by Camp and Inhibitors of Protein Phosphatases in One (Ipc Leukemia) Cell-Line. *Journal of Cell Science* **107**, 3363-3377
119. Conley, J. M., Brand, C. S., Bogard, A. S., Pratt, E. P., Xu, R., Hockerman, G. H., *et al.* (2013) Development of a high-throughput screening paradigm for the discovery of small-molecule modulators of adenylyl cyclase: identification of an adenylyl cyclase 2 inhibitor. *J Pharmacol Exp Ther* **347**, 276-287
120. Lerner, A., and Epstein, P. M. (2006) Cyclic nucleotide phosphodiesterases as targets for treatment of haematological malignancies. *Biochem J* **393**, 21-41
121. Scavennec, J., Carcassonne, Y., Gastaut, J. A., Blanc, A., and Cailla, H. L. (1981) Relationship between the levels of cyclic cytidine 3':5'-monophosphate, cyclic guanosine 3':5'-monophosphate, and cyclic adenosine 3':5'-monophosphate in urines and leukocytes and the type of human leukemias. *Cancer Res* **41**, 3222-3227
122. Peracchi, M., Lombardi, L., Maiolo, A. T., Bamonti-Catena, F., Toschi, V., Chiorboli, O., *et al.* (1983) Plasma and urine cyclic nucleotide levels in patients with acute and chronic leukemia. *Blood* **61**, 429-434
123. Russel, F. G., Koenderink, J. B., and Masereeuw, R. (2008) Multidrug resistance protein 4 (MRP4/ABCC4): a versatile efflux transporter for drugs and signalling molecules. *Trends Pharmacol Sci* **29**, 200-207
124. Perez, D. R., Simons, P. C., Smagley, Y., Sklar, L. A., and Chigaev, A. (2016) A high throughput flow cytometry assay for identification of inhibitors of 3', 5'-cyclic adenosine monophosphate efflux. In *High Throughput Screening: Methods and Protocols* (Janzen, W. P., ed) pp. 227-244, Humana Press
125. Schimmer, A. D., Jitkova, Y., Gronda, M., Wang, Z., Brandwein, J., Chen, C., *et al.* (2012) A phase I study of the metal ionophore clioquinol in patients with advanced hematologic malignancies. *Clin Lymphoma Myeloma Leuk* **12**, 330-336
126. Chen, W., Luo, Y., Liu, L., Zhou, H., Xu, B., Han, X., *et al.* (2010) Cryptotanshinone inhibits cancer cell proliferation by suppressing Mammalian target of

- rapamycin-mediated cyclin D1 expression and Rb phosphorylation. *Cancer Prev Res (Phila)* **3**, 1015-1025
127. Guzman, M. L., Rossi, R. M., Neelakantan, S., Li, X., Corbett, C. A., Hassane, D. C., *et al.* (2007) An orally bioavailable parthenolide analog selectively eradicates acute myelogenous leukemia stem and progenitor cells. *Blood* **110**, 4427-4435
 128. Wu, T. S., Liao, Y. C., Yu, F. Y., Chang, C. H., and Liu, B. H. (2008) Mechanism of patulin-induced apoptosis in human leukemia cells (HL-60). *Toxicol Lett* **183**, 105-111
 129. Chigaev, A., Waller, A., Amit, O., and Sklar, L. A. (2008) G α s-coupled receptor signaling actively down-regulates α 4 β 1-integrin affinity: a possible mechanism for cell de-adhesion. *BMC Immunol* **9**, 26
 130. Chigaev, A., Smagley, Y., and Sklar, L. A. (2011) Nitric oxide/cGMP pathway signaling actively down-regulates α 4 β 1-integrin affinity: an unexpected mechanism for inducing cell de-adhesion. *BMC Immunol* **12**, 28
 131. Andersson, A., Eden, P., Lindgren, D., Nilsson, J., Lassen, C., Heldrup, J., *et al.* (2005) Gene expression profiling of leukemic cell lines reveals conserved molecular signatures among subtypes with specific genetic aberrations. *Leukemia* **19**, 1042-1050
 132. Borst, P., de Wolf, C., and van de Wetering, K. (2007) Multidrug resistance-associated proteins 3, 4, and 5. *Pflugers Arch* **453**, 661-673
 133. Takeuchi, K., Shibata, M., Kashiya, E., and Umehara, K. (2012) Expression levels of multidrug resistance-associated protein 4 (MRP4) in human leukemia and lymphoma cell lines, and the inhibitory effects of the MRP-specific inhibitor MK-571 on methotrexate distribution in rats. *Exp Ther Med* **4**, 524-532
 134. Baumann, K. (2013) Stem cells: A metabolic switch. *Nat Rev Mol Cell Biol* **14**, 64-65
 135. Felipe Rico, J., Hassane, D. C., and Guzman, M. L. (2013) Acute myelogenous leukemia stem cells: from Bench to Bedside. *Cancer Lett* **338**, 4-9
 136. Chen, Z. S., and Tiwari, A. K. (2011) Multidrug resistance proteins (MRPs/ABCCs) in cancer chemotherapy and genetic diseases. *FEBS J* **278**, 3226-3245

137. Wu, T. S., Yu, F. Y., Su, C. C., Kan, J. C., Chung, C. P., and Liu, B. H. (2005) Activation of ERK mitogen-activated protein kinase in human cells by the mycotoxin patulin. *Toxicol Appl Pharmacol* **207**, 103-111
138. Fribley, A. M., Cruz, P. G., Miller, J. R., Callaghan, M. U., Cai, P., Narula, N., *et al.* (2011) Complementary cell-based high-throughput screens identify novel modulators of the unfolded protein response. *J Biomol Screen* **16**, 825-835
139. Hothi, P., Martins, T. J., Chen, L. P., Deleyrolle, L., Yoon, J. G., Reynolds, B., *et al.* (2012) High-Throughput Chemical Screens Identify Disulfiram as an Inhibitor of Human Glioblastoma Stem Cells. *Oncotarget* **3**, 1124-1136
140. Kawauchiya, T., Takumi, R., Kudo, Y., Takamori, A., Sasagawa, T., Takahashi, K., *et al.* (2011) Correlation between the destruction of tight junction by patulin treatment and increase of phosphorylation of ZO-1 in Caco-2 human colon cancer cells. *Toxicol Lett* **205**, 196-202
141. Mohan, H. M., Collins, D., Maher, S., Walsh, E. G., Winter, D. C., O'Brien, P. J., *et al.* (2012) The mycotoxin patulin increases colonic epithelial permeability in vitro. *Food Chem Toxicol* **50**, 4097-4102
142. McLaughlin, J., Lambert, D., Padfield, P. J., Burt, J. P., and O'Neill, C. A. (2009) The mycotoxin patulin, modulates tight junctions in caco-2 cells. *Toxicol In Vitro* **23**, 83-89
143. Kwon, O., Soung, N. K., Thimmegowda, N. R., Jeong, S. J., Jang, J. H., Moon, D. O., *et al.* (2012) Patulin induces colorectal cancer cells apoptosis through EGR-1 dependent ATF3 up-regulation. *Cell Signal* **24**, 943-950
144. Liu, B. H., Wu, T. S., Yu, F. Y., and Su, C. C. (2007) Induction of oxidative stress response by the mycotoxin patulin in mammalian cells. *Toxicol Sci* **95**, 340-347
145. Zhou, S. M., Jiang, L. P., Geng, C. Y., Cao, J., and Zhong, L. F. (2010) Patulin-induced oxidative DNA damage and p53 modulation in HepG2 cells. *Toxicol* **55**, 390-395
146. Czyz, M., Koprowska, K., and Sztiller-Sikorska, M. (2013) Parthenolide reduces the frequency of ABCB5-positive cells and clonogenic capacity of melanoma cells from anchorage independent melanospheres. *Cancer Biol Ther* **14**, 135-145
147. Czyz, M., Lesiak-Mieczkowska, K., Koprowska, K., Szulawska-Mroczek, A., and Wozniak, M. (2010) Cell context-dependent activities of parthenolide in primary and metastatic melanoma cells. *Br J Pharmacol* **160**, 1144-1157

148. Hehner, S. P., Hofmann, T. G., Droge, W., and Schmitz, M. L. (1999) The antiinflammatory sesquiterpene lactone parthenolide inhibits NF-kappa B by targeting the I kappa B kinase complex. *J Immunol* **163**, 5617-5623
149. Kwok, B. H., Koh, B., Ndubuisi, M. I., Elofsson, M., and Crews, C. M. (2001) The anti-inflammatory natural product parthenolide from the medicinal herb Feverfew directly binds to and inhibits IkappaB kinase. *Chem Biol* **8**, 759-766
150. Dai, Y., Guzman, M. L., Chen, S., Wang, L., Yeung, S. K., Pei, X. Y., *et al.* (2010) The NF (Nuclear factor)-kappaB inhibitor parthenolide interacts with histone deacetylase inhibitors to induce MKK7/JNK1-dependent apoptosis in human acute myeloid leukaemia cells. *Br J Haematol* **151**, 70-83
151. Steele, A. J., Jones, D. T., Ganeshaguru, K., Duke, V. M., Yogashangary, B. C., North, J. M., *et al.* (2006) The sesquiterpene lactone parthenolide induces selective apoptosis of B-chronic lymphocytic leukemia cells in vitro. *Leukemia* **20**, 1073-1079
152. Zhou, J., Zhang, H., Gu, P., Bai, J., Margolick, J. B., and Zhang, Y. (2008) NF-kappaB pathway inhibitors preferentially inhibit breast cancer stem-like cells. *Breast Cancer Res Treat* **111**, 419-427
153. Chen, T., Li, M., Zhang, R., and Wang, H. (2009) Dihydroartemisinin induces apoptosis and sensitizes human ovarian cancer cells to carboplatin therapy. *J Cell Mol Med* **13**, 1358-1370
154. Disbrow, G. L., Baege, A. C., Kierpiec, K. A., Yuan, H., Centeno, J. A., Thibodeaux, C. A., *et al.* (2005) Dihydroartemisinin is cytotoxic to papillomavirus-expressing epithelial cells in vitro and in vivo. *Cancer Res* **65**, 10854-10861
155. Dell'Eva, R., Pfeffer, U., Vene, R., Anfosso, L., Forlani, A., Albini, A., *et al.* (2004) Inhibition of angiogenesis in vivo and growth of Kaposi's sarcoma xenograft tumors by the anti-malarial artesunate. *Biochem Pharmacol* **68**, 2359-2366
156. Jiang, Z., Chai, J., Chuang, H. H., Li, S., Wang, T., Cheng, Y., *et al.* (2012) Artesunate induces G0/G1 cell cycle arrest and iron-mediated mitochondrial apoptosis in A431 human epidermoid carcinoma cells. *Anticancer Drugs* **23**, 606-613
157. Bachmeier, B., Fichtner, I., Killian, P. H., Kronschi, E., Pfeffer, U., and Efferth, T. (2011) Development of resistance towards artesunate in MDA-MB-231 human breast cancer cells. *PLoS One* **6**, e20550

158. Hamacher-Brady, A., Stein, H. A., Turschner, S., Toegel, I., Mora, R., Jennewein, N., *et al.* (2011) Artesunate activates mitochondrial apoptosis in breast cancer cells via iron-catalyzed lysosomal reactive oxygen species production. *J Biol Chem* **286**, 6587-6601
159. Hou, J., Wang, D., Zhang, R., and Wang, H. (2008) Experimental therapy of hepatoma with artemisinin and its derivatives: in vitro and in vivo activity, chemosensitization, and mechanisms of action. *Clin Cancer Res* **14**, 5519-5530
160. Du, J. H., Zhang, H. D., Ma, Z. J., and Ji, K. M. (2010) Artesunate induces oncosis-like cell death in vitro and has antitumor activity against pancreatic cancer xenografts in vivo. *Cancer Chemother Pharmacol* **65**, 895-902
161. Youns, M., Efferth, T., Reichling, J., Fellenberg, K., Bauer, A., and Hoheisel, J. D. (2009) Gene expression profiling identifies novel key players involved in the cytotoxic effect of Artesunate on pancreatic cancer cells. *Biochem Pharmacol* **78**, 273-283
162. Chen, H., Shi, L., Yang, X., Li, S., Guo, X., and Pan, L. (2010) Artesunate inhibiting angiogenesis induced by human myeloma RPMI8226 cells. *Int J Hematol* **92**, 587-597
163. Efferth, T., Davey, M., Olbrich, A., Rucker, G., Gebhart, E., and Davey, R. (2002) Activity of drugs from traditional Chinese medicine toward sensitive and MDR1- or MRP1-overexpressing multidrug-resistant human CCRF-CEM leukemia cells. *Blood Cells Mol Dis* **28**, 160-168
164. Efferth, T., Giaisi, M., Merling, A., Krammer, P. H., and Li-Weber, M. (2007) Artesunate induces ROS-mediated apoptosis in doxorubicin-resistant T leukemia cells. *PLoS One* **2**, e693
165. Steinbrück, L., Pereira, G., and Efferth, T. (2010) Effects of Artesunate on Cytokinesis and G2/M Cell Cycle Progression of Tumour Cells and Budding Yeast. *Cancer Genomics - Proteomics* **7**, 337-346
166. Zhou, H. J., Wang, W. Q., Wu, G. D., Lee, J., and Li, A. (2007) Artesunate inhibits angiogenesis and downregulates vascular endothelial growth factor expression in chronic myeloid leukemia K562 cells. *Vascul Pharmacol* **47**, 131-138
167. Li, L. N., Zhang, H. D., Yuan, S. J., Yang, D. X., Wang, L., and Sun, Z. X. (2008) Differential sensitivity of colorectal cancer cell lines to artesunate is associated with expression of beta-catenin and E-cadherin. *Eur J Pharmacol* **588**, 1-8

168. Michaelis, M., Kleinschmidt, M. C., Barth, S., Rothweiler, F., Geiler, J., Breitling, R., *et al.* (2010) Anti-cancer effects of artesunate in a panel of chemoresistant neuroblastoma cell lines. *Biochem Pharmacol* **79**, 130-136
169. Rasheed, S. A., Efferth, T., Asangani, I. A., and Allgayer, H. (2010) First evidence that the antimalarial drug artesunate inhibits invasion and in vivo metastasis in lung cancer by targeting essential extracellular proteases. *Int J Cancer* **127**, 1475-1485
170. Xu, Q., Li, Z. X., Peng, H. Q., Sun, Z. W., Cheng, R. L., Ye, Z. M., *et al.* (2011) Artesunate inhibits growth and induces apoptosis in human osteosarcoma HOS cell line in vitro and in vivo. *J Zhejiang Univ Sci B* **12**, 247-255
171. Jiao, Y., Ge, C. M., Meng, Q. H., Cao, J. P., Tong, J., and Fan, S. J. (2007) Dihydroartemisinin is an inhibitor of ovarian cancer cell growth. *Acta Pharmacol Sin* **28**, 1045-1056
172. Ba, Q., Zhou, N., Duan, J., Chen, T., Hao, M., Yang, X., *et al.* (2012) Dihydroartemisinin exerts its anticancer activity through depleting cellular iron via transferrin receptor-1. *PLoS One* **7**, e42703
173. Zhang, C. Z., Zhang, H., Yun, J., Chen, G. G., and Lai, P. B. (2012) Dihydroartemisinin exhibits antitumor activity toward hepatocellular carcinoma in vitro and in vivo. *Biochem Pharmacol* **83**, 1278-1289
174. Cabello, C. M., Lamore, S. D., Bair, W. B., 3rd, Qiao, S., Azimian, S., Lesson, J. L., *et al.* (2012) The redox antimalarial dihydroartemisinin targets human metastatic melanoma cells but not primary melanocytes with induction of NOXA-dependent apoptosis. *Invest New Drugs* **30**, 1289-1301
175. Chen, H., Sun, B., Pan, S., Jiang, H., and Sun, X. (2009) Dihydroartemisinin inhibits growth of pancreatic cancer cells in vitro and in vivo. *Anticancer Drugs* **20**, 131-140
176. Chen, H., Sun, B., Wang, S., Pan, S., Gao, Y., Bai, X., *et al.* (2010) Growth inhibitory effects of dihydroartemisinin on pancreatic cancer cells: involvement of cell cycle arrest and inactivation of nuclear factor-kappaB. *J Cancer Res Clin Oncol* **136**, 897-903
177. Kong, R., Jia, G., Cheng, Z. X., Wang, Y. W., Mu, M., Wang, S. J., *et al.* (2012) Dihydroartemisinin enhances Apo2L/TRAIL-mediated apoptosis in pancreatic cancer cells via ROS-mediated up-regulation of death receptor 5. *PLoS One* **7**, e37222

178. Wang, S. J., Gao, Y., Chen, H., Kong, R., Jiang, H. C., Pan, S. H., *et al.* (2010) Dihydroartemisinin inactivates NF-kappaB and potentiates the anti-tumor effect of gemcitabine on pancreatic cancer both in vitro and in vivo. *Cancer Lett* **293**, 99-108
179. Wang, S. J., Sun, B., Cheng, Z. X., Zhou, H. X., Gao, Y., Kong, R., *et al.* (2011) Dihydroartemisinin inhibits angiogenesis in pancreatic cancer by targeting the NF-kappaB pathway. *Cancer Chemother Pharmacol* **68**, 1421-1430
180. Chen, M., Chen, T. S., Lu, Y. Y., Liu, C. Y., and Qu, J. L. (2012) Dihydroartemisinin-induced apoptosis is not dependent on the translocation of Bim to the endoplasmic reticulum in human lung adenocarcinoma cells. *Pathol Oncol Res* **18**, 809-816
181. Lu, Y. Y., Chen, T. S., Wang, X. P., and Li, L. (2010) Single-cell analysis of dihydroartemisinin-induced apoptosis through reactive oxygen species-mediated caspase-8 activation and mitochondrial pathway in ASTC-a-1 cells using fluorescence imaging techniques. *J Biomed Opt* **15**, 046028
182. Zhou, H. J., Zhang, J. L., Li, A., Wang, Z., and Lou, X. E. (2010) Dihydroartemisinin improves the efficiency of chemotherapeutics in lung carcinomas in vivo and inhibits murine Lewis lung carcinoma cell line growth in vitro. *Cancer Chemother Pharmacol* **66**, 21-29
183. Gao, N., Budhraja, A., Cheng, S., Liu, E. H., Huang, C., Chen, J., *et al.* (2011) Interruption of the MEK/ERK signaling cascade promotes dihydroartemisinin-induced apoptosis in vitro and in vivo. *Apoptosis* **16**, 511-523
184. Handrick, R., Ontikatzte, T., Bauer, K. D., Freier, F., Rubel, A., Durig, J., *et al.* (2010) Dihydroartemisinin induces apoptosis by a Bak-dependent intrinsic pathway. *Mol Cancer Ther* **9**, 2497-2510
185. Lee, J., Zhou, H. J., and Wu, X. H. (2006) Dihydroartemisinin downregulates vascular endothelial growth factor expression and induces apoptosis in chronic myeloid leukemia K562 cells. *Cancer Chemother Pharmacol* **57**, 213-220
186. Lu, J. J., Meng, L. H., Cai, Y. J., Chen, Q., Tong, L. J., Lin, L. P., *et al.* (2008) Dihydroartemisinin induces apoptosis in HL-60 leukemia cells dependent of iron and p38 mitogen-activated protein kinase activation but independent of reactive oxygen species. *Cancer Biol Ther* **7**, 1017-1023

187. Wang, Z., Hu, W., Zhang, J. L., Wu, X. H., and Zhou, H. J. (2012) Dihydroartemisinin induces autophagy and inhibits the growth of iron-loaded human myeloid leukemia K562 cells via ROS toxicity. *FEBS Open Bio* **2**, 103-112
188. Wu, X. H., Zhou, H. J., and Lee, J. (2006) Dihydroartemisinin inhibits angiogenesis induced by multiple myeloma RPMI8226 cells under hypoxic conditions via downregulation of vascular endothelial growth factor expression and suppression of vascular endothelial growth factor secretion. *Anticancer Drugs* **17**, 839-848
189. He, Q., Shi, J., Shen, X. L., An, J., Sun, H., Wang, L., *et al.* (2010) Dihydroartemisinin upregulates death receptor 5 expression and cooperates with TRAIL to induce apoptosis in human prostate cancer cells. *Cancer Biol Ther* **9**, 819-824
190. Huang, X. J., Ma, Z. Q., Zhang, W. P., Lu, Y. B., and Wei, E. Q. (2007) Dihydroartemisinin exerts cytotoxic effects and inhibits hypoxia inducible factor-1alpha activation in C6 glioma cells. *J Pharm Pharmacol* **59**, 849-856
191. Ji, Y., Zhang, Y. C., Pei, L. B., Shi, L. L., Yan, J. L., and Ma, X. H. (2011) Anti-tumor effects of dihydroartemisinin on human osteosarcoma. *Mol Cell Biochem* **351**, 99-108
192. Cao, B., Li, J., Zhu, J., Shen, M., Han, K., Zhang, Z., *et al.* (2013) The antiparasitic clioquinol induces apoptosis in leukemia and myeloma cells by inhibiting histone deacetylase activity. *J Biol Chem* **288**, 34181-34189
193. Mao, X., Li, X., Sprangers, R., Wang, X., Venugopal, A., Wood, T., *et al.* (2009) Clioquinol inhibits the proteasome and displays preclinical activity in leukemia and myeloma. *Leukemia* **23**, 585-590
194. Ding, W. Q., Liu, B., Vaught, J. L., Yamauchi, H., and Lind, S. E. (2005) Anticancer activity of the antibiotic clioquinol. *Cancer Res* **65**, 3389-3395
195. Daniel, K. G., Chen, D., Orlu, S., Cui, Q. C., Miller, F. R., and Dou, Q. P. (2005) Clioquinol and pyrrolidine dithiocarbamate complex with copper to form proteasome inhibitors and apoptosis inducers in human breast cancer cells. *Breast Cancer Res* **7**, R897-908
196. Zheng, J., Benbrook, D. M., Yu, H. J., and Ding, W. Q. (2011) Clioquinol Suppresses Cyclin D1 Gene Expression through Transcriptional and Post-transcriptional Mechanisms. *Anticancer Research* **31**, 2739-2747

197. Du, T., Filiz, G., Caragounis, A., Crouch, P. J., and White, A. R. (2008) Cloiquinol promotes cancer cell toxicity through tumor necrosis factor alpha release from macrophages. *J Pharmacol Exp Ther* **324**, 360-367
198. Yu, H., Zhou, Y., Lind, S. E., and Ding, W. Q. (2009) Cloiquinol targets zinc to lysosomes in human cancer cells. *Biochem J* **417**, 133-139
199. Yu, H., Lou, J. R., and Ding, W. Q. (2010) Cloiquinol independently targets NF-kappaB and lysosome pathways in human cancer cells. *Anticancer Res* **30**, 2087-2092
200. Chen, D., Cui, Q. C., Yang, H., Barrea, R. A., Sarkar, F. H., Sheng, S., *et al.* (2007) Cloiquinol, a therapeutic agent for Alzheimer's disease, has proteasome-inhibitory, androgen receptor-suppressing, apoptosis-inducing, and antitumor activities in human prostate cancer cells and xenografts. *Cancer Res* **67**, 1636-1644
201. Ge, Y., Cheng, R., Zhou, Y., Shen, J., Peng, L., Xu, X., *et al.* (2012) Cryptotanshinone induces cell cycle arrest and apoptosis of multidrug resistant human chronic myeloid leukemia cells by inhibiting the activity of eukaryotic initiation factor 4E. *Mol Cell Biochem* **368**, 17-25
202. Jung, J. H., Kwon, T.-R., Jeong, S.-J., Kim, E.-O., Sohn, E. J., Yun, M., *et al.* (2013) Apoptosis Induced by Tanshinone IIA and Cryptotanshinone Is Mediated by Distinct JAK/STAT3/5 and SHP1/2 Signaling in Chronic Myeloid Leukemia K562 Cells. *Evidence-Based Complementary and Alternative Medicine* **2013**, 10
203. Shin, D. S., Kim, H. N., Shin, K. D., Yoon, Y. J., Kim, S. J., Han, D. C., *et al.* (2009) Cryptotanshinone inhibits constitutive signal transducer and activator of transcription 3 function through blocking the dimerization in DU145 prostate cancer cells. *Cancer Res* **69**, 193-202
204. Wu, C. Y., Hsieh, C. Y., Huang, K. E., Chang, C., and Kang, H. Y. (2012) Cryptotanshinone down-regulates androgen receptor signaling by modulating lysine-specific demethylase 1 function. *Int J Cancer* **131**, 1423-1434
205. Nizamutdinova, I. T., Lee, G. W., Son, K. H., Jeon, S. J., Kang, S. S., Kim, Y. S., *et al.* (1992) Tanshinone I effectively induces apoptosis in estrogen receptor-positive (MCF-7) and estrogen receptor-negative (MDA-MB-231) breast cancer cells. *International Journal of Oncology*
206. Chen, L., Zheng, S. Z., Sun, Z. G., Wang, A. Y., Huang, C. H., Punchard, N. A., *et al.* (2011) Cryptotanshinone has diverse effects on cell cycle events in melanoma

cell lines with different metastatic capacity. *Cancer Chemother Pharmacol* **68**, 17-27

207. Tse, A. K., Chow, K. Y., Cao, H. H., Cheng, C. Y., Kwan, H. Y., Yu, H., *et al.* (2013) The herbal compound cryptotanshinone restores sensitivity in cancer cells that are resistant to the tumor necrosis factor-related apoptosis-inducing ligand. *J Biol Chem* **288**, 29923-29933
208. Neelakantan, S., Nasim, S., Guzman, M. L., Jordan, C. T., and Crooks, P. A. (2009) Aminoparthenolides as novel anti-leukemic agents: Discovery of the NF-kappaB inhibitor, DMAPT (LC-1). *Bioorg Med Chem Lett* **19**, 4346-4349
209. Cheng, G., and Xie, L. (2011) Parthenolide induces apoptosis and cell cycle arrest of human 5637 bladder cancer cells in vitro. *Molecules* **16**, 6758-6768
210. Zunino, S. J., Storms, D. H., and Ducore, J. M. (2010) Parthenolide treatment activates stress signaling proteins in high-risk acute lymphoblastic leukemia cells with chromosomal translocation t(4;11). *Int J Oncol* **37**, 1307-1313
211. Kishida, Y., Yoshikawa, H., and Myoui, A. (2007) Parthenolide, a natural inhibitor of Nuclear Factor-kappaB, inhibits lung colonization of murine osteosarcoma cells. *Clin Cancer Res* **13**, 59-67
212. Liu, J. W., Cai, M. X., Xin, Y., Wu, Q. S., Ma, J., Yang, P., *et al.* (2010) Parthenolide induces proliferation inhibition and apoptosis of pancreatic cancer cells in vitro. *J Exp Clin Cancer Res* **29**, 108
213. Kreuger, M. R., Grootjans, S., Biavatti, M. W., Vandenabeele, P., and D'Herde, K. (2012) Sesquiterpene lactones as drugs with multiple targets in cancer treatment: focus on parthenolide. *Anticancer Drugs* **23**, 883-896
214. Saadane, A., Eastman, J., Berger, M., and Bonfield, T. L. (2011) Parthenolide inhibits ERK and AP-1 which are dysregulated and contribute to excessive IL-8 expression and secretion in cystic fibrosis cells. *J Inflamm (Lond)* **8**, 26
215. Mathema, V. B., Koh, Y. S., Thakuri, B. C., and Sillanpaa, M. (2012) Parthenolide, a sesquiterpene lactone, expresses multiple anti-cancer and anti-inflammatory activities. *Inflammation* **35**, 560-565
216. Efferth, T., Sauerbrey, A., Olbrich, A., Gebhart, E., Rauch, P., Weber, H. O., *et al.* (2003) Molecular modes of action of artesunate in tumor cell lines. *Mol Pharmacol* **64**, 382-394

217. Konkimalla, V. B., Blunder, M., Korn, B., Soomro, S. A., Jansen, H., Chang, W., *et al.* (2008) Effect of artemisinins and other endoperoxides on nitric oxide-related signaling pathway in RAW 264.7 mouse macrophage cells. *Nitric Oxide* **19**, 184-191
218. Cheng, C., Ho, W. E., Goh, F. Y., Guan, S. P., Kong, L. R., Lai, W. Q., *et al.* (2011) Anti-malarial drug artesunate attenuates experimental allergic asthma via inhibition of the phosphoinositide 3-kinase/Akt pathway. *PLoS One* **6**, e20932
219. Saxena, N., Ansari, K. M., Kumar, R., Dhawan, A., Dwivedi, P. D., and Das, M. (2009) Patulin causes DNA damage leading to cell cycle arrest and apoptosis through modulation of Bax, p(53) and p(21/WAF1) proteins in skin of mice. *Toxicol Appl Pharmacol* **234**, 192-201
220. Guo, X., Dong, Y., Yin, S., Zhao, C., Huo, Y., Fan, L., *et al.* (2013) Patulin induces pro-survival functions via autophagy inhibition and p62 accumulation. *Cell Death Dis* **4**, e822
221. Lupescu, A., Jilani, K., Zbidah, M., and Lang, F. (2013) Patulin-induced suicidal erythrocyte death. *Cell Physiol Biochem* **32**, 291-299
222. de Melo, F. T., de Oliveira, I. M., Greggio, S., Dacosta, J. C., Guecheva, T. N., Saffi, J., *et al.* (2012) DNA damage in organs of mice treated acutely with patulin, a known mycotoxin. *Food Chem Toxicol* **50**, 3548-3555
223. Naviglio, S., Caraglia, M., Abbruzzese, A., Chiosi, E., Di Gesto, D., Marra, M., *et al.* (2009) Protein kinase A as a biological target in cancer therapy. *Expert Opinion on Therapeutic Targets* **13**, 83-92
224. Savai, R., Pullamsetti, S. S., Banat, G.-A., Weissmann, N., Ghofrani, H. A., Grimminger, F., *et al.* (2010) Targeting cancer with phosphodiesterase inhibitors. *Expert Opinion on Investigational Drugs* **19**, 117-131
225. Guillemin, M. C., Raffoux, E., Vitoux, D., Kogan, S., Soilihi, H., Lallemand-Breitenbach, V., *et al.* (2002) In vivo activation of cAMP signaling induces growth arrest and differentiation in acute promyelocytic leukemia. *J Exp Med* **196**, 1373-1380
226. Adema, A., Floor, K., Smid, K., Honeywell, R., Scheffer, G., Jansen, G., *et al.* (2014) Overexpression of MRP4 (ABCC4) and MRP5 (ABCC5) confer resistance to the nucleoside analogs cytarabine and troxacitabine, but not gemcitabine. *SpringerPlus* **3**, 732

227. Keppler, D. (2011) Multidrug resistance proteins (MRPs, ABCs): importance for pathophysiology and drug therapy. *Handb Exp Pharmacol*, 299-323
228. Koczor, C. A., Torres, R. A., and Lewis, W. (2012) The role of transporters in the toxicity of nucleoside and nucleotide analogs. *Expert Opin Drug Metab Toxicol* **8**, 665-676
229. Okada, C. Y., and Rechsteiner, M. (1982) Introduction of macromolecules into cultured mammalian cells by osmotic lysis of pinocytotic vesicles. *Cell* **29**, 33-41
230. Chigaev, A., and Sklar, L. A. (2012) Overview: assays for studying integrin-dependent cell adhesion. *Methods Mol Biol* **757**, 3-14
231. Prossnitz, E. R. (1997) Desensitization of N-formylpeptide receptor-mediated activation is dependent upon receptor phosphorylation. *Journal of Biological Chemistry* **272**, 15213-15219
232. Liu, Y., Easton, J., Shao, Y., Maciaszek, J., Wang, Z., Wilkinson, M. R., *et al.* (2017) The genomic landscape of pediatric and young adult T-lineage acute lymphoblastic leukemia. *Nature genetics* **49**, 1211-1218
233. Schrappe, M., Valsecchi, M. G., Bartram, C. R., Schrauder, A., Panzer-Grumayer, R., Moricke, A., *et al.* (2011) Late MRD response determines relapse risk overall and in subsets of childhood T-cell ALL: results of the AIEOP-BFM-ALL 2000 study. *Blood* **118**, 2077-2084
234. Gross, S., Rahal, R., Stransky, N., Lengauer, C., and Hoeflich, K. P. (2015) Targeting cancer with kinase inhibitors. *The Journal of clinical investigation* **125**, 1780-1789
235. Maude, S. L., Dolai, S., Delgado-Martin, C., Vincent, T., Robbins, A., Selvanathan, A., *et al.* (2015) Efficacy of JAK/STAT pathway inhibition in murine xenograft models of early T-cell precursor (ETP) acute lymphoblastic leukemia. *Blood* **125**, 1759-1767
236. Tyner, J. W., Yang, W. F., Bankhead, A., 3rd, Fan, G., Fletcher, L. B., Bryant, J., *et al.* (2013) Kinase pathway dependence in primary human leukemias determined by rapid inhibitor screening. *Cancer Res* **73**, 285-296
237. Jones, L., Carol, H., Evans, K., Richmond, J., Houghton, P. J., Smith, M. A., *et al.* (2016) A review of new agents evaluated against pediatric acute lymphoblastic leukemia by the Pediatric Preclinical Testing Program. *Leukemia* **30**, 2133-2141

238. Lhermitte, L., Ben Abdelali, R., Villarese, P., Bedjaoui, N., Guillemot, V., Trinquand, A., *et al.* (2013) Receptor kinase profiles identify a rationale for multitarget kinase inhibition in immature T-ALL. *Leukemia* **27**, 305-314
239. Ahmadi, M., Ahmadihosseini, Z., Allison, S. J., Begum, S., Rockley, K., Sadiq, M., *et al.* (2014) Hypoxia modulates the activity of a series of clinically approved tyrosine kinase inhibitors. *Br J Pharmacol* **171**, 224-236
240. Filippi, I., Naldini, A., and Carraro, F. (2011) Role of the hypoxic microenvironment in the antitumor activity of tyrosine kinase inhibitors. *Curr Med Chem* **18**, 2885-2892
241. Edwards, B. S., Gouveia, K., Oprea, T. I., and Sklar, L. A. (2014) The University of New Mexico Center for Molecular Discovery. *Comb Chem High Throughput Screen* **17**, 256-265
242. Dagklis, A., Demeyer, S., De Bie, J., Radaelli, E., Pauwels, D., Degryse, S., *et al.* (2016) Hedgehog pathway activation in T-cell acute lymphoblastic leukemia predicts response to SMO and GLI1 inhibitors. *Blood* **128**, 2642-2654
243. Coustan-Smith, E., Mullighan, C. G., Onciu, M., Behm, F. G., Raimondi, S. C., Pei, D., *et al.* (2009) Early T-cell precursor leukaemia: a subtype of very high-risk acute lymphoblastic leukaemia. *Lancet Oncol* **10**, 147-156
244. Frisimantas, V., Dobay, M. P., Rinaldi, A., Tchinda, J., Dunn, S. H., Kunz, J., *et al.* (2017) Ex vivo drug response profiling detects recurrent sensitivity patterns in drug-resistant acute lymphoblastic leukemia. *Blood* **129**, e26-e37
245. Laukkanen, S., Gronroos, T., Polonen, P., Kuusanmaki, H., Mehtonen, J., Cloos, J., *et al.* (2017) In silico and preclinical drug screening identifies dasatinib as a targeted therapy for T-ALL. *Blood Cancer J* **7**, e604
246. Ben-David, U., Ha, G., Tseng, Y. Y., Greenwald, N. F., Oh, C., Shih, J., *et al.* (2017) Patient-derived xenografts undergo mouse-specific tumor evolution. *Nature genetics* **49**, 1567-1575
247. Cooper, M. J., Cox, N. J., Zimmerman, E. I., Dewar, B. J., Duncan, J. S., Whittle, M. C., *et al.* (2013) Application of multiplexed kinase inhibitor beads to study kinome adaptations in drug-resistant leukemia. *PLoS One* **8**, e66755
248. Matlawska-Wasowska, K., Kang, H., Devidas, M., Wen, J., Harvey, R. C., Nickl, C. K., *et al.* (2016) MLL rearrangements impact outcome in HOXA-deregulated T-lineage acute lymphoblastic leukemia: a Children's Oncology Group Study. *Leukemia*

249. Zeidner, J. F., Foster, M. C., Blackford, A. L., Litzow, M. R., Morris, L. E., Strickland, S. A., *et al.* (2015) Randomized multicenter phase II study of flavopiridol (alvocidib), cytarabine, and mitoxantrone (FLAM) versus cytarabine/daunorubicin (7+3) in newly diagnosed acute myeloid leukemia. *Haematologica* **100**, 1172-1179
250. Palmer, A. C., and Sorger, P. K. (2017) Combination Cancer Therapy Can Confer Benefit via Patient-to-Patient Variability without Drug Additivity or Synergy. *Cell* **171**, 1678-1691 e1613
251. Lehar, J., Zimmermann, G. R., Krueger, A. S., Molnar, R. A., Ledell, J. T., Heilbut, A. M., *et al.* (2007) Chemical combination effects predict connectivity in biological systems. *Mol Syst Biol* **3**, 80
252. Yeh, P., Tschumi, A. I., and Kishony, R. (2006) Functional classification of drugs by properties of their pairwise interactions. *Nat Genet* **38**, 489-494
253. Berenbaum, M. (1989) What is synergy? *Pharmacol Rev* **41**, 93-141
254. Bliss, C. I. (1939) The toxicity of poisons applied jointly. *Annals of Applied Biology* **26**, 585-615
255. Loewe, S. (1953) The problem of synergism and antagonisms of combined drugs. *Arzneimittelforsch Drug Res* **3**, 285-290
256. Chou, T. C. (2010) Drug combination studies and their synergy quantification using the Chou-Talalay method. *Cancer Res* **70**, 440-446
257. Foucquier, J., and Guedj, M. (2015) Analysis of drug combinations: current methodological landscape. *Pharmacol Res Perspect* **3**, e00149
258. Yadav, B., Wennerberg, K., Aittokallio, T., and Tang, J. (2015) Searching for Drug Synergy in Complex Dose-Response Landscapes Using an Interaction Potency Model. *Comput Struct Biotechnol J* **13**, 504-513
259. Di Veroli, G. Y., Fornari, C., Wang, D., Mollard, S., Bramhall, J. L., Richards, F. M., *et al.* (2016) Combenefit: an interactive platform for the analysis and visualization of drug combinations. *Bioinformatics* **32**, 2866-2868
260. Chou, T. C., and Martin, N. (2005) CompuSyn for drug combinations: PC Software and User's Guide: a computer program for quantitation of synergism and antagonism in drug combinations, and the determination of IC50 and ED50 and LD50 values. Combo-Syn, Paramus, NJ, USA

261. Boik, J. C., and Narasimhan, B. (2010) An R Package for Assessing Drug Synergism/Antagonism. *J Stat Softw* **34**, 1-18
262. Mathews Griner, L. A., Guha, R., Shinn, P., Young, R. M., Keller, J. M., Liu, D., *et al.* (2014) High-throughput combinatorial screening identifies drugs that cooperate with ibrutinib to kill activated B-cell-like diffuse large B-cell lymphoma cells. *Proc Natl Acad Sci U S A* **111**, 2349-2354
263. Held, M. A., Langdon, C. G., Platt, J. T., Graham-Steed, T., Liu, Z., Chakraborty, A., *et al.* (2013) Genotype-selective combination therapies for melanoma identified by high-throughput drug screening. *Cancer Discov* **3**, 52-67
264. Edwards, B. S., and Sklar, L. A. (2015) Flow Cytometry: Impact on Early Drug Discovery. *J Biomol Screen* **20**, 689-707
265. Kashif, M., Andersson, C., Aberg, M., Nygren, P., Sjoblom, T., Hammerling, U., *et al.* (2014) A pragmatic definition of therapeutic synergy suitable for clinically relevant in vitro multicomponent analyses. *Mol Cancer Ther* **13**, 1964-1976
266. Fukuda, Y., Lian, S., and Schuetz, J. D. (2015) Leukemia and ABC transporters. *Adv Cancer Res* **125**, 171-196
267. Cho-Chung, Y. S., Nesterova, M., Becker, K. G., Srivastava, R., Park, Y. G., Lee, Y. N., *et al.* (2002) Dissecting the circuitry of protein kinase A and cAMP signaling in cancer genesis: antisense, microarray, gene overexpression, and transcription factor decoy. *Ann N Y Acad Sci* **968**, 22-36
268. Guo, Y., Kotova, E., Chen, Z. S., Lee, K., Hopper-Borge, E., Belinsky, M. G., *et al.* (2003) MRP8, ATP-binding cassette C11 (ABCC11), is a cyclic nucleotide efflux pump and a resistance factor for fluoropyrimidines 2',3'-dideoxycytidine and 9'-(2'-phosphonylmethoxyethyl)adenine. *J Biol Chem* **278**, 29509-29514
269. Chen, Z. S., Lee, K., and Kruh, G. D. (2001) Transport of cyclic nucleotides and estradiol 17-beta-D-glucuronide by multidrug resistance protein 4. Resistance to 6-mercaptopurine and 6-thioguanine. *J Biol Chem* **276**, 33747-33754
270. Kathawala, R. J., Wang, Y. J., Ashby, C. R., Jr., and Chen, Z. S. (2014) Recent advances regarding the role of ABC subfamily C member 10 (ABCC10) in the efflux of antitumor drugs. *Chin J Cancer* **33**, 223-230
271. Leggas, M., Adachi, M., Scheffer, G. L., Sun, D., Wielinga, P., Du, G., *et al.* (2004) Mrp4 confers resistance to topotecan and protects the brain from chemotherapy. *Mol Cell Biol* **24**, 7612-7621

272. Rickles, R. J., Pierce, L. T., Giordano, T. P., 3rd, Tam, W. F., McMillin, D. W., Delmore, J., *et al.* (2010) Adenosine A2A receptor agonists and PDE inhibitors: a synergistic multitarget mechanism discovered through systematic combination screening in B-cell malignancies. *Blood* **116**, 593-602
273. Follin-Arbelet, V., Misund, K., Hallan Naderi, E., Ugland, H., Sundan, A., and Blomhoff, H. K. (2015) The natural compound forskolin synergizes with dexamethasone to induce cell death in myeloma cells via BIM. *Sci Rep* **5**, 13001
274. Oprea-Lager, D. E., Bijnsdorp, I. V., Van Moorselaar, R. J., Van Den Eertwegh, A. J., Hoekstra, O. S., and Geldof, A. A. (2013) ABCC4 Decreases docetaxel and not cabazitaxel efficacy in prostate cancer cells in vitro. *Anticancer Res* **33**, 387-391
275. Perez, D. R., Edwards, B. S., Sklar, L. A., and Chigaev, A. (2018) High-Throughput Flow Cytometry Drug Combination Discovery with Novel Synergy Analysis Software, SynScreen. *SLAS Discov* **23**, 751-760
276. Perez, D. R., Nickl, C. K., Waller, A., Delgado-Martin, C., Woods, T., Sharma, N. D., *et al.* (2018) High-Throughput Flow Cytometry Identifies Small-Molecule Inhibitors for Drug Repurposing in T-ALL. *SLAS Discov* **23**, 732-741
277. Koefler, H. P., and Golde, D. W. (1980) Human myeloid leukemia cell lines: a review. *Blood* **56**, 344-350
278. Lange, B., Valtieri, M., Santoli, D., Caracciolo, D., Mavilio, F., Gemperlein, I., *et al.* (1987) Growth factor requirements of childhood acute leukemia: establishment of GM-CSF-dependent cell lines. *Blood* **70**, 192-199
279. Lai, C., Karp, J. E., and Hourigan, C. S. (2016) Precision medicine for acute myeloid leukemia. *Expert Rev Hematol* **9**, 1-3
280. Sriskanthadevan, S., Jeyaraju, D. V., Chung, T. E., Prabha, S., Xu, W., Skrtic, M., *et al.* (2015) AML cells have low spare reserve capacity in their respiratory chain that renders them susceptible to oxidative metabolic stress. *Blood* **125**, 2120-2130
281. Blom, K., Nygren, P., Alvarsson, J., Larsson, R., and Andersson, C. R. (2016) Ex Vivo Assessment of Drug Activity in Patient Tumor Cells as a Basis for Tailored Cancer Therapy. *J Lab Autom* **21**, 178-187
282. Li, K., Hu, C., Mei, C., Ren, Z., Vera, J. C., Zhuang, Z., *et al.* (2014) Sequential combination of decitabine and idarubicin synergistically enhances anti-

leukemia effect followed by demethylating Wnt pathway inhibitor promoters and downregulating Wnt pathway nuclear target. *J Transl Med* **12**, 167

283. Lee, M. J., Ye, A. S., Gardino, A. K., Heijink, A. M., Sorger, P. K., MacBeath, G., *et al.* (2012) Sequential application of anticancer drugs enhances cell death by rewiring apoptotic signaling networks. *Cell* **149**, 780-794
284. Drenberg, C. D., Buaboonnam, J., Orwick, S. J., Hu, S., Li, L., Fan, Y., *et al.* (2016) Evaluation of artemisinins for the treatment of acute myeloid leukemia. *Cancer Chemother Pharmacol* **77**, 1231-1243
285. Belinsky, M. G., Guo, P., Lee, K., Zhou, F., Kotova, E., Grinberg, A., *et al.* (2007) Multidrug resistance protein 4 protects bone marrow, thymus, spleen, and intestine from nucleotide analogue-induced damage. *Cancer Res* **67**, 262-268
286. Megias-Vericat, J. E., Montesinos, P., Herrero, M. J., Moscardo, F., Boso, V., Rojas, L., *et al.* (2017) Impact of ABC single nucleotide polymorphisms upon the efficacy and toxicity of induction chemotherapy in acute myeloid leukemia. *Leuk Lymphoma* **58**, 1197-1206
287. Brown, R. B., Madrid, N. J., Suzuki, H., and Ness, S. A. (2017) Optimized approach for Ion Proton RNA sequencing reveals details of RNA splicing and editing features of the transcriptome. *PLOS ONE* **12**, e0176675
288. Kang, H., Sharma, N. D., Nickl, C. K., Devidas, M., Loh, M. L., Hunger, S. P., *et al.* (2018) Dysregulated transcriptional networks in KMT2A- and MLLT10-rearranged T-ALL. *Biomarker Research* **6**, 27
289. Cahoon, L. (2009) The curious case of clioquinol. *Nature medicine* **15**, 356-359
290. Kono, R. (1971) Subacute myelo-optico-neuropathy, a new neurological disease prevailing in Japan. *Jpn J Med Sci Biol* **24**, 195-216
291. Meade, T. W. (1975) Subacute myelo-optic neuropathy and clioquinol. An epidemiological case-history for diagnosis. *Br J Prev Soc Med* **29**, 157-169
292. Eichhorn, G. L. (1979) Aging, genetics, and the environment: potential of errors introduced into genetic information transfer by metal ions. *Mech Ageing Dev* **9**, 291-301
293. Hare, D. J., Faux, N. G., Roberts, B. R., Volitakis, I., Martins, R. N., and Bush, A. I. (2016) Lead and manganese levels in serum and erythrocytes in Alzheimer's disease and mild cognitive impairment: results from the Australian Imaging, Biomarkers and Lifestyle Flagship Study of Ageing. *Metallomics* **8**, 628-632

294. Yevenes Ugarte, L. F., Fowler, C. J., Hung, Y. H., Finkelstein, D. I., Adlard, P. A., Masters, C. L., *et al.* (2014) PROTEIN AND METAL ALTERATIONS IN PLATELETS OF ALZHEIMER'S DISEASE PATIENTS. *Alzheimer's & Dementia: The Journal of the Alzheimer's Association* **10**, P518
295. Roberts, B. R., Doecke, J. D., Rembach, A., Yevenes, L. F., Fowler, C. J., McLean, C. A., *et al.* (2016) Rubidium and potassium levels are altered in Alzheimer's disease brain and blood but not in cerebrospinal fluid. *Acta Neuropathol Commun* **4**, 119
296. Helmuth, L. (2000) Neuroscience. An antibiotic to treat Alzheimer's? *Science* **290**, 1273-1274
297. Cherny, R. A., Atwood, C. S., Xilinas, M. E., Gray, D. N., Jones, W. D., McLean, C. A., *et al.* (2001) Treatment with a copper-zinc chelator markedly and rapidly inhibits beta-amyloid accumulation in Alzheimer's disease transgenic mice. *Neuron* **30**, 665-676
298. Ayton, S., Lei, P., and Bush, A. I. (2013) Metallostasis in Alzheimer's disease. *Free Radic Biol Med* **62**, 76-89
299. Cuajungco, M. P., and Faget, K. Y. (2003) Zinc takes the center stage: its paradoxical role in Alzheimer's disease. *Brain Res Brain Res Rev* **41**, 44-56
300. Grasso, G., Pietropaolo, A., Spoto, G., Pappalardo, G., Tundo, G. R., Ciaccio, C., *et al.* (2011) Copper(I) and copper(II) inhibit Abeta peptides proteolysis by insulin-degrading enzyme differently: implications for metallostasis alteration in Alzheimer's disease. *Chemistry* **17**, 2752-2762
301. Squitti, R. (2012) Metals in Alzheimer's disease: a systemic perspective. *Front Biosci (Landmark Ed)* **17**, 451-472
302. Liang, S. H., Southon, A. G., Fraser, B. H., Krause-Heuer, A. M., Zhang, B., Shoup, T. M., *et al.* (2015) Novel Fluorinated 8-Hydroxyquinoline Based Metal Ionophores for Exploring the Metal Hypothesis of Alzheimer's Disease. *ACS Med Chem Lett* **6**, 1025-1029
303. Huntington Study Group Reach, H. D. I. (2015) Safety, tolerability, and efficacy of PBT2 in Huntington's disease: a phase 2, randomised, double-blind, placebo-controlled trial. *Lancet Neurol* **14**, 39-47
304. Lannfelt, L., Blennow, K., Zetterberg, H., Batsman, S., Ames, D., Harrison, J., *et al.* (2008) Safety, efficacy, and biomarker findings of PBT2 in targeting Abeta

as a modifying therapy for Alzheimer's disease: a phase IIa, double-blind, randomised, placebo-controlled trial. *Lancet Neurol* **7**, 779-786

305. Ayton, S., Lei, P., and Bush, A. I. (2015) Biometals and their therapeutic implications in Alzheimer's disease. *Neurotherapeutics* **12**, 109-120
306. Billings, J. L., Hare, D. J., Nurjono, M., Volitakis, I., Cherny, R. A., Bush, A. I., *et al.* (2016) Effects of Neonatal Iron Feeding and Chronic Clioquinol Administration on the Parkinsonian Human A53T Transgenic Mouse. *ACS Chem Neurosci* **7**, 360-366
307. Finkelstein, D. I., Hare, D. J., Billings, J. L., Sedjahtera, A., Nurjono, M., Arthofer, E., *et al.* (2016) Clioquinol Improves Cognitive, Motor Function, and Microanatomy of the Alpha-Synuclein hA53T Transgenic Mice. *ACS Chem Neurosci* **7**, 119-129
308. Park, M. H., Lee, S. J., Byun, H. R., Kim, Y., Oh, Y. J., Koh, J. Y., *et al.* (2011) Clioquinol induces autophagy in cultured astrocytes and neurons by acting as a zinc ionophore. *Neurobiology of disease* **42**, 242-251
309. Seo, B. R., Lee, S. J., Cho, K. S., Yoon, Y. H., and Koh, J. Y. (2015) The zinc ionophore clioquinol reverses autophagy arrest in chloroquine-treated ARPE-19 cells and in APP/mutant presenilin-1-transfected Chinese hamster ovary cells. *Neurobiol Aging* **36**, 3228-3238
310. Tanida, I., Ueno, T., and Kominami, E. (2008) LC3 and Autophagy. *Methods Mol Biol* **445**, 77-88
311. Levy, J. M. M., Towers, C. G., and Thorburn, A. (2017) Targeting autophagy in cancer. *Nature reviews. Cancer* **17**, 528-542
312. Huang, Z., Wang, L., Chen, L., Zhang, Y., and Shi, P. (2015) Induction of cell cycle arrest via the p21, p27-cyclin E,A/Cdk2 pathway in SMMC-7721 hepatoma cells by clioquinol. *Acta Pharm* **65**, 463-471
313. Chigaev, A. (2015) Does aberrant membrane transport contribute to poor outcome in adult acute myeloid leukemia? *Front Pharmacol* **6**, 134
314. Copsel, S., Garcia, C., Diez, F., Vermeulem, M., Baldi, A., Bianciotti, L. G., *et al.* (2011) Multidrug resistance protein 4 (MRP4/ABCC4) regulates cAMP cellular levels and controls human leukemia cell proliferation and differentiation. *Journal of Biological Chemistry* **286**, 6979-6988

315. Perez, D., Simons, P. C., Smagley, Y., Sklar, L. A., and Chigaev, A. (2016) A High-Throughput Flow Cytometry Assay for Identification of Inhibitors of 3',5'-Cyclic Adenosine Monophosphate Efflux. *Methods Mol Biol* **1439**, 227-244
316. McInerney, M. P., Volitakis, I., Bush, A. I., Banks, W. A., Short, J. L., and Nicolazzo, J. A. (2018) Ionophore and Biometal Modulation of P-glycoprotein Expression and Function in Human Brain Microvascular Endothelial Cells. *Pharm Res* **35**, 83
317. Krishnamurthy, P., Schwab, M., Takenaka, K., Nachagari, D., Morgan, J., Leslie, M., *et al.* (2008) Transporter-mediated protection against thiopurine-induced hematopoietic toxicity. *Cancer Res* **68**, 4983-4989
318. Ban, H., Andoh, A., Imaeda, H., Kobori, A., Bamba, S., Tsujikawa, T., *et al.* (2010) The multidrug-resistance protein 4 polymorphism is a new factor accounting for thiopurine sensitivity in Japanese patients with inflammatory bowel disease. *J Gastroenterol* **45**, 1014-1021
319. Tanaka, Y., Manabe, A., Fukushima, H., Suzuki, R., Nakadate, H., Kondoh, K., *et al.* (2015) Multidrug resistance protein 4 (MRP4) polymorphisms impact the 6-mercaptopurine dose tolerance during maintenance therapy in Japanese childhood acute lymphoblastic leukemia. *Pharmacogenomics J* **15**, 380-384
320. Janke, D., Mehralivand, S., Strand, D., Godtel-Armbrust, U., Habermeier, A., Gradhand, U., *et al.* (2008) 6-mercaptopurine and 9-(2-phosphonyl-methoxyethyl) adenine (PMEA) transport altered by two missense mutations in the drug transporter gene ABCC4. *Hum Mutat* **29**, 659-669
321. Ablu, N., Chinn, L. W., Nakamura, T., Liu, L., Huang, C. C., Johns, S. J., *et al.* (2008) The human multidrug resistance protein 4 (MRP4, ABCC4): functional analysis of a highly polymorphic gene. *The Journal of pharmacology and experimental therapeutics* **325**, 859-868
322. Yoshiura, K., Kinoshita, A., Ishida, T., Ninokata, A., Ishikawa, T., Kaname, T., *et al.* (2006) A SNP in the ABCC11 gene is the determinant of human earwax type. *Nat Genet* **38**, 324-330
323. Nakano, M., Miwa, N., Hirano, A., Yoshiura, K., and Niikawa, N. (2009) A strong association of axillary osmidrosis with the wet earwax type determined by genotyping of the ABCC11 gene. *BMC Genet* **10**, 42
324. Super Science High School, C. (2009) Japanese map of the earwax gene frequency: a nationwide collaborative study by Super Science High School Consortium. *J Hum Genet* **54**, 499-503

325. Uemura, T., Oguri, T., Ozasa, H., Takakuwa, O., Miyazaki, M., Maeno, K., *et al.* (2010) ABCC11/MRP8 confers pemetrexed resistance in lung cancer. *Cancer Sci* **101**, 2404-2410
326. Toyoda, Y., and Ishikawa, T. (2010) Pharmacogenomics of human ABC transporter ABCC11 (MRP8): potential risk of breast cancer and chemotherapy failure. *Anticancer Agents Med Chem* **10**, 617-624
327. Petrakis, N. L. (1971) Cerumen genetics and human breast cancer. *Science* **173**, 347-349
328. Ota, I., Sakurai, A., Toyoda, Y., Morita, S., Sasaki, T., Chishima, T., *et al.* (2010) Association between breast cancer risk and the wild-type allele of human ABC transporter ABCC11. *Anticancer Res* **30**, 5189-5194
329. Beesley, J., Johnatty, S. E., Chen, X., Spurdle, A. B., Peterlongo, P., Barile, M., *et al.* (2011) No evidence for an association between the earwax-associated polymorphism in ABCC11 and breast cancer risk in Caucasian women. *Breast Cancer Res Treat* **126**, 235-239
330. Lang, T., Justenhoven, C., Winter, S., Baisch, C., Hamann, U., Harth, V., *et al.* (2011) The earwax-associated SNP c.538G>A (G180R) in ABCC11 is not associated with breast cancer risk in Europeans. *Breast Cancer Res Treat* **129**, 993-999
331. Yamada, A., Ishikawa, T., Ota, I., Kimura, M., Shimizu, D., Tanabe, M., *et al.* (2013) High expression of ATP-binding cassette transporter ABCC11 in breast tumors is associated with aggressive subtypes and low disease-free survival. *Breast Cancer Res Treat* **137**, 773-782
332. Yamada, A., Ishikawa, T., Takabe, K., and Endo, I. (2013) Earwax type and osmidrosis: prognostic factor for breast cancer? Response to letter to the editor. *Breast Cancer Res Treat* **138**, 652-653
333. Ramos-Espiritu, L., Diaz, A., Nardin, C., Saviola, A. J., Shaw, F., Plitt, T., *et al.* (2016) The metabolic/pH sensor soluble adenylyl cyclase is a tumor suppressor protein. *Oncotarget* **7**, 45597-45607
334. Grant, W. B. (2014) Trends in diet and Alzheimer's disease during the nutrition transition in Japan and developing countries. *J Alzheimers Dis* **38**, 611-620
335. Pozueta, J., Lefort, R., and Shelanski, M. L. (2013) Synaptic changes in Alzheimer's disease and its models. *Neuroscience* **251**, 51-65

336. Chigaev, A., and Sklar, L. A. (2012) Aspects of VLA-4 and LFA-1 regulation that may contribute to rolling and firm adhesion. *Frontiers in immunology* **3**, 242
337. Chigaev, A., Smagley, Y., Haynes, M. K., Ursu, O., Bologna, C. G., Halip, L., *et al.* (2015) FRET detection of lymphocyte function-associated antigen-1 conformational extension. *Molecular biology of the cell* **26**, 43-54
338. Chigaev, A., Smagley, Y., and Sklar, L. A. (2014) Carbon monoxide down-regulates alpha4beta1 integrin-specific ligand binding and cell adhesion: a possible mechanism for cell mobilization. *BMC immunology* **15**, 52
339. Chigaev, A., Waller, A., Amit, O., and Sklar, L. A. (2008) Galphas-coupled receptor signaling actively down-regulates alpha4beta1-integrin affinity: a possible mechanism for cell de-adhesion. *BMC.Immunol.* **9**, 26
340. Wang, Q., Klyubin, I., Wright, S., Griswold-Prenner, I., Rowan, M. J., and Anwyl, R. (2008) Alpha v integrins mediate beta-amyloid induced inhibition of long-term potentiation. *Neurobiol Aging* **29**, 1485-1493
341. Wang, Q. W., Rowan, M. J., and Anwyl, R. (2009) Inhibition of LTP by beta-amyloid is prevented by activation of beta2 adrenoceptors and stimulation of the cAMP/PKA signalling pathway. *Neurobiol Aging* **30**, 1608-1613
342. Li, S., Jin, M., Zhang, D., Yang, T., Koeglsperger, T., Fu, H., *et al.* (2013) Environmental novelty activates beta2-adrenergic signaling to prevent the impairment of hippocampal LTP by Abeta oligomers. *Neuron* **77**, 929-941
343. Barco, A., Alarcon, J. M., and Kandel, E. R. (2002) Expression of constitutively active CREB protein facilitates the late phase of long-term potentiation by enhancing synaptic capture. *Cell* **108**, 689-703
344. Zeitlin, R., Patel, S., Burgess, S., Arendash, G. W., and Echeverria, V. (2011) Caffeine induces beneficial changes in PKA signaling and JNK and ERK activities in the striatum and cortex of Alzheimer's transgenic mice. *Brain Res* **1417**, 127-136
345. Scott Bitner, R. (2012) Cyclic AMP response element-binding protein (CREB) phosphorylation: a mechanistic marker in the development of memory enhancing Alzheimer's disease therapeutics. *Biochem Pharmacol* **83**, 705-714
346. Du, H., Guo, L., Wu, X., Sosunov, A. A., McKhann, G. M., Chen, J. X., *et al.* (2014) Cyclophilin D deficiency rescues Abeta-impaired PKA/CREB signaling and alleviates synaptic degeneration. *Biochim Biophys Acta* **1842**, 2517-2527

347. Chen, Y., Huang, X., Zhang, Y. W., Rockenstein, E., Bu, G., Golde, T. E., *et al.* (2012) Alzheimer's beta-secretase (BACE1) regulates the cAMP/PKA/CREB pathway independently of beta-amyloid. *The Journal of neuroscience : the official journal of the Society for Neuroscience* **32**, 11390-11395
348. Liang, Z., Liu, F., Grundke-Iqbal, I., Iqbal, K., and Gong, C. X. (2007) Down-regulation of cAMP-dependent protein kinase by over-activated calpain in Alzheimer disease brain. *J Neurochem* **103**, 2462-2470
349. Shi, J., Qian, W., Yin, X., Iqbal, K., Grundke-Iqbal, I., Gu, X., *et al.* (2011) Cyclic AMP-dependent protein kinase regulates the alternative splicing of tau exon 10: a mechanism involved in tau pathology of Alzheimer disease. *The Journal of biological chemistry* **286**, 14639-14648
350. Hartz, A. M., and Bauer, B. (2011) ABC transporters in the CNS - an inventory. *Curr Pharm Biotechnol* **12**, 656-673
351. Wijesuriya, H. C., Bullock, J. Y., Faull, R. L., Hladky, S. B., and Barrand, M. A. (2010) ABC efflux transporters in brain vasculature of Alzheimer's subjects. *Brain Res* **1358**, 228-238
352. Martinez, M., Fernandez, E., Frank, A., Guaza, C., de la Fuente, M., and Hernanz, A. (1999) Increased cerebrospinal fluid cAMP levels in Alzheimer's disease. *Brain Res* **846**, 265-267
353. Martinez, M., Hernandez, A. I., and Hernanz, A. (2001) Increased cAMP immunostaining in cerebral vessels in Alzheimer's disease. *Brain Res* **922**, 148-152
354. Qosa, H., Mohamed, L. A., Alqahtani, S., Abuasal, B. S., Hill, R. A., and Kaddoumi, A. (2016) Transporters as Drug Targets in Neurological Diseases. *Clin Pharmacol Ther* **100**, 441-453
355. Murphy, M. P., and LeVine, H., 3rd. (2010) Alzheimer's disease and the amyloid-beta peptide. *J Alzheimers Dis* **19**, 311-323
356. Vitolo, O. V., Sant'Angelo, A., Costanzo, V., Battaglia, F., Arancio, O., and Shelanski, M. (2002) Amyloid beta -peptide inhibition of the PKA/CREB pathway and long-term potentiation: reversibility by drugs that enhance cAMP signaling. *Proceedings of the National Academy of Sciences of the United States of America* **99**, 13217-13221

357. Atkins, C. M., Oliva, A. A., Jr., Alonso, O. F., Pearse, D. D., Bramlett, H. M., and Dietrich, W. D. (2007) Modulation of the cAMP signaling pathway after traumatic brain injury. *Exp Neurol* **208**, 145-158
358. Zhao, L., Qian, Z. M., Zhang, C., Wing, H. Y., Du, F., and Ya, K. (2008) Amyloid beta-peptide 31-35-induced neuronal apoptosis is mediated by caspase-dependent pathways via cAMP-dependent protein kinase A activation. *Aging Cell* **7**, 47-57
359. Kraft, P., Schwarz, T., Gob, E., Heydenreich, N., Brede, M., Meuth, S. G., *et al.* (2013) The phosphodiesterase-4 inhibitor rolipram protects from ischemic stroke in mice by reducing blood-brain-barrier damage, inflammation and thrombosis. *Exp Neurol* **247**, 80-90
360. Chagtoo, M., George, N., Pathak, N., Tiwari, S., Godbole, M. M., and Ladilov, Y. (2017) Inhibition of Intracellular Type 10 Adenylyl Cyclase Protects Cortical Neurons Against Reperfusion-Induced Mitochondrial Injury and Apoptosis. *Mol Neurobiol*
361. Yu, X. Y., Lin, S. G., Chen, X., Zhou, Z. W., Liang, J., Duan, W., *et al.* (2007) Transport of cryptotanshinone, a major active triterpenoid in *Salvia miltiorrhiza* Bunge widely used in the treatment of stroke and Alzheimer's disease, across the blood-brain barrier. *Curr Drug Metab* **8**, 365-378
362. Mei, Z., Zhang, F., Tao, L., Zheng, W., Cao, Y., Wang, Z., *et al.* (2009) Cryptotanshinone, a compound from *Salvia miltiorrhiza* modulates amyloid precursor protein metabolism and attenuates beta-amyloid deposition through upregulating alpha-secretase in vivo and in vitro. *Neurosci Lett* **452**, 90-95
363. Yoo, K. Y., and Park, S. Y. (2012) Terpenoids as potential anti-Alzheimer's disease therapeutics. *Molecules* **17**, 3524-3538
364. Zhang, X. Z., Qian, S. S., Zhang, Y. J., and Wang, R. Q. (2016) *Salvia miltiorrhiza*: A source for anti-Alzheimer's disease drugs. *Pharm Biol* **54**, 18-24
365. Cheepala, S., Hulot, J. S., Morgan, J. A., Sassi, Y., Zhang, W., Naren, A. P., *et al.* (2013) Cyclic nucleotide compartmentalization: contributions of phosphodiesterases and ATP-binding cassette transporters. *Annu Rev Pharmacol Toxicol* **53**, 231-253
366. Cripe, L. D., Uno, H., Paietta, E. M., Litzow, M. R., Ketterling, R. P., Bennett, J. M., *et al.* (2010) Zosuquidar, a novel modulator of P-glycoprotein, does not improve the outcome of older patients with newly diagnosed acute myeloid

- leukemia: a randomized, placebo-controlled trial of the Eastern Cooperative Oncology Group 3999. *Blood* **116**, 4077-4085
367. Kim, D. H., and Lerner, A. (1998) Type 4 Cyclic Adenosine Monophosphate Phosphodiesterase as a Therapeutic Target in Chronic Lymphocytic Leukemia. *Blood* **92**, 2484-2494
368. Degerman, E., Belfrage, P., and Manganiello, V. C. (1997) Structure, localization, and regulation of cGMP-inhibited phosphodiesterase (PDE3). *J Biol Chem* **272**, 6823-6826
369. Meng, X., Matlawska-Wasowska, K., Girodon, F., Mazel, T., Willman, C. L., Atlas, S., *et al.* (2011) GSI-I (Z-LLNle-CHO) inhibits γ -secretase and the proteasome to trigger cell death in precursor-B acute lymphoblastic leukemia. *Leukemia* **25**, 1135
370. Matlawska-Wasowska, K., Ward, E., Stevens, S., Wang, Y., Herbst, R., Winter, S. S., *et al.* (2013) Macrophage and NK-mediated killing of precursor-B acute lymphoblastic leukemia cells targeted with a-fucosylated anti-CD19 humanized antibodies. *Leukemia* **27**, 1263
371. Matlawska-Wasowska, K., Kang, H., Devidas, M., Wen, J., Harvey, R. C., Nickl, C. K., *et al.* (2016) MLL rearrangements impact outcome in HOXA-deregulated T-lineage acute lymphoblastic leukemia: a Children's Oncology Group Study. *Leukemia* **30**, 1909-1912